

U.S. EPR Rod Ejection Accident Methodology

ANP-10286NP-A
Revision 0

Topical Report

November 2011

AREVA NP Inc.

(c) 2011 AREVA NP Inc.

Copyright © 2011

**AREVA NP Inc.
All Rights Reserved**



OFFICIAL USE ONLY – ENCLOSURE 2 CONTAINS SECURITY RELATED INFORMATION

**UNITED STATES
NUCLEAR REGULATORY COMMISSION
WASHINGTON, D.C. 20555-0001**

November 29, 2011

Mr. Pedro Salas
Manager, Corporate Regulatory Affairs
AREVA NP, Inc.
3315 Old Forrest Road
P.O. Box 10935
Lynchburg, VA 24506-0935

**SUBJECT: FINAL SAFETY EVALUATION REPORT REGARDING ANP-10286P,
"U.S. EPR ROD EJECTION ACCIDENT METHODOLOGY TOPICAL REPORT"**

Dear Mr. Salas:

By letter dated November 20, 2007 (Agencywide Documents Access and Management System (ADAMS) Accession No. ML073310620), as supplemented by letters dated July 10, 2008 (ADAMS ML081970349), October 3, 2008 (ADAMS ML082880500), and March 26, 2009 (ADAMS ML090890175), AREVA NP, Inc., (AREVA) submitted for U.S. Nuclear Regulatory Commission (NRC) staff review Topical Report (TR) ANP-10286P, "U.S. EPR Rod Ejection Accident Methodology Topical Report," ADAMS ML073310629 (proprietary), ADAMS ML073310622 (nonproprietary). On July 19, 2010, an NRC draft safety evaluation (SE) regarding our approval of ANP-10286P was provided for your review and comments. By letter dated July 19, 2010, AREVA NP, Inc., commented on the draft SE. The staff's disposition of AREVA NP, Inc.'s comments on the draft SE are discussed in the attachment to the final SE enclosed in this letter. A public version of the final SE is contained in Enclosure 1. A non-public, or proprietary, version of the final SE is contained in Enclosure 2.

The staff has found that ANP-10286P, Revision 0, is acceptable for referencing in licensing applications for U.S. EPR to the extent specified and under the limitations delineated in the TR and in the enclosed SE. The SE defines the basis for acceptance of the TR.

Our acceptance applies only to material provided in the subject TR. We do not intend to repeat our review of the acceptable material described in the TR. When the TR appears as a reference in license applications, our review will ensure that the material presented applies to the specific plant involved. Regulatory applications that deviate from this TR will be subject to a plant-specific review in accordance with applicable review standards.

Document transmitted herewith contains sensitive unclassified information. When separated from the enclosure, this document is "DECONTROLLED."

OFFICIAL USE ONLY – ENCLOSURE 2 CONTAINS SECURITY RELATED INFORMATION

In accordance with the guidance provided on the NRC website, we request that AREVA publish accepted proprietary and non-proprietary versions of this TR within three months of receipt of this letter. The accepted versions shall incorporate this letter and the enclosed SE after the title page. Also, they must contain historical review information, including NRC requests for additional information and your responses. The accepted versions shall include an "-A" (designating accepted) following the TR identification symbol.

If future changes to the NRC's regulatory requirements affect the acceptability of this TR, AREVA will be expected to revise the TR appropriately, or justify its continued applicability for subsequent referencing.

If you have any questions, please contact me at Getachew.Tesfaye@nrc.gov or 301-415-3361.

Sincerely,

A handwritten signature in black ink, appearing to read "Getachew Tesfaye". The signature is fluid and cursive, with a long horizontal stroke extending to the right.

Getachew Tesfaye, Senior Project Manager
EPR Projects Branch
Division of New Reactor Licensing
Office of New Reactors

Docket No.: 52-020

Enclosure:
Final Safety Evaluation Report

cc: w/o encl: U.S. EPR Mailing List

DC AREVA - EPR Mailing List

(Revised 11/16/2011)

cc:

Ms. Michele Boyd
Legislative Director
Energy Program
Public Citizens Critical Mass Energy
and Environmental Program
215 Pennsylvania Avenue, SE
Washington, DC 20003

Dr. Charles L. King
Licensing Manager, IRIS Project
Westinghouse Electric Company
Science and Technology Department
20 International Drive
Windsor, CT 06095

Ms. Sherry McFaden
AREVA NP Inc.
3315 Old Forest Road, OF-16
Lynchburg, VA 24501

Mr. Tony Robinson
AREVA NP, Inc.
3315 Old Forest Road
Lynchburg, VA 24501

Mr. Steve Seitz
AREVA NP Canada Ltd.
100 Dean Road
East Lyme, CT 06333

Mr. Robert E. Sweeney
IBEX ESI
4641 Montgomery Avenue
Suite 350
Bethesda, MD 20814

Mr. Gary Wright, Director
Division of Nuclear Facility Safety
Illinois Emergency Management Agency
1035 Outer Park Drive
Springfield, IL 62704

DC AREVA - EPR Mailing List

Email

alau@washdc.whitecase.com (Albie Lau)
APH@NEI.org (Adrian Heymer)
awc@nei.org (Anne W. Cottingham)
bgattoni@roe.com (William (Bill) Gattoni)
BrinkmCB@westinghouse.com (Charles Brinkman)
cwaltman@roe.com (C. Waltman)
darrell.gardner@areva.com (Darrell Gardner)
david.hinds@ge.com (David Hinds)
david.lewis@pillsburylaw.com (David Lewis)
dennis.williford@areva.com (Dennis Williford)
erg-xl@cox.net (Eddie R. Grant)
gcesare@enercon.com (Guy Cesare)
greg.gibson@unistarnuclear.com (Greg Gibson)
james.beard@gene.ge.com (James Beard)
james.p.mcquighan@constellation.com (Jim McQuighan)
jason.parker@pillsburylaw.com (Jason Parker)
jerald.head@ge.com (Jerald G. Head)
jim.riccio@wdc.greenpeace.org (James Riccio)
Joseph_Hegner@dom.com (Joseph Hegner)
junichi_uchiyama@mnes-us.com (Junichi Uchiyama)
KSutton@morganlewis.com (Kathryn M. Sutton)
kwaugh@impact-net.org (Kenneth O. Waugh)
lchandler@morganlewis.com (Lawrence J. Chandler)
Len.Gucwa.ext@areva.com (Len Gucwa)
Marc.Brooks@dhs.gov (Marc Brooks)
maria.webb@pillsburylaw.com (Maria Webb)
mark.beaumont@wsms.com (Mark Beaumont)
Martin.Bryan.ext@AREVA.com (Martin Bryan)
matias.travieso-diaz@pillsburylaw.com (Matias Travieso-Diaz)
mbowling@numarkassoc.com (Marty Bowling)
media@nei.org (Scott Peterson)
mike_moran@fpl.com (Mike Moran)
MSF@nei.org (Marvin Fertel)
mwetterhahn@winston.com (M. Wetterhahn)
nirsnet@nirs.org (Michael Mariotte)
Nuclaw@mindspring.com (Robert Temple)
patriciaL.campbell@ge.com (Patricia L. Campbell)
paul.gaukler@pillsburylaw.com (Paul Gaukler)
Paul@beyondnuclear.org (Paul Gunter)
pbessette@morganlewis.com (Paul Bessette)
RJB@NEI.org (Russell Bell)
rrsgarro@pplweb.com (Rocco Sgarro)
sabinski@suddenlink.net (Steve A. Bennett)

DC AREVA - EPR Mailing List

sandra.sloan@areva.com (Sandra Sloan)
sfrantz@morganlewis.com (Stephen P. Frantz)
stephan.moen@ge.com (Stephan Moen)
Steve.Graham@hse.gsi.gov.uk (Steve Graham)
steven.hucik@ge.com (Steven Hucik)
strambgb@westinghouse.com (George Stramback)
tkkibler@scana.com (Tria Kibler)
tlharpster@pplweb.com (Terry Harpster)
tom.miller@hq.doe.gov (Tom Miller)
trsmith@winston.com (Tyson Smith)
Vanessa.quinn@dhs.gov (Vanessa Quinn)
vijukrp@westinghouse.com (Ronald P. Vijuk)
Wanda.K.Marshall@dom.com (Wanda K. Marshall)
wayne.marquino@ge.com (Wayne Marquino)
whorin@winston.com (W. Horin)

ENCLOSURE 1

ML110050349

SAFETY EVALUATION BY THE OFFICE OF NEW REACTORS
TOPICAL REPORT ANP-10286P, REVISION 0
"U.S. EPR ROD EJECTION ACCIDENT METHODOLOGY TOPICAL REPORT"
AREVA NP, INC.
DOCKET NO. 52-020

1.0 INTRODUCTION

1.1. SUMMARY

By letter dated November 20, 2007 (Agencywide Documents Access and Management System [ADAMS] Accession Number ML073310620), as supplemented by letters dated July 10, 2008 (ADAMS ML081970349), October 3, 2008 (ADAMS ML082880500), and March 26, 2009 (ADAMS ML090890175), AREVA NP, Inc., (AREVA) submitted for U.S. Nuclear Regulatory Commission (NRC) staff review and approval Topical Report (TR) ANP-10286P, "U.S. EPR Rod Ejection Accident Methodology Topical Report" ADAMS ML073310629 (proprietary), ADAMS ML073310622 (nonproprietary) [1]. This Safety Evaluation Report (SER) is based on the submitted Licensing Topical Report, the information obtained during a number of meetings and conference calls with the applicant, and formal requests for additional information (RAIs).

In the document ANP-10286P [1], the applicant describes a method of analyzing the consequences of a control rod ejection accident (REA) for the U.S. EPR. The methodology is based on a 3-D nodal kinetics solution with both thermal-hydraulic and fuel temperature feedback. In addition, there is a separate peak rod thermal evaluation using an open channel thermal-hydraulic model. This methodology includes updated models for determining the trip detection, control rod insertion and effective fuel temperature.

The review is carried out in conformance with the regulatory guidance as summarized in NUREG-0800, "Standard Review Plan for the Review of Safety Analysis Reports for Nuclear Power Plants: LWR Edition" (SRP) [2] Section 15.4.8, "Spectrum of Rod Ejection Accidents (PWR)," and SRP Section 4.2, "Fuel System Design," Appendix B, "Interim Acceptance Criteria and Guidance for the Reactivity Initiated Accidents."

The rod ejection accident is analyzed using two primary codes, NEMO-K [3] and LYNXT [3]. The former is used to carry out the 3-D kinetic calculation while the control rod is being ejected from the core, and LYNXT (coupled with COPERNIC [3]) is primarily used to determine the number of failed rods. In addition, it is necessary under certain conditions that a system level code, in this case S-RELAP [3], be used to determine the state points in the core, which are used to determine the number of failed rods. Rod failure is defined by either the addition of, at least, 110 cal/g (197.4 BTU/lb) during the initial transient, or if the specified acceptable fuel design limit (SAFDL) limits are violated on the value of the minimum departure from nucleate boiling ratio (MDNBR).

The staff's evaluations presented in this report are divided into several sections that cover: (1) Code and Code Updates Descriptions, (2) Selected Transient Responses, and (3) Independent Validation. Summaries of these sections are provided as follows:

- 1) Code and Code Updates Descriptions – Sections 3.3 and 3.4 of this report include short descriptions of the codes used in the applicant's analysis as well as a description of the updates (if applicable). These include CASMO-3G, COPERNIC, NEMO-K, and LYNXT. These descriptions are followed by a discussion of the changes made to NEMO-K and LYNXT since the submittal of ANP-10263P, "Codes and Methods Applicability Report for the U.S. EPR" [3]. NEMO-K has an improved trip detection and control rod insertion model that mimics the behavior of the actual trip signal processing closely. In addition, the rod insertion model allows for rod acceleration and slowing down at either end of its stroke. An improved determination of the effective fuel temperature is included in NEMO-K. This is particularly important since this temperature controls Doppler feedback, which is the most important shutdown mechanism in the near term. The improved effective temperature model is validated against calculations carried out using APOLLO2 and MCNP. The changes introduced in LYNXT involve an improved gap thermal property model.
- 2) Selected Transient Responses – Section 3.5 of this report describes the categories of transient responses analyzed by the applicant and provides the staff's evaluation. There are two transient categories in the REA scenarios. The first are those transients that are terminated within approximately the first 5 seconds (sec.) by the ex-core detectors; the second are those transients that carry on until they are terminated by a system level trip signal. One of each of these transients is evaluated by the staff. In addition, the method of determining the number of failed rods is reviewed by the staff.
- 3) Independent Confirmatory Analysis – Section 3.6 of this report presents two sets of confirmatory analyses used by the staff to support the safety evaluation. The first set of confirmatory analyses involved the staff using an independent code package to analyze the limiting cases presented by the applicant. The second set of confirmatory analyses involved a comparison of the staff's analysis of the Special Power Excursion Reactor Test (SPERT) using TRITON/TRACE [4,5] to the applicant's NEMO-K based analysis.

1.2. DESCRIPTION OF A GENERIC ROD EJECTION ACCIDENT TRANSIENT EVENT

Rod Ejection Accidents are a class of accident transients that pressurized water reactor (PWR) vendors are required to analyze in order to meet the requirements of General Design Criterion (GDC) 28, "Reactivity Limits," (as described in SRP Section 15.4.8) in order to obtain an NRC license for a particular reactor design. The following discussion is based on descriptions presented in the Topical Report.

The accident is initiated by the sudden ejection of a control rod from the core of a critical reactor. Initially, the reactor can be at hot full power (HFP), or hot zero power (HZP), and, in addition, the core could be at beginning of cycle (BOC) or end of cycle (EOC). Thus, a total of at least four different combinations exist to be analyzed. Partial power situations might be considered in particular cases to explore bounding conditions. Furthermore, the possibility that simultaneous depressurizations of the primary coolant system occurs must be considered, since the ejection of the rod could damage the pressure vessel and create a coolant leakage path. In general, there are a large number of initial conditions that can affect the transient response, and its ultimate termination.

In a typical REA, a control rod is rapidly ejected and accelerated by the system pressure, resulting in a step change in reactivity. The sudden addition of reactivity results in a

corresponding increase in power and fuel temperature. The only feedback mechanism that can counter this power increase is the Doppler Effect associated with the fertile component of the fuel (^{238}U). As a result of the increase in power, the fuel temperature increases and the Doppler feedback becomes progressively more negative until it reverses the power increase, resulting in a typical power pulse. Finally, the ex-core power detectors trip the scram system and the transient is terminated. The duration of the transient is approximately 5 sec., which is short enough to ignore all system related changes to the coolant temperature and pressure.

However, if the time frame is long enough that system level thermal hydraulic changes are significant, a second transient type results. This can occur at HFP when the control rods are mostly withdrawn. In this case, the power increase is comparatively small, causing a small amount of negative Doppler feedback and, thus, a small pulse followed by a slow increase in reactor power. In addition, the primary system boundary may be compromised due to the ejected rod creating a small break loss of coolant. In this case, a system level response is necessary, since transient termination will be due to activation of reactor trips associated with system response.

Two important results from a REA analysis are of primary interest. First, the number of fuel rods that have failed as a result of the transient, and second, whether or not any of the regulatory requirements have been violated (see Section 2 of this report). Two rod failure mechanisms are important in REA transients:

- 1) Those that occur during the initial power pulse, caused by pellet clad mechanical interaction (PCMI).
- 2) Those due to fuel clad failure caused by violation of the Minimum Departure from Nucleate Boiling Ratio (MDNBR) limits. There is an accepted limit (to be discussed below) known as the specified acceptable fuel design limit, which will be referred to in connection with the MDNBR.

If none of the regulatory requirements are violated, the transient analysis is considered complete. However, if there is any violation of these regulatory requirements, it is necessary to re-configure the core design or reactor system to ensure compliance.

2.0 REGULATORY CRITERIA

2.1. REQUIREMENTS

The applicant submitted ANP-10286P [1] in order to support the rod ejection analysis summarized within the U.S. EPR Final Safety Analysis Report (FSAR). As such, the regulatory requirements and guidance outlined by SRP Section 15.4.8, "Spectrum of Rod Ejection Accidents (PWR)," and SRP Section 4.2, "Fuel System Design," Appendix B, "Interim Acceptance Criteria and Guidance for the Reactivity Initiated Accidents," were used by the staff in the review of this topical report. These requirements concern cladding failure, coolability, and radiological release. Radiological release was not addressed explicitly in ANP-10286P [1], so this requirement must be addressed when an applicant applies the methodology presented in ANP-10286P [1] to the review of a rod ejection event. The following is a summary of the applicable criteria.

GDC 13, "Instrumentation and Control," requires the provision of instrumentation that is capable of monitoring variables and systems over their anticipated ranges to assure adequate safety,

and of controls that can maintain these variables and systems within prescribed operating ranges.

GDC 28, "Reactivity Limits," assures that the effects of postulated reactivity accidents can neither damage the reactor coolant pressure boundary nor result in sufficient disturbance to impair the core cooling capability.

2.2. RELEVANT GUIDANCE

SRP Section 4.2, Appendix B provides the interim acceptance criteria and guidance for Reactivity Initiated Accidents, of which the Rod Ejection Accident is a subset. By following the provided guidance, an applicant demonstrates compliance with GDC 28. A brief description of the guidance from SRP Section 4.2, Appendix B is provided below:

1) Cladding failure

The PCMI due to the sudden rise in power during the pulse phase of a REA requires a limit regarding energy (cal/g) as a function of clad thickness (clad thickness change due to oxidation). The oxide thickness increases with burnup. The applicant has estimated that for a maximum burnup of 62 GWD/MT, the oxide thickness/wall thickness is 0.061, which implies an energy deposition limit of 110 cal/g (198 BTU/lb) for PCMI failures to occur. Additionally, clad failures can occur in cases which the pin internal pressure is below system pressure when the total enthalpy exceeds 170 cal/g (306 BTU/lb), and for cases that the pin internal pressure is above system pressure when the total energy exceeds 150 cal/g (270 BTU/lb). Both of these limits apply for core power levels below five percent. Finally, violating the thermal design limits for all power levels above five percent is assumed to lead to clad failure. These requirements, as they relate to SAFDLs are captured in GDC 10, "Reactor Design."

2) Coolability

Pin cooling is assumed failed for all pins with a total enthalpy of 230 cal/g (414 BTU/lb). In addition, pin cooling is assumed to fail in cases in which there is incipient fuel melting. Furthermore, cooling failure will occur for all cases in which there is a failure to preserve the reactor pressure boundary, reactor internals, and fuel assembly structural integrity. Finally, a loss of coolable geometry will result following clad and fuel fragmentation, and clad ballooning. These requirements are captured in GDC 27, "Combined Reactivity Control Systems Capability," and GDC 35, "Emergency Core Cooling," as they relate to control rod insertability and core coolability.

3) Radiological Impact

Radiological impact will not be explicitly discussed in this report. However, SRP Section 4.2 Appendix B provides guidance related to the calculation of fission product inventory that would be available after an event. This inventory is to include both the steady-state gap inventory (further guidance is provided in RG 1.183 and RG 1.195) as well as fission gas released during the event. SRP Section 4.2 Appendix B provides a correlation between gas release and maximum fuel enthalpy increase that can be used to calculate the transient fission gas release.

The above limits summarize the guidance used to demonstrate compliance with GDC 28, which must be met in carrying out the analyses outlined in Section 3.2, Figures 2 and 3 of this report. These limits are used at the decision points regarding fuel temperature and cal/g determinations, and the number of failed rods that imply unacceptable radiological release.

3.0 SUMMARY OF TECHNICAL INFORMATION

In this chapter, the applicant's methodology is summarized and the codes used by the applicant in the methodology are briefly described, including their input, output, and analytic modeling.

3.1. OUTLINE OF ROD EJECTION ACCIDENT PHYSICAL PHENOMENA, MODELING, AND OVERALL METHODOLOGY

In this section, an outline is given of the various physical phenomena that govern the progression of an REA transient, and the implied requirements that are placed on the numerical algorithms to be used. Broadly, the initial response of the core to an REA is generally a skewed increase in the power, which severely impacts the fuel temperature and cooling of the core in selected assemblies. In all these analyses, temperature-dependent cross-section data and temperature- and pressure-dependent thermo-physical properties are necessary in order to model the event accurately.

The core power shape is most accurately determined by using a 3-D space-time kinetic calculation. In the applicant's model, the cross-section data is a function of temperature, burnup, and composition.

The fluid dynamics and heat transfer calculations used by the applicant were carried out on the most highly challenged fuel assemblies recognizing every fuel rod, and allowing for both axial and transverse flow. This calculation takes input from the 3-D kinetics calculation or the system level calculation, and the variable thermo-physical data used in the above calculation is also used in this analysis. The primary output from this analysis is the number of failed rods, either due to PCMI or due to violation of the SAFDL limits.

Finally, for those transients that go on for more than approximately 5 sec., a system level code is required to determine the coolant temperature and pressure, and to determine any phase change in the cases where the pressure is dropping. This code takes input from the 3-D kinetics code NEMO-K, and the variable thermo-physical data used in the above calculations. The system level code traditionally uses a point kinetic model, but in this application this model is turned off, and a power versus (vs.) time characteristic is obtained from the 3-D kinetic calculation and used as a driving function.

Rod failure due to PCMI is determined by a threshold value of enthalpy deposited per gram of fuel material (cal/g) in conformance with SRP Section 4.2, Appendix B. All rods that exceed this limit are assumed failed and occur during the initial power pulse phase of the transient. In the longer term, additional rod failure may occur due to violation of the SAFDL limit (MDNBR < SAFDL). Rods that fail and have an energy deposition above 31.2 cal/gm are ascribed a higher radiological worth than rods that fail below this value. This enhancement in worth is recognized by multiplying the number of rods by a transient fission gas release (TFGR) factor, which is a function of the enthalpy rise (threshold of 31.2 cal/gm), to arrive at an equivalent number of rods failed. Thus, to obtain the total number of rods failed for radiological release consideration, those that fail and have a prompt enthalpy rise above 31.2 cal/gm are multiplied by a TFGR factor and added to the number of rods failed below this value. The

radiological consequences of this total number of failed rods is compared to the regulatory requirements of 10 CFR 100.11, "Determination of exclusion area, low population zone, and population center distance," or 10 CFR 50.67, "Accident Source Term," as indicated in SRP Section 15.4.8 to determine acceptability. Figure 1 of this report illustrates the methodology used by the applicant to analyze the REA event.

The starting point is determined by the design for fuel pins, which are assembled into a fuel assembly, and which finally are combined to form the reactor core. Following this step, the state of the reactor before the rod ejection accident is defined; this includes burnup, power level, location of rod to be ejected, system state points, etc. In addition, the regulatory limits as listed in Section 2 of this report are defined, and the code suite to be used is selected based on the expected transient. The later step is important, since the inter-linkage of the various codes that supply the solution as the transient progresses is dependent on the expected outcome of the transient. This point has been made above in connection with the reactor scram and transient termination depending on the amount of reactivity insertion requiring either an ex-core detector, or a system level scram mode.

Once all the above preparatory work has been carried out the analysis step can be initiated. The details of this step are discussed in Section 3.2 of this report, in which the detailed inter-linkage of the various codes and associated information are described. Following the analysis step, a decision is made regarding whether or not the core design under consideration can successfully survive the imposed transient. If any of the regulatory requirements listed in Section 2 of this report are violated, the reactor core needs to be re-configured and the process repeated until all requirements are satisfied. If the transient is completed without violating any regulatory requirements, the analysis is considered complete (see Section 2 of this report).

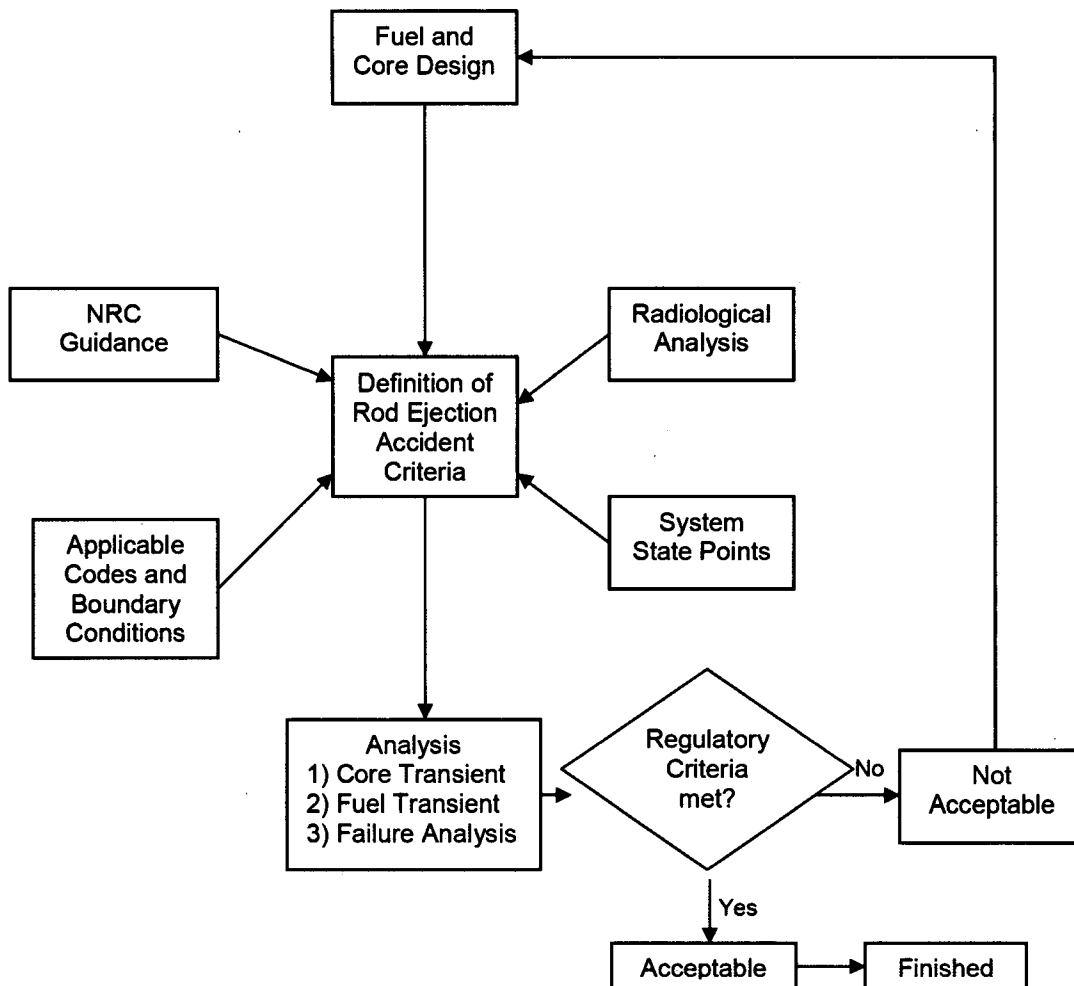


Figure 1 – Overall Core-Fuel Rod Ejection Accident Analysis Methodology.

3.2. DETAILS OF ANALYSIS METHODOLOGY

This section summarizes the linkages of the codes, the information being transmitted along the links, and the sequence of codes used by the applicant in ANP-10286P [1]. The code linkages are shown in Figures 2 and 3 of this report. The primary codes are NEMO-K, LYNXT, and S-RELAP, which cover the initial power pulse, thermal-hydraulic response of the most highly challenged fuel assemblies and rods, and the system response, respectively. More detailed descriptions of the codes, particularly NEMO-K are given in Section 3.3.3 of this report. The codes CASMO-3G and COPERNIC supply temperature, pressure, and composition dependent input to the above three codes. Furthermore, as outlined above, REA transients are divided into two broad groups: (1) Those that are terminated by ex-core detectors within approximately 5 sec.; and (2) those that need to be terminated by system level trip signals and extend beyond 5 sec. The linkages shown in Figures 2 and 3 of this report for these two time frames are:

- 1) The first time frame is defined as 0 – 5 sec., Figure 2 of this report. NEMO-K is used to calculate the core power pulse, with input from CASMO-3G and COPERNIC.

CASMO-3G is used to supply temperature-dependent cross-section data, and COPERNIC calculates thermo-physical data and pin power shape. If the scram system is activated, the transient is over and the analysis proceeds to the LYNXT step to determine the number of failed rods. LYNXT takes input from COPERNIC and NEMO-K to determine the fuel temperature and the cal/g added to the fuel. If these parameters are outside acceptable limits, then the design needs to be modified. However, if they are within limits, the MDNBR needs to be checked by comparing to the SAFDL limits. If the MDNBR is greater than the SAFDL limit, then no fuel failure is implied for the assumed transient. However, if the MDNBR is below the SAFDL limit, an estimate of the number of failed fuel rods needs to be made. The most accurate manner of determining the number of failed pins would be to obtain a rod-by-rod power distribution vs. time from a 3-D neutronics and thermal-hydraulic calculation to determine the MDNBR, which can then be compared to the SAFDL limit. However, this option is not realistic and, thus, an acceptable practical approximate method is necessary. In Section 3.3 of this report, the method used by the applicant is outlined. A final tally of the number of failed rods is made, and then a determination is made whether or not the number of failed rods is within regulatory limits as discussed in Section 2 of this report. If the number of failed rods is within the regulatory limit the transient is over, if it exceeds the limit then the core needs to be re-designed.

- 2) The second time frame (greater than 5 sec. in Figure 3 of this report) begins after the coolant has made a complete circuit of the primary system. Thus, the system code S-RELAP5 is used to generate input for LYNXT in order to determine the number of failed rods. The S-RELAP5 code is driven by a total power input derived from NEMO-K. S-RELAP5 has the major system scram functions built in and, thus, eventually one of these is tripped and the system will scram, ending the transient. The determination of the number of failed rods in this case is simpler than in the short transient case, since the transient progresses in a quasi-static manner at this stage. The details of the method used to determine the number of failed fuel rods is outlined in Section 3.3 of this report. A final tally of the number of failed rods is made and then a determination is made whether or not the number of failed rods is within regulatory limits. If the number of failed rods is within the regulatory limit, the analysis is considered acceptable and complete; if it exceeds the limit, then the core needs to be re-designed.

Figures 2 and 3 of this report show that there are three points following in which the transient is terminated in an acceptable manner, and two terminations that imply that the reactor needs to be re-designed because it failed one of the regulatory requirements.

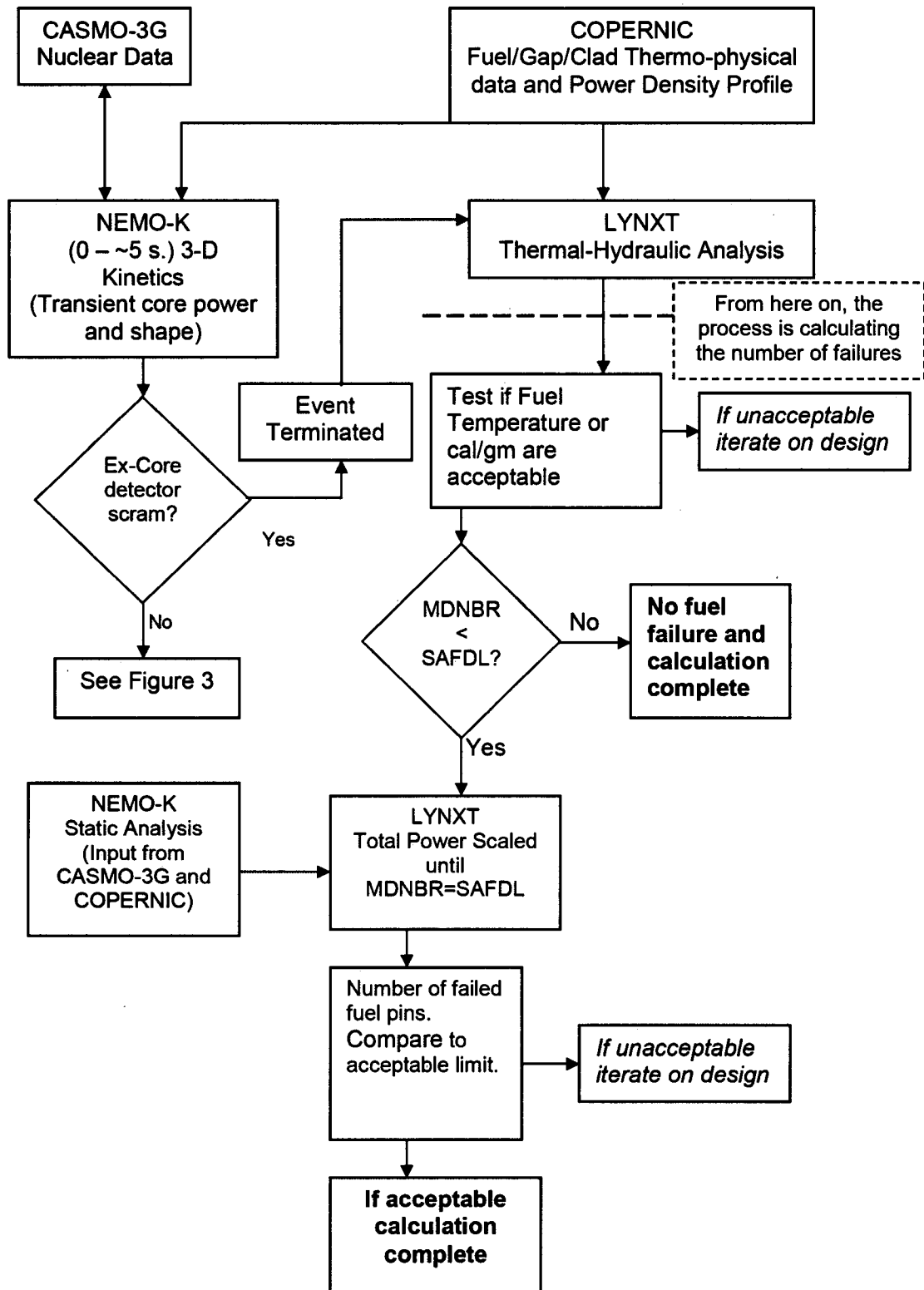


Figure 2 – Details of Analysis Methodology (0 - ~ 5 sec.)

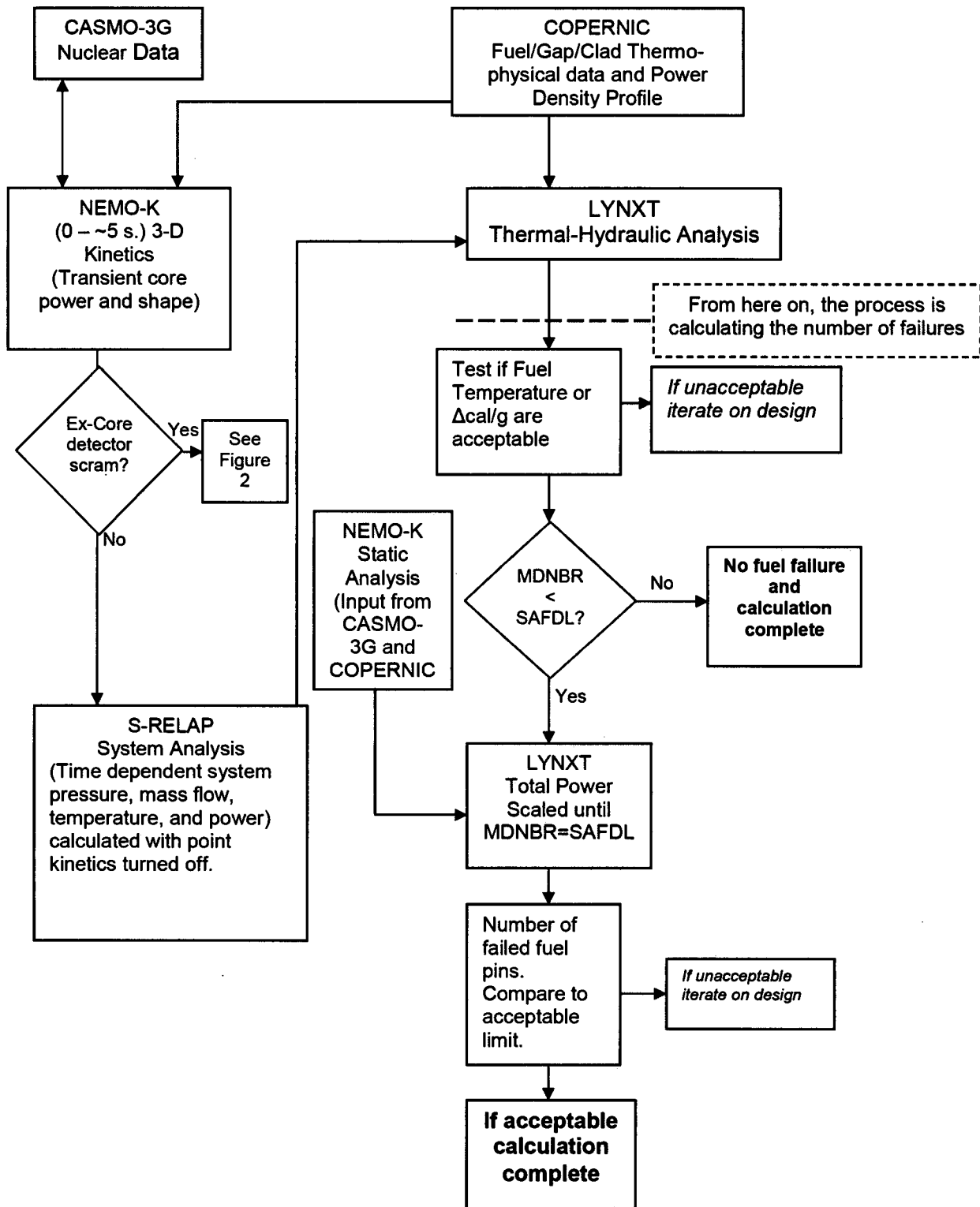


Figure 3 – Details of Analysis Methodology (greater than approximately 5 sec.)

3.3. CODE DESCRIPTIONS

3.3.1. CASMO-3G

CASMO-3G [3] is used to generate the temperature-dependent few-group nuclear data libraries for use in NEMO-K. CASMO-3G takes input from a processing code, which makes the Evaluated Nuclear Data File (ENDF/B) compilations compatible with the input to CASMO-3G. CASMO-3G models a unit assembly that consists of a two dimensional slice through the assembly, in which individual rods are recognized in all their detail (each rod has a pellet, gap, and clad). This calculation uses reflective boundary conditions, and leakage effects are included by assuming that the leakage can be approximated by a fundamental mode. In this case, spatial flux varies as approximately $e^{iB_1 r}$ using the B_1 approximation, which implies P_1 scattering. In this manner, the global leakage effect can be accounted for in determining the neutron energy spectrum over which the cross-sections will be averaged. These calculations are repeated for each assembly type (loading and burnup), and for various temperatures, resulting in a multi-dimensional table of few group cross-section as a function of these variables.

The CASMO-3G table is accessed by NEMO-K as the transient progresses. Due to variation of the fuel temperature, the resonance range cross-section changes as a result of the Doppler effect, and these cross-section changes play a pivotal role in the progression of the transient. In general, it is, thus, important to generate cross-section input for NEMO-K on a sufficiently fine mesh in order to capture all temperature peaks.

3.3.2. COPERNIC

COPERNIC [3] is used to prepare input for both NEMO-K and LYNXT. It defines thermo-physical properties for the fuel, gap, and clad material, including conductivity and specific heat. The properties for the fuel are a function of temperature and burnup. Clad properties are a function of the oxide film buildup on the surface, which is also determined by COPERNIC. Finally, the gap thermal properties are determined and tabulated. The thermal properties are a complex function of burnup that affects the composition of gap gas, gap size, surface temperatures of the pellet and the clad, and contact pressure once the gap closes due to creep. It is desirable to use a constant gap size model in NEMO-K and LYNXT and, thus, an appropriate multi-dimensional table must be created that preserves the functional dependence described above, while not varying the gap size. [

]. These three parameters capture all the dependencies implied above.

In order to create the desired table, the applicant runs [

]. These calculations are repeated for various burnup levels, which finally result in a complete table of gap thermal properties that capture all the complex interactions in the desired format.

3.3.3. NEMO-K

NEMO-K [3] solves the three dimensional space-time kinetic multi-group neutron diffusion equations, and it is possible to run NEMO-K in both the static and time-dependent modes. Generally, core transients require that the calculations recognize simultaneous variations in neutron flux, fuel pin temperature, and core coolant conditions.

The neutron flux algorithm evaluates the requirements for specific cross-sections, based on fuel temperature, coolant temperature and density, etc., and determines the three dimensional neutron flux shape and associated power. The cross-section input is obtained from specially prepared tables created by CASMO-3G calculations. Output from this step includes the power generated in the fuel and the power directly deposited in the coolant.

The fuel pin model uses thermo-physical properties determined by COPERNIC to calculate the fuel pin temperature. Inputs to this model are the power shape within the pellet, the clad wall temperature, and the fuel model time step. Outputs from the model are the Doppler effective temperature, which is used in the neutron model to select the appropriate cross-section, and heat flux at the clad surface.

The coolant model conserves mass and energy to determine the coolant properties, including temperature and density. Input to the model are the heat flux at the clad surface, power directly deposited in the coolant, inlet coolant temperature and volumetric flow rate, the system pressure, and the thermal-hydraulic time step.

As approved in ANP-10263P-A [3], NEMO-K is suitable for both rapid REA transients and slow rod drop transients. In addition, with appropriate bounding parameters and assumptions, it can be used for safety related transient simulations.

3.3.3.1. Modifications to NEMO-K

In this section, the two most important modifications to the original NEMO-K code are outlined. They include a more realistic trip detection-control rod insertion, and fuel effective temperature determination models. In addition to these models, there are other changes considered minor by the staff. These concern the editing of fuel enthalpy changes and application of adjustment factors to selected parameters. These parameters include: Fuel and gap conductivity; cross-section changes due to temperature; and cross-section changes due to control rod position. These adjustment factors are included by the applicant to account for additional conservatism in the calculation.

3.3.3.1.1. Trip detection and control rod insertion model

The U.S. EPR uses an ex-core rate lagged power trip signal to sense if an REA has occurred, and to subsequently scram the core. This trip function has three components, including an ex-core detector signal, a rate lagging processor for the signal, and a control rod insertion model. NEMO-K has models that simulate the functions implied by these actions and/or processes. The ex-core detectors are located in each quadrant surrounding the pressure vessel, which causes the ex-core response to differ from the core average when an off center rod is ejected. In addition, they measure the rate of power change, and if this is outside of threshold values, a trip signal is sent. These signals are processed with a suitable rate lagging function that is compared to trip values. Once the trip signal is exceeded, a time delay is employed before the control rods are moved to scram the core. The activation of the signal requires two detectors out of four total detectors to respond. This is known as 2/4 logic.

The ex-core detectors measure the fast flux exiting the core, and are calibrated to the actual conditions within the core. The in-core assembly powers are multiplied by weighting factors to correlate in-core conditions to the ex-core signals. The weighting factors are determined by transport calculations. In addition, the overall ex-core response is calibrated against measured thermal power.

to be determined. A simple solution to this problem used by the applicant was to use a volume averaged temperature. The original model (the Rowland model) used in NEMO-K for determining a time dependent fuel temperature was a model that combined the fuel surface and centerline temperatures given below and found on page 6-6 of ANP-10286P [1]. The following equation is known as the Rowland model:

$$T_{\text{eff}} = T_s \cdot wt_{\text{sc}} + T_{\text{cl}} (1-wt_{\text{sc}})$$

Where:

- T_{eff} = Effective flat profile fuel temperature
- T_s = Fuel surface temperature
- T_{cl} = Fuel centerline temperature
- wt_{sc} = Weight factor for Rowland model

NEMO-K was modified to include an improved weighted effective flat fuel temperature that [

]. This relationship is given below:

$$[\quad]$$

Where:

- [
-]

The weight factor used in the Rowland formulation of T_{eff} (wt_{sc}) is obtained by assuming that the pellet temperature varies as function of radius squared, which is characteristic of fresh fuel. Based on this assumption the value of wt_{sc} is 0.7, which is used in all subsequent calculations regardless of burnup. The improved formulation of T_{eff} includes an average temperature term and a weighted temperature difference across the pellet. [

] Typically, the value of [], which is used in all subsequent calculations regardless of burnup.

In RAI-12 [7], the staff requested that the applicant provide additional validation of the improved methodology to determine the effective temperature. In an October 3, 2008, response to RAI-12 [7], the applicant validated the improved determination of T_{eff} by comparing calculated values, using the methods outlined above, to independent values determined using the APOLLO2 code [6]. The staff notes that the APOLLO2 code has not been validated or approved for U.S. EPR use. However, based on the staff's approval of APOLLO2 for use in the operating fleet and a review of the applicable limitations and parameters, the staff concluded that for the purposes of providing additional assurance regarding the validity of the Rowland model, the use of APOLLO2 is reasonable. The staff did not review or approve APOLLO2 for any other use for the U.S. EPR design.

The validation was carried out by comparing ^{238}U capture rate and reactivity for variable fuel temperatures within the pin to a constant temperature distribution within a pin. The value of the constant temperature that yielded the same ^{238}U capture rate and reactivity as the variable temperature case was considered T_{eff} as determined by the APOLLO2 code. This value of T_{eff} was then compared to values determined by the above two methods based on the variable temperature distribution used in the pin. A series of variable temperature distributions characteristic of steady state and transient conditions for a variety of burn-ups were used in the

validation exercise. It was found that for steady state fresh fuel conditions all three values of T_{eff} were in good agreement. However, under all other conditions investigated it was found that the new T_{eff} formulation agreed with APOLLO2 determinations of T_{eff} to within $\pm 2K$, while the Rowland formulation deviated from the APOLLO2 value by 23K – 65K for transient cases.

Application of the above study to the transient being investigated indicates that, for the case of fresh fuel, when the temperature distribution is expected to be parabolic, these two formulations give similar results, provided that the appropriate values are chosen for the respective weight factors. However, under transient conditions the original method underestimates the Doppler effect. This deviation increases for transients starting with low initial reactor power. Thus, the largest difference in Doppler effect is expected for transients initiated when the reactor is at hot zero power. Under these conditions, the control rods are at or close to their maximum insertion, and over approximately \$1.0 of reactivity could be inserted upon ejection of the rod.

3.3.4. LYNXT

LYNXT is an open channel thermal-hydraulic code that includes a fuel thermal model. The open channel aspects of the code allow both axial and cross-channel flow, thus recognizing flow around the fuel pins. This flow model allows for the determination of more accurate fuel pin surface temperatures, which are important in the current application to determine the MDNBR value for the fuel pin of interest and whether or not it meets the SAFDL limits.

The fuel thermal model allows for both axial and radial heat conduction. The following two fuel rod models are included as options in the code:

- 1) The Constant Gap/Constant Properties (CG/CP) model is the simplest option. As the name implies, the pellet/clad gap and the thermo-physical properties remain invariant, with the exception of the fuel conductivity that can be represented by a third order polynomial.
- 2) The Variable Gap/Temperature Dependent Properties (VG/TDP) model is the most realistic. In this case, all the thermo-physical properties and the pellet gap are permitted to vary with temperature. In the case of the pellet/gap variation, both the temperature and pressure difference between the coolant and the gap gas pressure are accounted for. The fuel rod model in this case is based on fuel performance codes such as COPERNIC.

In this analysis, the LYNXT code is used to determine:

- 1) The MDNBR value of the fuel rod being analyzed, and to determine if it meets the SAFDL limits
- 2) The fuel centerline temperature and margin to incipient fuel melting
- 3) The enthalpy added to the fuel during the transient, and to determine if it meets acceptable limits

3.3.4.1. Modifications to LYNXT

Modifications to LYNXT were minimal in nature, and did not involve changes to the fuel rod modeling. This model is based on a solution to the two dimensional conduction equation, with

radial and axial dependence. Briefly, in the approved version of the code the fuel rod model either uses the constant gap/constant properties (CG/CP), or variable gap/temperature dependent properties (VG/TDP) representation. The later model being the most elaborate since it allows for the gap between the pellet and clad to change during the transient.

ANP-10286P [1] did not contain sufficient information regarding the thermo-physical properties used in LYNXT, the use of the CG/TDP model, and its validation against the COPERNIC code. In RAI-14, RAI-15, RAI-16, RAI-17, RAI-24, RAI-27, and RAI-31 [7], the staff requested that the applicant provide additional information to improve understanding of LYNXT. In an October 3, 2008, response to RAI-14, RAI-15, RAI-16, RAI-24, RAI-27, and RAI-31 [7] the applicant provided justification for the use of the property tables for the fuel, clad, and gap. In addition, the CG/TDP model was justified and validated against comparisons with the COPERNIC code, which more accurately represents the test problem. The staff concludes that the responses provide adequate supporting documentation for the LYNXT modification. Portions of these responses are included in the discussion below.

There are two enhancements to the approved LYNXT code. First, the number of solution locations is increased. Second, the modified LYNXT code implements a combination of the CG/CP and VG/TDP models, resulting in a CG/TDP model. The increased number of solution locations allows for a more accurate representation of the radial power profile, including those that peak on the outside, which can occur at EOC. The CG/TDP model requires that the following parameters stay invariant during the transient:

- 1) Fuel pellet dimension
- 2) Pellet/clad gap
- 3) Gas inventory in gap
- 4) Radial power profile

However, it does allow the following properties to be entered in tabular form:

- 1) Thermal properties for fuel and clad as a function of temperature.
- 2) Specific heat for fuel and clad as a function of temperature.
- 3) Gap conductance []. The varying gap dimensions during the transient are accounted for by suitably varying the gap thermal properties in the tabular input.
- 4) Fuel enthalpy as a function of temperature.

The staff reviewed these model changes based on the information provided in ANP-10286P [1] and responses to RAI-14, RAI-15, RAI-16, RAI-17, RAI-24, RAI-27, and RAI-31 [7]. The staff concludes that the model changes more accurately represent, and remain bounding of, the thermal phenomena occurring during a rod ejection accident (particularly at EOC) and are, therefore, acceptable for use.

3.3.5. S-RELAP

S-RELAP5 uses a volume and junction model to solve the conservation of mass, momentum, and energy equations, similar to all other RELAP based codes. S-RELAP5 is used for both loss-of-coolant-accident (LOCA) and non-LOCA transients that involve changes to the thermal-hydraulic state points of the reactor. S-RELAP5 takes thermo-physical input from the steam tables for the coolant, and the properties determined by COPERNIC for the fuel. In addition, many of the reactor trip setpoints specific to the U.S. EPR system are included in the code. Thus, any condition that may change pressure, inlet temperature and/or flow rate during an REA can be modeled using this code.

It is traditional in the system level codes such as RELAP to use a point kinetics model to determine the transient reactor power. In this application (REA), the applicant disabled the point kinetics capability and instead used a power vs. time characteristic for transients that need a system level calculation. In these cases, the reactor power versus time response is either obtained directly from NEMO-K or considered to be conservatively defined higher than the NEMO-K results with time following the completion of the initial transient pulse of the event. In the former case where NEMO-K powers are used directly, iterations would be required between NEMO-K and S-RELAP5 until the power/thermal conditions are converged between NEMO-K and S-RELAP5. The staff considers the approximation in the latter case to be conservative with respect to power, since increasing fuel and coolant temperatures and decreasing system pressure would generally lead to a decrease in power.

3.3.6. Conclusions

The code suite used by the applicant for analyzing the rod ejection event for the U.S. EPR design includes codes previously approved for the applicant's operating fleet that were subsequently approved for use in the U.S. EPR design in ANP-10263P-A [3]. Based on the approval of ANP-10263P-A [3], the staff's review of the application of these codes to the analysis of the U.S. EPR rod ejection analysis, and the similarities to the operating fleet rod ejection analysis code suite, the staff concludes that the code suite detailed in ANP-10286P, "U.S. EPR Rod Ejection Accident Methodology Topical Report" [1], is applicable for analyzing the U.S. EPR response to an REA and conforms to the guidance provided in SRP Section 15.4.8.

Based on the evaluations provided in Section 3.3.3.1 of this report, the staff concludes that the changes presented in NEMO-K as compared with the previously approved version in ANP-10263P-A [3] more accurately represent the fuel temperature and provide an improved trip detection and control rod insertion model. Therefore, these modifications are approved for use in REA analyses for the U.S. EPR. The staff's review only applies to REA analyses for U.S. EPR and any other use of the modified version of NEMO-K presented in ANP-10286P [1] would require further NRC review and approval.

The staff also concludes that the changes presented in LYNXT as compared with the previously approved version in ANP-10263P-A [3] more accurately represent heat conduction by creating a constant gap / temperature dependent properties model and increasing the number of solution locations. Based on the evaluations provided in Section 3.3.4.1 of this report, these modifications are approved for use in REA analyses for the U.S. EPR. The staff's review only applies to REA analyses for U.S. EPR and any other use of this modified version of LYNXT would require further NRC review and approval.

The applicant verified the CG/TDP model by comparison with independently determined parameters (fuel temperatures, etc.) using higher fidelity codes and benchmark problem results in ANP-10286P [1]. These parameters include:

- 1) Analytic and fuel performance benchmark problems
- 2) Comparisons to COPERNIC, which used a form of a VG/TDP model

The code comparisons indicate that the CG/TDP model based on input gap conductance tables agrees with the benchmark solutions to []. Comparisons to the dynamic COPERNIC calculations, which used a more accurate form of a VG/TDP model, indicate that the CG/TDP model in LYNXT consistently over-predicts the fuel temperature. The over-prediction is highest during the peak of the transient pulse, and then reverts to an over-prediction of []. The duration of the pulse is very small and, thus, the overall over-prediction of the energy deposited is expected to be []. The applicant concluded from these comparisons that the LYNXT CG/TDP model combination conservatively predicts the fuel temperature and, thus, the gap conductance fitting tables used in this model are an acceptable method to predict the fuel melt and MDNBR conditions for REA event analysis. The staff reviewed the applicant's comparisons and concurs with the applicant's conclusion.

3.4. SELECTED TRANSIENT RESPONSE

In this section, applications of the code system outlined in Section 2 of this report to two different types of REA transients are described. Topical Report ANP-10286P [1] did not include enough detail for the staff to conclude if the spectrum of rod ejection events was accurately modeled. In RAI-26 [7], the staff requested that the applicant provide an event timeline and description of the various REA events. In an October 3, 2008, response to RAI-26 [7], the applicant responded with a detailed explanation of the various scenarios that were analyzed along with respective timelines. The staff concludes that the response adequately demonstrates the ability of the methodology to handle the spectrum of REA events. The staff also used select portions of this response for comparison in the independent confirmatory analyses [13]. The transients discussed follow two distinct trajectories in time; the first is initiated by a significant reactivity input and is terminated by an ex-core detector trip signal, while the second experiences a smaller reactivity input and is terminated by a system level scram. In the case of the U.S. EPR, these transients occur at EOC and BOC respectively, and are discussed in ANP-10286P [1], Chapter 8. Because of the buildup of transuranic elements at EOC, the value of the effective total delayed neutron fraction (β_{eff}) is lower than the value at BOC. This fact, together with the fact that the control rods are worth more at EOC, ensures that the added reactivity exceeds \$1.0 for transients up to 40 percent of full power. At BOC, the added reactivity is always below \$1.0, and consequently, the transient power is not expected to be as sudden and as peaked. At EOC, the moderator and Doppler feedback are both negative, while at BOC only, the Doppler feedback is negative and the moderator feedback is small but positive as listed in ANP-10286P [1], Table 7-1. Moderator feedback plays a secondary role in the initial part of the transient. Only if it continues beyond the initial power pulse, and the remainder of the system is involved, does the moderator effect become important. In the following two sections, the progression through these transient types is outlined. These sections should be read while consulting Figures 2 and 3 of this report.

The objective of an REA event analysis is to determine the number of failed fuel rods following the termination of the event. In order to assure that this number is as conservative as possible

while still remaining realistic, the input parameters and boundary conditions to the analysis are chosen to yield conservative results. These conservative limits are summarized in ANP-10286P [1], Table 7-3. ANP-10286P [1] did not contain sufficient information regarding the sensitivity of the number of fuel rods to the assumptions made in the analysis. In RAI-34 and RAI-35 [8], the staff requested that the applicant provide additional information related to these topics. In a March 26, 2009, response to RAI-34 and RAI-35 [8], the applicant provided the primary conservatisms in the REA methodology that result in the maximum defensible number of failed rods. These are listed below:

- 1) The deterministic choice of ejecting the highest worth control rod
- 2) Adding a 15 percent uncertainty to the ejected control rod
- 3) Adding uncertainties to the Doppler and moderator temperature coefficients, and β_{eff}
- 4) The reference cycle has an additional bias on the ejected rod worth, Doppler and moderator temperature coefficients, and β_{eff} that allow for possible variations introduced by further cycles
- 5) Peaking factor uncertainties of [] for the peak rod power ($F_{\Delta H}$) and [] for the peak local power (F_Q) are added

Based on the staff's review of these conservatisms, the staff concludes that the number of failed fuel rods determined by the applicant's methodology is a conservative upper limit.

3.4.1. Transient involving approximately \$1.0 of reactivity

The analysis is started by preparing the appropriate nuclear data library using CASMO-3G, and the thermo-physical property input data and pellet power profile using COPERNIC. These two data files and appropriate NEMO-K input, which involves initial conditions, spatial grid configuration, and transient termination conditions completes the input preparation. At this stage, the NEMO-K calculation can be carried out, which results in a reactor trip following approximately 1.0 sec., since an ex-core overpower trip signal is sent to the scram system at this time. An illustration of these power pulses is presented in Figure 26-2 of the October 3, 2008, response to RAI-26 [7] for several EOC starting points. It is seen that they are very sharp, and with peak values almost double the reactor full power. However, the Doppler effect is very efficient at reversing the power rise and the ex-core detectors are responsible for ensuring a reactor scram after approximately 1.0 sec. It takes approximately 3 sec. to fully insert the control rods and shut the reactor down. Output from NEMO-K in the form of transient core power, axial power profiles, and rod power profiles, which includes allowances to account for other possible reactor designs, forms the input to LYNXT. The LYNXT code also uses input from COPERNIC. At this stage, the fluid dynamic and heat transfer analysis can be carried out for the transient. The primary output from this analysis is the level of compliance with the relevant regulatory guidelines concerning maximum fuel temperature, maximum enthalpy rise in fuel, DNBR limits, and the number of rods failed. The minimum DNBR values, as a ratio of MDNBR to SAFDL, vary as a function of time during the transient. If the ratio dips below unity, rods are potentially failed.

3.4.2. Transient involving less than \$1.0 of reactivity

In RAI-26 [7], the staff requested that the applicant provide an event timeline and description for various REA events, including transients involving less than \$1.0 of reactivity. In an October 3, 2008, response to RAI-26 [7], the applicant provided examples of transients that do not reach a trip signal in the traditional manner for an REA occur at BOC and EOC HFP. In these cases, a system analysis is required, since the duration of the transient is longer than the coolant transit time around the primary circuit. In ANP-10286P [1], S-RELAP is used to carry out the system calculations, which take input from NEMO-K. The S-RELAP5 calculation continues the analysis into the regime where NEMO-K does not apply, since it does not recognize the remainder of the system. In addition, in these transient calculations the primary system has been compromised by a hole caused by the control rod ejection. The primary system boundary break is assumed to be 2.95 in. (7.5 cm) in diameter, and conforms to the control rod flange size. This added boundary condition will affect the system pressure, since there will be a slow leak out of the break. The simulation continues until a trip in the S-RELAP5 model is reached. Results for this type of transient are shown in Table 26-3 and 26-4 of the response to RAI-26 [7]. It is seen in the October 3, 2008, response to RAI-26 [7] that the pressure decreases, essentially monotonically, while the inlet temperature increases almost linearly. The transient would eventually trip, either because of low system pressure or high secondary steam pressure. In these cases, the transient is slow enough that the core is essentially in equilibrium with the thermal parameters. Thus, a quasi-static approach is appropriate for this analysis and the complication of coupled space-time analysis is not needed. Thus, using various thermal boundary conditions obtained from S-RELAP5, a series of static calculations are run using NEMO-K in its static mode to determine power shapes and magnitudes following a rod removal. The bounding conditions, for example maximum power, are evaluated using LYNXT to determine the response of the fuel rods. The staff reviewed the applicant's approach as presented in ANP-10286P [1] and supplemented by the October 3, 2008, response to RAI-26 [7] and agrees with the assumptions used. Additionally, the staff concludes that the methodology presented is acceptable for modeling transients involving less than \$1.0 of reactivity.

The above section outlines the reactor response to a typical rod ejection transient. Two transients are considered: the first one involves a rapid scram of the reactor due to ex-core detectors, and the second one has a longer duration and is terminated by a system level trip. ANP-10286P [1] did not contain sufficient information regarding the application of the LYNXT code in these analyses, and thus the staff requested additional information. In an October 3, 2008, response to RAI-30, RAI-31, and RAI-32 [7], the applicant provided justification as to why the pin power distribution is conservative, explained differences between the COPERNIC and LYNXT results, and explained the analysis of the application of LYNXT in the BOC hot zero power transient. The primary difference between LYNXT and COPERNIC regarding fuel temperature is the coarseness of the grid used to determine the thermo-physical properties in LYNXT. This leads to abrupt changes in the calculated temperature, which are not seen in the COPERNIC calculations. The staff concludes that these discussions adequately address the issues raised by the staff.

3.4.3. Determination of the number of failed rods

ANP-10286P [1] does not contain sufficient information regarding the calculation of the number of failed fuel rods following a REA transient. In RAI-28 [7], the staff requested that the applicant provide additional information to explain this calculation methodology. In an October 3, 2008, response to RAI-28 [7], the applicant provided an explanation of the methodology used in determining the number of failed rods regardless of the length of the transient event.

As discussed below, the staff concludes that the response satisfactorily provides the information requested in the RAI. Portions of the response to this RAI are included in the following evaluation discussion.

In the case of each transient, two different rod failures need to be considered in order to conform to the guidance provided in SRP Section 4.2, Appendix B regarding cladding failure and radiological impacts: (1) Rods that fail during the initial transient event, which is controlled by the energy deposition (cal/g) added during the transient; and (2) rods that fail to meet the MDNBR value defined by the SAFDL. Therefore, the MDNBR/SAFDL ratio must be determined and those rods below unity are considered failed. Fuel rod failure during the initial transient did not occur in the transients considered in ANP-10286P [1], since the failure criterion, or addition of 110 cal/g (197.4 BTU/lb), was never met. Thus, all rod failures for this reactor are due to the second mechanism described above. To quantify this mechanism, the values of $F_{\Delta H}$ and F_Q as determined by LYNXT with input from NEMO-K, corresponding to the conditions for a fuel rod when the MDNBR/SAFDL ratio is unity, are used as the failure criterion. Thus, any rod for which $F_{\Delta H}$ or F_Q exceed these values is considered failed. The most accurate manner of determining the number of failed pins would be to obtain a rod-by-rod power distribution vs. time from a three dimensional neutronics/thermal-hydraulic calculation to determine the MDNBR. However, this option is not realistic and the staff agrees that a practical approximate method that captures the salient phenomena is acceptable.

The applicant has determined that the [

The information presented by the applicant is contained in Figures 28-1 to 28-3 in the October 3, 2008, response to RAI-28 [7]. [

]. This fact is used to simplify the determination of fuel rod or assembly power at which the MDNBR calculation is carried out.

In order to determine if the MDNBR condition is reached for an arbitrary fuel rod, the following procedure is used: (1) Selected assemblies that have been analyzed using NEMO-K in full transient mode are analyzed using LYNXT to determine the power vs. time response at which DNB occurs; (2) this power vs. time response is determined by scaling the power profile until the DNB conditions are satisfied; (3) the scaling factor that corresponds to this power level is known as the "multiplier," and [

] the transient values can also be determined.

Representative samples of different fuel assembly responses are analyzed for which the full space-time kinetic and thermal hydraulic method was used. The fuel assemblies for which a full 3-D analysis has been carried out will be referred to as FA3-D. These assemblies are chosen in such a manner as to characterize the bulk of the core response to the transient. Two pieces of information are obtained from this analysis for each of the fuel assemblies: [

- 1)
- 2)
- 3)
- 4)

].

For those cases that are terminated by a system trip, and determined by analysis using S-RELAP5, the transient vs. static correlation is not necessary since the time dependence is relatively weak, and a quasi-static approach is sufficient. The coolant pressure and temperature change with time, but the power is essentially constant. In order to find the values of $F_{\Delta H}$ and F_Q at which the DNBR limits are exceeded, LYNXT calculations are repeated using input from S-RELAP5 and NEMO-K. Generally, the peak assembly power is scaled until it reaches the MDNBR design limits. The scaled values of $F_{\Delta H}$ and F_Q for this fuel rod then become the failure criterion for each fuel rod in the core. Any fuel rod that exceeds the $F_{\Delta H}$ and F_Q failure criteria is assumed to be failed.

The implication of conservatisms and contingencies that are assumed in the estimate of rod failures, which covers uncertainties and future fuel cycle designs, was made by removing them and re-evaluating the rod failure census. The primary sources of conservatism are:

- 1) The highest worth rod is chosen to be ejected. The worth is further increased by 15 percent to account for uncertainties.
- 2) Uncertainties are applied to the Doppler temperature coefficient, moderator temperature coefficient, beta-effective, and the peaking factors.
- 3) The reference cycle configured for the analysis has additional biases concerning the rod worth, Doppler temperature coefficient, moderator temperature coefficient, beta-effective, and the peaking factors.
- 4) The most extreme assemblies are chosen for the [

].

An analysis by the applicant, reported in ANP-10286P [1], used this methodology with the full complement of uncertainties for the BOC HFP case and predicted rod failures in both the dynamic and the quasi-static phases of the transient. ANP-10286P [1] did not contain sufficient information regarding the sensitivity of the number of failed rods to uncertainties that were included in the analysis. In RAI-34 and RAI-35 [8], the staff requested that the applicant provide additional information related to this sensitivity. In a March 26, 2009, response to RAI-34 and RAI-35 [8], the applicant removed the uncertainties included in the ANP-10286P [1] analysis and re-estimated the number of failed rods. This analysis was carried out for both the rapid transients, characterized by an ex-core detector scram, and the longer transients that rely on a system level scram. If the transient is re-analyzed with the uncertainties removed the results

shown in Table 1 of this report are obtained. The results shown in this table are based on ANP-10286P [1], Table 8-3, and the March 26, 2009, responses to RAI-34 and RAI-35 [8].

Table 1 – Percent of rods failed with and without uncertainties

	Dynamic phase	Quasi-static phase
With uncertainties	0.3	7.2
Without uncertainties	-	0.6

It is seen that there is a significant reduction in the percentage of rods failed by removing the uncertainties. The staff concludes from this result that the analysis presented in ANP-10286P [1] would cover a wide range of fuel cycle designs.

3.4.4. Conclusions

The staff reviewed the application of the code system outlined in Section 2 of this report for large and small REA transients, (i.e., transients that are terminated by either ex-core detectors or system trips, respectively). Based on the applicant's analysis of the events, RAI responses, and comparison to similar confirmatory analyses performed by the staff as detailed in Section 3.4 of this report, the staff concludes that the applicant's U.S. EPR REA methodology as presented in ANP-10286P [1] conforms to the appropriate guidelines in SRP Section 4.2, Appendix B, and the criteria listed in GDC 13 and GDC 28. The staff concludes that the methodology presented in ANP-10286P [1] can be used to analyze the REA event for the U.S. EPR design.

3.5. CONFIRMATORY ANALYSES

3.5.1. Introduction

Confirmatory calculations of reactivity insertion accidents and related phenomena were carried out as a guide in the understanding of the various physical phenomena involved in the transient, and as an independent check of the applicant's analysis techniques. Specifically, two confirmatory analyses were performed: (1) An independent confirmatory analysis by the staff of the most limiting case provided in Reference 1 using the TRITON/TRACE code package, and (2) a new analysis performed by the applicant of select SPERT [12] experimental rod ejection data. This SPERT data came from a reactor test conducted in 1965 [12], and provides a benchmark with which to validate analytical methods.

3.5.2. Independent Confirmatory Analyses

The TRITON/TRACE code package was used to assist in the review of the applicant's code package [10 and 13]. Specifically, confirmatory analyses were used to investigate the analysis results for the most limiting case and the NEMO-K model changes as presented in ANP-10286P [1]. The independent confirmatory analyses showed nearly identical energy deposition calculations for the most limiting case.

The staff modified the internal confirmatory runs to include the original and modified temperature models from NEMO-K to investigate the fuel temperature model changes

introduced into NEMO-K. In order to perform the confirmatory calculations, the staff requested detailed design information. In a July 10, 2008, response to RAI-1 and RAI-2 [9], the applicant provided this information. The staff developed models for each fuel type and generated cross-sections in which all the relevant physical variables were parameterized. The most limiting event proposed in ANP-10286P [1] was used in this confirmatory calculation to assist in the staff's review of the applicant's calculations. The results of the rod ejection simulations are shown in Figures 4, 5 and 6 of this report. The staff's TRACE model predicts a rod worth of \$1.33 which, compared to the applicant's prediction of \$1.35, further indicates that the models are consistent with one another. The maximum power predicted by TRACE of 240 percent compares well to the applicant's prediction of approximately 210 percent. Figure 6 of this report summarizes the fuel temperature calculation results using three different effective fuel temperature models referred to as the Rowland's, volume, and AREVA models. These models represent, respectively: (1) A linear combination of the fuel centerline and surface temperatures; (2) a simple volumetric average of the radial temperature profile in the fuel; and (3) a combination of both the linear and volumetric approach. As shown in the results, TRACE predicts very little impact of these different models on the predicted fission power, but a noticeable, yet relatively insignificant, effect on the fuel temperature can be seen. TRACE predicts a maximum fuel temperature of 850 Kelvin which is consistent with the applicant's prediction of 785 Kelvin. Most importantly, however, the TRACE-predicted enthalpy deposition is approximately 30 cal/g which is well below the acceptance criterion of 110 cal/g as specified by SRP Section 4.2, Appendix B. For completeness, the components of reactivity are shown in Figure 7 of this report.

The changes did not lead to any unexpected anomalies and the results compared well with the results reported in ANP-10286P [1].

No additional RAIs were generated as a result of the confirmatory analyses.

3.5.3. SPERT Analysis

In this section, results of an independent analysis of the applicant's REA transient by the NRC, and validating analyses of SPERT experimental data by both NRC and the applicant are presented. In order to provide additional validation of the applicant's rod ejection accident methodology, the applicant was asked to model test cases from the SPERT reactivity accident experiments [11]. The SPERT-III E-Core reactor is a small PWR designed to investigate power excursions. The maximum number of assemblies that can be loaded in the core is 68, which results in a high-leakage core design when compared with the U.S. EPR core with 241 assemblies. The applicant's REA code package was designed to analyze large PWR cores instead of small reactor cores, and it is expected by the staff for some differences to occur due to modeling limitations. Regardless, expected differences due to modeling limitations would be relatively small and the overall predicted reactor response would reasonably match experimental results.

As detailed in a March 26, 2009, response to RAI-36 [8], the applicant validated the COPERNIC-NEMO-LYNXT REA analysis methodology by analyzing two rod ejection transients carried out at the SPERT facility and documented in IDO-17036, "SPERT III Reactor Facility, E-Core Revision" [13]. Test 60 (H2P) and Test 86 (H2F) from IDO-17036 [12] were chosen as the two candidate experiments for comparison. The Test 60 power vs. time experimental results were compared to analytical results obtained using the methodology and code package outlined in ANP-10286P [1]. The calculated peak power is 439 MW and the measured peak power is reported as 410 ±41 MW. The calculated integrated power at the peak is 8.6 MW-sec.

and the measured integrated power is reported as 8.5 ± 1.1 MW-sec. The staff notes that these calculated values are within the measurement uncertainty of the test. This resolves the question raised by RAI-36 [8], and acts as a further validation of the methodology outlined in ANP-10286P [1].

The Test 86 power vs. time experimental results were compared to analytical results obtained using the methodology and code package outlined in ANP-10286P [1]. The calculated peak power response is in agreement with the measured response, yielding a calculated peak power of 604 MW compared to a measured value of 610 ± 60 MW. The calculated time integrated power, or the time integrated power above the initial power, at the peak is 13.7 MW-sec. and the measured is reported as 17 ± 2 MW-sec. The calculated result for the integrated power for this test is outside of the quoted measured uncertainty. A possible cause of the difference between the measured and calculated integrated power for Test 86 could be a higher uncertainty in the measured results attributed to the at power conditions than reported, or a lack of refinement in the model to represent the small SPERT III-E core configuration which is not typical of a PWR.

In the first comparison between NRC and the applicant's calculations of an REA the agreement is very good, particularly considering that completely different codes were used in the two analyses. In the second comparison both NRC and the applicant's analyses agreed well with the SPERT experimental data, essentially validating both methods for carrying out rod ejection accidents.

3.5.4. Conclusions

Three NRC confirmatory analyses of the U.S. EPR, using TRACE/PARCS, were performed to assist in the review of ANP-10286P [1]. The TRACE/PARCS models were consistent with the applicant's models while maintaining as much analytical independence as possible. The only calculation by the applicant used to develop the staff's models was the equilibrium BOC exposure. The staff's REA simulations served to independently support the staff's review of the applicant's predictions and guide the development of RAIs. The resulting agreement between the staff's independent confirmatory calculations and the applicant's U.S. EPR REA analysis adds further support to the staff's review that shows that the U.S. EPR REA methodology acceptably models the REA event and that the U.S. EPR reactor response should meet regulatory requirements as outlined in Section 2 of this report.

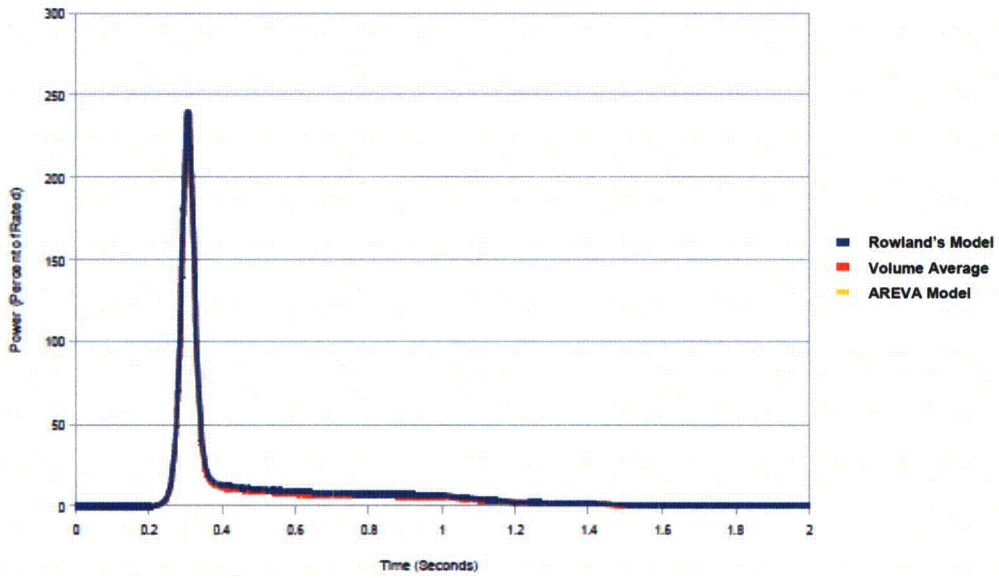


Figure 4 – Fission Power Following Rod Ejection

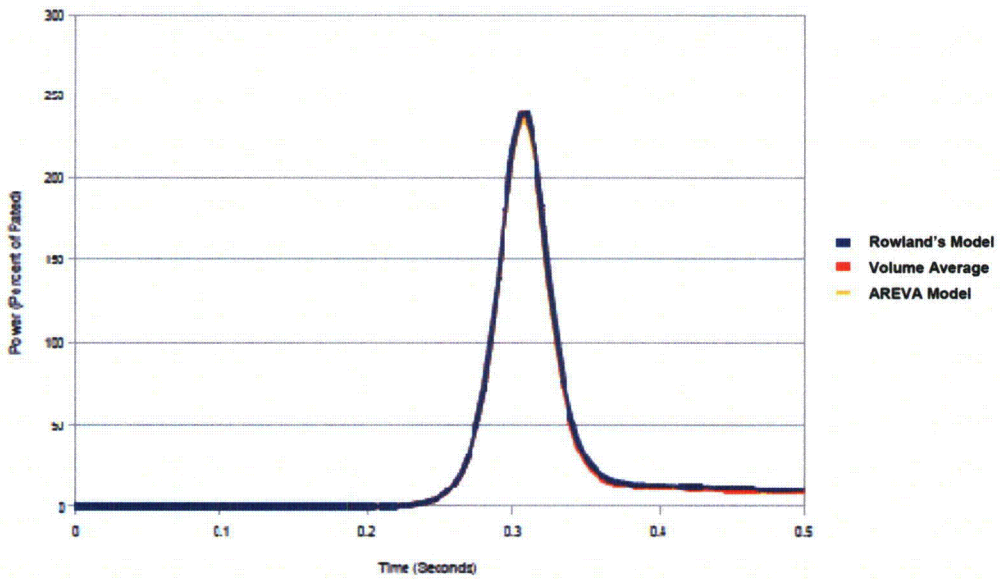


Figure 5 – Fission Power Following Rod Ejection (Zoom)

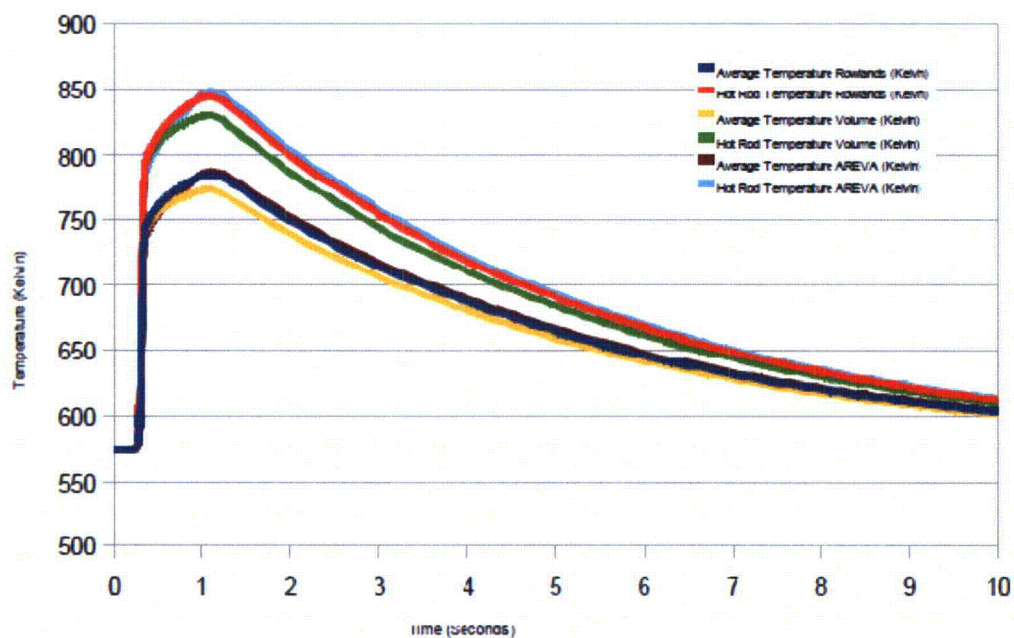


Figure 6 – Fuel Temperature Calculation for U.S. EPR Rod Ejection Comparing Different Effective Fuel Temperature Models

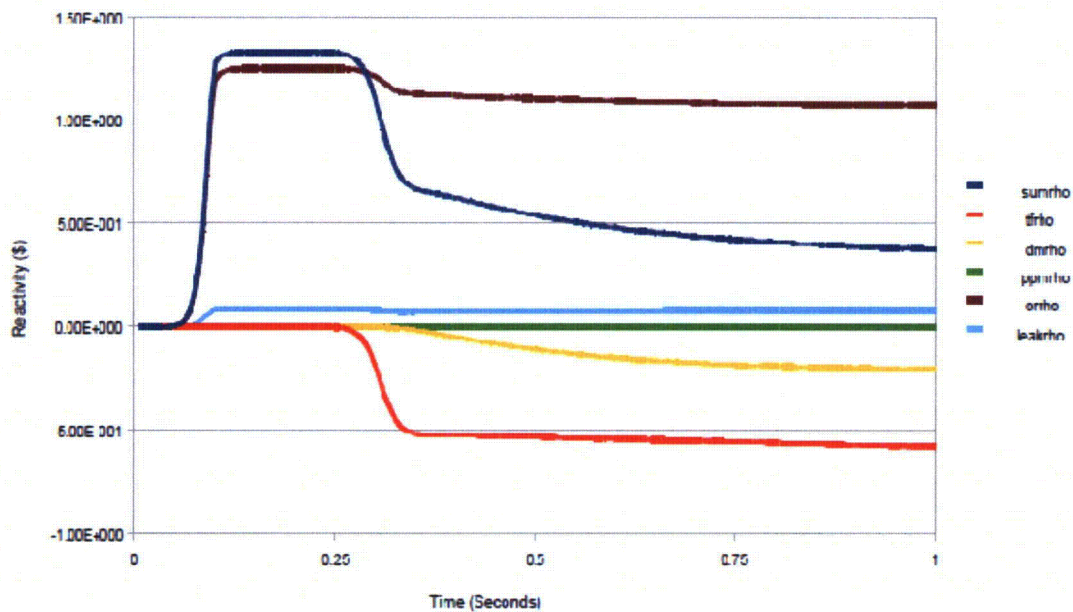


Figure 7 – Reactivity Balance Following Rod Ejection (Rowland's Effective Fuel Temperature Model)

4.0 CONCLUSIONS

The staff has reviewed the applicant's rod ejection analysis methodology documented in ANP-10286P [1]. From this review, the staff concludes from this review that this methodology is acceptable for performing rod ejection analyses for the U.S. EPR nuclear power plant design, and that results generated by the methodology presented in ANP-10286P [1] can accurately determine whether or not the regulatory requirements outlined in Section 2 of this report are satisfied. Using this methodology, the applicant has analyzed the U.S. EPR rod ejection accident based on inputs listed in ANP-10286P [1] and RAI responses [7, 8, and 9]. The staff concludes that the use of the methodology described in ANP-10286P [1], for the U.S. EPR design and within the boundaries and limitations set forth within ANP-10286P [1] and Section 5 of this report, will result in the satisfaction of GDC 13 and GDC 18, due to the resulting conformance with the guidance provided in SRP Sections 15.4.8 and 4.2, Appendix B.

Additionally, based on the present review, the staff reaches the following conclusions regarding the updates concerning the NEMO-K and LYNXT codes:

1. The revised effective temperature model and the trip detection and control rod activation model used in NEMO-K are approved for use in rod ejection accident (REA) analyses.
2. The modified constant gap/temperature dependent properties (CG/TDP) model used in LYNXT is approved for use in REA analyses.
3. The transient phase fuel rod failure census model, based on a linear relationship for the ratio of post-to-pre-ejection fuel rod power determined by transient calculations and static calculations, is acceptable for REA analyses.

5.0 RESTRICTIONS AND LIMITATIONS

Based on the review of TR ANP-10286P [1], the staff imposes the following restrictions and limitations:

5.1. LIMITATION NO. 1 – APPROVAL OF NEW CODE MODELS

The models of NEMO-K and LYNXT as submitted in ANP-10286P [1] are different than the code models previously approved in ANP-10263P-A [3]. The staff's review of the code modifications found in ANP-10286P [1] only pertains to their use in reactivity initiated accident analyses as described by ANP-10286P [1]. The approval of this topical report does not in any way imply an approval of these new models of NEMO-K and LYNXT for any other purpose.

5.2. LIMITATION NO. 2 - DESIGN APPLICABILITY

Per the methodology and analysis detailed in ANP-10286P [1], the staff's review and approval is limited to the U.S. EPR reactor design.

5.3. LIMITATION NO. 3 - FUEL DESIGN

The REA analysis presented in ANP-10286P [1] is based on the fuel and nuclear design of the U.S. EPR as presented in Revision 0 of the U.S. EPR Final Safety Analysis Report. This analysis is applicable to core designs bounded by the parameters listed in Table 9-1 of ANP-10286P [1]. Any core designs that are not bounded by ANP-10286P [1] will need to be addressed separately following the methodology presented in ANP-10286P [1].

6.0 REFERENCES

1. ANP-10286P, "U.S. EPR Rod Ejection Accident Methodology Topical Report," November 2007 (ML073310622).
2. NUREG-0800, Revision 3, "Standard Review Plan for the Review of Safety Analysis Reports for Nuclear Power Plants: LWR Edition, Section 15.4.8, Spectrum of Rod Ejection Accidents (PWR)," March 2007 (ML070550014).
3. ANP-10263P-A, "Codes and Methods Applicability Report for the U.S. EPR," August 2006, (ML062270395).
4. "SCALE 5.1," ORNL/TM-2005/39, Oak Ridge National Laboratory, November 2006.
5. "TRACE 5.0 Theory Manual: Field Equations, Solution Methods and Physical Models," U.S. NRC, (ML071000097).
6. BAW-10228PA, "Science," Framatome Cogema Fuels, December 2000 (ML010110422).
7. "Response to Second Request for Additional Information - ANP-10286P 'U.S. EPR Rod Ejection Accident Methodology Topical Report'," October 3, 2008 (ML082880502).
8. "Response to a Third Request for Additional Information Regarding ANP-10286P, 'U.S. EPR Rod Ejection Accident Methodology Topical Report'," March 26, 2009 (ML090890175).
9. "Response to Request for Additional Information Regarding ANP-10286P, 'U.S. EPR Rod Ejection Accident Methodology Topical Report'," July 10, 2008 (ML081970402).
10. Ulses, A. P, "TRACE Calculations of U.S. EPR using a 3-D Kinetics Model," January 29, 2009 (ML090300045).
11. McCardell, R. K., et al., "Reactivity Accident Test Results and Analyses for the SPERT III E-Core – A Small, Oxide-Fueled, Pressurized-Water Reactor," March 1969 (ML080320431).
12. Dugone J., "SPERT III Reactor Facility, E-Core Revision," IDO-17036, U.S. Atomic Energy Commission, November 1965.
13. Ulses, A.P. "Final Results of US EPR RIA and Setpoint Confirmatory Calculations," May 27, 2009 (ML091420248)

7.0 ACRONYMS

BOC	beginning of cycle
CFR	<i>Code of Federal Regulations</i>
CG	constant gap
CP	constant properties
DNBR	departure from nucleate boiling ratio
ENDF	Evaluated Nuclear Data Base File
EOC	end of cycle
FSAR	Final Safety Analysis Report
GDC	General Design Criterion
HFP	hot full power
HZP	hot zero power
LOCA	loss-of-coolant-accident
MDNBR	minimum departure from nucleate boiling ratio
NRC	Nuclear Regulatory Commission
PCMI	pellet clad mechanical interaction
PWR	pressurized water reactor
RAI	request for additional information
REA	rod ejection accident
SER	Safety Evaluation Report
SAFDL	specified acceptable fuel design limit
sec.	seconds
SPERT	special power excursion reactor test
SRP	Standard Review Plan
TDP	temperature dependent properties
TFGR	transient fission gas release
TR	Topical Report
VG	variable gap

Attachment
The Staffs Disposition of AREVA's comments on the Draft SE

COMMENT 1

AREVA commented in Section 1.0 that 31.2 cal/gm is the value above which increase fission gas release must be considered, not the failure point.

DISPOSITION

The value was corrected to 110 cal/g.

COMMENT 2

AREVA noted in item 3 of Section 1.1 that LYNXT was not used for the SPERT comparison.

DISPOSITION

Staff corrected text to delete reference to LYNXT.

COMMENT 3

AREVA noted in bullet 2 of Section 2.2 that the requirements are that the pressure boundary integrity, the reactor internals integrity, and the fuel assembly integrity need to be evaluated if the fuel rod bursts, not the reverse. The evaluation of this is eliminated in the method by not allowing the fuel rod to burst.

DISPOSITION

NRC staff note that this section only deals with the description of the relevant NRC guidance regarding coolability and does not make any judgement on the whether or not the topical report meets the guidance or requirements. No changes were made to the text.

COMMENT 4

AREVA noted in bullet 3 of Section 2.2 that the step was performed regardless of the failure mechanism.

DISPOSITION

This section was re-written to focus on describing the relevant NRC guidance.

COMMENT 5

AREVA noted on page 5 that the methodology accounts for increase fission gas release whether the failure is due to DNB or PCMI as long as the failure occurs above 31.2 cal/gm.

DISPOSITION

NRC staff updated the text in the last paragraph of page 5 for clarity and accuracy.

COMMENT 6

AREVA noted on page 6 that there is no Section 1.4 in the topical report, and inquired which Section was referred to in the text of the SER.

DISPOSITION

NRC staff updated the reference to point to Section 3.2 of the SER.

COMMENT 7

AREVA noted on bullet 2 of Section 3.2 that the input to S-RELAP5 is either form NEMO-K of a conservative value relative to the NEMO-K value, and that the sample problem characteristics are an example instead of a method.

DISPOSITION

NRC staff deleted text referring to the input power variation used for S-RELAP5.

COMMENT 8

AREVA noted on Figure 2 that the box with "Ex-core detecto" is missing some text.

DISPOSITION

NRC staff corrected the figure.

COMMENT 9

AREVA noted on Figure 3 that S-REALP should be S-RELAP5 in boxes and that the words "No scram" in the NEMO-K box were incorrect.

DISPOSITION

NRC staff corrected the figure.

COMMENT 10

AREVA noted in Section 3.3.2 that the COPERNIC calculation was not described correctly.

DISPOSITION

NRC staff removed the incorrect statement.

COMMENT 11

AREVA noted in Section 3.3.5 that the COPERNIC the SER language suggested that only a conservative flat response with time is allowed to be used, and that this statement could be interpreted that NEMO-K powers cannot be used in SRELAP5.

DISPOSITION

NRC staff updated the text in the final paragraph of Section 3.3.5 to address the above concern.

COMMENT 12

AREVA noted in Section 3.3.6 that the two statements regarding the staff's review were very broad and outside the context of this topical report.

DISPOSITION

NRC staff note that this statement is also captured in the conclusions contained in Section 4.0. No changes were made to the text.

COMMENT 13

AREVA noted in Section 3.3.6 that COPERNIC does not have "the VG/TDP" model but has a similar model.

DISPOSITION

NRC staff corrected the text to state that a form of a VG/TDP model was used.

COMMENT 14

AREVA noted in Section 3.4.1 that the statement "It takes approximately 1.5 seconds . . ." should be consistent with Figure 6-1.

DISPOSITION

NRC staff corrected the text to 3 seconds.

COMMENT 15

AREVA noted in the fourth paragraph of Section 3.4.3 that in this context the term DNB is more appropriate than DNBR.

DISPOSITION

NRC staff corrected the text to use DNB instead of DNBR.

COMMENT 16

AREVA noted that Figures 4 through 7 were difficult to read, and better figures may be desirable.

DISPOSITION

NRC staff were unable to obtain better figures for use in the SER. No changes were made to the SER.

COMMENT 17

AREVA noted in Section 4.0 that while AREVA would prefer that these changes be approved for all reactivity insertion accidents it is clear that the NRC wants to be more restrictive in its approval, and that the language in the numbered list was not consistent with Section 5.0 of the SER.

DISPOSITION

NRC staff changed the text to be consistent with Section 5.0 of the SER.

COMMENT 18

AREVA noted in Section 5.0 that the topical report requested approval of a set of models, not a set of coding.

DISPOSITION

NRC staff changed the text of Limitation No. 1 to reference models instead of codes.



November 20, 2007
NRC:07:065

Document Control Desk
U.S. Nuclear Regulatory Commission
Washington, D.C. 20555-0001

Request for Review and Approval of ANP-10286P, "U.S. EPR Rod Ejection Accident Methodology Topical Report"

Ref. 1: Letter, Ronnie L. Gardner (AREVA NP Inc.) to Document Control Desk (NRC),
"Proposed Plan for the Pre-Application Review of the U.S. EPR," NRC:07:007,
February 14, 2007.

AREVA NP Inc. (AREVA NP) requests the NRC's review and approval of the enclosure, ANP-10286P, "U.S. EPR Rod Ejection Methodology Topical Report." This report was identified as a pre-application submittal for the U.S. EPR in Attachment 1 of Reference 1. In Reference 1, this report was referred to as the "U.S. EPR Reactivity Insertion Accident Methodology Topical Report."

AREVA NP requests that the NRC issue a Safety Evaluation Report (SER) that approves this topical report which will be used to support AREVA NP's U.S. EPR design. AREVA NP plans to reference this topical report in its Design Certification application for the U.S. EPR. AREVA NP requests that the NRC complete its review of the enclosed report and issue the SER by November of 2008.

Proprietary and non-proprietary versions of the topical report are enclosed on CDs.

AREVA NP considers some of the material contained in the enclosed document to be proprietary. As required by 10 CFR 2.390(b), an affidavit is enclosed to support the withholding of the information from public disclosure.

If you have any questions related to this submittal, please contact Ms. Sandra M. Sloan, Regulatory Affairs Manager for New Plants Deployment. She may be reached by telephone at 434-832-2369 or by e-mail at sandra.sloan@areva.com.

Sincerely,

A handwritten signature in cursive script that reads "Ronnie L. Gardner".

Ronnie L. Gardner, Manager
Site Operations and Corporate Regulatory Affairs
AREVA NP Inc.

AREVA NP INC.

An AREVA and Siemens company

Document Control Desk
November 20, 2007

NRC:07:065
Page 2

Enclosures

cc: L. J. Burkhart
G. Tesfaye
Project 733

requested qualifies under 10 CFR 2.390(a)(4) "Trade secrets and commercial or financial information."

6. The following criteria are customarily applied by AREVA NP to determine whether information should be classified as proprietary:

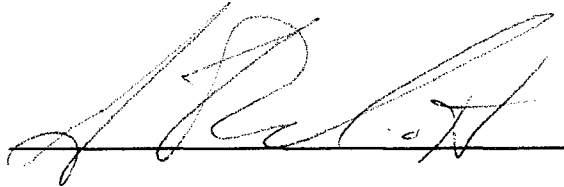
- (a) The information reveals details of AREVA NP's research and development plans and programs or their results.
- (b) Use of the information by a competitor would permit the competitor to significantly reduce its expenditures, in time or resources, to design, produce, or market a similar product or service.
- (c) The information includes test data or analytical techniques concerning a process, methodology, or component, the application of which results in a competitive advantage for AREVA NP.
- (d) The information reveals certain distinguishing aspects of a process, methodology, or component, the exclusive use of which provides a competitive advantage for AREVA NP in product optimization or marketability.
- (e) The information is vital to a competitive advantage held by AREVA NP, would be helpful to competitors to AREVA NP, and would likely cause substantial harm to the competitive position of AREVA NP.

The information in the Document is considered proprietary for the reasons set forth in paragraphs 6(b) and 6(c) above.

7. In accordance with AREVA NP's policies governing the protection and control of information, proprietary information contained in this Document have been made available, on a limited basis, to others outside AREVA NP only as required and under suitable agreement providing for nondisclosure and limited use of the information.

8. AREVA NP policy requires that proprietary information be kept in a secured file or area and distributed on a need-to-know basis.

9. The foregoing statements are true and correct to the best of my knowledge, information, and belief.



SUBSCRIBED before me this 19th
day of November, 2007.



Sherry L. McFaden
NOTARY PUBLIC, COMMONWEALTH OF VIRGINIA
MY COMMISSION EXPIRES: 10/31/10
Reg. # 7079129





UNITED STATES
NUCLEAR REGULATORY COMMISSION
WASHINGTON, D.C. 20555-0001

March 14, 2008

Mr. Ronnie L. Gardner, Manager
Site Operations and Corporate Regulatory Affairs
AREVA NP Inc.
3315 Old Forest Road
P.O. Box 10935
Lynchburg, VA 24506-0935

SUBJECT: AREVA NP INC. - ACCEPTANCE FOR REVIEW OF ANP-10286, "US EPR ROD EJECTION ACCIDENT METHODOLOGY TOPICAL REPORT"

Dear Mr. Gardner:

By letter dated November 20, 2007, AREVA NP Inc. (AREVA) submitted for U.S. Nuclear Regulatory Commission (NRC) staff review ANP-10286, "US EPR Rod Ejection Accident methodology Topical Report," Revision 0. The NRC staff has performed an acceptance review of the subject topical report and has found that the material presented is sufficient to begin our comprehensive review. The NRC staff expects to issue any requests for additional information (RAI) by December 31, 2008, and issue its draft safety evaluation by May 31, 2009. The staff also estimates that the review will require approximately 750 staff hours including project management efforts, and 1000 contractor hours.

The review schedule milestones and estimated review costs were discussed and agreed upon in a telephone conference between your staff and the NRC staff on February 19, 2008 and March 11, 2008. The schedule and cost estimates are based on a timely resolution of one round of RAI. Should there be a need for more RAIs beyond the December 31, 2008 date, the estimates will be adjusted accordingly.

Per AREVA's request, post-submittal meetings and or telephone conferences will be scheduled at a mutually agreed upon time, most likely prior to issuing RAIs.

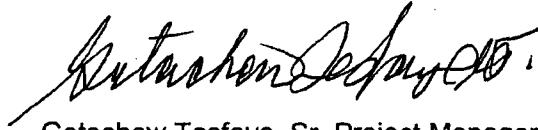
Section 170.21 of Title 10 of the *Code of Federal Regulations* requires that topical reports are subject to fees based on the full cost of the review. You did not request a fee exemption; therefore, NRC staff hours will be billed accordingly.

R. Gardner

- 2 -

If you have any questions regarding this matter, please contact me at 301-415-3361 or via email at gxt2@nrc.gov.

Sincerely,

A handwritten signature in black ink, appearing to read "Getachew Tesfaye". The signature is fluid and cursive, with a long horizontal stroke extending to the left.

Getachew Tesfaye, Sr. Project Manager
EPR Projects Branch
Division of New Reactor Licensing
Office of New Reactors

Docket No. 50-020

cc: See next page

DC AREVA - EPR Mailing List

cc:

Mr. Glenn H. Archinoff
AECL Technologies
481 North Frederick Avenue
Suite 405
Gaithersburg, MD 20877

Marty Bowling
NUMARK Project Manager
86 WestBay Drive
Kilmarnock, VA 22482

Ms. Michele Boyd
Legislative Director
Energy Program
Public Citizens Critical Mass Energy
and Environmental Program
215 Pennsylvania Avenue, SE
Washington, DC 20003

W. Craig Conklin, Director
Chemical and Nuclear Preparedness &
Protection Division (CNPPD)
Office of Infrastructure Protection
Department of Homeland Security
Washington, DC 20528

Mr. Marvin Fertel
Senior Vice President
and Chief Nuclear Officer
Nuclear Energy Institute
1776 I Street, NW
Suite 400
Washington, DC 20006-3708

Mr. Ray Ganthner
Senior Vice President
AREVA, NP, Inc. 3315
Old Forest Road
P.O. Box 10935
Lynchburg, VA 24506-0935

Mr. Paul Gaukler
Pillsbury, Winthrop, Shaw, Pittman
2300 N Street, NW
Washington, DC 20037

Dr. Charles L. King
Licensing Manager, IRIS Project
Westinghouse Electric Company
Science and Technology Department
20 International Drive
Windsor, CT 06095

Ms. Sherry McFaden
Framatome NP, Inc.
3315 Old Forest Road, OF-16
Lynchburg, VA 24501

Vanessa E. Quinn, Acting Director
Technological Hazards Division
National Preparedness Directorate
Federal Emergency Management Agency
500 C Street, NW
Washington, DC 20472

Mr. Steve Seitz
AREVA
100 Dean Road
East Lyme, CT 06333

Mr. Robert E. Sweeney
IBEX ESI
4641 Montgomery Avenue
Suite 350
Bethesda, MD 20814

Russ Wells
Advisory Engineer, New Plants Deployment
AREVA NP, Inc.
3315 Old Forest Road, P.O. Box 10935
Mail Stop Of-34
Lynchburg, VA 24506-0935
Mr. Gary Wright, Director
Division of Nuclear Facility Safety
Illinois Emergency Management Agency
1035 Outer Park Drive
Springfield, IL 62704

Email

alex.miller@hse.gsi.gov.uk (Alex Miller)
APH@NEI.org (Adrian Heymer)
awc@nei.org (Anne W. Cottingham)
bennettS2@bv.com (Steve A. Bennett)
bob.brown@ge.com (Robert E. Brown)
BrinkmCB@westinghouse.com (Charles Brinkman)
carey.fleming@constellation.com (Carey Fleming)
chris.maslak@ge.com (Chris Maslak)
cwaltman@roe.com (C. Waltman)
david.hinds@ge.com (David Hinds)
david.lewis@pillsburylaw.com (David Lewis)
dlochbaum@UCSUSA.org (David Lochbaum)
erg-xl@cox.net (Eddie R. Grant)
frankq@hursttech.com (Frank Quinn)
gcesare@enercon.com (Guy Cesare)
greshaja@westinghouse.com (James Gresham)
james.beard@gene.ge.com (James Beard)
jason.parker@pillsburylaw.com (Jason B. Parker)
jcurtiss@winston.com (Jim Curtiss)
jgutierrez@morganlewis.com (Jay M. Gutierrez)
jim.riccio@wdc.greenpeace.org (James Riccio)
JJD1@nrc.gov (John Donohue)
JJNesrsta@cpsenergy.com (James J. Nesrsta)
John.O'Neill@pillsburylaw.com (John O'Neill)
Joseph_Hegner@dom.com (Joseph Hegner)
junichi_uchiyama@mnes-us.com (Junichi Uchiyama)
KSutton@morganlewis.com (Kathryn M. Sutton)
kwaugh@impact-net.org (Kenneth O. Waugh)
maria.webb@pillsburylaw.com (Maria Webb)
mark.beaumont@wsms.com (Mark Beaumont)
matias.travieso-diaz@pillsburylaw.com (Matias Travieso-Diaz)
media@nei.org (Scott Peterson)
mike_moran@fpl.com (Mike Moran)
mwetterhahn@winston.com (M. Wetterhahn)
nirsnet@nirs.org (Michael Mariotte)
patriciaL.campbell@ge.com (Patricia L. Campbell)
paul.gaukler@pillsburylaw.com (Paul Gaukler)
Paul@beyondnuclear.org (Paul Gunter)
pshastings@duke-energy.com (Peter Hastings)
RJB@NEI.org (Russell Bell)
RKTemple@cpsenergy.com (R.K. Temple)
roberta.swain@ge.com (Roberta Swain)
rod.krich@unistarnuclear.com (Mr. Rod Krich)
Ronda.pederson@areva.com (Ronda Pederson)
Russell.Wells@Areva.com (Russ Wells)
sandra.sloan@areva.com (Sandra Sloan)
sfrantz@morganlewis.com (Stephen P. Frantz)

steven.hucik@ge.com (Steven Hucik)
tjh2@nrc.gov (Thomas Herrity)
tkkibler@scana.com (Tria Kibler)
tom.miller@hq.doe.gov (Tom Miller)
trsmith@winston.com (Tyson Smith)
VictorB@bv.com (Bill Victor)
vijukrp@westinghouse.com (Ronald P. Vijuk)
Wanda.K.Marshall@dom.com (Wanda K. Marshall)
waraksre@westinghouse.com (Rosemarie E. Waraks)
wayne.marquino@ge.com (Wayne Marquino)
whorin@winston.com (W. Horin)



UNITED STATES
NUCLEAR REGULATORY COMMISSION
WASHINGTON, D.C. 20555-0001

May 15, 2008

Mr. Ronnie L. Gardner
AREVA NP Inc.
3315 Old Forest Road
P.O. Box 10935
Lynchburg, VA 24506-0935

SUBJECT: REQUEST FOR ADDITIONAL INFORMATION REGARDING ANP-10286, "US EPR ROD EJECTION ACCIDENT METHODOLOGY TOPICAL REPORT"

Dear Mr. Gardner:

By letter dated November 20, 2007, which can be accessed through NRC'S Agencywide Document Access and Management (ADAMS) Accession No. ML073310620, AREVA NP submitted for U.S. Nuclear Regulatory Commission (NRC) staff review Topical Report ANP-10286, "Rod Ejection Accident Methodology." The staff is reviewing the topical report and has determined that additional information is required. Our questions are provided in the enclosure.

A draft of the request for additional information (RAI) was provided to you on May 5, 2008 (ADAMS Accession No. ML081140030), and discussed with your staff in a post submittal telephone conference on May 8, 2008. As a result of that discussion the staff agreed to modify Draft RAIs 1d and 2b.

In addition, AREVA NP requested and the staff agreed that AREVA NP will provide responses to the RAIs within 60 days of the date of the letter.

If you have any questions regarding this matter, I may be reached at 301-415-3361.

Sincerely,

A handwritten signature in cursive script, reading "Getachew Tesfaye, Sr.".

Getachew Tesfaye, Sr., Project Manager
EPR Projects Branch
Division of New Reactor Licensing
Office of New Reactors

Docket No. 52-020

Enclosure: Request for Additional Information

cc: DC AREVA – EPR Mailing List

REQUEST FOR ADDITIONAL INFORMATION (RAI)

ANP-10285P, "U. S. EPR RO EJECTION ACCIDENT

METHODOLOGY TOPICAL REPORT"

DOCKET NO. 52-020

RAI-1. Please provide the following data that was used in the development of the cross sections in the Rod Ejection Accident (RIA) analyses:

- a. axial and radial enrichments,
- b. poison loading,
- c. pellet densities,
- d. composition and dimensions of cladding materials, control rods, guide tubes, etc.

RAI-2. Please provide the following modeling data that was used in the RIA analyses:

- a. core loading map,
- b. associated 3-d nodal exposure.

Enclosure



July 10, 2008
NRC:08:044

Document Control Desk
U.S. Nuclear Regulatory Commission
Washington, D.C. 20555-0001

Response to Request for Additional Information Regarding ANP-10286P, "U.S. EPR Rod Ejection Accident Methodology Topical Report"

- Ref. 1: Letter, Ronnie L. Gardner (AREVA NP Inc.) to Document Control Desk (NRC), "Request for Review and Approval of ANP-10286P, 'U.S. EPR Rod Ejection Accident Methodology Topical Report'," NRC:07:065, November 20, 2007.
- Ref. 2: Letter, Getachew Tesfaye (NRC) to Ronnie L. Gardner (AREVA NP Inc.), "Request for Additional Information Regarding ANP-10286, 'U.S. EPR Rod Ejection Accident Methodology Topical Report'," May 16, 2008.
- Ref. 3: Letter, Getachew Tesfaye (NRC) to Ronnie L. Gardner (AREVA NP Inc.), "AREVA NP INC. – Acceptance for Review of ANP-10286, 'U.S. EPR Rod Ejection Accident Methodology Topical Report'," March 14, 2008.

AREVA NP Inc. (AREVA NP) requested the NRC's review and approval of topical report ANP-10286P, "U.S. EPR Rod Ejection Accident Methodology Topical Report" in Reference 1. The NRC provided a request for additional information (RAI) regarding this topical report in Reference 2. The response to that RAI is enclosed with this letter, ANP-10286PQ1, "Response to Request for Additional Information—ANP-10286P."

The responses to the two RAI questions posed in Reference 2 (including the associated data files) are provided on the enclosed compact disk (CD) and do not contain any information that AREVA NP considers to be proprietary.

AREVA NP references topical report ANP-10286P in the Final Safety Analysis Report for the U.S. EPR. Reference 3 states that the NRC plans to complete its review of the topical report and issue the draft safety evaluation by May 31, 2009. AREVA NP understands that this timely response to the RAI supports the scheduled deliverable of the draft safety evaluation.

If you have any questions related to this submittal, please contact Ms. Sandra M. Sloan, Regulatory Affairs Manager for New Plants Deployment. She may be reached by telephone at 434-832-2369 or by e-mail at sandra.sloan@areva.com.

Sincerely,

A handwritten signature in cursive script that reads "Ronnie L. Gardner".

Ronnie L. Gardner, Manager
Corporate Regulatory Affairs
AREVA NP Inc.

AREVA NP INC.

An AREVA and Siemens company

Document Control Desk
July 10, 2008

NRC:08:044
Page 2

Enclosure

cc: J. Rycyna
G. Tesfaye
Docket No. 52-020

**Response to Request for Additional Information Regarding ANP-10286P,
“U.S. EPR Rod Ejection Accident Methodology Topical Report”**

- RAI-1.** *Please provide the following data that was used in the development of the cross sections in the Rod Ejection Accident (RIA) analyses:*
- a. axial and radial enrichments,*
 - b. poison loading,*
 - c. pellet densities,*
 - d. composition and dimensions of cladding materials, control rods, guide tubes, etc.*

Response to RAI-1:

The following information is used in the development of the cross sections in the analysis of the rod ejection accident (REA). The fuel assembly data are representative of Cycle 1 and the equilibrium cycle of an 18-month core design. Table 1-1 presents the data relevant to the fuel rod, and Table 1-2 presents general fuel assembly data. Table 1-3 presents control rod data.

The fuel assembly layouts, including radial and axial U^{235} enrichment values and Gd enrichment, for the fuel types in Cycle 1 are shown in Figure 1-1 through Figure 1-7. The same information for the fuel assemblies in the equilibrium cycle are shown in Figure 1-8 through Figure 1-17. These figures are for Cycle 1 and the equilibrium cycle, respectively.

Table 1-1—Fuel Rod Data

Parameter	Value
Fuel pellet diameter	0.3225 in
Clad inner diameter	0.3291 in
Clad outer diameter	0.3740 in
Fuel pellet % theoretical density ^a	96%
Pellet end void F-factor ^b	0.990
Clad material	M5™
M5™ Clad material density	6.5 g/cm ³
M5™ Clad material composition ^c Zircaloy	100%

^a Stack density can be calculated using the following equations:

for UO₂ fuel: $d = TD * (1-f_{void}) * f_{TD}$,

for UO₂-Gd₂O₃ fuel: $d = [TD - (2.65*P)/(P+0.67145*(1-P))] * (1-f_{void}) * f_{TD}$

where TD = theoretical density of UO₂ (10.96 g/cm³)

f_{void} = effective pellet void volume fraction

f_{TD} = fraction of theoretical density

P = weight fraction of Gd₂O₃ in the UO₂-Gd₂O₃ fuel mixture

^b Equivalent to (1- f_{void}) from equation in note (a) - includes dish void fraction and the outward land taper void fraction

^c M5™ is a proprietary variant of Zr1NB. 100% Zr is a reasonable approximation to M5™

Table 1-2—General Fuel Assembly Data

Parameter	Value
Lattice Dimension	17x17
Assembly pitch	8.4661 in
Fuel rod pitch	0.496 in
Active fuel length	165.354 in
Guide tube inner diameter ^a	0.4508 in
Guide tube outer diameter ^a	0.4902 in
Guide tube material ^a	M5™ ^b
Number of spacer grids in active fuel region	8
Grid material	M5™ ^b
Mass per grid	2.822 lb _m
Grid height	1.75 in

^a Instrument tubes have same dimensions and material as guide tubes

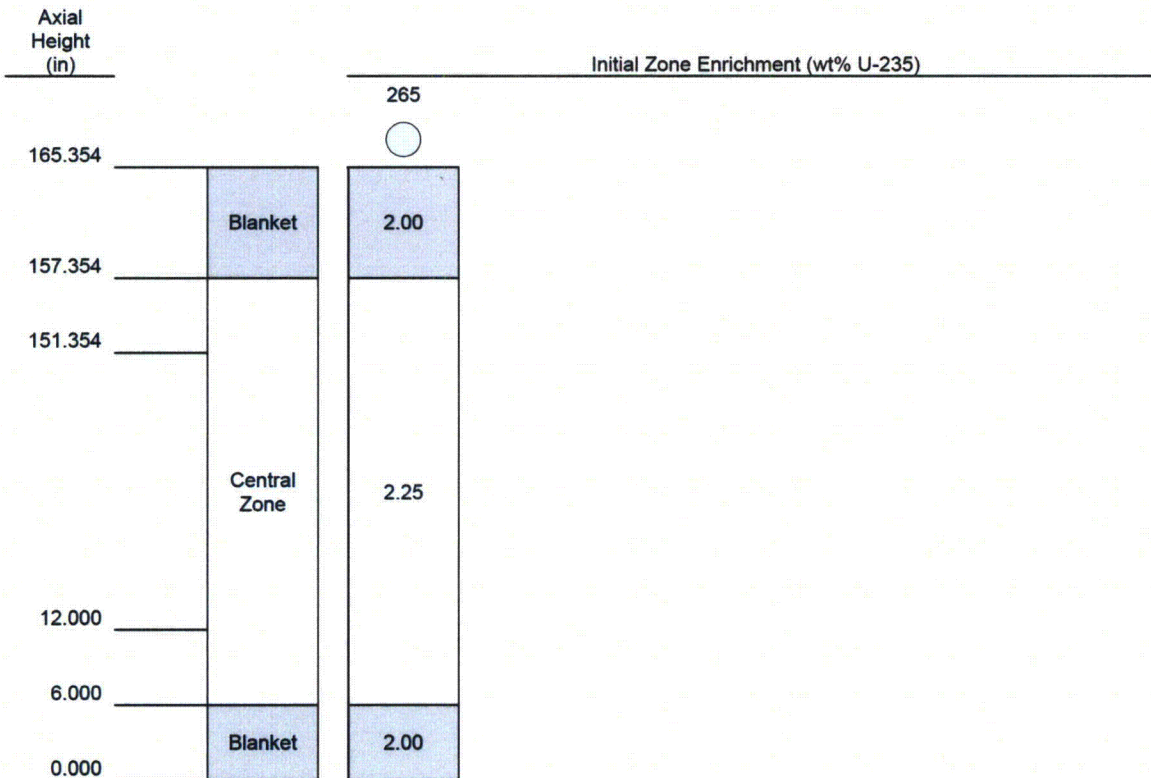
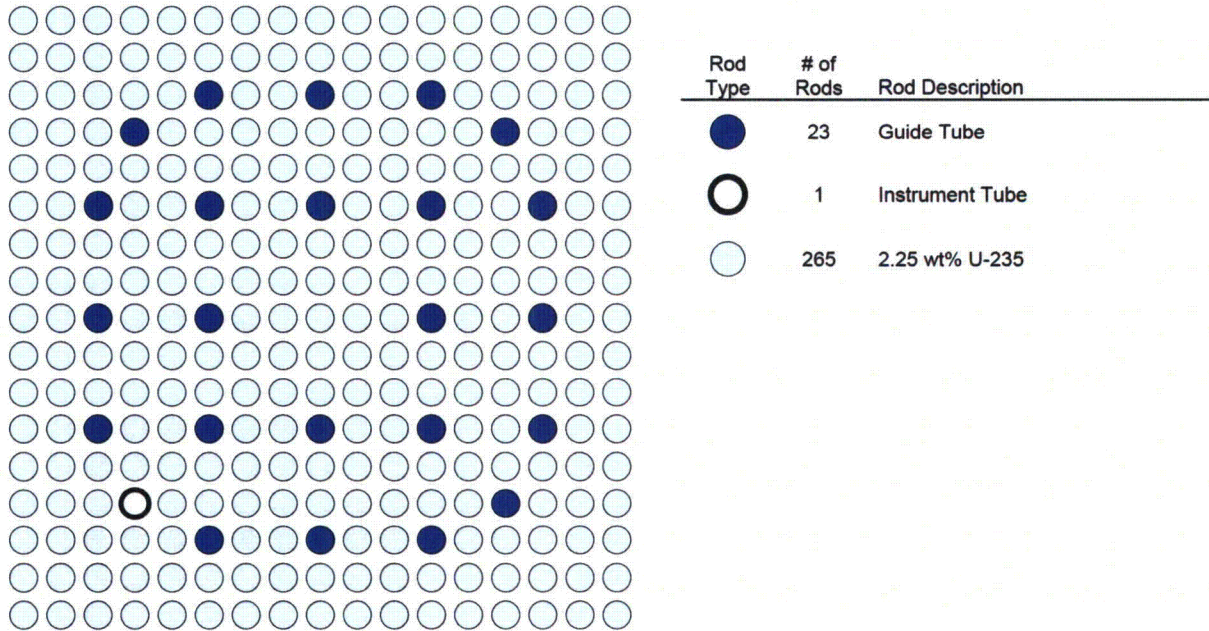
^b See Table 1-1 for M5™ composition

Table 1-3—Control Rod Data

Parameter	Value
Absorber inner diameter	0.174 in
Absorber outer diameter ^a	0.341 in
Absorber material	AgInCd
AgInCd composition	
Silver (Ag)	80%
Indium (In)	15%
Cadmium (Cd)	5%
AgInCd density	10.17 g/cm ³
Control rod cladding inner diameter	0.344 in
Control rod cladding outer diameter	0.381 in
Control rod cladding material	AISI 316L
Control rod cladding density	7.97 g/cm ³
Number of control rods per rod cluster control assembly	24

^a Dimension is for upper region. Lower region is not modeled as part of the REA topical report.

**Figure 1-1—Fuel Assembly Layout, Cycle 1, Batch A1
 2.25 wt% U-235, No Gd**



**Figure 1-2—Fuel Assembly Layout, Cycle 1, Batch A2
 2.25 wt% U-235, 4X4 Gd**

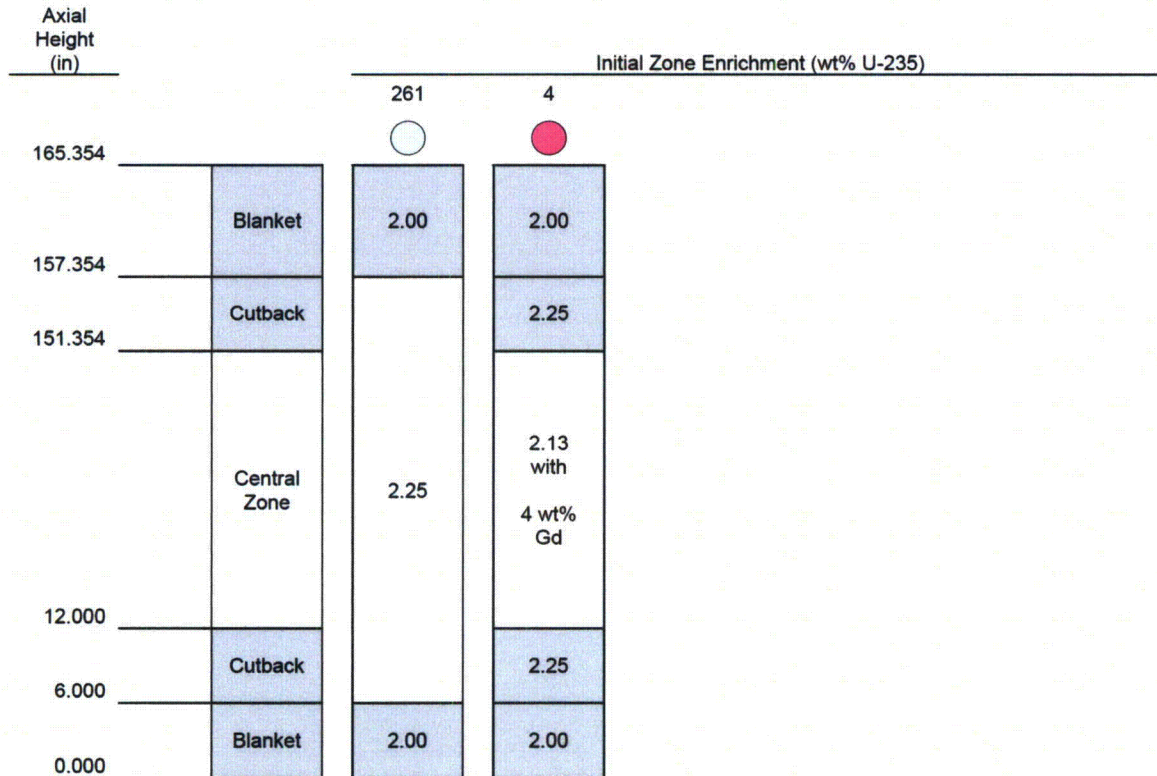
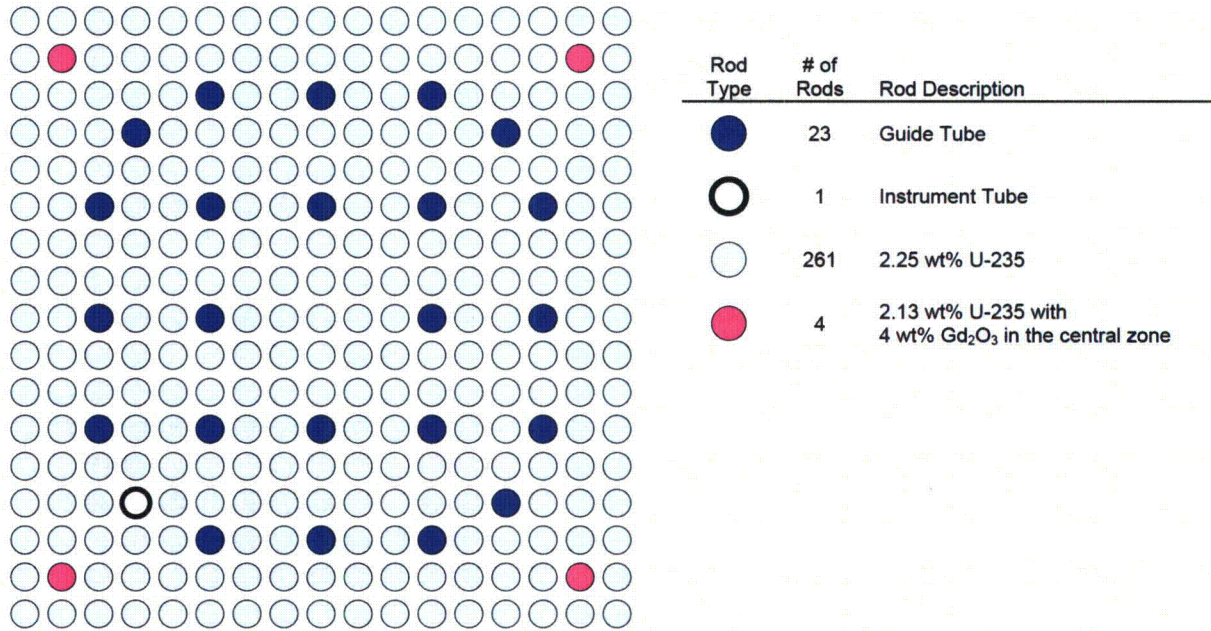


Figure 1-3—Fuel Assembly Layout, Cycle 1, Batch B1
2.70 wt% U-235, 8X8 + 4X4 Gd

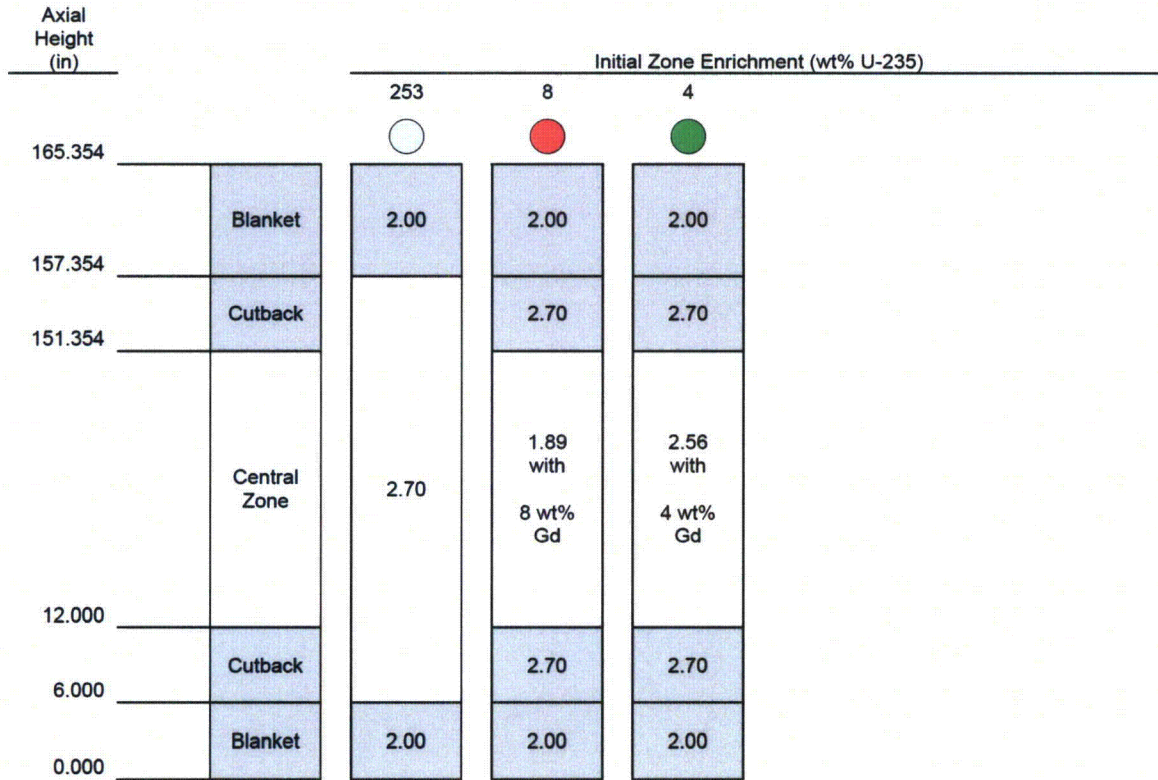
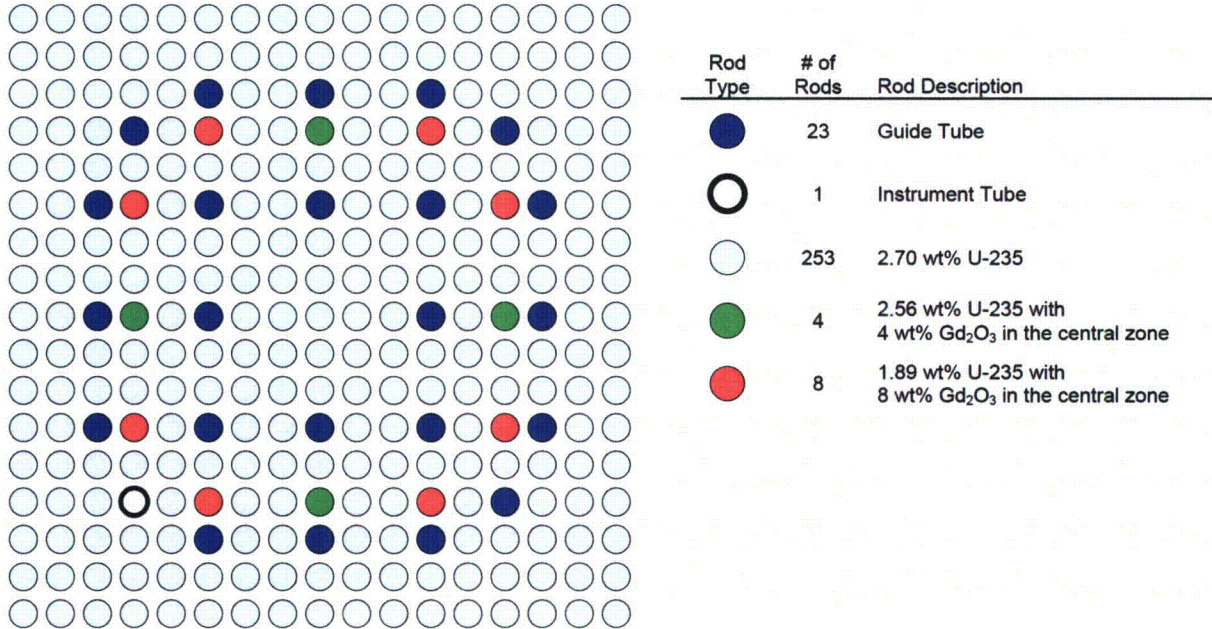


Figure 1-4—Fuel Assembly Layout, Cycle 1, Batch B2
2.70 wt% U-235, 12X8 + 4X2 Gd

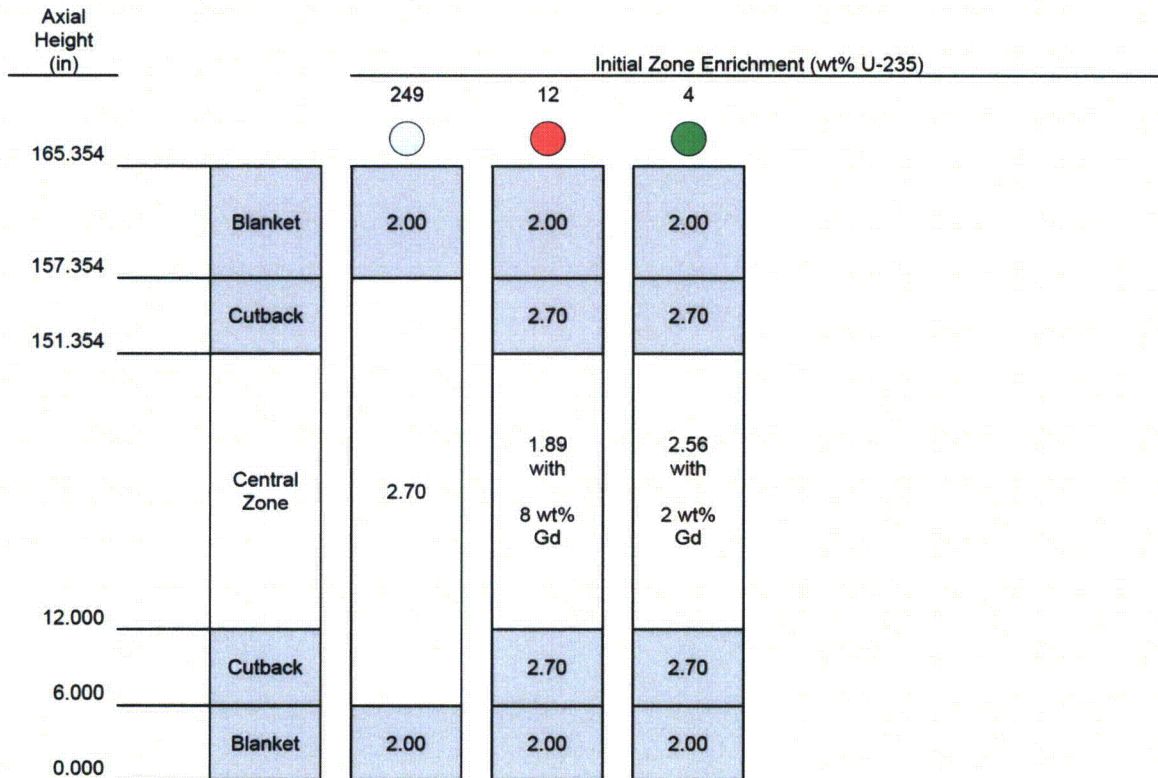
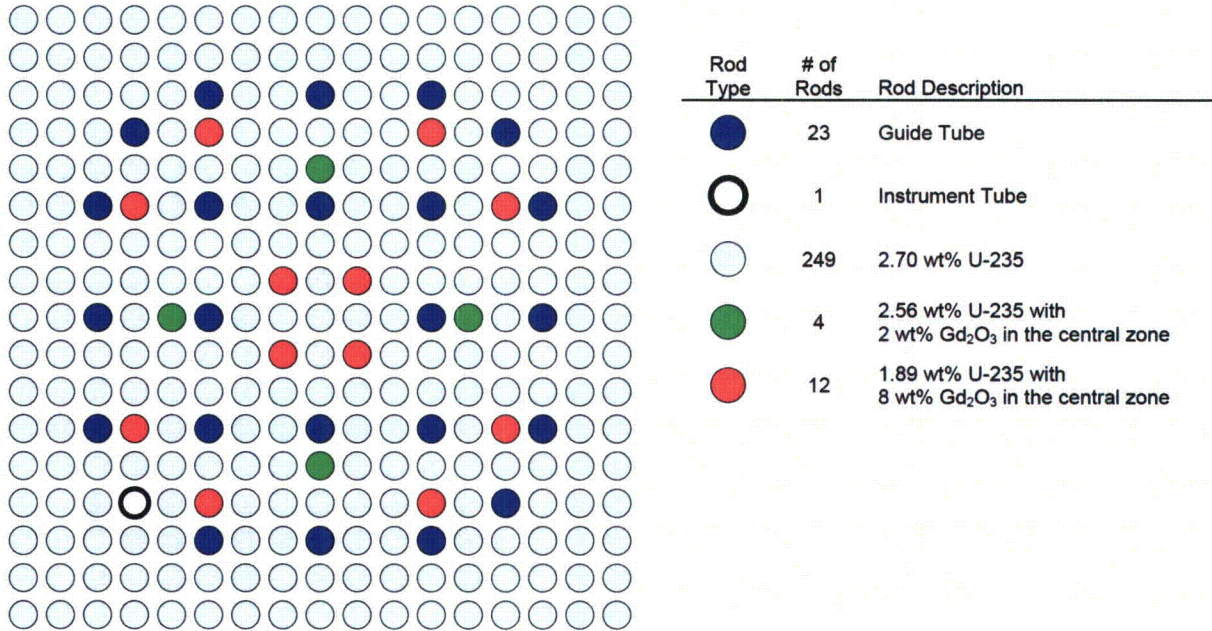


Figure 1-5—Fuel Assembly Layout, Cycle 1, Batch C1
2.70 wt% U-235, 4X6 + 4X2 Gd

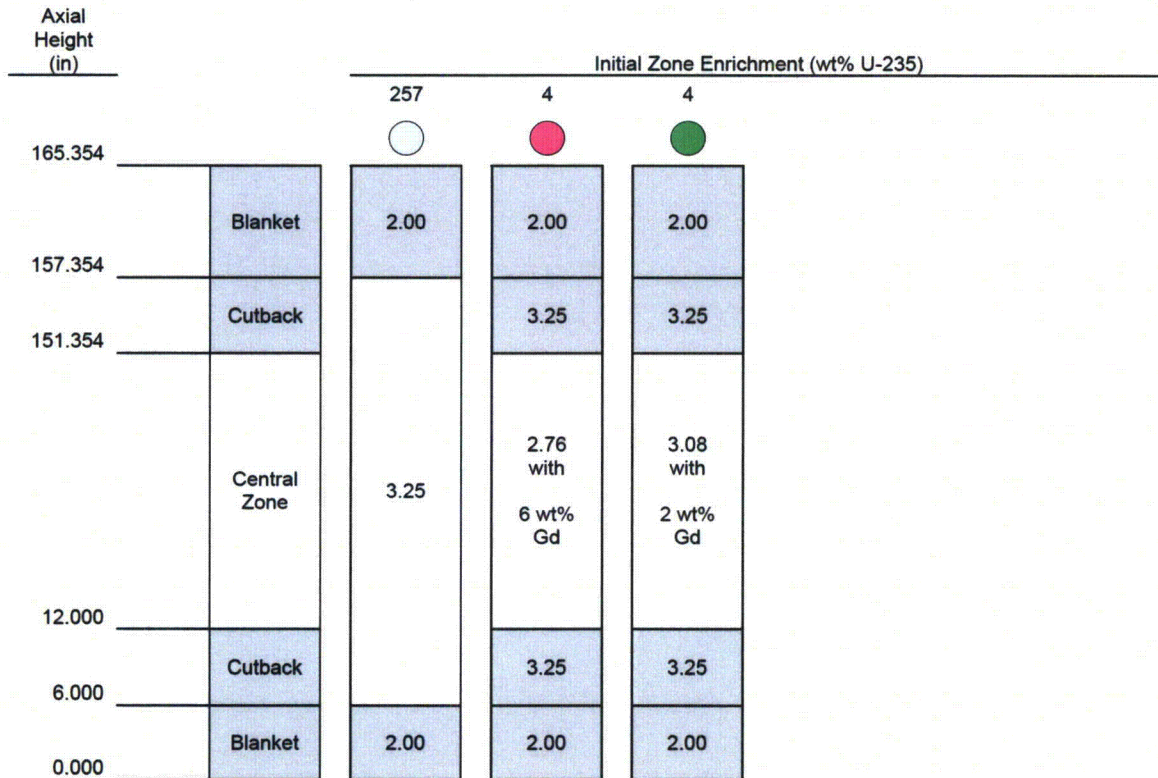
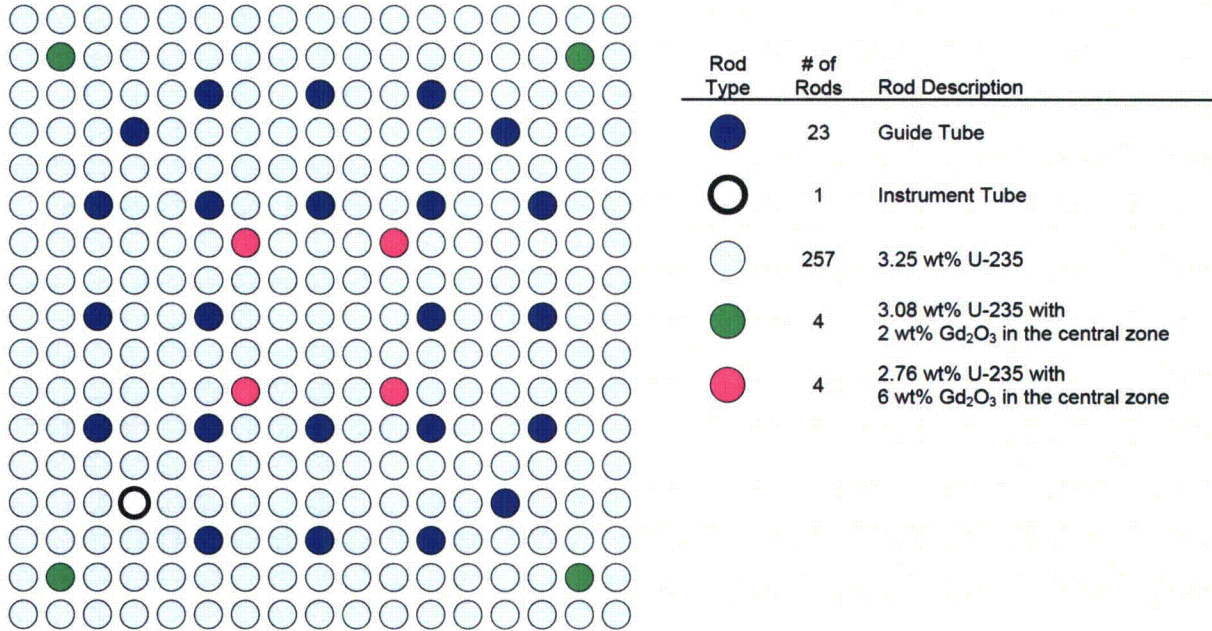


Figure 1-6—Fuel Assembly Layout, Cycle 1, Batch C2
3.25 wt% U-235, 8X6 + 4X2 Gd

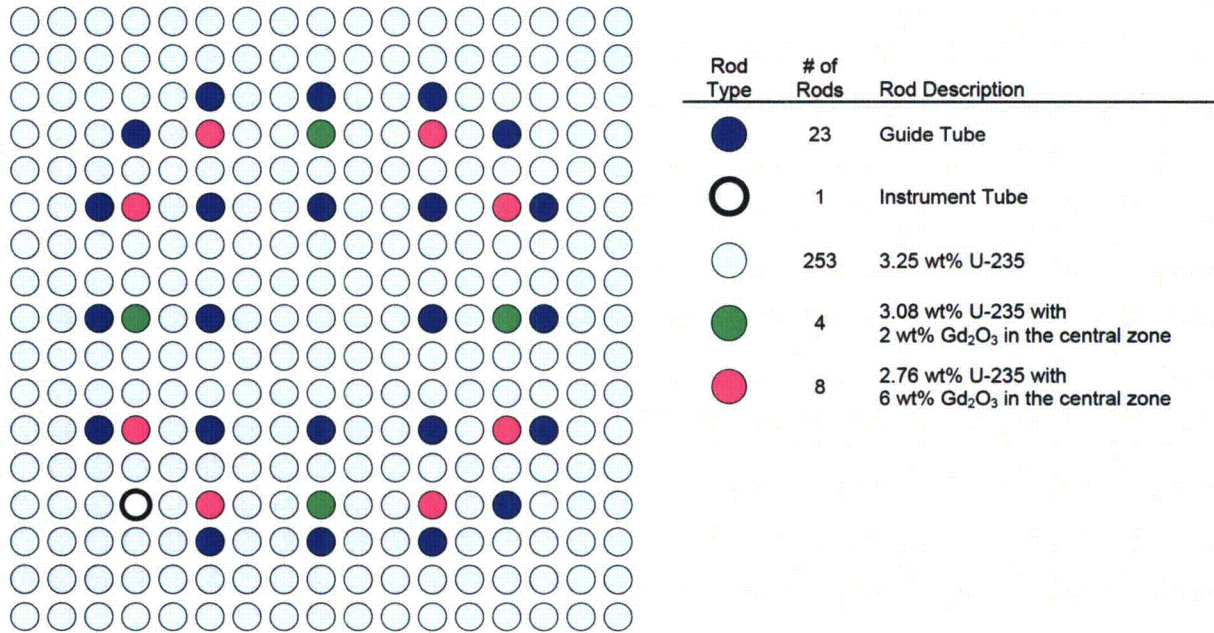
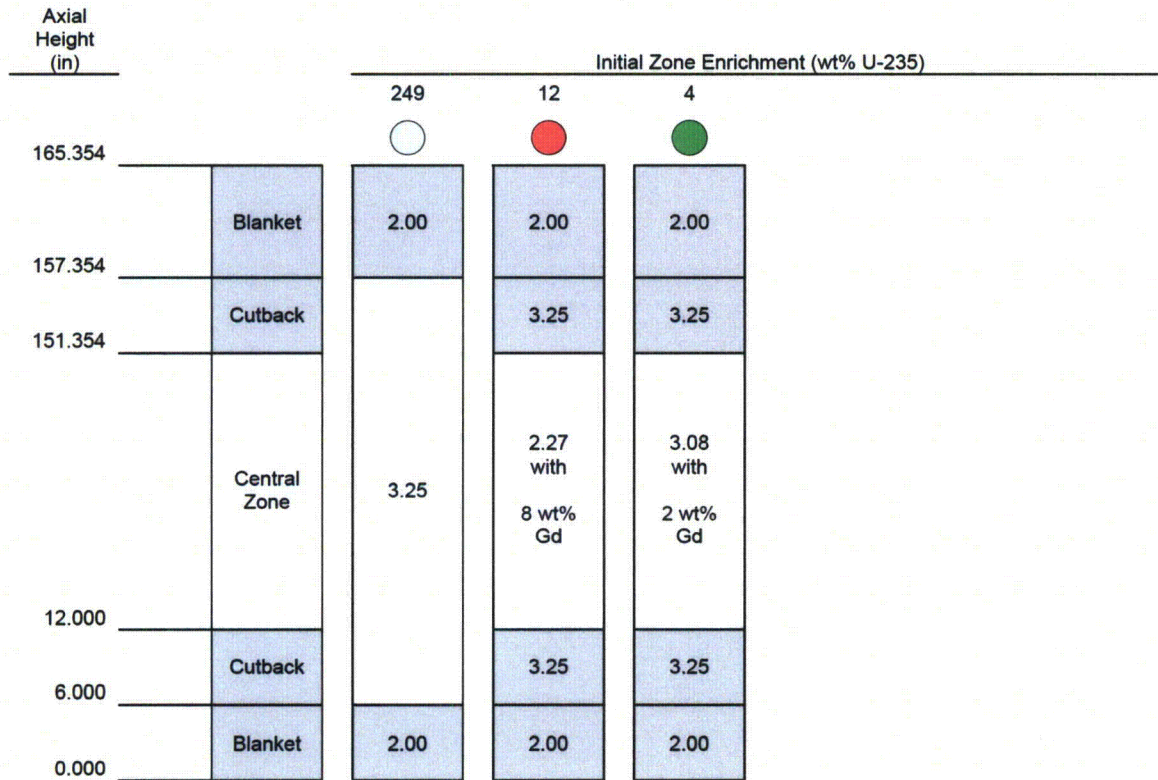
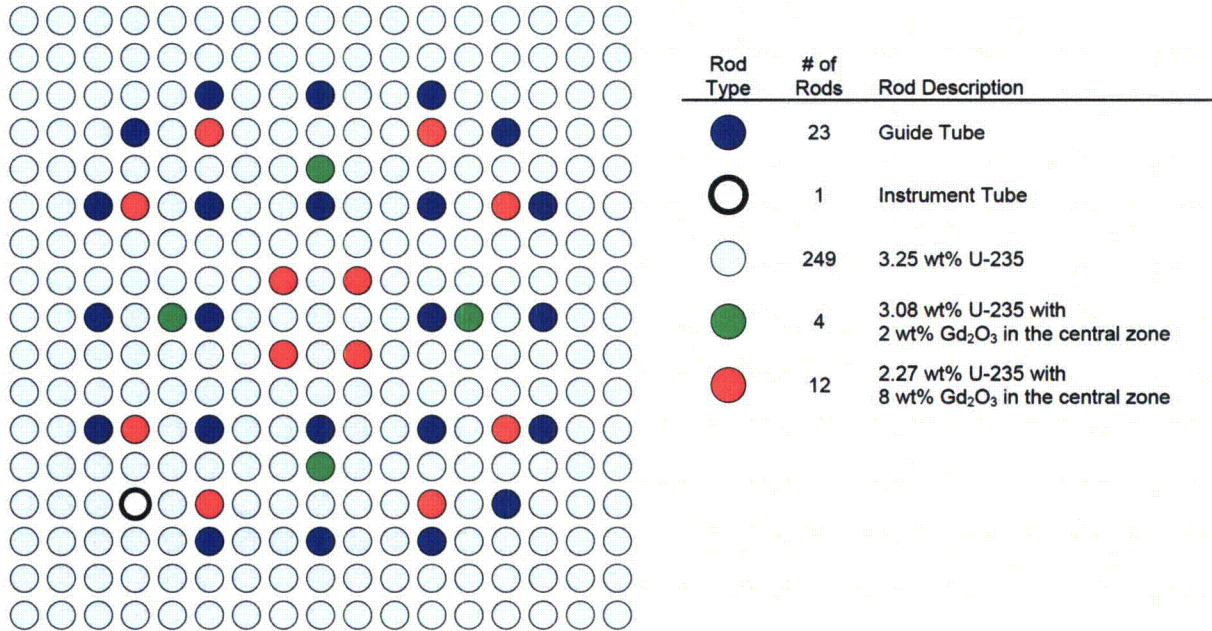
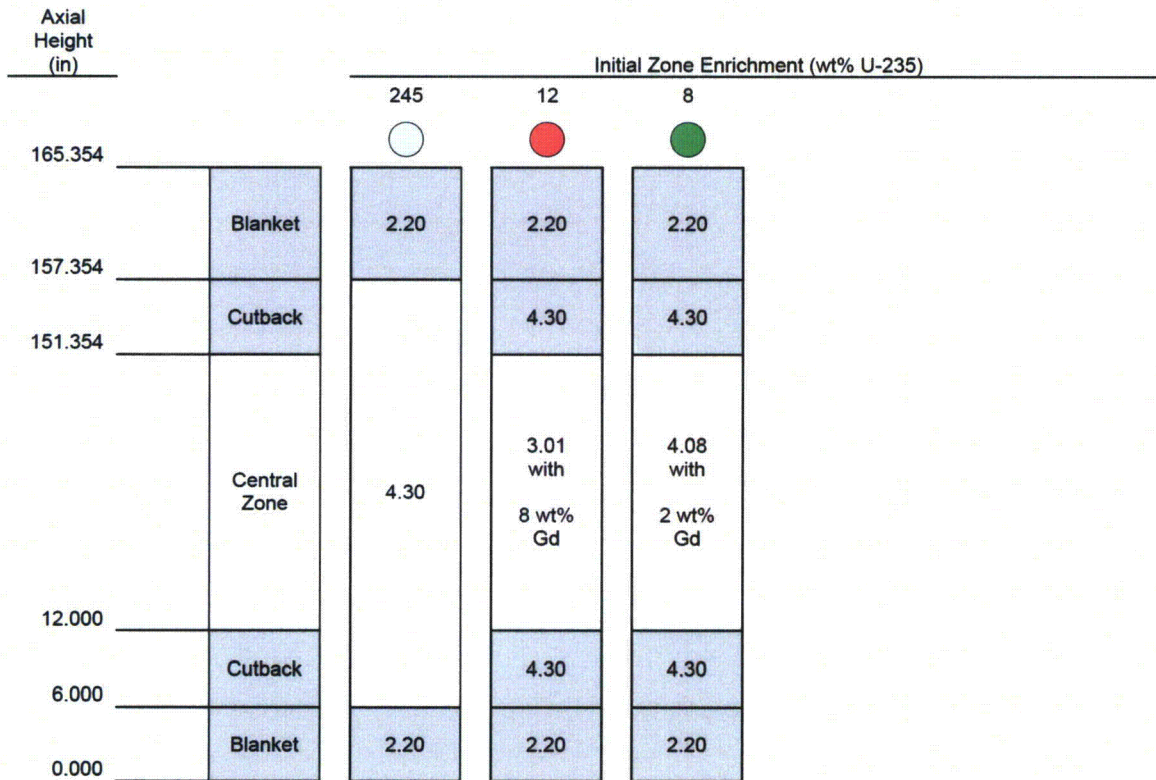
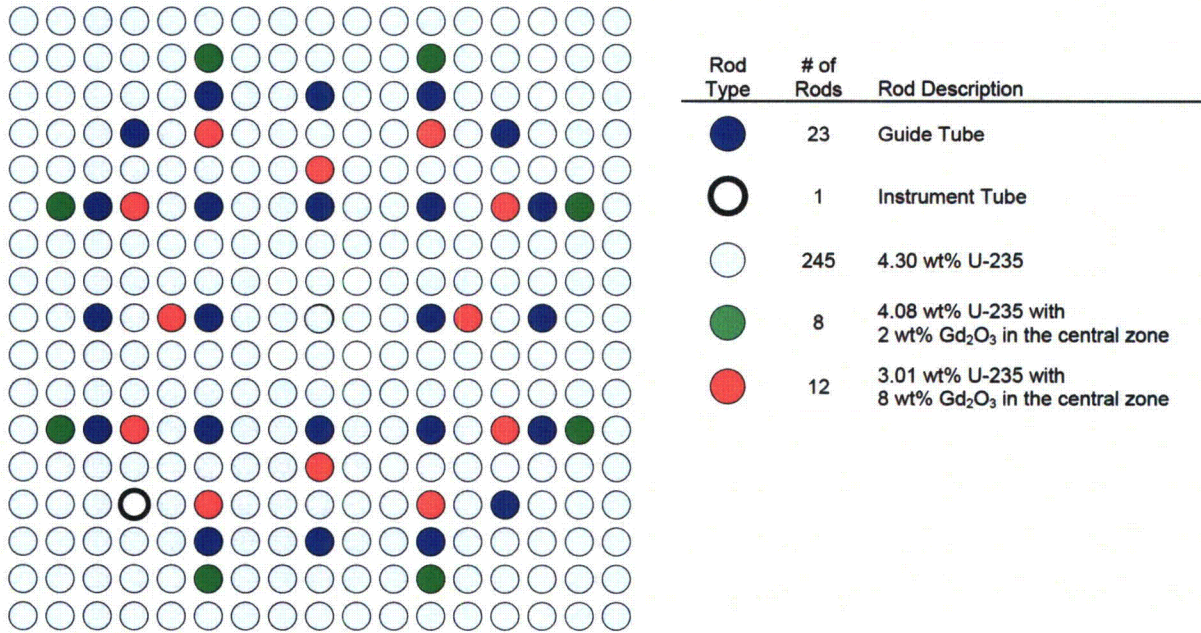


Figure 1-7—Fuel Assembly Layout, Cycle 1, Batch C3
3.25 wt% U-235, 12X8 + 4X2 Gd



**Figure 1-8—Fuel Assembly Layout, Equilibrium Cycle, Batch XX1
 4.30 wt% U-235 12X8 + 8X2 Gd**



**Figure 1-9—Fuel Assembly Layout, Equilibrium Cycle, Batch XX2
 4.30 wt% U-235 16X8 Gd**

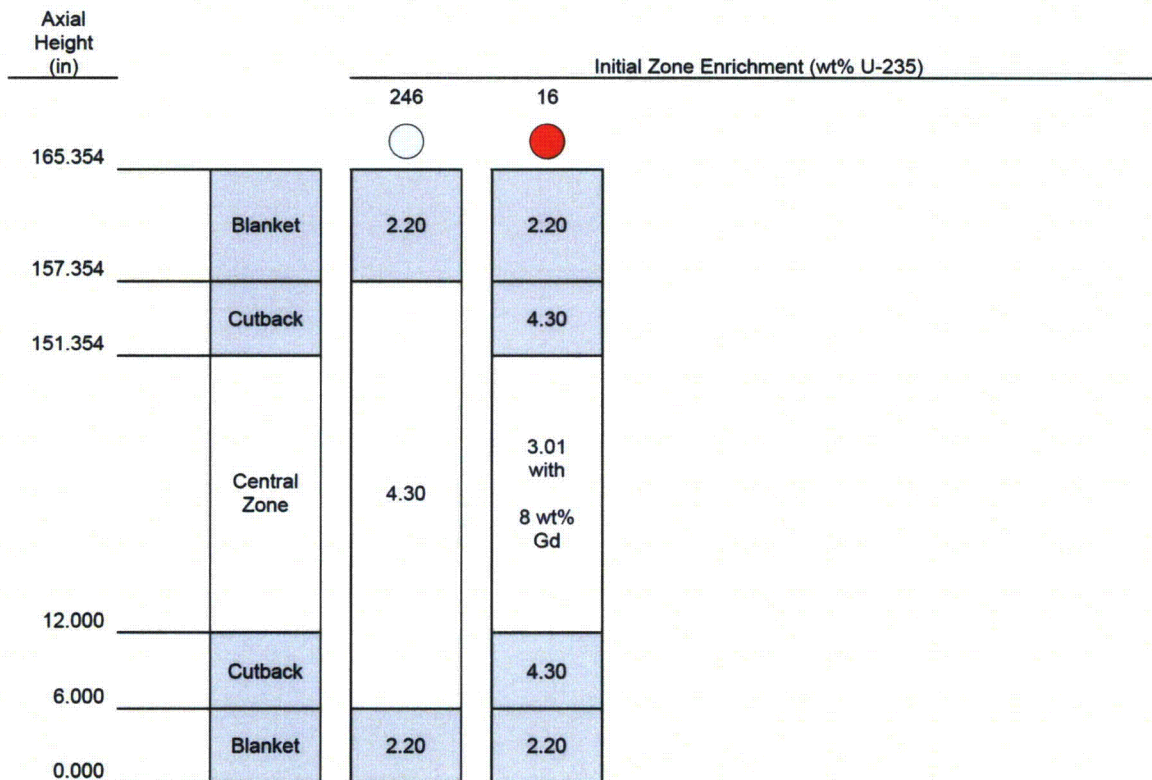
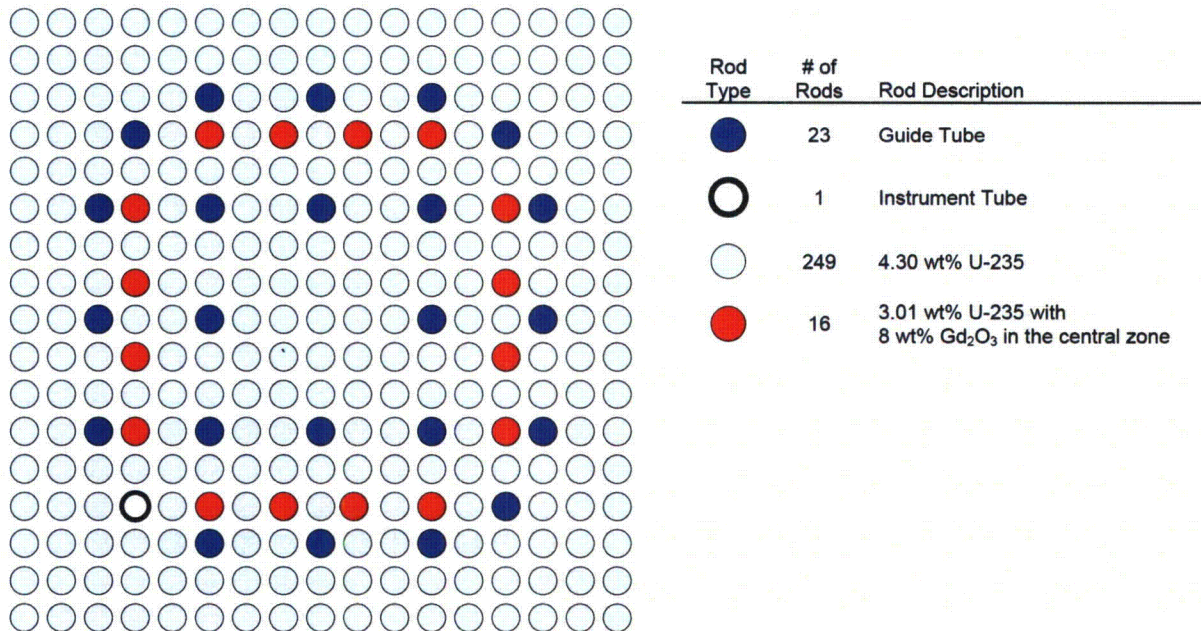


**Figure 1-10—Fuel Assembly Layout, Equilibrium Cycle, Batch XX3
 4.30 wt% U-235 16X8 + 5X2 Gd**

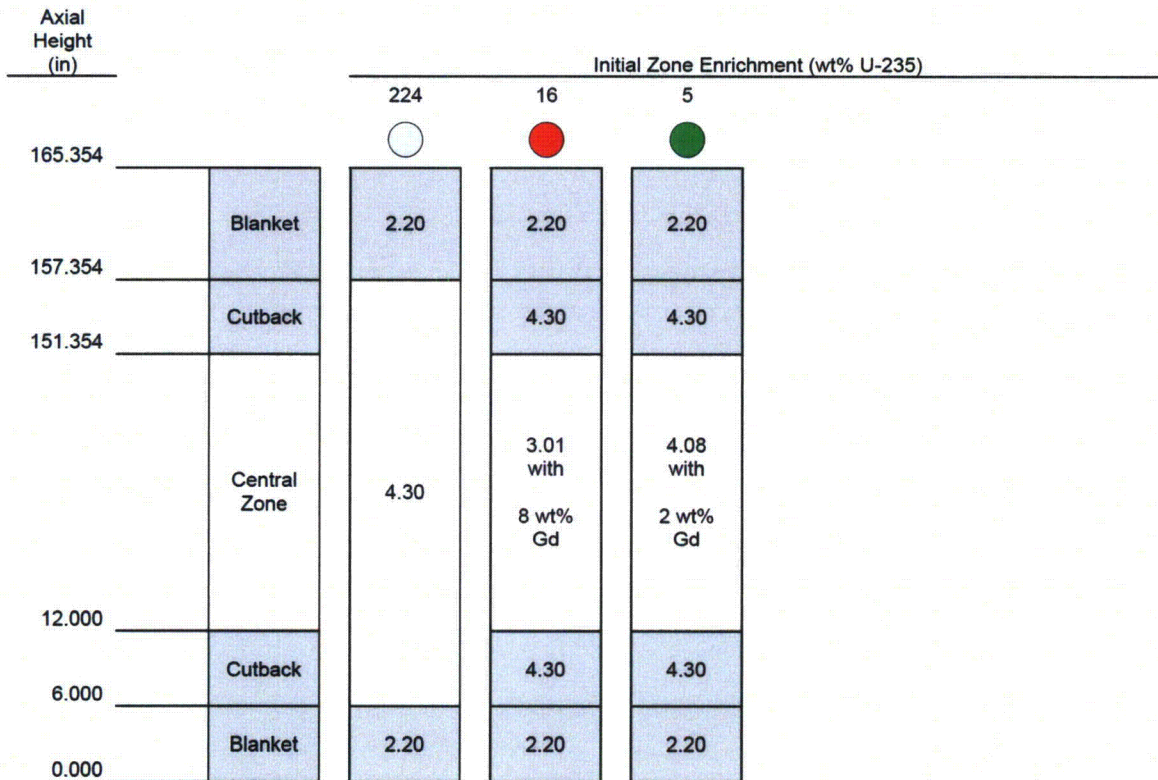
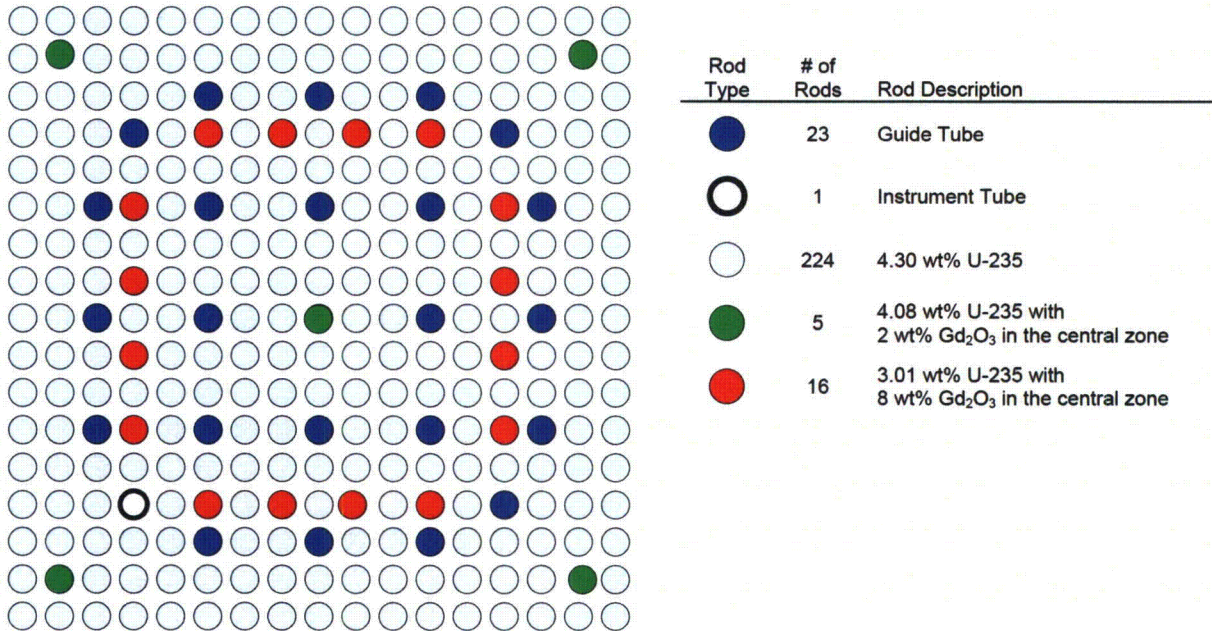
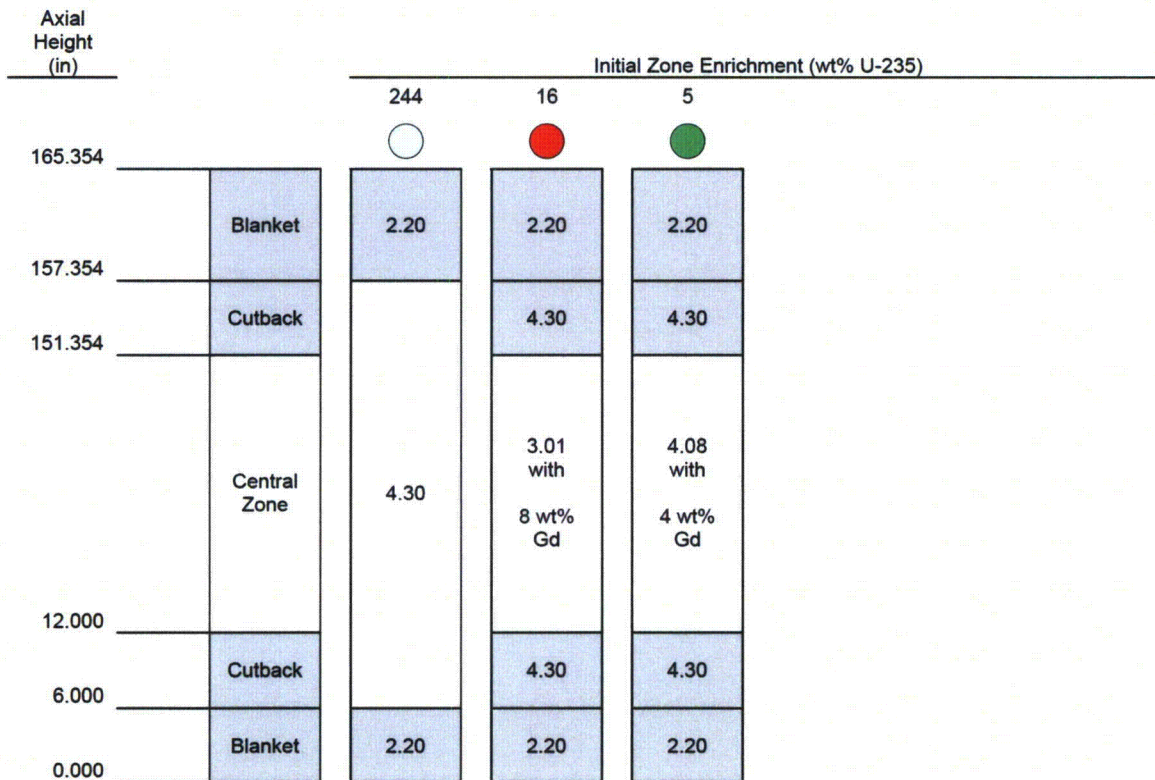
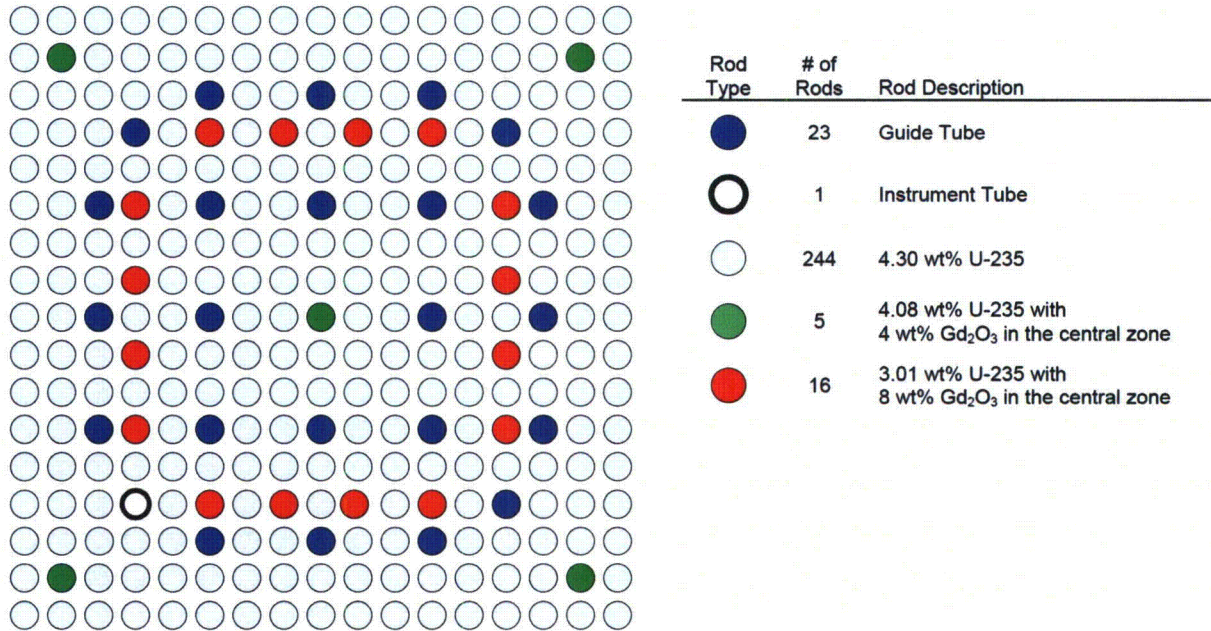
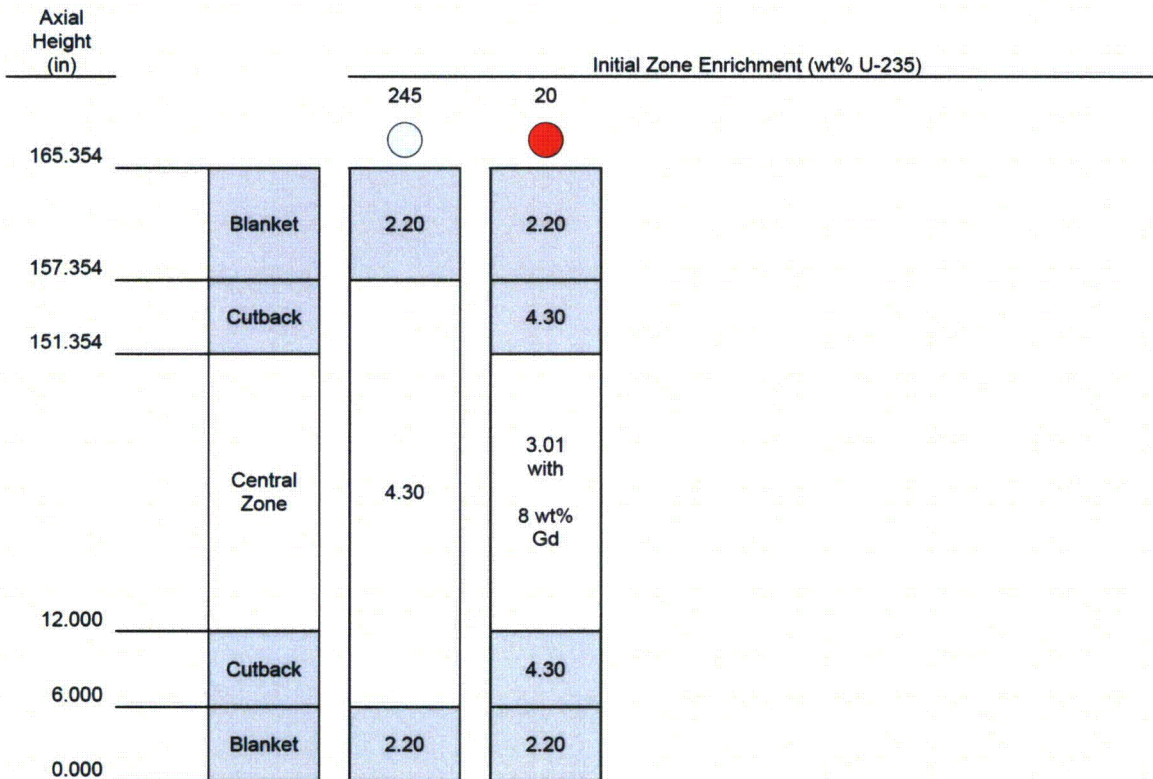
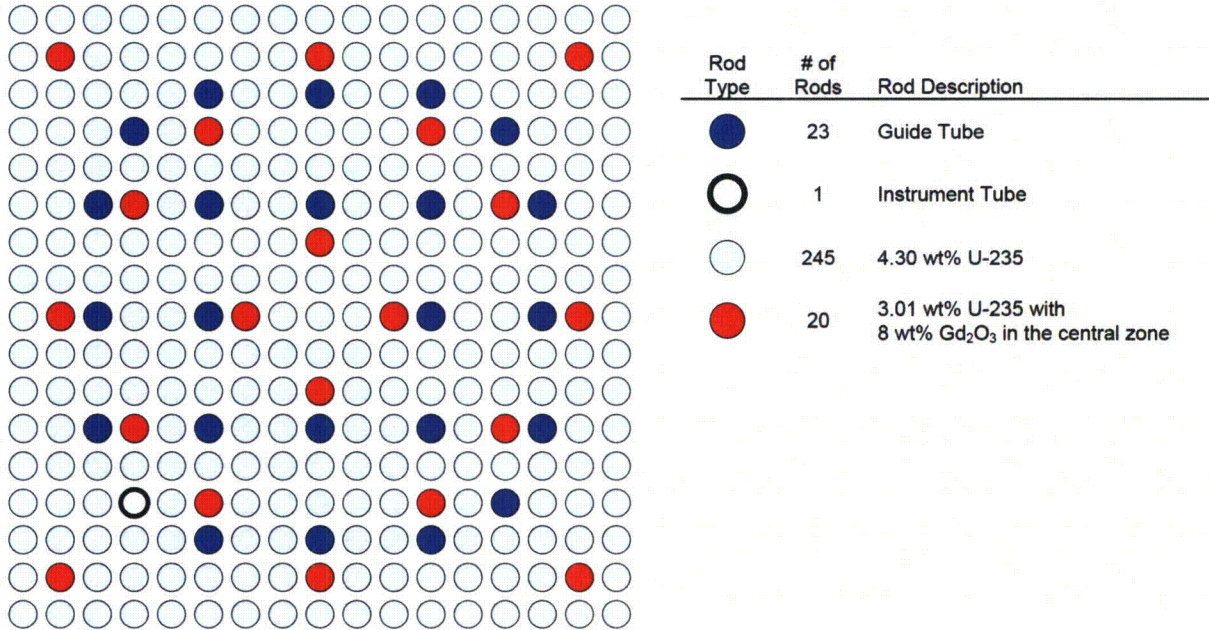


Figure 1-11—Fuel Assembly Layout, Equilibrium Cycle, Batch XX4
4.30 wt% U-235 16X8 + 5X4 Gd



**Figure 1-12—Fuel Assembly Layout, Equilibrium Cycle, Batch XX5
 4.30 wt% U-235 20X8 Gd**



**Figure 1-13—Fuel Assembly Layout, Equilibrium Cycle, Batch XX6
 4.80 wt% U-235 8X2 Gd**

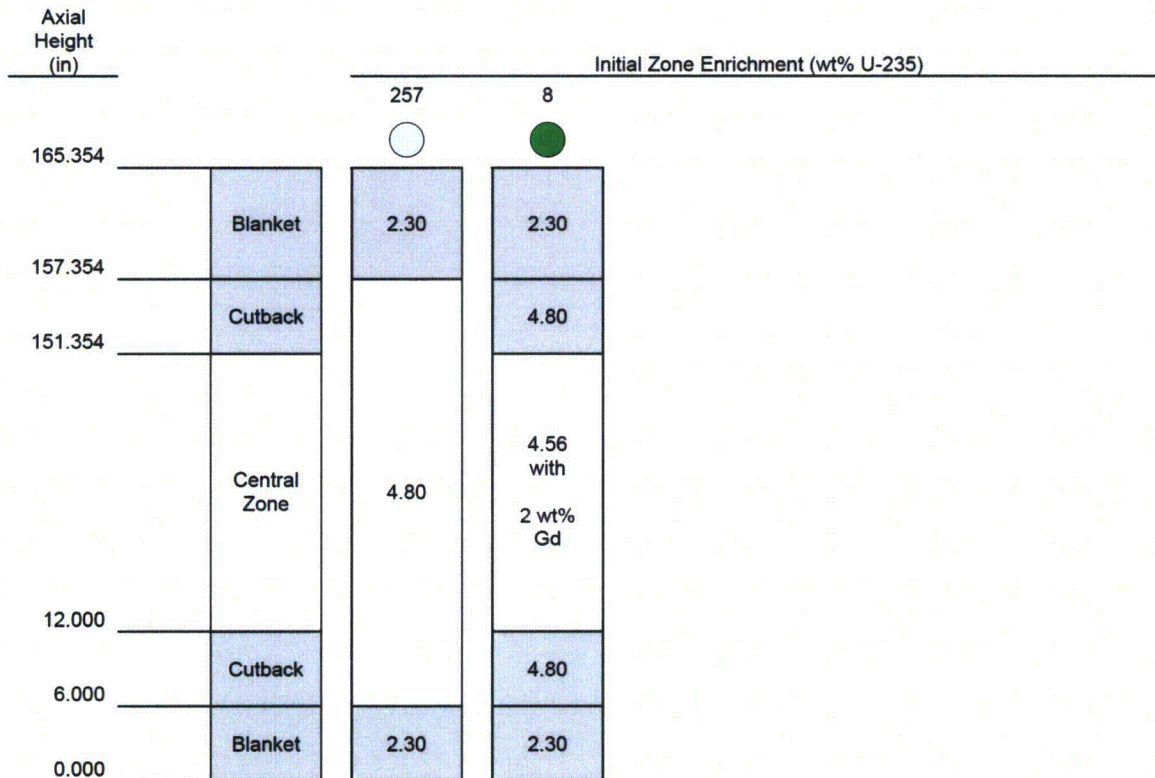
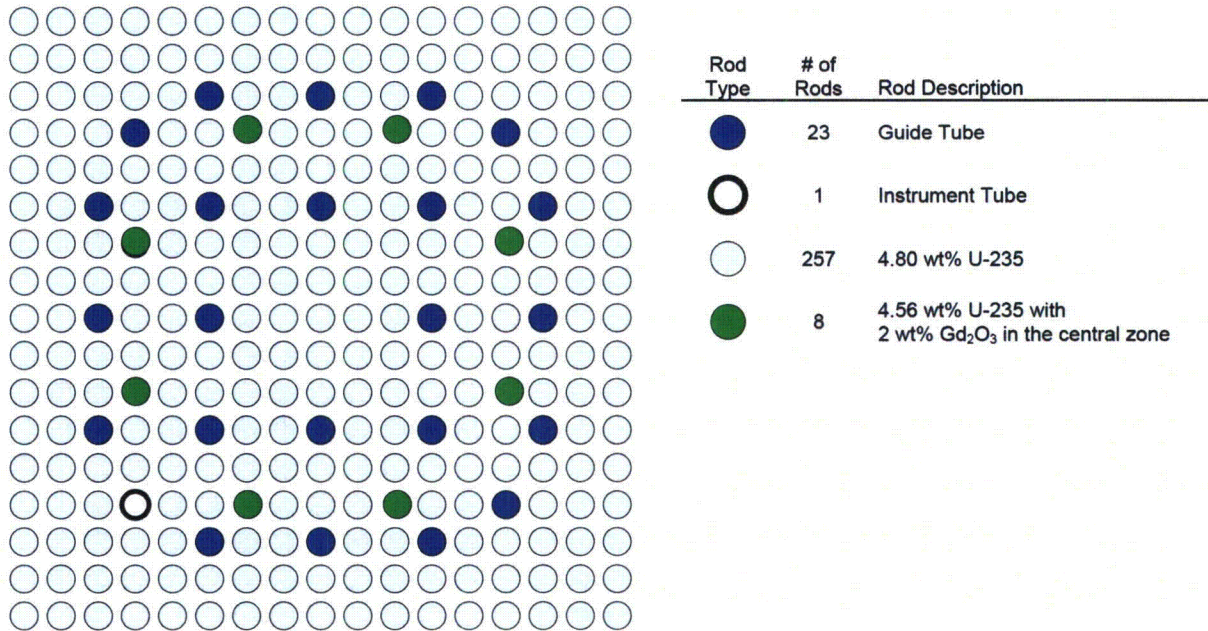


**Figure 1-14—Fuel Assembly Layout, Equilibrium Cycle, Batch XX7
 4.80 wt% U-235 12X8 Gd**

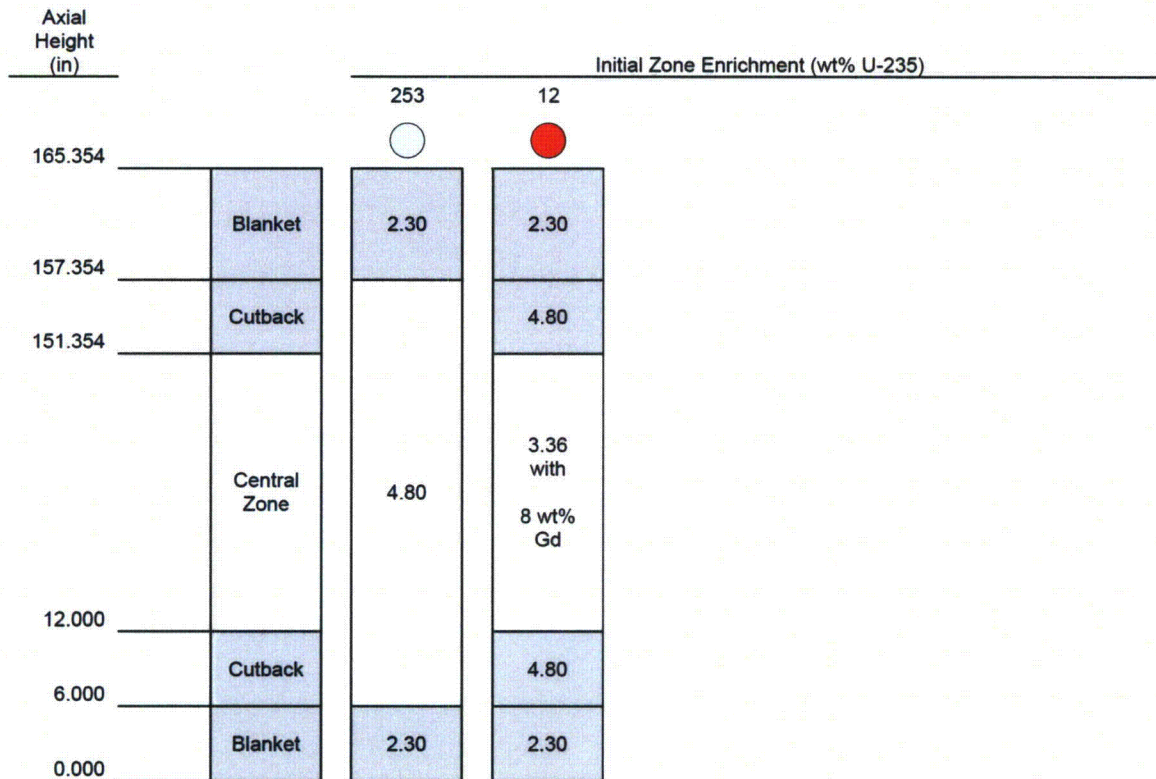
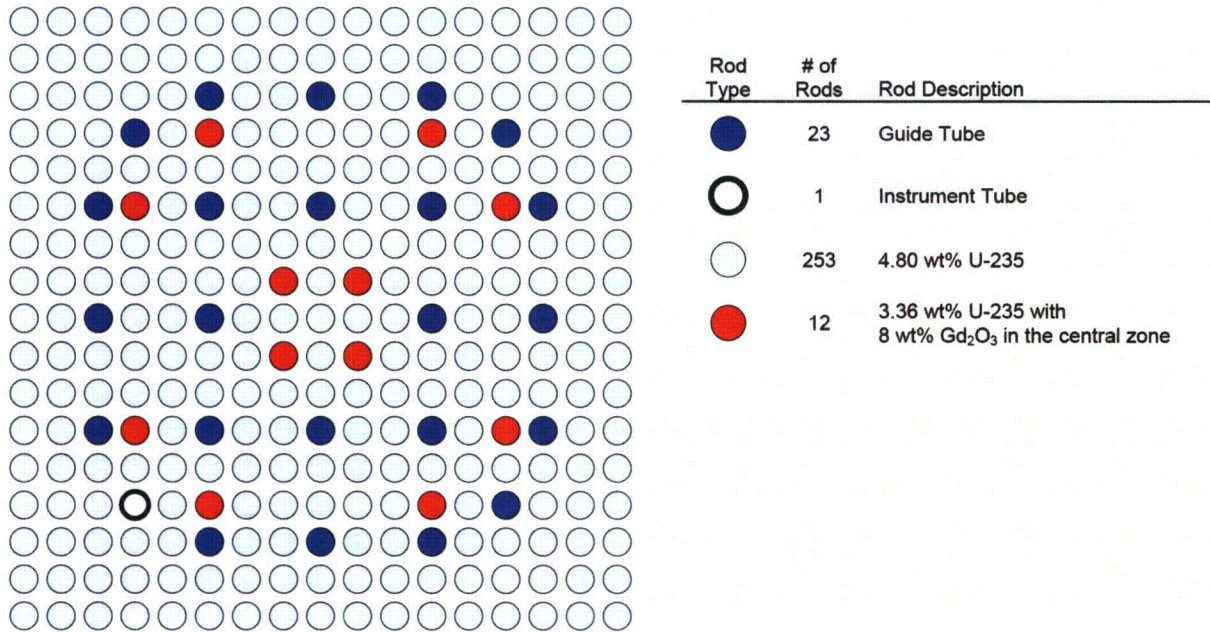


**Figure 1-15—Fuel Assembly Layout, Equilibrium Cycle, Batch XX8
 4.80 wt% U-235 12X8 + 8X2 Gd**

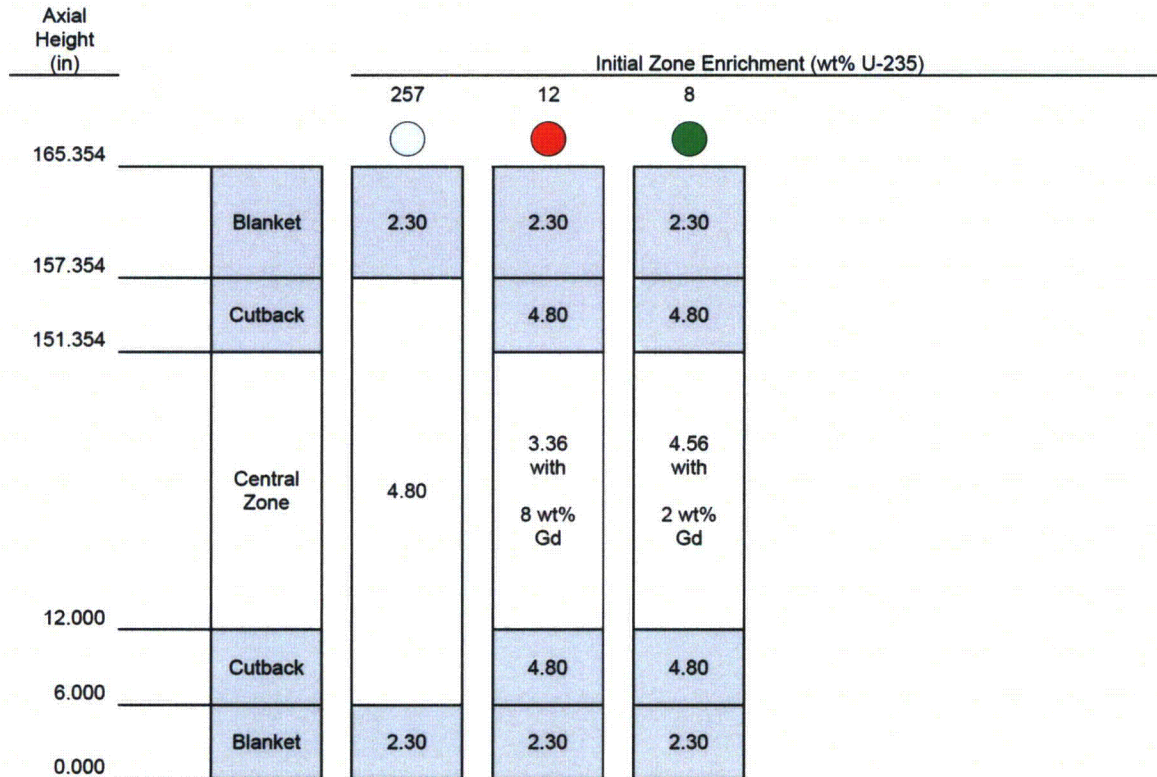
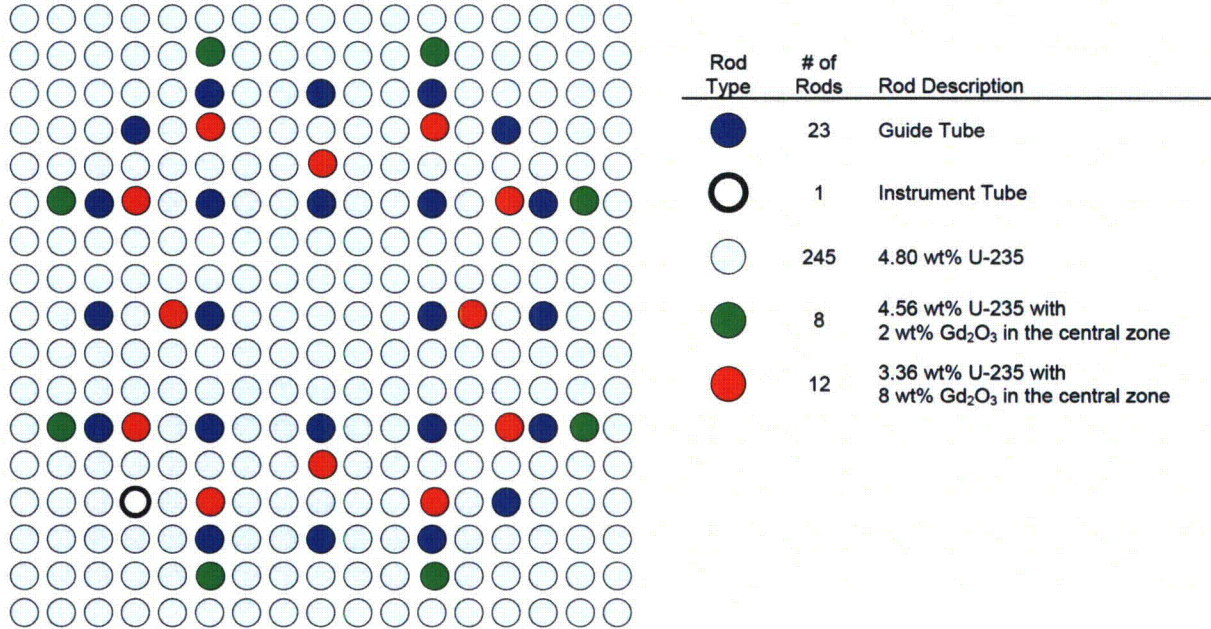


**Figure 1-16—Fuel Assembly Layout, Equilibrium Cycle, Batch XX9
 4.80 wt% U-235 16X8 + 5X4 Gd**

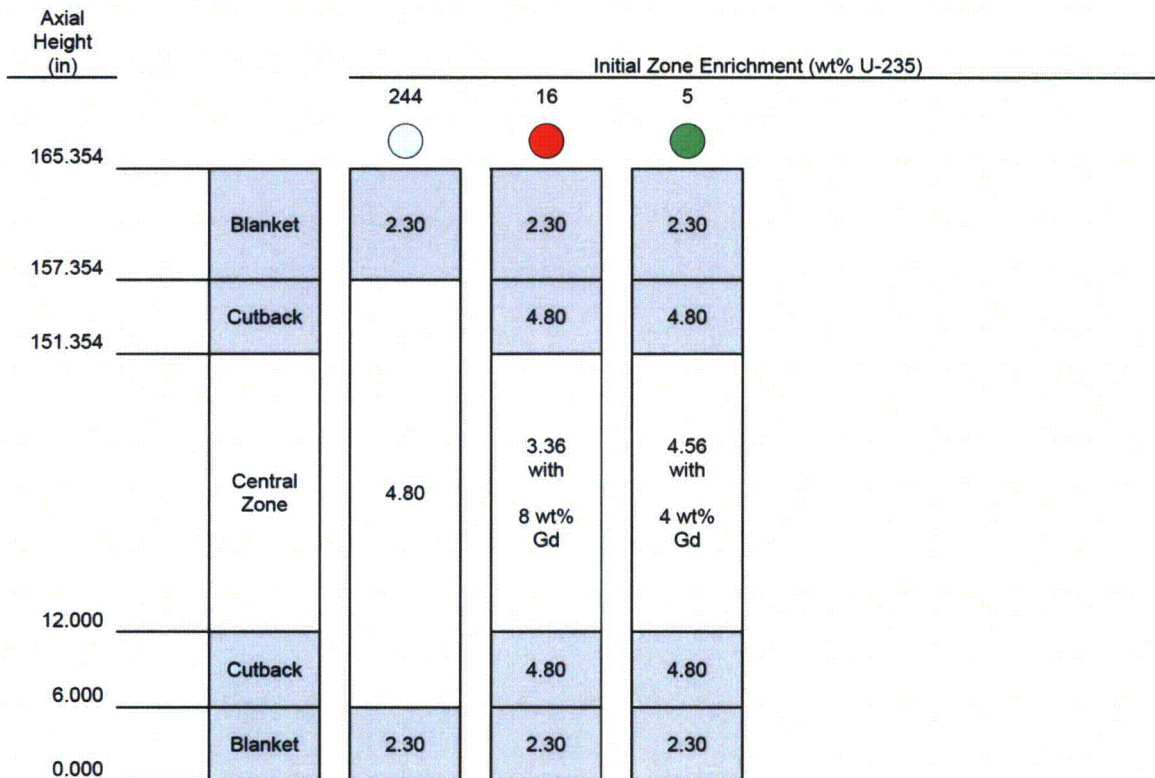
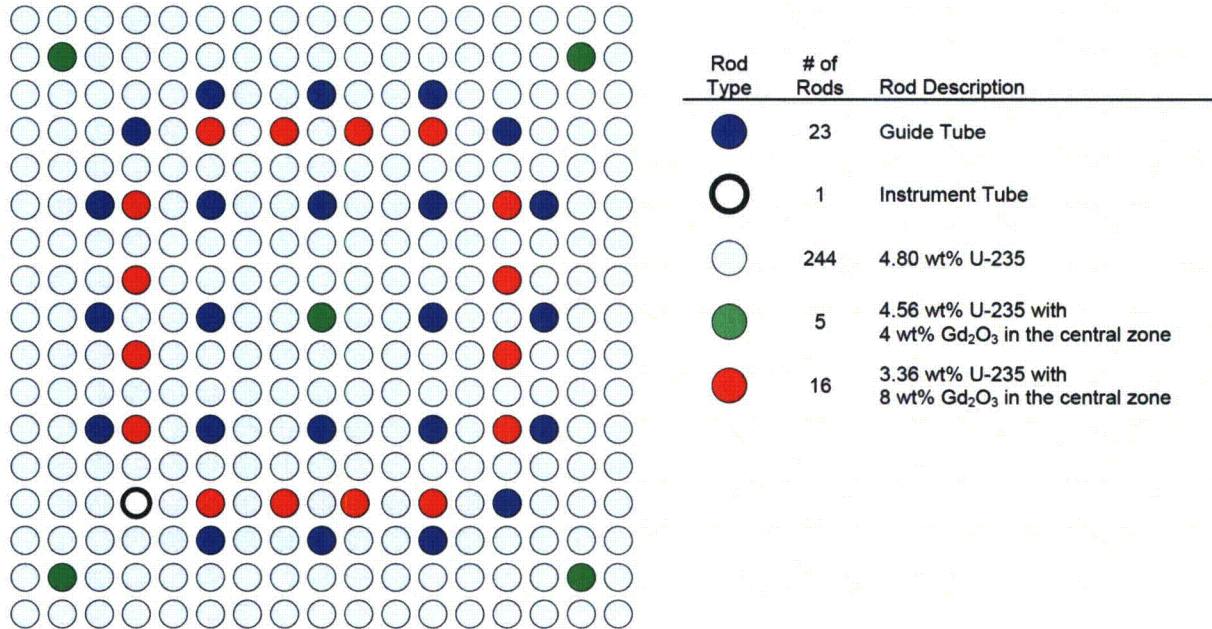
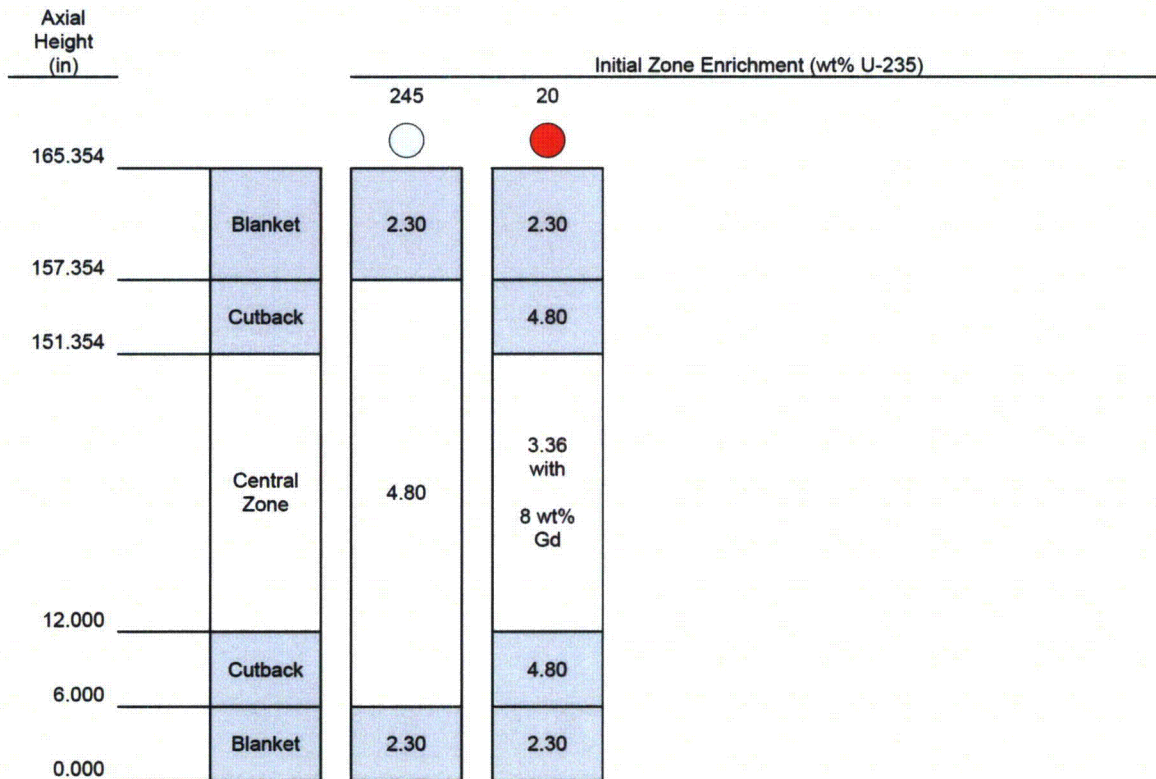
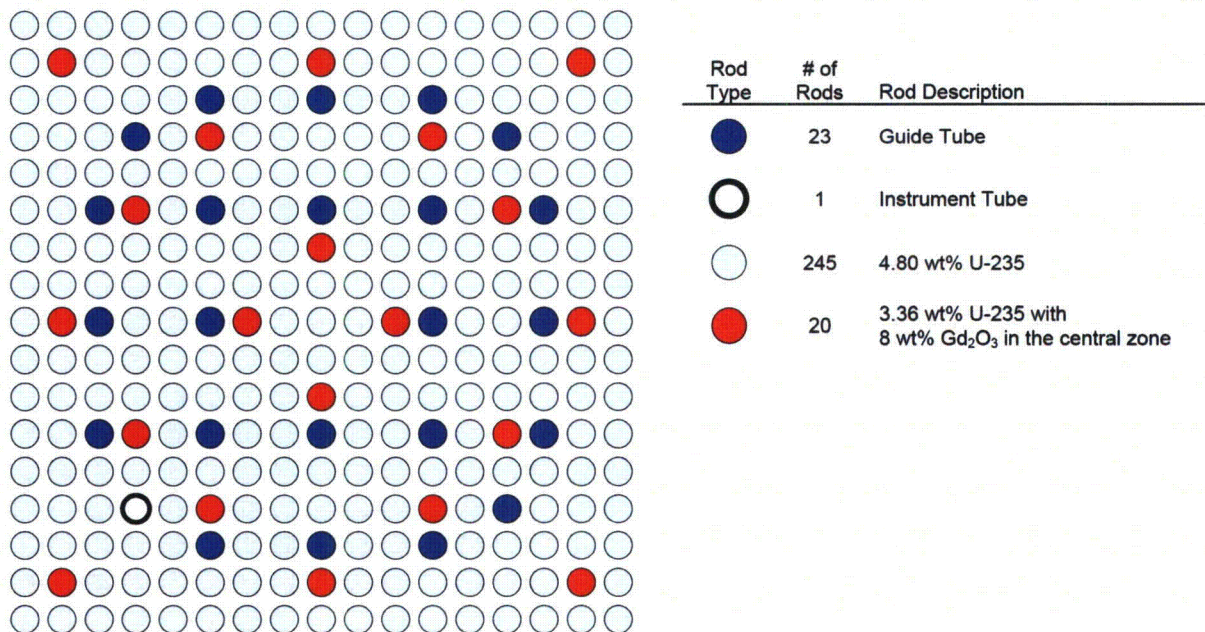


**Figure 1-17—Fuel Assembly Layout, Equilibrium Cycle, Batch XX10
 4.80 wt% U-235 20X8 Gd**



- RAI-2.** *Please provide the following modeling data that was used in the RIA analyses:*
- a. *core loading map,*
 - b. *associated 3-d nodal exposure.*

Response to RAI-2:

The following information is provided to model the core at the burnups represented in the REA analysis presented in ANP-10286P. Figure 2-1 and Figure 2-2 show the core loading maps for Cycle 1 and the equilibrium cycle, respectively. Control rod locations are shown in Figure 2-3. Three shutdown banks (Banks SA, SB, and SC) and four control banks (D, C, B, A) are shown. Bank D is the lead bank.

The 3-D nodal exposures are provided in the following ASCII punch files, which are contained on the enclosed compact disc and are readable with a text editor (e.g., Microsoft Wordpad®):

Cycle 1: c1_data_dep.pch.txt (cksum: 3868873889 165728)
Equilibrium cycle: eq_data_dep.pch.txt (cksum: 1364008463 165728)

In the punch files, the 3-D nodal exposures are written to keyword 'BURNUP' in the following way (core numbering can be see in the Cycle 1 loading map shown in Figure 2-1):

- The first assembly presented is at the top left of the core map (core location F17)
- Each row is completed before the next row is started (e.g., F17...M17, D16...P16, C15...R15, etc.)
- Values are given for all fuel assemblies in the core for one complete axial layer at a time
- The first axial layer presented is at the bottom of the active fuel
- The first 'BURNUP' set corresponds to beginning-of-cycle (BOC), 4 effective fuel power days (EFPD); the second 'BURNUP' set corresponds to end-of-cycle (EOC), 547 EFPD

The 3-D nodal exposures are shown for select assemblies in Table 2-1 through Table 2-4 to enable cross checking with computer generated files.

Axial profiles for fuel and moderator temperature at BOC (4 EFPD) and EOC (547 EFPD) are given in Table 2-5 for Cycle 1 and Table 2-6 for the equilibrium cycle. These profiles are applicable to all fuel types.

A value of 3.64 percent is used for the core bypass flow.

**Table 2-1—3-D Nodal Burnups (GWd/MTU) for Select Assemblies,
 Cycle 1, BOC (4 EFPD)**

Axial Layer	Node Height (cm)	ASSEMBLY (CORE LOCATION)							
		F17	P16	J09	R08	E07	J06	N05	M01
2 - bottom	15.24	0.031	0.030	0.086	0.081	0.082	0.080	0.084	0.031
3	15.24	0.060	0.059	0.190	0.162	0.177	0.160	0.182	0.060
4	17.698	0.081	0.078	0.199	0.159	0.172	0.162	0.176	0.081
5	17.698	0.094	0.090	0.205	0.164	0.173	0.168	0.177	0.094
6	17.698	0.101	0.096	0.211	0.169	0.177	0.174	0.181	0.101
7	17.698	0.106	0.100	0.215	0.174	0.180	0.177	0.184	0.106
8	17.698	0.108	0.102	0.218	0.177	0.182	0.180	0.187	0.108
9	17.698	0.109	0.104	0.220	0.178	0.184	0.182	0.188	0.109
10	17.698	0.110	0.104	0.221	0.179	0.184	0.183	0.189	0.110
11	17.698	0.109	0.104	0.221	0.178	0.184	0.183	0.188	0.109
12	17.698	0.108	0.103	0.220	0.176	0.183	0.182	0.186	0.108
13	17.698	0.107	0.101	0.218	0.174	0.181	0.180	0.184	0.107
14	17.698	0.105	0.099	0.215	0.171	0.179	0.178	0.181	0.105
15	17.698	0.102	0.097	0.212	0.167	0.175	0.176	0.177	0.102
16	17.698	0.099	0.094	0.207	0.163	0.172	0.172	0.173	0.099
17	17.698	0.096	0.091	0.203	0.158	0.167	0.168	0.168	0.096
18	17.698	0.093	0.088	0.197	0.152	0.162	0.164	0.162	0.093
19	17.698	0.088	0.084	0.191	0.146	0.157	0.159	0.156	0.088
20	17.698	0.083	0.079	0.183	0.139	0.150	0.153	0.148	0.083
21	17.698	0.078	0.074	0.175	0.131	0.144	0.147	0.141	0.078
22	17.698	0.070	0.067	0.164	0.122	0.138	0.140	0.132	0.070
23	17.698	0.060	0.058	0.146	0.113	0.134	0.134	0.119	0.060
24	15.24	0.046	0.045	0.099	0.110	0.139	0.136	0.086	0.046
25 - top	20.32	0.023	0.023	0.036	0.053	0.064	0.068	0.032	0.023

**Table 2-2—3-D Nodal Burnups (GWd/MTU) for Select Assemblies,
 Cycle 1, EOC (547 EFPD)**

Axial Layer	Node Height (cm)	ASSEMBLY (CORE LOCATION)							
		F17	P16	J09	R08	E07	J06	N05	M01
2 - bottom	15.24	3.686	3.696	9.506	9.201	9.517	9.210	9.605	3.686
3	15.24	6.774	6.748	19.369	17.350	19.219	17.247	19.475	6.774
4	17.698	8.848	8.794	23.361	20.590	22.582	20.420	22.939	8.848
5	17.698	10.023	9.961	25.518	22.572	24.619	22.366	25.018	10.023
6	17.698	10.569	10.510	26.487	23.507	25.583	23.279	25.996	10.569
7	17.698	10.799	10.745	26.858	23.871	25.957	23.645	26.369	10.799
8	17.698	10.878	10.828	26.946	23.962	26.049	23.753	26.453	10.878
9	17.698	10.891	10.842	26.914	23.934	26.019	23.751	26.408	10.891
10	17.698	10.878	10.831	26.839	23.862	25.944	23.709	26.317	10.878
11	17.698	10.861	10.812	26.757	23.782	25.861	23.662	26.217	10.861
12	17.698	10.846	10.796	26.683	23.709	25.786	23.621	26.122	10.846
13	17.698	10.836	10.786	26.621	23.646	25.722	23.593	26.039	10.836
14	17.698	10.833	10.781	26.572	23.595	25.671	23.578	25.968	10.833
15	17.698	10.836	10.782	26.534	23.553	25.629	23.572	25.906	10.836
16	17.698	10.840	10.784	26.501	23.514	25.590	23.571	25.846	10.840
17	17.698	10.841	10.782	26.460	23.464	25.541	23.562	25.773	10.841
18	17.698	10.826	10.763	26.386	23.378	25.453	23.521	25.659	10.826
19	17.698	10.770	10.701	26.227	23.206	25.275	23.402	25.449	10.770
20	17.698	10.629	10.552	25.886	22.853	24.915	23.123	25.043	10.629
21	17.698	10.325	10.238	25.175	22.155	24.214	22.541	24.252	10.325
22	17.698	9.722	9.626	23.737	20.819	22.921	21.422	22.741	9.722
23	17.698	8.587	8.493	20.488	18.428	20.759	19.457	19.551	8.587
24	15.24	6.755	6.685	12.883	15.267	17.928	16.780	12.561	6.755
25 - top	20.32	3.646	3.627	5.023	7.795	8.827	8.993	4.898	3.646

**Table 2-3—3-D Nodal Burnups (GWd/MTU) for Select Assemblies,
 Equilibrium Cycle, BOC (4 EFPD)**

Axial Layer	Node Height (cm)	ASSEMBLY (CORE LOCATION)							
		F17	P16	J09	R08	E07	J06	N05	M01
2 - bottom	15.24	18.738	15.992	14.383	7.308	10.172	0.049	9.975	18.674
3	15.24	40.310	34.831	31.785	16.733	22.141	0.125	21.792	40.172
4	17.698	47.808	41.232	37.767	19.585	25.779	0.133	25.640	47.638
5	17.698	51.215	44.145	40.596	21.177	27.744	0.144	27.601	51.034
6	17.698	52.423	45.147	41.651	21.827	28.491	0.153	28.318	52.241
7	17.698	52.826	45.455	41.979	22.030	28.718	0.161	28.526	52.645
8	17.698	52.946	45.526	42.028	22.049	28.740	0.169	28.541	52.767
9	17.698	52.971	45.520	41.975	21.995	28.685	0.178	28.484	52.794
10	17.698	52.967	45.492	41.889	21.915	28.603	0.186	28.402	52.793
11	17.698	52.959	45.462	41.794	21.827	28.512	0.194	28.313	52.787
12	17.698	52.953	45.435	41.700	21.739	28.420	0.201	28.222	52.784
13	17.698	52.952	45.411	41.608	21.652	28.327	0.208	28.132	52.785
14	17.698	52.954	45.391	41.519	21.566	28.235	0.215	28.041	52.790
15	17.698	52.959	45.372	41.431	21.480	28.141	0.221	27.949	52.798
16	17.698	52.965	45.355	41.342	21.392	28.043	0.225	27.854	52.806
17	17.698	52.966	45.333	41.246	21.298	27.937	0.229	27.750	52.810
18	17.698	52.948	45.295	41.128	21.187	27.809	0.231	27.627	52.794
19	17.698	52.874	45.212	40.954	21.037	27.632	0.232	27.459	52.723
20	17.698	52.656	45.008	40.643	20.799	27.346	0.230	27.190	52.509
21	17.698	52.081	44.499	40.014	20.367	26.819	0.226	26.689	51.939
22	17.698	50.628	43.233	38.659	19.526	25.776	0.217	25.677	50.493
23	17.698	47.082	40.174	35.749	17.937	23.706	0.203	23.598	46.962
24	15.24	40.277	34.440	30.541	15.634	20.681	0.194	20.326	40.184
25 - top	20.32	18.771	15.883	13.784	6.812	9.560	0.076	9.340	18.728

**Table 2-4—3-D Nodal Burnups (GWd/MTU) for Select Assemblies,
 Equilibrium Cycle, EOC (547 EFPD)**

Axial Layer	Node Height (cm)	ASSEMBLY (CORE LOCATION)							
		F17	P16	J09	R08	E07	J06	N05	M01
2 - bottom	15.24	21.341	18.678	21.301	16.018	19.233	10.026	19.129	21.281
3	15.24	45.379	40.190	45.362	35.101	40.156	21.770	40.046	45.252
4	17.698	53.742	47.663	53.695	41.730	47.180	25.248	47.301	53.585
5	17.698	57.513	51.060	57.343	44.787	50.475	27.112	50.620	57.346
6	17.698	58.880	52.264	58.638	45.897	51.716	27.811	51.853	58.711
7	17.698	59.357	52.664	59.068	46.228	52.123	28.019	52.245	59.190
8	17.698	59.513	52.782	59.193	46.260	52.204	28.038	52.309	59.348
9	17.698	59.558	52.806	59.216	46.181	52.163	27.991	52.249	59.395
10	17.698	59.570	52.801	59.209	46.065	52.080	27.922	52.146	59.409
11	17.698	59.575	52.793	59.198	45.940	51.985	27.849	52.030	59.416
12	17.698	59.584	52.787	59.190	45.814	51.888	27.778	51.913	59.427
13	17.698	59.597	52.785	59.188	45.691	51.793	27.709	51.796	59.442
14	17.698	59.615	52.788	59.191	45.570	51.700	27.642	51.680	59.463
15	17.698	59.638	52.795	59.198	45.450	51.607	27.576	51.564	59.488
16	17.698	59.662	52.802	59.206	45.328	51.509	27.510	51.442	59.514
17	17.698	59.679	52.804	59.209	45.195	51.398	27.437	51.306	59.534
18	17.698	59.673	52.785	59.190	45.033	51.251	27.344	51.132	59.530
19	17.698	59.602	52.710	59.105	44.797	51.019	27.203	50.871	59.461
20	17.698	59.363	52.486	58.853	44.388	50.592	26.949	50.408	59.226
21	17.698	58.720	51.898	58.178	43.585	49.736	26.448	49.487	58.586
22	17.698	57.104	50.424	56.461	41.895	47.958	25.420	47.549	56.978
23	17.698	53.193	46.860	51.923	38.282	44.299	23.374	43.049	53.080
24	15.24	45.553	40.061	41.135	32.044	38.014	20.402	32.890	45.465
25 - top	20.32	21.434	18.646	18.141	14.292	18.139	9.416	14.380	21.393

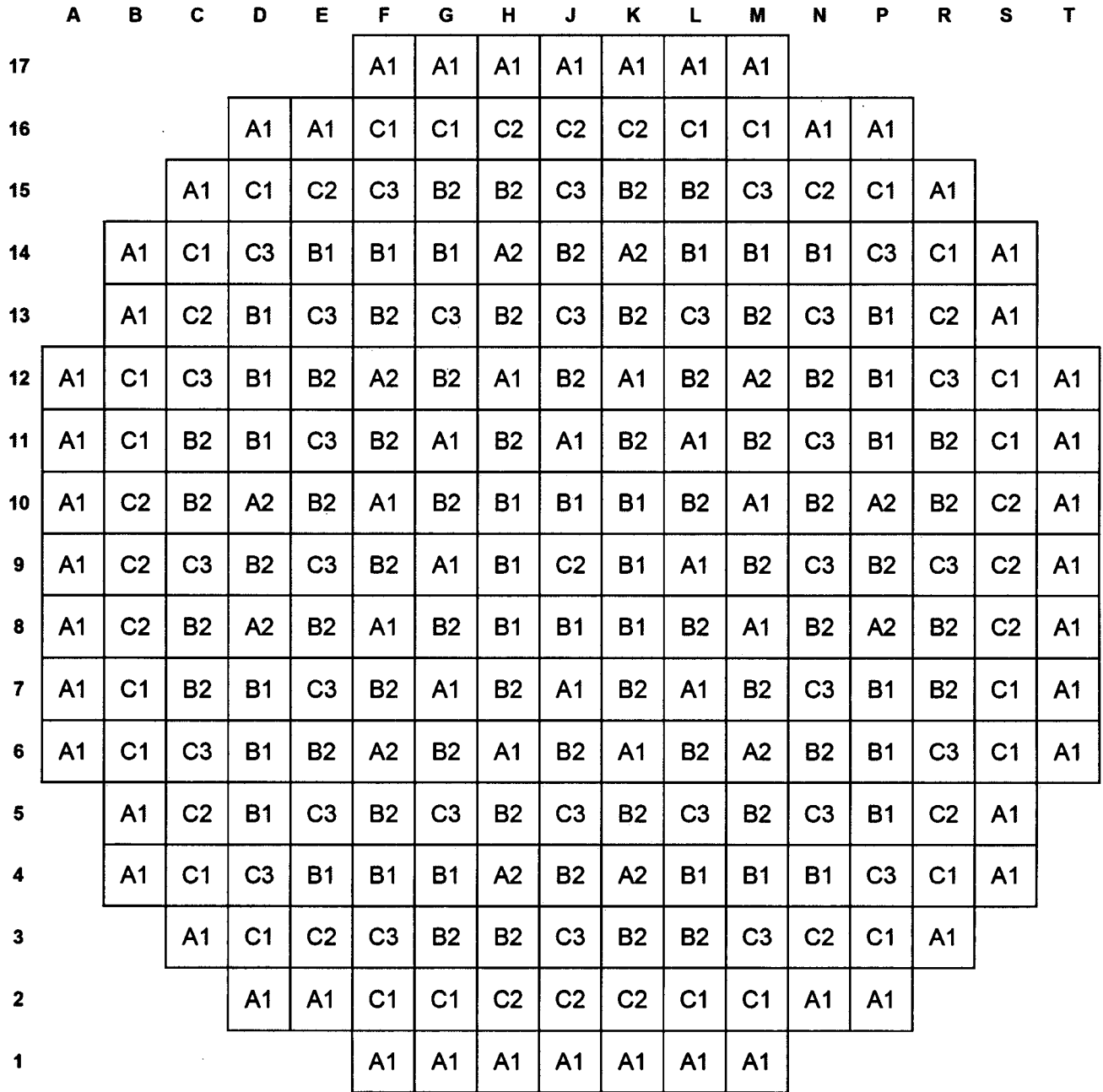
Table 2-5—Cycle 1 Axial Temperature Profiles, BOC and EOC

Axial Layer	Node Height (cm)	BOC (4 EFPD)		EOC (547 EFPD)	
		Fuel Temp (°F)	Mod Temp (°F)	Fuel Temp (°F)	Mod Temp (°F)
2 - BOTTOM	15.24	810.3	564.1	774.0	564.0
3	15.24	1066.9	565.9	961.3	565.4
4	17.698	1103.3	568.6	1041.9	567.8
5	17.698	1131.1	571.7	1088.5	570.6
6	17.698	1151.9	574.9	1111.2	573.7
7	17.698	1166.1	578.1	1121.8	576.7
8	17.698	1175.1	581.3	1126.7	579.8
9	17.698	1179.9	584.5	1129.2	582.9
10	17.698	1181.3	587.7	1130.9	585.9
11	17.698	1180.0	590.9	1132.3	588.9
12	17.698	1176.4	593.9	1133.9	591.8
13	17.698	1170.8	596.9	1135.8	594.7
14	17.698	1163.5	599.8	1137.8	597.6
15	17.698	1154.6	602.7	1140.0	600.4
16	17.698	1144.1	605.4	1142.3	603.2
17	17.698	1132.1	608.0	1144.5	606.0
18	17.698	1118.2	610.6	1145.9	608.7
19	17.698	1102.4	613.0	1145.7	611.4
20	17.698	1084.4	615.3	1141.9	614.0
21	17.698	1063.6	617.4	1131.0	616.5
22	17.698	1039.6	619.5	1107.2	618.9
23	17.698	1012.6	621.3	1060.9	621.1
24	15.24	985.5	622.9	988.7	622.8
25 - TOP	20.32	799.4	624.1	813.6	624.0

Table 2-6—Equilibrium Cycle Axial Temperature Profiles, BOC and EOC

Axial Layer	Node Height (cm)	BOC (4 EFPD)		EOC (547 EFPD)	
		Fuel Temp (°F)	Mod Temp (°F)	Fuel Temp (°F)	Mod Temp (°F)
2 - BOTTOM	15.24	715.7	563.8	763.5	563.9
3	15.24	907.4	565.1	946.8	565.5
4	17.698	949.9	567.2	1003.8	568.0
5	17.698	978.3	569.6	1032.4	570.9
6	17.698	999.2	572.2	1044.7	573.9
7	17.698	1017.4	574.9	1050.6	576.9
8	17.698	1034.8	577.6	1053.9	580.0
9	17.698	1051.8	580.4	1056.4	583.0
10	17.698	1068.3	583.2	1058.6	585.9
11	17.698	1084.2	586.1	1060.7	588.9
12	17.698	1099.1	589.1	1062.8	591.8
13	17.698	1112.9	592.0	1065.0	594.6
14	17.698	1125.3	595.0	1067.1	597.4
15	17.698	1136.0	598.0	1069.2	600.2
16	17.698	1144.8	601.0	1071.3	602.9
17	17.698	1151.4	604.0	1073.3	605.6
18	17.698	1155.3	606.9	1075.0	608.3
19	17.698	1155.8	609.8	1076.0	610.9
20	17.698	1152.0	612.6	1075.4	613.5
21	17.698	1141.9	615.3	1071.2	615.9
22	17.698	1122.0	617.9	1059.1	618.3
23	17.698	1085.5	620.3	1030.0	620.5
24	15.24	1031.6	622.2	977.1	622.3
25 - TOP	20.32	799.9	623.5	804.2	623.5

Figure 2-1—Cycle 1 Core Loading Map



A1	2.25 wt% CZE with No Gd
A2	2.25 wt% CZE with 4 rods at 4 wt% Gd
B1	2.70 wt% CZE with 8 rods at 8 wt% and 4 rods at 4 wt% Gd
B2	2.70 wt% CZE with 12 rods at 8 wt% and 4 rods at 2 wt% Gd

C1	3.25 wt% CZE with 4 rods at 6 wt% and 4 rods at 2 wt% Gd
C2	3.25 wt% CZE with 8 rods at 6 wt% and 4 rods at 2 wt% Gd
C3	3.25 wt% CZE with 12 rods at 8 wt% and 4 rods at 2 wt% Gd

Figure 2-2—Equilibrium Cycle Core Loading Map

	A	B	C	D	E	F	G	H	J	K	L	M	N	P	R	S	T
17						XX8 S 8 3	XX7 G16 2	XX10 C12 2	XX7 S12 2	XX10 C 6 2	XX7 L16 2	XX9 P13 2					
16			XX8 H16 2	XX6 D15 2	XX7 F16	XX7 G16	XX8 H16	XX7 M16 1	XX8 K16	XX7 L16	XX7 M16	XX6 P15 2	XX8 K16 2				
15		XX9 D13 2	XX6 D15	XX7 G16 1	XX10 F15	XX10 C12 1	XX6 D15 1	XX6 P15 1	XX7 S12 1	XX10 R12 1	XX10 M15	XX7 L16 1	XX6 P15	XX9 N14 2			
14	XX8 B10 2	XX6 C14	XX8 H16 1	XX9 E14	XX3 D 9 1	XX1 G14	XX4 E10 1	XX3 J14	XX4 N10 1	XX1 L14	XX5 K11 1	XX9 N14	XX8 S10 1	XX6 R14	XX8 S10 2		
13	XX6 C14 2	XX7 B11 1	XX9 D13	XX1 G14 1	XX3 F13	XX3 E12 1	XX4 H13	XX5 L10 1	XX4 K13	XX3 N12 1	XX3 M13	XX1 P11 1	XX9 P13	XX7 S11 1	XX6 R14 2		
12	XX9 E14 2	XX7 B12	XX10 C12	XX5 G10 1	XX3 E12	XX3 F 9 1	XX2 G12	XX2 F11 1	XX3 J12	XX1 L14 1	XX2 L12	XX3 J12 1	XX3 N12	XX3 J14 1	XX10 R12	XX7 S12	XX8 H 2 3
11	XX7 B11 2	XX7 B11	XX10 F15 1	XX1 D11	XX3 F13 1	XX2 F11	XX2 G12 1	XX5 H11	XX9 P13 1	XX5 K11	XX2 M11 1	XX2 M11	XX3 M13 1	XX1 P11	XX10 M15 1	XX7 S11	XX7 S11 2
10	XX10 M 3 2	XX8 B10	XX7 F16 1	XX4 H13 1	XX4 E10	XX1 D11 1	XX5 G10	XX9 D13 1	XX8 K16 1	XX9 N14 1	XX5 L10	XX2 L12 1	XX4 N10	XX4 K13 1	XX6 R14 1	XX8 S10	XX10 M15 2
9	XX7 F16 2	XX7 B12 1	XX6 C14 1	XX3 D 9	XX5 H11 1	XX3 F 9	XX9 E14 1	XX8 B10 1	XX7 S 6 2	XX8 S 8 1	XX9 N 4 1	XX3 M 9	XX5 K 7 1	XX3 P 9	XX6 R 4 1	XX7 S 6 1	XX7 M 2 2
8	XX10 F 3 2	XX8 B 8	XX6 C 4 1	XX4 H 5 1	XX4 E 8	XX2 G 6 1	XX5 G 8	XX9 E 4 1	XX8 H 2 1	XX9 P 5 1	XX5 L 8	XX1 P 7 1	XX4 N 8	XX4 K 5 1	XX7 M 2 1	XX8 S 8	XX10 F15 2
7	XX7 B 7 2	XX7 B 7	XX10 F 3 1	XX1 D 7	XX3 F 5 1	XX2 F 7	XX2 F 7	XX5 H 7	XX9 D 5 1	XX5 K 7	XX2 L 6 1	XX2 M 7	XX3 M 5 1	XX1 P 7	XX10 M 3 1	XX7 S 7	XX7 S 7 2
6	XX8 K16 3	XX7 B 6	XX10 C 6	XX3 J 4 1	XX3 E 6	XX3 J 6 1	XX2 G 6	XX1 G 4 1	XX3 J 6	XX2 M 7 1	XX2 L 6	XX3 M 9 1	XX3 N 6	XX5 L 8 1	XX10 R 6	XX7 S 6	XX9 N 4 2
5	XX6 C 4 2	XX7 B 7 1	XX9 D 5	XX1 D 7 1	XX3 F 5	XX3 E 6 1	XX4 H 5	XX5 G 8 1	XX4 K 5	XX3 N 6 1	XX3 M 5	XX1 L 4 1	XX9 P 5	XX7 S 7 1	XX6 R 4 2		
4	XX8 B 8 2	XX6 C 4	XX8 B 8 1	XX9 E 4	XX5 H 7 1	XX1 G 4	XX4 E 8 1	XX3 J 4	XX4 N 8 1	XX1 L 4	XX3 P 9 1	XX9 N 4	XX8 K 2 1	XX6 R 4	XX8 S 8 2		
3		XX9 E 4 2	XX6 D 3	XX7 G 2 1	XX10 F 3	XX10 C 6 1	XX7 B 6 1	XX6 D 3 1	XX6 P 3 1	XX10 R 6 1	XX10 M 3	XX7 L 2 1	XX6 P 3	XX9 P 5 2			
2			XX8 H 2 2	XX6 D 3 2	XX7 F 2	XX7 G 2	XX8 H 2	XX7 F 2 1	XX8 K 2	XX7 L 2	XX7 M 2	XX6 P 3 2	XX8 K 2 2	Fuel Type Initial Core Location Number of Burns			
1						XX9 D 5 2	XX7 G 2 2	XX10 R12 2	XX7 B 6 2	XX10 R 6 2	XX7 L 2 2	XX8 B10 3					

XX1	4.30 wt% CZE with 12 rods at 8 wt% and 8 rods at 2 wt% Gd
XX2	4.30 wt% CZE with 16 rods at 8 wt% Gd
XX3	4.30 wt% CZE with 16 rods at 8 wt% and 5 rods at 2 wt% Gd
XX4	4.30 wt% CZE with 16 rods at 8 wt% and 5 rods at 4 wt% Gd
XX5	4.30 wt% CZE with 20 rods at 8 wt% Gd

XX6	4.80 wt% CZE with 8 rods at 2 wt% Gd
XX7	4.80 wt% CZE with 12 rods at 8 wt% Gd
XX8	4.80 wt% CZE with 12 rods at 8 wt% and 8 rods at 2 wt% Gd
XX9	4.80 wt% CZE with 16 rods at 8 wt% and 5 rods at 4 wt% Gd
XX10	4.80 wt% CZE with 20 rods at 8 wt% Gd



UNITED STATES
NUCLEAR REGULATORY COMMISSION
WASHINGTON, D.C. 20555-0001

August 7, 2008

Mr. Ronnie L. Gardner
AREVA NP Inc.
3315 Old Forest Road
P.O. Box 10935
Lynchburg, VA 24506-0935

SUBJECT: SECOND REQUEST FOR ADDITIONAL INFORMATION REGARDING ANP-10286P, "US EPR ROD EJECTION ACCIDENT METHODOLOGY TOPICAL REPORT"

Dear Mr. Gardner:

By letter dated November 20, 2007, which can be accessed through NRC'S Agencywide Document Access and Management (ADAMS) Accession No. ML073310620, AREVA NP submitted for U.S. Nuclear Regulatory Commission (NRC) staff review Topical Report ANP-10286P, "Rod Ejection Accident Methodology." The staff is reviewing the topical report and has determined that additional information is required. Our questions are provided in the enclosure.

A draft of the second request for additional information (RAI) was provided to you on June 25, 2008 (ADAMS Accession No. ML081850297), and discussed with your staff in a post submittal telephone conference on July 2, 2008. As a result of that discussion, the staff agreed to delete the last draft RAI question and renumber the remaining questions for consistency with the first set of RAI.

In addition, AREVA NP requested and the staff agreed that AREVA NP will provide responses to the RAIs within 60 days of the date of this letter.

If you have any questions regarding this matter, I may be reached at 301-415-3361.

Sincerely,

A handwritten signature in black ink, appearing to read "Getachew Tesfaye, Sr.", written in a cursive style.

Getachew Tesfaye, Sr., Project Manager
EPR Projects Branch
Division of New Reactor Licensing
Office of New Reactors

Docket No. 52-020

Enclosure:
Request for Additional Information

cc: DC AREVA – EPR Mailing List

DC AREVA - EPR Mailing List

cc:

Mr. Glenn H. Archinoff
AECL Technologies
481 North Frederick Avenue
Suite 405
Gaithersburg, MD 20877

Mr. Robert E. Sweeney
IBEX ESI
4641 Montgomery Avenue
Suite 350
Bethesda, MD 20814

Marty Bowling
NUMARK Project Manager
86 WestBay Drive
Kilmarnock, VA 22482

Russ Well
Advisory Engineering
New Plants Development
3315 Forest Road
P.O. Box 10935
Mail Stop OF-34
Lynchburg, VA 24506

Ms. Michele Boyd
Legislative Director
Energy Program
Public Citizens Critical Mass Energy
and Environmental Program
215 Pennsylvania Avenue, SE
Washington, DC 20003

Mr. Gary Wright, Director
Division of Nuclear Facility Safety
Illinois Emergency Management Agency
1035 Outer Park Drive
Springfield, IL 62704

Mr. Ray Ganthner
Senior Vice President
AREVA, NP, Inc. 3315
Old Forest Road
P.O. Box 10935
Lynchburg, VA 24506-0935

Dr. Charles L. King
Licensing Manager, IRIS Project
Westinghouse Electric Company
Science and Technology Department
20 International Drive
Windsor, CT 06095

Ms. Sherry McFaden
Framatome NP, Inc.
3315 Old Forest Road, OF-16
Lynchburg, VA 24501

Mr. Steve Seitz
AREVA
100 Dean Road
East Lyme, CT 06333

DC AREVA - EPR Mailing List

Email

alex.miller@hse.gsi.gov.uk (Alex Miller)
APH@NEI.org (Adrian Heymer)
awc@nei.org (Anne W. Cottingham)
bennettS2@bv.com (Steve A. Bennett)
bob.brown@ge.com (Robert E. Brown)
BrinkmCB@westinghouse.com (Charles Brinkman)
carey.fleming@constellation.com (Carey Fleming)
chris.maslak@ge.com (Chris Maslak)
cwaltman@roe.com (C. Waltman)
david.hinds@ge.com (David Hinds)
david.lewis@pillsburylaw.com (David Lewis)
dlochbaum@UCSUSA.org (David Lochbaum)
erg-xl@cox.net (Eddie R. Grant)
frankq@hursttech.com (Frank Quinn)
gcesare@enercon.com (Guy Cesare)
greshaja@westinghouse.com (James Gresham)
james.beard@gene.ge.com (James Beard)
james.p.mcquighan@constellation.com (Jim McQuighan)
jason.parker@pillsburylaw.com (Jason Parker)
jgutierrez@morganlewis.com (Jay M. Gutierrez)
jim.riccio@wdc.greenpeace.org (James Riccio)
JJD1@nrc.gov (John Donohue)
JJNesrsta@cpsenergy.com (James J. Nesrsta)
John.O'Neill@pillsburylaw.com (John O'Neill)
Joseph_Hegner@dom.com (Joseph Hegner)
junichi_uchiyama@mnes-us.com (Junichi Uchiyama)
KSutton@morganlewis.com (Kathryn M. Sutton)
kwaugh@impact-net.org (Kenneth O. Waugh)
Marc.Brooks@dhs.gov (Marc Brooks)
maria.webb@pillsburylaw.com (Maria Webb)
mark.beaumont@wsms.com (Mark Beaumont)
matias.travieso-diaz@pillsburylaw.com (Matias Travieso-Diaz)
media@nei.org (Scott Peterson)
mike_moran@fpl.com (Mike Moran)
MSF@nei.org (Marvin Fertel)
mwetterhahn@winston.com (M. Wetterhahn)
nirsnet@nirs.org (Michael Mariotte)
patriciaL.campbell@ge.com (Patricia L. Campbell)
paul.gaukler@pillsburylaw.com (Paul Gaukler)
Paul@beyondnuclear.org (Paul Gunter)
pshastings@duke-energy.com (Peter Hastings)
RJB@NEI.org (Russell Bell)
RKTemple@cpsenergy.com (R.K. Temple)
roberta.swain@ge.com (Roberta Swain)

DC AREVA - EPR Mailing List

Ronda.pederson@areva.com (Ronda Pederson)
sandra.sloan@areva.com (Sandra Sloan)
sfrantz@morganlewis.com (Stephen P. Frantz)
steven.hucik@ge.com (Steven Hucik)
tkkibler@scana.com (Tria Kibler)
tom.miller@hq.doe.gov (Tom Miller)
trsmith@winston.com (Tyson Smith)
Vanessa.quinn@dhs.gov (Vanessa Quinn)
VictorB@bv.com (Bill Victor)
vijukrp@westinghouse.com (Ronald P. Vijuk)
Wanda.K.Marshall@dom.com (Wanda K. Marshall)
wayne.marquino@ge.com (Wayne Marquino)
whorin@winston.com (W. Horin)

SECOND REQUEST FOR ADDITIONAL INFORMATION (RAI)

ANP-10286P, "U. S. EPR ROD EJECTION ACCIDENT

METHODOLOGY TOPICAL REPORT"

DOCKET NO. 52-020

- RAI-3 Section 2.1.1 – Please provide the basis (e.g. experimental, mechanistic, etc.) for the oxide buildup model referred to in the report.
- RAI-4 Section 2.3 – Please provide a more detailed discussion concerning TFGR and FGRF.
- RAI-5 Section 4.1.4 – (Table 4-1) The knowledge ratio (KR) for fuel feedback is given as 96. Doppler feedback is generally ± 10 percent at best. Please explain how the uncertainty in the DTC is determined throughout the burnup range?
- RAI-6 Table 4-1 – Please explain what method is used to determine β_{eff} and the associated uncertainty.
- RAI-7 Section 4.1.6 – Please elaborate on the last sentence in Section 4.1.6 to explain how and why the sensitivity of the trip reactivity to "at power" events determines the level of conservatism of the trip reactivity.
- RAI-8 Section 4.1.10 – Please clarify whether there is a provision to account for direct heating of the coolant due to the increase in neutron and gamma ray flux during the transient.
- RAI-9 Section 4.2.8 – When MDNBR is exceeded, the topical report stated that static heat transfer, CHF, and failure are conservatively assumed. Please provide justification for this position.
- RAI-10 Section 6.2.1 – Please clarify whether the lead time constant and the lagged signal time constant are consistent with the reactor design. Provide their respective values.
- RAI-11 Section 6.2.3 – Please provide a typical magnitude of the adjustment factors used in sensitivity analyses.
- RAI-12 Section 6.2.4 – Does NEMO-K calculate the temperatures, or are they calculated by LYNXT and passed to NEMO-K? If they are passed to NEMO-K, is the connection a dynamic one? Has the relationship developed for T_{eff} been validated against another method? If another method has been used, please describe it and discuss the accuracy of that method.
- RAI-13 Section 6.3.2 – Is there a case in which the power profile within the pellet changes during the transient? If there is no provision for this change in profile, what is the effect of not allowing the change?

- RAI-14 Section 6.3.3.1 – The CG/TDP model was validated for BOL conditions against various methods. Has this same validation also been carried out for EOL conditions, or is the validation at EOL conditions limited to only a comparison with COPERNIC?
- RAI-15 Section 6.3.3.2 – Table 6-3 summarizes the comparison between LYNXT and COPERNIC. Please elaborate on how the results are determined.
- RAI-16 Section 6.3.4 – Is there a standard set of data for the thermal properties of the fuel and clad, gap conductance, and radial power profile that are used as input to these analyses, or are they calculated as needed by one of the detail codes? If there is a standard set please list them or give appropriate references.
- RAI-17 Section 7.0 – To what do the uncertainties in Table 7-1 refer? REA analysis values seem to be further from PRISM range values than uncertainties. Please provide proper references and explanations.
- RAI-18 Section 7.1.3 – Is the value DTC uncertainty of ± 10 percent equally valid for BOL and EOL conditions? Please explain its burn-up dependency.
- RAI-19 Section 7.1.7 – Are combinations of the uncertainties listed in Table 7-3 evaluated when performing uncertainty analyses? If so, please explain what combinations are evaluated.
- RAI-20 Section 7.2.1 – Have sensitivity calculations been carried out using different node selections? If so, explain the node sensitivity analysis results.
- RAI-21 Section 7.2.4 – Please clarify whether NEMO-K and LYNXT use the same nodal distribution.
- RAI-22 Section 7.2.5 – In Fig 7-10 the no-gadolinia case does not bound the gadolinia cases over the entire time span, which appears to be contradictory to statements in Section 7.2.5. Please explain this discrepancy.
- RAI-23 Section 8.5 – Please provide more information as to why no fuel rod failures are reported. For example, is it due to: a reactor trip terminating the transient, negative feedback reversing the trend, thermal inertia in the system reducing the temperatures, all of the above, etc.?
- RAI-24 Please list the model assumptions used to generate the LYNXT to COPERNIC transient model comparison.
- RAI-25 Supply and describe a flowchart on code and data process linkages that explain the analysis flow path for the REA event.
- RAI-26 Provide an event timeline and description for various REA events (include events that trip and events that don't trip the plant) to explain the parameter responses. Additionally, please explain the process by which the incore DNBR trip time estimates were made.

- RAI-27 Provide a description of the thermal properties tables' inputs to LYNXT.
- RAI-28 Please provide an example to describe the process by which the failed fuel rod census is performed using the transient pin to static pin power ratios.
- RAI-29 Provide an explanation about the calibration for the high rate flux trip and provide a sample response of the rate lagged filter. (Section 6.2.1, 6.2.1.2, Table 8-1).
- RAI-30 Section 7.2.4 – Please explain why the assembly pin power radial power distribution in LYNXT is conservative for the assumed power distribution within the fuel assembly of interest.
- RAI-31 Please provide an explanation for the discontinuities of the LYNXT results relative to the COPERNIC temperature transients in Figures 6-23 and 6-27.
- RAI-32 Please explain why the BOC HZP was not analyzed in LYNXT in Sections 8.1 and 8.3.



October 3, 2008
NRC:08:078

Document Control Desk
U.S. Nuclear Regulatory Commission
Washington, D.C. 20555-0001

Response to a Second Request for Additional Information Regarding ANP-10286P, "U.S. EPR Rod Ejection Accident Methodology Topical Report"

- Ref. 1: Letter, Ronnie L. Gardner (AREVA NP Inc.) to Document Control Desk (NRC), "Request for Review and Approval of ANP-10286P, 'U.S. EPR Rod Ejection Accident Methodology Topical Report'," NRC:07:065, November 20, 2007.
- Ref. 2: Letter, Getachew Tesfaye (NRC) to Ronnie L. Gardner (AREVA NP Inc.), "Second Request for Additional Information Regarding ANP-10286P, 'U.S. EPR Rod Ejection Accident Methodology Topical Report'," August 7, 2008.
- Ref. 3: Letter, Getachew Tesfaye (NRC) to Sandra M. Sloan (AREVA NP Inc.), "AREVA NP Inc. - U.S. EPR Standard Design Certification Application Review Schedule," March 26, 2008.

AREVA NP Inc. (AREVA NP) requested the NRC's review and approval of topical report ANP-10286P, "U.S. EPR Rod Ejection Accident Methodology Topical Report" in Reference 1. The NRC provided a second Request for Additional Information (RAI) regarding this topical report in Reference 2. The response to the RAI is enclosed with this letter, ANP-10286Q2P, "Response to Second Request for Additional Information – ANP-10286P, 'U.S. EPR Rod Ejection Accident Methodology Topical Report'."

AREVA NP references the topical report ANP-10286P in the Final Safety Analysis Report for the U.S. EPR. Reference 3 states that the NRC plans to complete its review of the topical report and issue the draft safety evaluation by May 31, 2009. AREVA NP understands that this timely response to the RAI supports the scheduled deliverable of the draft safety evaluation.

AREVA NP considers some of the material contained in the attachments to this letter to be proprietary. As required by 10 CFR 2.390(b), an affidavit is enclosed to support the withholding of the information from public disclosure. Proprietary and non-proprietary versions of the response are provided on the enclosed compact disks (CDs).

If you have any questions related to this submittal, please contact Ms. Sandra M. Sloan, Regulatory Affairs Manager for New Plants. She may be reached by telephone at 434-832-2369 or by e-mail at sandra.sloan@areva.com.

Sincerely,

A handwritten signature in cursive script that reads "Ronnie L. Gardner".

Ronnie L. Gardner, Manager
Corporate Regulatory Affairs
AREVA NP Inc.

AREVA NP INC.

An AREVA and Siemens company

Enclosures

cc: J. Rycyna
G. Tesfaye
Docket No. 52-020

accordance with 10 CFR 2.390. The information for which withholding from disclosure is requested qualifies under 10 CFR 2.390(a)(4) "Trade secrets and commercial or financial information".

6. The following criteria are customarily applied by AREVA NP to determine whether information should be classified as proprietary:

- (a) The information reveals details of AREVA NP's research and development plans and programs or their results.
- (b) Use of the information by a competitor would permit the competitor to significantly reduce its expenditures, in time or resources, to design, produce, or market a similar product or service.
- (c) The information includes test data or analytical techniques concerning a process, methodology, or component, the application of which results in a competitive advantage for AREVA NP.
- (d) The information reveals certain distinguishing aspects of a process, methodology, or component, the exclusive use of which provides a competitive advantage for AREVA NP in product optimization or marketability.
- (e) The information is vital to a competitive advantage held by AREVA NP, would be helpful to competitors to AREVA NP, and would likely cause substantial harm to the competitive position of AREVA NP.

The information in the Document is considered proprietary for the reasons set forth in paragraphs 6(b) and 6(c) above.

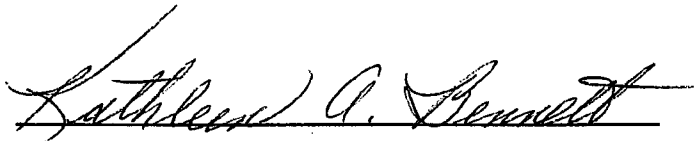
7. In accordance with AREVA NP's policies governing the protection and control of information, proprietary information contained in this Document has been made available, on a limited basis, to others outside AREVA NP only as required and under suitable agreement providing for nondisclosure and limited use of the information.

8. AREVA NP policy requires that proprietary information be kept in a secured file or area and distributed on a need-to-know basis.

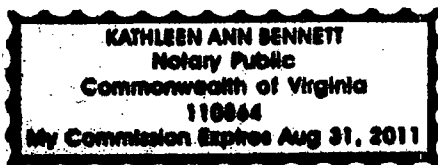
9. The foregoing statements are true and correct to the best of my knowledge, information, and belief.



SUBSCRIBED before me this 3rd
day of October, 2008.



Kathleen A. Bennett
NOTARY PUBLIC, COMMONWEALTH OF VIRGINIA
MY COMMISSION EXPIRES: 8/31/2011



Response to

Second Request for Additional Information – ANP-10286P

“U.S. EPR Rod Ejection Accident Methodology Topical Report”

**Response to Second Request for Additional Information – ANP-10286P
“U.S. EPR Rod Ejection Accident methodology Topical Report”**

RAI-3. *Section 2.1.1 – Please provide the basis (e.g. experimental, mechanistic, etc.) for the oxide buildup model referred to in the report.*

Response to RAI-3:

The corrosion calibration database is described in Section 8.1.3.2 of BAW-10231PA, COPERNIC Fuel Rod Design Computer Code (Topical Report Reference 2). A comparison plot of measured and predicted is provided in BAW-10231PA, Figure 8-15. BAW-10231PA, Figure 8-16 provides the oxide thickness as a function of rod average burnup. For hydriding, an experimental validation is given in Section 8.2.3.2, Figure 8-26, and Figure 8-27 of BAW-10231PA. The maximum corrosion layer thickness of 35 μm referenced in Topical Report (TR) Section 2.1.1 was predicted from the maximum burnup point of the fuel rod performance evaluation under an enveloping power history.

RAI-4. *Section 2.3 – Please provide a more detailed discussion concerning TFGR and FGFR*

Response to RAI-4:

Conformance with Standard Review Plan (SRP) 4.2 (TR Reference 1), regarding radiological fission gas release (FGR) dependence on prompt fuel enthalpy dependence, requires a coupling between fuel failures, local energy depositions, and radiological releases. TFGR is the Transient FGR expression from SRP 4.2, Appendix B, Section D. The number of pins that fail due to exceeding the DNBR limit, F, is predicted from the NEMO-K neutronics and LYNXT thermal hydraulics calculations. The maximum allowed number of fuel rods that can fail due only to departure from nucleate boiling ratio (DNBR) failures, A, is determined by radiological consequence calculations in accordance with Regulatory Guide 1.183 and SRP 15.0.3. This analysis has a percent of fission gas release from the pellets specified to determine the radiological inventory of a particular pin to determine the dose from the release. From a dose calculation for a DNBR failure, a correlation can be made between the dose from additional TFGR and a DNBR failure. The correlation is used to determine the equivalent number of additional rods to be considered failed, FGFR. The equivalent total number of fuel rods failed (EQP) is the sum of those failed due to DNBR, F, and the equivalent number of additional rods due to the TFGR.

For example, if the base release inventory for a fuel rod failure exceeding DNBR is 10 percent FGR and the enthalpy rise of the pin yields a TFGR of 5 percent, then for this fuel rod, the total fission gas release would be 15 percent. This amount of release is equivalent to 1.5 failures for the value of EQP for this pin rather than 1.0. This calculation would be repeated for all fuel rods that have an enthalpy rise greater than 31.2 $\Delta\text{cal/g}$. The sum of the individual rod EQPs is then compared against the value of A. For the U.S. EPR, the maximum number of equivalent failures is 30 percent of the core (i.e., 19,159 fuel rods) and no additional fuel failures needed to be considered because the peak enthalpy rise for all the rod ejection cases was less than 31.2 $\Delta\text{cal/g}$.

RAI-5. Section 4.1.4 – (Table 4-1) The knowledge ratio (KR) for fuel feedback is given as 96. Doppler feedback is generally ± 10 percent at best. Please explain how the uncertainty in the DTC is determined throughout the burnup range?

Response to RAI-5:

A 10 percent uncertainty was determined based on the underprediction of the Doppler Power Coefficients (DPC) compared to measurements. Table 5-1 lists the DPC predictions to measurements for NEMO from the NEMO computer code in BAW-10180A-01, NEMO – Nodal Expansion Method Optimized (Reference 1) and for NEMO using the fuel temperature model with T_{eff} in TR Section 6.2.4. The predictions of these models underestimate the measured magnitude of the DPC by approximately 20 percent with either model. The DPC is proportional to the Doppler Temperature Coefficient (DTC) with the proportional constant being the ratio of the fuel temperature change to the percent power change. The bias could be from either the DTC or the fuel temperature predictions. These benchmarks are performed at beginning of cycle (BOC) for a cycle 1 core which has less than 6 EFPD of irradiation. Because the fuel properties for fuel with zero burnup are well characterized, it is unlikely that every pin in the core is biased low in the fuel temperature predictions. Therefore, a significant portion of underprediction in the DPC magnitude is probably due to the DTC component of the DPC. Having a lower prediction for the magnitude of the DTC is conservative for the ejected rod application due to a resultant lower negative reactivity feedback. Due to this conservatism and the 10 percent additional uncertainty, sufficient conservatism exists in the model, and no additional penalty was assessed as a function of burnup.

Table 5-1—Doppler Power Coefficient Comparisons to Measured

Power Level, %	Measured DPC, pcm/%full power	NEMO with TACO3 Average Fuel Temperature DPC (% Difference $\{(M-P)/M*100\}$)	NEMO with COPERNIC dynamic fuel rod model and T_{eff} DPC (% Difference $\{(M-P)/M*100\}$)
30	-13.6	-11.1 (-18%)	[]
50	-12.7	-10.4 (-18%)	[]
75	-11.6	-9.2 (-21%)	[]

References for RAI-5:

1. BAW-10180A-01, NEMO – Nodal Expansion Method Optimized, Revision 1, July 1993.

RAI-6. Table 4-1 – Please explain what method is used to determine β_{eff} and the associated uncertainty.

Response to RAI-6:

The method to calculate the core average β_{eff} is the sum of the beta fractions for each of the major fissionable isotopes (i.e., U-235, U-238, Pu-239, Pu-241) weighted by the respective fission rates for each simulator node. An effectiveness factor of [] is applied. The core average betas are scaled to bound the uncertainty and the amount of excess margin for future designs and these scaled betas are input to NEMO-K to use for the transient. TR Sections

4.1.5 and 7.1.4 provide the rationale for this uncertainty. Also, BAW-10120PA "Comparison of Core Physics Calculations with Measurements," (Reference 1) Section 3.2.3 describes β_{eff} uncertainties and defines a 5 percent uncertainty for β_{eff} .

References for RAI-6:

1. BAW-10120PA, "Comparison of Core Physics Calculations with Measurements," J. J. Woods et al, July 1979.

RAI-7. *Section 4.1.6 – Please elaborate on the last sentence in Section 4.1.6 to explain how and why the sensitivity of the trip reactivity to "at power" events determines the level of conservatism of the trip reactivity.*

Response to RAI-7:

The last sentence in Section 4.1.6 is intended to address the importance of trip reactivity for the ejected rod event at power even though the Phenomena Importance Ranking Tables (PIRT) analysis did not rate trip reactivity as an important parameter. The insertion of the rods may affect the timing of the severity of the departure from nucleate boiling (DNB) response as core power decreases. The trip reactivity is evaluated in TR Section 7.1.7, Table 7-3 to illustrate the difference between a nominal control rod worth and the rod worth reduced by 9 percent. The reduced scram rod worth simulates a limiting trippable rod worth by reducing the worth by the uncertainty and excluding the ejected rod. The total rod worth uncertainty reduction is 10 percent for shutdown margin calculations; however, the reactivity worth of the inserted bank from which a rod is ejected is increased by more than 15 percent. The net effect on the total tripped worth was 9 percent for the case studied. The sensitivity case showed only a [] percent core power difference at [] percent power. Since the sensitivity is small to trippable worth and the slightly higher power results in a conservative estimate of DNBR, the ejected rod model uses an approximate 10% worth reduction of the remaining banks to be tripped.

RAI-8. *Section 4.1.10 – Please clarify whether there is a provision to account for direct heating of the coolant due to the increase in neutron and gamma ray flux during the transient.*

Response to RAI-8:

The provision to account for direct heating of the coolant is made by depositing into the coolant a fraction of the total power produced. For the U.S. EPR, the fractional heat deposited in the coolant was 2.6 percent of the total power produced. Because this fraction is applied to the power produced with time, the power deposited in the water is proportional to the transient power produced by the pin. This direct heating provision is included in both the NEMO-K and LYNXT simulations.

RAI-9. *Section 4.2.8 – When MDNBR is exceeded, the topical report stated that static heat transfer, CHF, and failure are conservatively assumed. Please provide justification for this position.*

Response to RAI-9:

BAW-10156A (TR Reference 7) addresses a CHF correlation developed from static testing in transient heat transfer analyses. Appendix G of BAW-10156A provides the response to an RAI and justification for performing transient CHF evaluations with transient system boundary conditions and steady-state CHF correlations. BAW-10156A, Appendix Section B.4 (Heat Transfer Correlations) and Appendix pages D-3 through D-6 (logic for selecting the heat transfer mode) provide descriptions of the heat transfer package implemented into the LYNXT computer code.

RAI-10. *Section 6.2.1 – Please clarify whether the lead time constant and the lagged signal time constant are consistent with the reactor design. Provide their respective values.*

Response to RAI-10:

TR Table 8-1 provides the values for the analysis for the lag rate constant and the gain constant. The gain constant is another name for the derivative lead time constant defined in the signal filter equation in TR Section 6.2.1.2. The values used in the sample calculations are both 30 seconds and are specified as inputs for reactor safety analysis. Any modifications to the signal parameter values based on actual circuitry design or implementation will be evaluated for impact on the analysis as indicated in Note b to the ejected rod analysis checklist in TR Table 9-1. A small sensitivity to these constants is shown in the response to question RAI-29 for transients with power changes occurring for less than a second.

RAI-11. *Section 6.2.3 – Please provide a typical magnitude of the adjustment factors used in sensitivity analyses.*

Response to RAI-11:

The result of using the adjustment factors in TR Section 6.2.3 that are used in the sensitivity analysis in TR Section 7.1.7 are shown in TR Table 7-3 in terms of percent change. For fuel conductivity and gap conductance, the relationship between adjustment factors and the uncertainty is given by the equation $(100 + \% \text{ uncertainty})/100$. Because the Doppler coefficient and the rod worth are calculated values by the code, the adjustment factors on the cross sections for Doppler and rod worth require an iteration process to obtain the target percent difference. The equation is an approximation to serve as the initialization point for the iteration process for these factors.

RAI-12. *Section 6.2.4 – Does NEMO-K calculate the temperatures, or are they calculated by LYNXT and passed to NEMO-K? If they are passed to NEMO-K, is the connection a dynamic one? Has the relationship developed for T_{eff} been validated against another method? If another method has been used, please describe it and discuss the accuracy of that method.*

Response to RAI-12:

NEMO-K calculates a dynamic fuel temperature using a 1D concentric radial ring fuel rod model as described in BAW-10221PA (TR Reference 6) and is not dependent upon LYNXT for its fuel and moderator temperature calculations. Both NEMO-K and LYNXT use COPERNIC based fuel and clad properties and both use the same gap conductivity model. The fraction of core power and power distribution versus time from NEMO-K are passed to LYNXT.

The relationship for T-effective temperature (T_{eff}) has been validated with the computer code APOLLO2 described in BAW-10228PA, (Reference 1). The reactivity and U-238 capture rate of several snapshot fuel temperature distributions at steady state conditions and those temperatures expected during a Reactivity Initiated Accident (RIA) event were examined with APOLLO2. Calculations were repeated with a uniform fuel temperature until the reactivity and U-238 capture rates were equivalent to the non-uniform temperature distributions. This uniform temperature was defined as the effective temperature and compared to the values predicted by Rowland's formula and the new T_{eff} formula. Fifteen cases were run for each temperature distribution, which spanned burnups from 0 to 60 GWD/MTU and U-235 enrichments from [] weight percent (w/o). Results showed that Rowland's formula resulted in nearly the same temperature as the new T_{eff} formula for steady state cases, and that both agreed with the APOLLO2 effective temperature. For the transient fuel temperature cases, the new T_{eff} definition showed substantial improvement reducing the mean prediction error of T_{eff} from a range [] K for the Rowlands formula down to a range of [] K. Both models had about a [] K standard deviation. The APOLLO2 temperature solution was benchmarked to Monte Carlo N-Particle (MCNP) transport code calculations. In addition, the T_{eff} method was compared in TR Table 7-3 to an average temperature formulation and was found to yield slightly more limiting results than a simple average weighting.

References for RAI-12:

1. BAW-10228PA, "Science," Framatome Cogema Fuels, December 2000.

RAI-13. *Section 6.3.2 – Is there a case in which the power profile within the pellet changes during the transient? If there is no provision for this change in profile, what is the effect of not allowing the change?*

Response to RAI-13:

The radial power profile does not change during the transient. The conditions that do change during a transient do not affect the radial power profile. The pellet radial power profile is primarily a function of burnup and initial enrichment. These two conditions are not affected by transient behavior. The burnup determines the amount of plutonium created in the rim of the pellet from U-238 resonance absorptions. At high burnups, the rim power can be twice as high as the average pellet power. The initial enrichment also has an effect, but it is less pronounced.

Initially, the higher enrichment has a slightly higher surface power because of the higher self shielding of thermal flux. As the plutonium is created on the rim, the plutonium power fraction is less in a higher enrichment pellet, and the surface power is smaller than a lower enriched pellet at the same burnup. The initial enrichment and burnup for the pellet are initial conditions for the transient and the pellet radial power profile remains fixed during the transient. A sensitivity study was performed on the neutronics solution assuming all the fuel was 2.0 w/o fuel and 5.0 w/o fuel with little or no sensitivity to the NEMO-K results (see TR Table 7-3).

RAI-14. *Section 6.3.3.1 – The CG/TDP model was validated for BOL conditions against various methods. Has this same validation also been carried out for EOL conditions, or is the validation at EOL conditions limited to only a comparison with COPERNIC?*

Response to RAI-14:

The purpose of the validation calculations at BOL conditions was to demonstrate continuity to existing results in Section 6.2.2 of BAW-10156A (TR Reference 7) and that the LYNXT fuel rod model remains valid for predicting fuel temperatures with each of the fuel options. No additional comparisons of LYNXT to LYNXT model option were performed for end of life (EOL) conditions. The BOL and EOL comparisons were made only for different transients with LYNXT and COPERNIC in order to show that the CG/TDP model provides similar results to the COPERNIC detailed model.

RAI-15. *Section 6.3.3.2 – Table 6-3 summarizes the comparison between LYNXT and COPERNIC. Please elaborate on how the results are determined.*

Response to RAI-15:

At each common time point in the two computer code simulations, the ratio of the respective fuel and cladding temperature results from the two codes is calculated. The ratio is the COPERNIC result divided by the LYNXT Constant Gap/Temperature Dependent Property (CG/TDP) result. For each of the four transients (hot zero power (HZP) EOL, hot full power (HFP) EOL, HZP beginning of life (BOL), and HFP BOL), the average, standard deviation, maximum, and minimum of the ratios during the transient simulation are calculated and tabulated in TR Table 6-3. The sample size reported in TR Table 6-3 is the number of common time points during the transient.

A revision to TR Table 6-3 was made as part of the response to RAI-31. The marked-up TR Table 6-3 is attached to this RAI response.

RAI-16. *Section 6.3.4 – Is there a standard set of data for the thermal properties of the fuel and clad, gap conductance, and radial power profile that are used as input to these analyses, or are they calculated as needed by one of the detail codes? If there is a standard set please list them or give appropriate references.*

Response to RAI-16:

The thermal properties are a standard set for the fuel rod design generated by using fuel and clad thermal property correlations in BAW-10231PA (TR Reference 2). A set of tables as a

function of temperature at a particular fuel rod burnup are input to LYNXT. These tables are available for different fuel pellet initial porosities, U-235 enrichments, and gadolinia content. Table 16-1, Table 16-2, and Table 16-3 provide a representative set for the fuel rod material compositions and burnups considered for the sample calculations in the topical report. Each fuel rod design can have a set of properties used for finer detail and response or a set of constant values can be used. NEMO-K uses the correlations in the form of the BAW-10231PA equations.

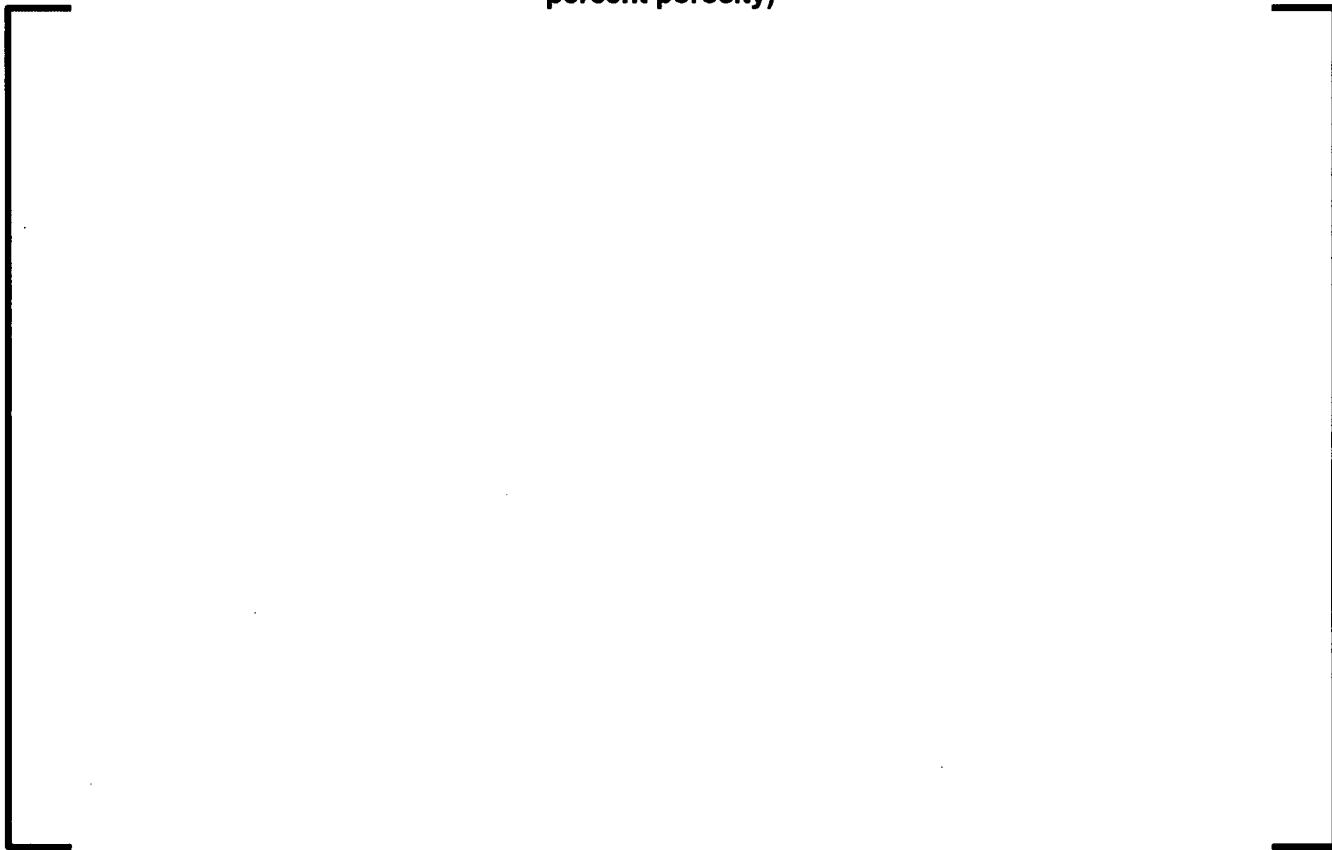
The fuel rod to cladding gas gap conductance (HGAP) used in the TR sample problem are given in Table 16-4. The HGAP is represented as a [] used as index interpolation points for HGAP. The [] index points for the TR sample problem calculations are []. The [] index points for the TR sample problem calculations are []. Both LYNXT and NEMO-K use a tabular input for this property.

The fuel pellet radial power profile used in the TR sample problem calculations consists of an array of normalized power density as a function of normalized radial position. This power profile is enrichment and burnup dependent. The values for UO₂ fuel pellets with [] w/o enriched U-235 at various levels of burnup are given in Table 16-5. These values are taken from the standard depletion dependent power profiles provided in the COPERNIC computer code BAW-10231PA. For fuel pellets loaded with gadolinia, the sets of pellet power profiles used for the TR sample problem are provided in Table 16-6 and Table 16-7 for fuel pellets loaded with [] w/o and [] w/o gadolinia, respectively.

Table 16-1—Cladding Thermal Properties from COPERNIC Correlations

A large, empty rectangular frame with a black border, positioned centrally on the page. It is intended to contain the data for Table 16-1, but the content is missing.

Table 16-2—UO₂ Fuel Thermal Properties from COPERNIC Correlations (4 percent porosity)

A large, empty rectangular frame with a black border, positioned centrally on the page. It appears to be a placeholder for a table that has been redacted or is otherwise missing from the document. The frame is oriented vertically and spans most of the width and height of the page's content area.

**Table 16-3—Gadolinia Fuel Thermal Properties from COPERNIC
Correlations at 50 GWd/tU (4 percent porosity)**



**Table 16-4—Burnup Dependent Gap Conductance Tables for 5 w/o U-235
enriched UO₂**

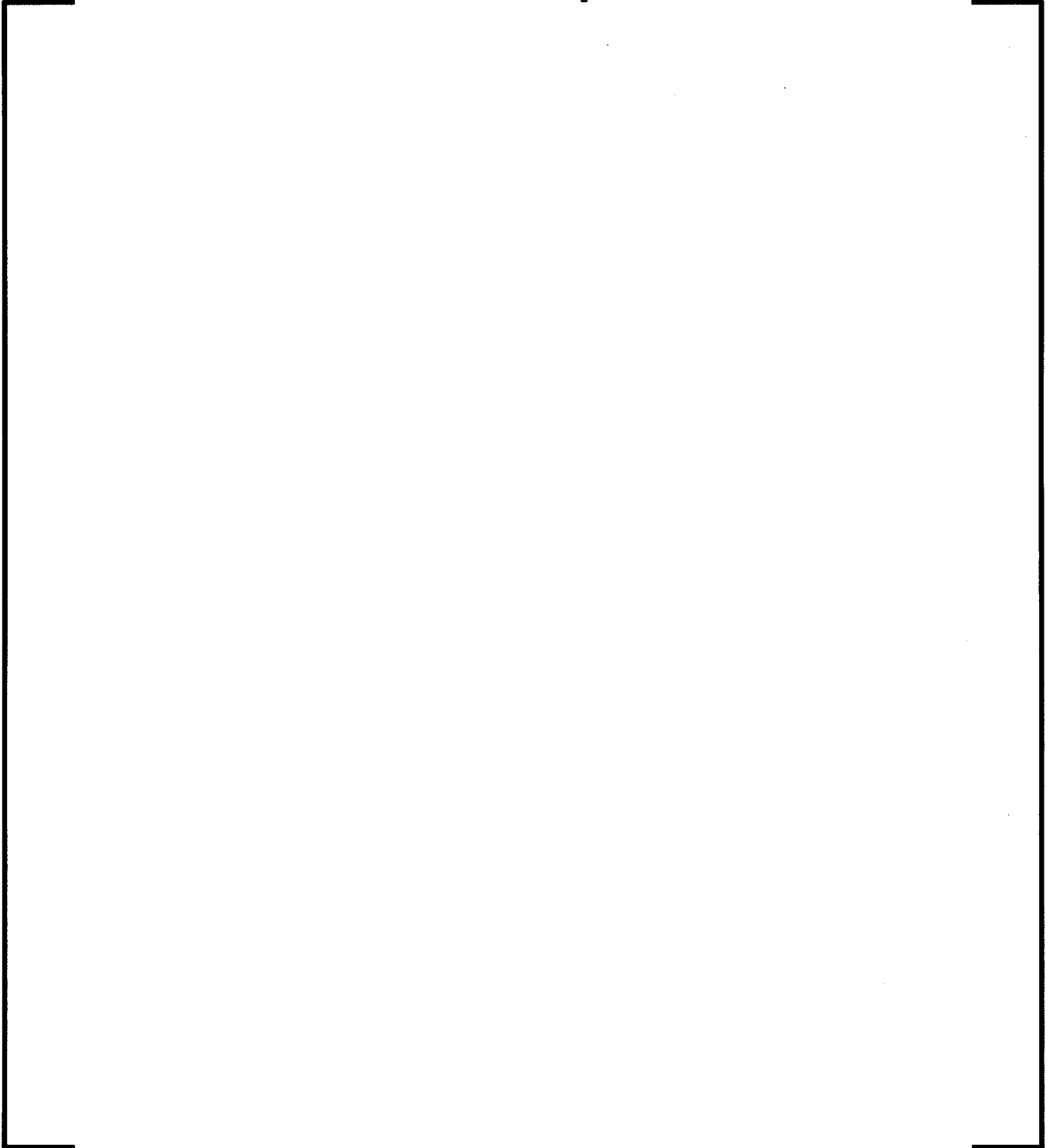


Table 16-5—Pellet Radial Power Profile for UO₂ with 5 w/o enriched U-235



Table 16-6—Pellet Radial Power Profile for UO_2 : Gd_2O_3 with 4.85 w/o U-235 enriched and 4 w/o gadolinia

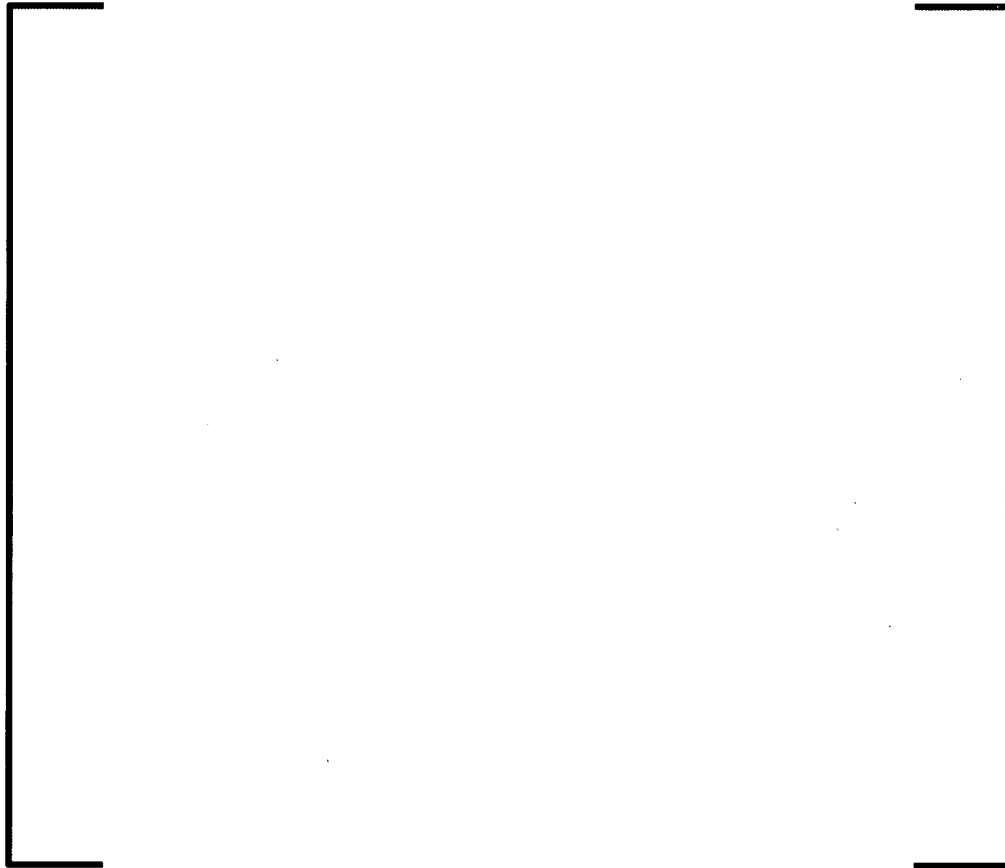


Table 16-7—Pellet Radial Power Profile for UO₂: Gd₂O₃ with 3.57 w/o U-235 enriched and 8 w/o gadolinia



RAI-17. *Section 7.0 – To what do the uncertainties in Table 7-1 refer? REA analysis values seem to be further from PRISM range values than uncertainties. Please provide proper references and explanations.*

Response to RAI-17:

The uncertainties referred to in TR Table 7-1 are the uncertainties to be applied to the calculated values from PRISM. The analyzed value should always be greater than the PRISM value with the uncertainty applied. The purpose of TR Table 7-1 is to show the difference between nominal value at the insertion limit and the REA analysis value. The amount between the PRISM calculated values and the REA analysis value is to account for the uncertainty, abnormal xenon distribution, and extra conservatism that can be used for future design margin. For example, the BOC Cycle 1 calculated ejected rod reactivity worth was 180 percent milli- $\Delta k/k$ (pcm). At adverse xenon conditions, the ejected worth became 291 pcm and increasing it by 15 percent results in a value of 335 pcm. This latter value is included in TR Table 9-2. The difference between 335 pcm and the REA analysis value of 433 pcm is amount of margin between this cycle and the analysis limit for this parameter.

RAI-18. *Section 7.1.3 – Is the value DTC uncertainty of ± 10 percent equally valid for BOL and EOL conditions? Please explain its burn-up dependency.*

Response to RAI-18:

The uncertainty of ± 10 percent is equally valid for all burnup conditions. Because U-238 dominates the Doppler temperature effect and the concentration of U-238 does not vary significantly with burnup, the same uncertainty value for BOC and EOC is appropriate. The Doppler temperature coefficient becomes more negative with burnup as Pu-240 is created. The DTC difference from BOC to EOC of Cycle 1 is approximately a [] percent increase in magnitude, which is indicative of the Pu-240 contribution to DTC. However, even if the error of Doppler contribution of Pu-240 was twice the assumed value of 10 percent, the implied error would increase [] percent, which is an insignificant amount relative to the overall conservatism described in the response to RAI-5.

For clarification, in the context of the topical report, the use of the terms BOC and EOC is in reference to burnup point in a particular operating cycle between core reloads. For the topical report, the use of the terms BOL and EOL refer to the operational duty time of a fuel rod, which may stretch over several core operating cycles. The DTC for the topical report is treated as a core wide parameter; therefore, the response in the paragraph above refers to BOC/EOC conditions instead of BOL/EOL conditions.

RAI-19. *Section 7.1.7 – Are combinations of the uncertainties listed in Table 7-3 evaluated when performing uncertainty analyses? If so, please explain what combinations are evaluated.*

Response to RAI-19:

The sensitivity studies were performed at the conditions listed in TR Table 7-3. When more than one “ Δ Case Conditions” is listed within a row, all of the listed changes were made in the input to obtain a single output sensitivity for each transient examined.

RAI-20. *Section 7.2.1 – Have sensitivity calculations been carried out using different node selections? If so, explain the node sensitivity analysis results.*

Response to RAI-20:

The LYNXT radial model nodalization is the same channel geometry as the baseline model used in other MDNBR analyses for the U.S. EPR (e.g., U.S. EPR FSAR Tier 2, Chapter 15 events). This radial geometry is presented in TR Figure 7-8. The axial nodalization used is based on the fuel assembly grid spacer locations and a reduced number of nodes from the baseline model for computational efficiency given the large number of time steps required. No other node selection sensitivity was performed.

RAI-21. *Section 7.2.4 – Please clarify whether NEMO-K and LYNXT use the same nodal distribution.*

Response to RAI-21:

NEMO-K and LYNXT are independent models; therefore, they are not required to use the same nodal distribution. The axial power shape data passed to LYNXT model input from NEMO-K model output is converted to the axial elevation spacing required by LYNXT. The fuel rod powers supplied to LYNXT from NEMO-K are calculated from the $F_{\Delta H}$ power transient of the fuel assembly of interest and its neighboring assemblies. The powers are mapped to the LYNXT model geometry with an intra-assembly radial power distribution. This radial power distribution is discussed further in the response to RAI-30.

RAI-22. *Section 7.2.5 – In Fig 7-10 the no-gadolinia case does not bound the gadolinia cases over the entire time span, which appears to be contradictory to statements in Section 7.2.5. Please explain this discrepancy.*

Response to RAI-22:

While TR Section 7.2.5 states that UO_2 is bounding, it was meant to be bounding in terms of the maximum temperature achieved during the transient, not that the UO_2 fuel temperature was bounding over the gadolinia fuel temperature at every time step.

TR Section 7.2.5, page 7-9 will be revised as follows:

“Note that the fuel temperatures with gadolinia are higher when operating at the same linear heat rate as UO_2 . When the transient temperatures for gadolinia fuel are adjusted by the power reduction factor, the maximum temperature during the transient is bounded by the UO_2 maximum temperature.”

A marked-up TR page 7-9 which reflects this change is attached to this RAI response.

RAI-23. *Section 8.5 – Please provide more information as to why no fuel rod failures are reported. For example, is it due to: a reactor trip terminating the transient, negative feedback reversing the trend, thermal inertia in the system reducing the temperatures, all of the above, etc.?*

Response to RAI-23:

TR Table 8-3, TR Table 8-4, and TR Table 8-5 summarize the results from the spectrum of rod ejections for a spectrum of initial power levels at BOC and EOC. There are no failures reported for events that tripped on high rate of flux on the excore detectors and that had minimum departure from nucleate boiling ratio (MDNBR) greater than the specified acceptable fuel design limits (SAFDL) during the transient. Therefore, no failures are reported for the BOC 35 percent power, EOC HZP, EOC 25 percent power, and EOC 35 percent power cases. The transient pulse is limited by the Doppler reactivity worth of the fuel rod heat up to counter the ejected rod worth and then ultimately terminated by the reactor scram.

The failed fuel rod census is performed for the transients where the fuel rod conditions reach the MDNBR SAFDL threshold for the potential of fuel failure. None of the cases for the TR sample problem have an enthalpy rise that exceeds 31.2 Δ cal/gm; therefore, the TFGR augmented fuel failure consideration is not needed. The response to RAI-28 describes the process by which the fuel failure census is completed. As shown in TR Figure 8-20 and Figure 8-35, the MDNBR of the bounding peak fuel rod for the 60 percent power cases only briefly crosses the SAFDL threshold by a small amount. It includes a multiplier on the initial peaking to bound cycle to cycle variations. However, the actual core power distribution that is used for the census only applies the uncertainties with no allowance for cycle to cycle variation and this power distribution did not have any fuel rods with heating rates where the MDNBR is exceeded.

RAI-24. *Please list the model assumptions used to generate the LYNXT to COPERNIC transient model comparison.*

Response to RAI-24:

The LYNXT to COPERNIC models were designed to investigate the performance of the LYNXT CG/TDP fuel rod model using the tabular fuel thermal properties compared to the COPERNIC full detailed capability model. The modelling assumptions used for the LYNXT to COPERNIC transient model comparison are listed below:

- A model of a single fuel rod with the same pellet radial power profile.
- Uniform power distribution in the axial direction to allow a single axial node to be compared.
- Same power history transient for the fuel. Time dependent inputs for LYNXT were linearly interpolated between no more than 101 input values. COPERNIC uses step values with a significantly finer mesh.
- Constant outer wall cladding temperature (set by creating nearly infinite heat transfer coefficient).
- Fuel pellet mesh—COPERNIC used 5 equal area nodes each with 4 equal area sub-nodes. LYNXT used ten collocation points for twelve radial temperature values.
- Cladding mesh—COPERNIC used 4 equal area nodes. LYNXT used two collocation points.
- Constant burnup profile within the fuel pellet so that fuel rod thermal properties are nearly the same.
- Fuel and cladding thermal properties (conductivity, specific heat, gap conductance)—COPERNIC uses inherent functions of the computer code fuel performance correlations. LYNXT uses tables of properties as a function of temperature (as described in the response to RAI-16).

RAI-25. *Supply and describe a flowchart on code and data process linkages that explain the analysis flow path for the REA event.*

Response to RAI-25:

A flowchart on code and data process linkages is presented in Figure 25-1.

COPERNIC calculations are run to obtain gap conductivity tables for both NEMO and LYNXT. The fuel property correlation equations from COPERNIC are used in NEMO-K. The fuel property equations from COPERNIC are used to create fitting tables in LYNXT for conductivities and heat capacities for the clad and fuel.

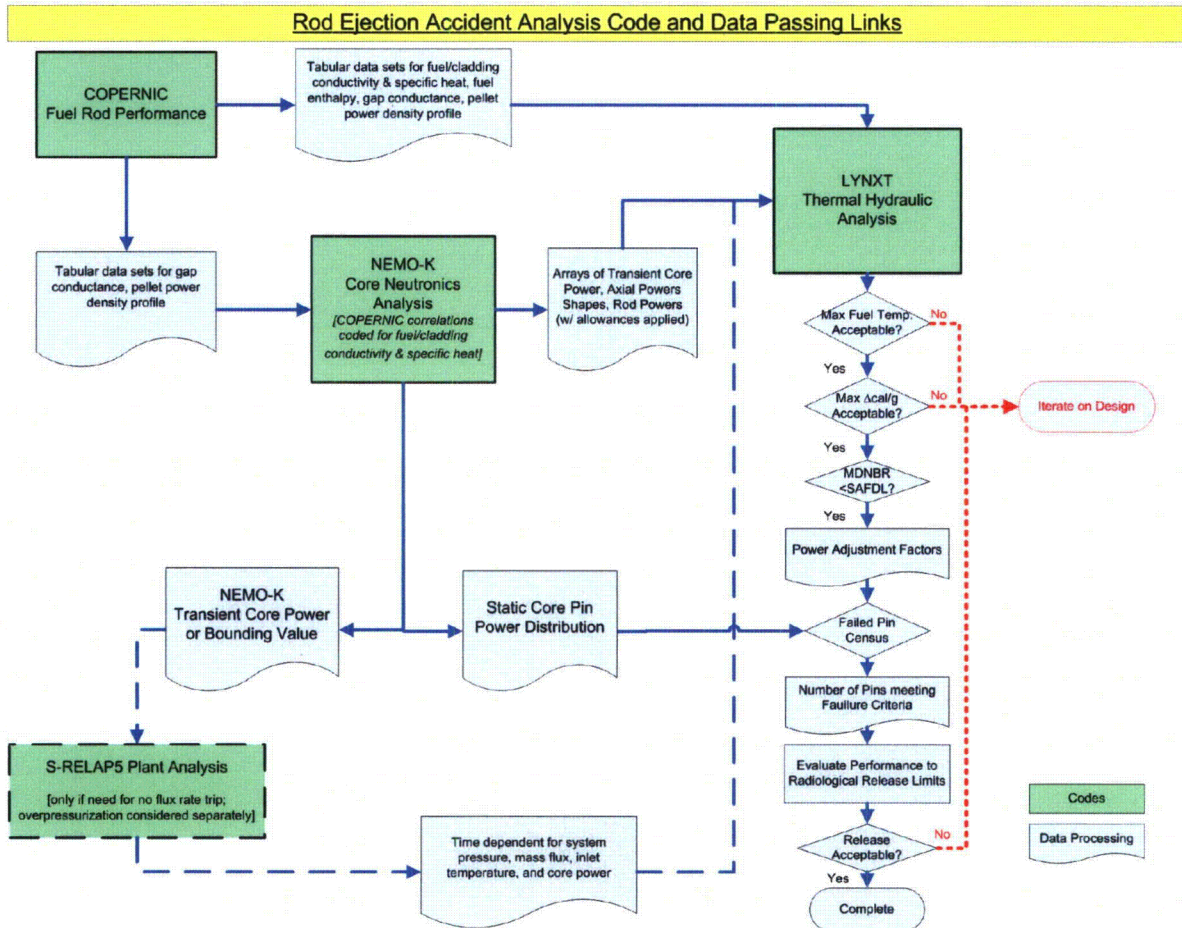
The ejected rod transient is simulated with NEMO-K at each of the plant initial conditions outlined in the topical. The core power, $F_{\Delta H}$ for the peak pin of interest, and axial powers versus time are extracted from NEMO-K and processed to create inputs for LYNXT.

Two cases (i.e., []) are run with LYNXT for each of the plant conditions as described in the TR Sections 4.2.7 and 7.2.5. The results are reviewed relative to their respective limiting conditions, as discussed in TR Section 2.0 and TR Table 2-1. If the fuel temperature or enthalpy rise is above the SRP 4.2 guidance, the design conditions must be re-evaluated. If these parameters are acceptable at this point, the fuel rod failure census process is followed as described in the response to RAI-28.

If a reactor trip does not occur during the power pulse, both kinetic and static NEMO-K cases are run to bound the power versus time response. This power history information is passed to S-RELAP5 to model the plant system response. The time dependent response of the inlet temperature, flow, and pressure from S-RELAP5 is input to LYNXT to obtain the fuel thermal response for times beyond approximately 5 seconds.

Once the fuel failure census is completed for an iteration of the design, the number of rods is compared against the maximum number of rods that may be failed for radiological release consequences as discussed in TR Section 2.3. If the number of fuel rods considered failed exceeds the limit, the design conditions must be re-evaluated.

Figure 25-1—Calculation Flow Interfaces



RAI-26. Provide an event timeline and description for various REA events (include events that trip and events that don't trip the plant) to explain the parameter responses. Additionally, please explain the process by which the incore DNBR trip time estimates were made.

Response to RAI-26:

An REA event timeline begins with the speed of withdrawal and worth of the ejected rod. The degree of insertion is set by the power dependent insertion limit (PDIL) curve. TR Figure 7-2 depicts the insertion level as a function of power and the extra insertion assumed for the topical report sample problem analysis. For higher powers, only one bank is allowed to be inserted (the "D" bank that includes the N05 and J09 control rod locations). At lower power levels overlap with the "C" bank is allowed, and this is how the total steps is greater than the full travel range of 416 steps.

The minimum time to eject a rod from full insertion was 0.1 second; therefore, for each power level, the time to eject is shortened based on the insertion level of the rod. Table 26-1 provides

the times assumed to eject the rods from various power dependent rod positions for BOC and EOC analysis. Table 26-1 also shows the timing sequence to the peak core fraction of power and the minimum or SAFDL MDNBR values. The first one second of the NEMO-K core power histories for the spectrum of power levels considered at BOC and EOC are presented in Figure 26-1 and Figure 26-2, respectively. Each transient has an initial rapid power rise that is limited by the Doppler reactivity feedback of the fuel rod heat up.

For cases that have reactor trips initiated by the excore flux rate signal, control rods begin to move into the core after an allowance for instrument and signal delays. As shown in TR Table 8-4 and TR Table 8-5, the banks begin insertion between 0.825 and 1.00 seconds for all the rod ejections accidents with the high flux rate trip. The rods are simulated to take 3.5 seconds to become fully inserted after they begin to move. As the rods move in, the axial power distribution shapes and maximum F_Q values will shift. The changes in the F_Q appear in the power transient figures, primarily after about 1.5 seconds into the transient due to the time required for the rods to be inserted enough to significantly affect the axial power distribution. The rod ejection accident events that have a trip on the excore neutron signal need no further consideration of the plant boundary conditions because the event is over before the coolant loop transport time has been reached.

As an example of a power history with a reactor trip on high flux rate, an event timeline is provided for the BOC 35 percent power TR sample problem case in Table 26-2.

For transients with no initial excore flux rate reactor trip, further consideration of the event is needed for the fuel rod performance because the plant boundary conditions for inlet temperature, core flow, and system pressure now become more important. As described in TR Sections 6.4 and 8.3, the NEMO-K power transient was provided as input to the S-RELAP5 plant model in order to determine the core thermal performance boundary conditions. A maximum break area was assumed to be the size of the inside diameter or the control rod flange to cause the most rapid depressurization. The BOC 25 percent power, BOC HFP, and EOC HFP transients required the further S-RELAP5 calculations are described in TR Section 8.3.

The system pressure and core inlet temperature for the BOC 25 percent power case are provided in TR Figure 8-12. The transient history of the system pressure, core inlet temperature, core inlet mass flux, and core power normalized to their initial value for this event are shown in Figure 26-3. The transient is terminated at [] seconds due to a reactor trip on high S/G pressure. An event timeline of important parameters for this rod ejection transient is provided in Table 26-3. As reported in TR Table 8-3, the predicted number failures with S-RELAP5 plant thermal boundary conditions at the time of the reactor trip was 1.8 percent.

The system pressure and core inlet temperature for the BOC HFP case are provided in TR Figure 8-13. The transient history of the system pressure, core inlet temperature, core inlet mass flux, and core power normalized to their initial value for this event are shown in Figure 26-4. The transient is terminated at [] seconds due to a reactor trip on low saturation margin and low primary pressure. An event timeline of the BOC HFP power transient for this rod ejection transient is provided in Table 26-4. For the EOC HFP case, a similar sequence to the BOC HFP case of events is followed.

In addition to the change to the power distribution transient, the DNBR performance is impacted by the decrease in system pressure and the increase in the core inlet temperature increase. A

plot of the pressure versus temperature during this transient is shown in Figure 26-5. The time horizon is such that the upper left corner of the plot (high pressure and low temperature) are the initial conditions and the lower right corner of the plot (low pressure and high temperature) are the conditions at the time of the S RELAP5 predicted reactor trip. The MDNBR resulting from the bounding LYNXT calculations for the BOC HFP case is shown in TR Figure 8-23 and is shown for the EOC HFP case in TR Figure 8-38. The fuel rod failure census is performed (as described in the response to RAI-28) with the final S-RELAP5 boundary conditions and with boundary conditions at several time points leading to the end of the transient. The maximum break area causes the maximum reduction in pressure and the worst boundary conditions for DBNR performance.

The pressure and temperature and a certain fuel rod heating rate can be used as inputs to create a MDNBR response that simulates the DNBR online monitoring system. The online DNBR monitoring system and transient analysis methodology is described in ANP-10287P, "Incore Trip Setpoint and Transient Methodology for U.S. EPR Topical Report," (Reference 1). In Figure 26-5, the two Pressure-Temperature (P-T) threshold lines are estimates of the pressure and temperature conditions required to have MDNBR= [] with a fraction of core power of 100 percent and 105 percent. The value to use for the MDNBR threshold was selected for the sample problem calculations as representative of the setpoint threshold that is established in accordance with ANP-10287P. The estimate of Low DNBR reactor trip occurring before 30 seconds is determined by the time just before the P-T crosses the MDNBR= [] threshold line for the fraction of power (FOP) equal to 1.00 (P= [] psia, T= [] °F). The actual time of a reactor trip would be dependent on the size of the break area, the Low DNBR reactor trip setpoint, and the fraction of core power during the event.

References for RAI 26:

1. ANP-10287P, Revision 0, "Incore Trip Setpoint and Transient Methodology for U.S. EPR Topical Report," AREVA NP Inc., November 2007.

Table 26-1—Rod Ejection and Peak Power/MDNBR Times from Spectrum of Power Levels at BOC and EOC

Initial Power Level (%FP)	RCCA N05 Initial Position (Steps Inserted)	Time to Eject (sec)	Time to Peak Power at BOC (sec)	Time to Limiting MDNBR at BOC (sec)	Time to Peak Power at EOC (sec)	Time to Limiting MDNBR at EOC (sec)
0	411	0.100	N/A	N/A	0.292	0.325 Min
25	411	0.100	0.115	17.0 SAFDL	0.132	0.170 Min
35	384	0.094	0.194	1.10 Min	0.123	0.170 Min
60	308	0.075	0.097	0.74 SAFDL	0.100	0.32 SAFDL
100	140	0.035	0.044	0.99 SAFDL	0.056	0.79 SAFDL

Table 26-2—Event Timeline for BOC 35 percent Power Transient

Event	Time (seconds)
Ejection beginning	0.000
Rod N05 fully ejected	0.094
High Neutron Flux Rate of Change Reactor Trip is reached	0.125
Peak Power Reached of 68.7 percent full power	0.194
Safety Bank Scram Rods begin to move	0.850
Minimum MDNBR is reached	1.100
Maximum Peak Fuel Enthalpy Rise is reached	1.350
Maximum Peak Fuel Temperature is reached	1.700

Table 26-3—Event Timeline for BOC 25 percent Power Transient

Event	Time (seconds)
Ejection beginning	0.000
Rod N05 Fully Ejected	0.100
Peak Power Reached of 53.1 percent full power	0.469
Core Outlet Temperature rapid rise due to power increase	2.00
Depressurization slows due to core outlet temperature rise	2.00 – 5.00
Core Inlet Temperature begin to rise after flow loop transport	≈9.00
Core Inlet Mass Flux begins to lower due to lower density of coolant	≈9.00
MDNBR reaches SAFLD level	17.00
Reactor Trip Setpoint reached (High S/G Pressure)	24.94
Reactor Trip	25.44
Turbine Trip	26.44
Safety Bank Scram Rods fully inserted	29.34

Table 26-4—Event Timeline for BOC HFP Power Transient

Event	Time (seconds)
Ejection beginning	0.000
Rod N05 Fully Ejected	0.035
Peak Power Reached of 110.2 percent full power	0.121
MDNBR reaches SAFDL level	0.900
Peak Cladding Temperature begins Post-CHF transition	1.350
Core Outlet Temperature rapid rise due to power increase	2.00
Depressurization slows due to core outlet temperature rise	2.00 – 5.00
Peak Fuel Average Temperature begins post CHF transition	5.000
Peak Fuel Temperature begins post-CHF transition	9.500
Core Inlet Temperature begin to rise after flow loop transport	≈10.00
Core Inlet Mass Flux begins to lower due to lower density of coolant	≈10.00
MDNBR estimated to reach Low DNBR reactor trip setpoint	<30.00
Reactor Trip Setpoint reached (Low Saturation Margin/Low Primary Pressure)	59.454
Reactor Trip	60.435
Turbine Trip	61.035
Safety Bank Scram Rods fully inserted	64.335

Figure 26-1—Fraction of Power versus Transient Time for BOC REA

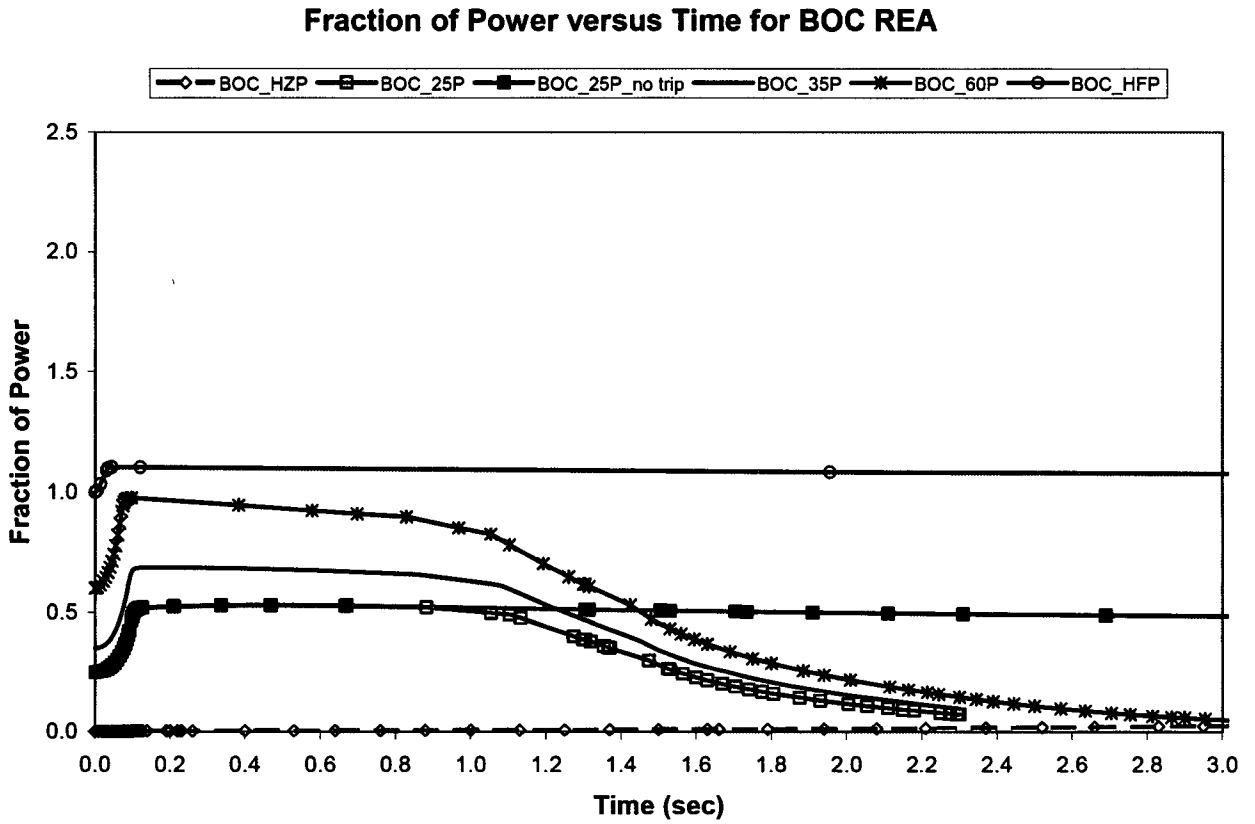
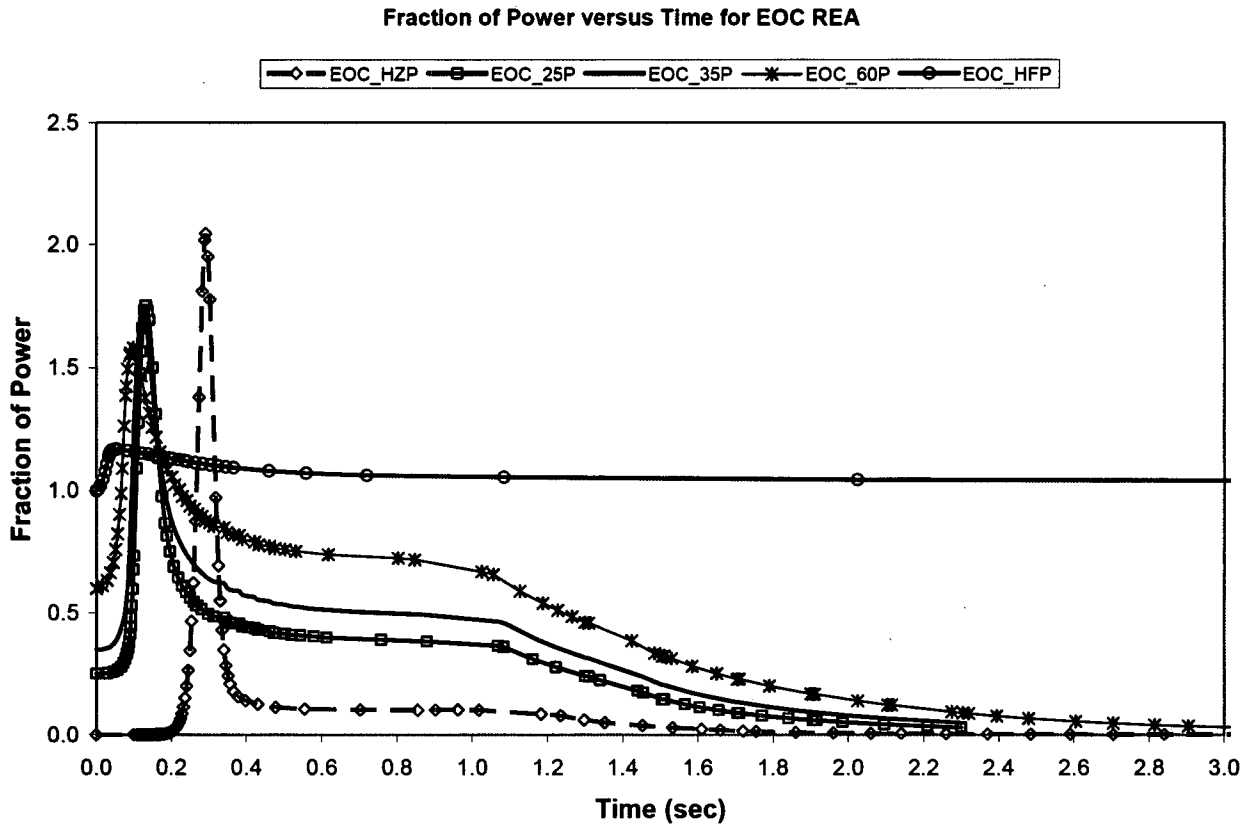


Figure 26-2—Fraction of Power versus Transient Time for EOC REA



**Figure 26-3—S-RELAP5 Normalized Boundary Conditions for 25 percent
power BOC Rod Ejection**



**Figure 26-4—S-RELAP5 Normalized Boundary Conditions for BOC HFP
Rod Ejection**



**Figure 26-5—Pressure and Temperature Conditions for BOC HFP
S-RELAP5 Case and MDNBR=1.8**



RAI-27. *Provide a description of the thermal properties tables' inputs to LYNXT.*

Response to RAI-27:

The fuel rod thermal properties tables that are input to LYNXT for the LYNXT Constant Gap/Temperature Dependent Properties (CG/TDP) option are input as pairs of temperatures and thermal property value at that temperature. The properties are the fuel thermal conductivity, fuel specific heat, cladding thermal conductivity, and cladding specific heat. The gap conductance property is input as a [

]. Additionally, the fuel enthalpy can be input as a function of fuel temperature in order for LYNXT to determine the total enthalpy and change in enthalpy at the radial locations in the fuel pellet. The attribute of the radial pellet power profile is input as a function of radial position. The radial power shape is an important attribute for determining the steady state and transient temperature distributions at different burnup conditions. The response to RAI-16 further describes the values in the thermal properties tables used to determine the COPERNIC computer code for the U.S. EPR fuel types.

[

]

Example Calculation

[] assemblies are used to represent the range of radial/axial power behavior during the transient. These assemblies are chosen over a range of [] with the corresponding highest []. Assemblies [] are chosen for the fuel rod failure census. The [] for these assemblies are shown in Figure 28-1. In this BOC HFP example, the N05 fuel assembly has the highest [].

The transient power histories for the chosen assemblies/rods, including appropriate uncertainties, are analyzed with the thermal-hydraulic code LYNXT. The power versus time response of the assembly is iteratively scaled up or down by a multiplier until the DNBR reaches the design limit. The multipliers determined for the [] fuel assemblies of this example are provided in Table 28-1. For this example, the data in the column labeled "Multiplier" in Table 28-1 are the multipliers for the respective assemblies. For example, any fuel rod that has a pre-ejection $F_{\Delta H} \geq [1.473]$ that has a transient power history shape like assembly [] will fail. A similar relationship applies to the [] fuel assemblies.

[

[] The values for the fuel assemblies used in the example are provided in Table 28-2. These multipliers behave linearly as shown in Figure 28-4. Since both correlations are linear, interpolation between the initial $F_{\Delta H}$ values can be used to obtain the $F_{\Delta H}$ or F_Q that would fail the fuel rod.

The pre-ejection fuel rod power is available for fuel rods in the core from the static calculation. The static post ejection failure limit for $F_{\Delta H}$ and F_Q are interpolated from the [] available values. If the fuel rod has a post ejection $F_{\Delta H}$ or F_Q greater than equal to the respective limit interpolated from its initial $F_{\Delta H}$, the fuel rod is assumed failed. This process is repeated for each analyzed power level. For the BOC HFP case, the number of pins estimated to be below the MDNBR design limit in the first few seconds of the transient (prompt response) was 0.3 percent.

For the cases that do not trip, as in the HFP BOC case, the core continues to operate in a near steady state neutronic condition so that a failure census is needed to account for the system degradation with time. The pressure slowly degrades due to primary coolant leakage through the assumed hole left by the ejected rod. Since this is a near steady state neutronic problem, the initial power distribution is no longer relevant; only the current power distribution contributes to the heat flux. The process of finding the $F_{\Delta H}$ and F_Q values that exceed the DNBR limit is repeated with LYNXT based on the pressure, flow, and inlet temperature provided by S-RELAP5 and the steady state peaking from NEMO-K. For the HFP static case at BOC, the peak assembly power is scaled in LYNXT until it reaches the MDNBR design limit. The values of $F_{\Delta H}$ and F_Q for this case become the failure criteria for each rod in the core. Any pin exceeding the $F_{\Delta H}$ or F_Q failure criteria is assumed failed. The number of pins estimated to be below the DNBR design limit was 7.2 percent.

Table 28-1—BOC_HFP Example Fuel Failure Census $F_{\Delta H}$ Threshold Determination



Table 28-2—BOC_HFP Example Fuel Failure Static Post-ejection $F_{\Delta H}$ and F_Q Threshold Determination



Where:

- mult = $F_{\Delta H}$ multiplier factor from Table 28-1 that brings the fuel rod to the MDNBR SAFDL
- fdh0 = initial maximum F_{QH} of fuel rods in the selected fuel assembly
- fdh1 = post-ejection maximum F_{QH} of fuel rods in the selected fuel assembly
- fq1 = post-ejection maximum F_Q of fuel rods in the selected fuel assembly

Figure 28-1—Transient Versus Static Peaking Ratios at 0.150 Seconds



Figure 28-2—Transient Versus Static Peaking Ratios at 0.044 Seconds



Figure 28-3—Transient Versus Static Peaking Ratios at 0.250 Seconds



Figure 28-4—Post Ejection Static DNBR Peaking Limits



RAI-29. *Provide an explanation about the calibration for the high rate flux trip and provide a sample response of the rate lagged filter. (Section 6.2.1, 6.2.1.2, Table 8-1).*

Response to RAI-29:

The high flux rate trip is described in U.S. EPR FSAR Tier 2, Section 7.2.1.2.3. The high flux rate is determined from the excore power range detection system signal which is described in U.S. EPR FSAR Tier 2, Section 7.1.1.5.3. The general calibration procedure and surveillance requirement is described in U.S. EPR FSAR Tier 2, Chapter 16, Section 3.3.1. The high rate flux trip is a fixed setting and is not calibrated. The flux rate signal is calculated by the digital protection system using excore detector signal. The definitions and equations in TR Sections 6.2.1.1 and 6.2.1.2 implemented in NEMO-K allow the simulation of these excore protection systems. A calibration is simulated in NEMO-K at the conditions to initialize the indicated power and imbalance of the top and bottom detectors for the four excore detectors. This is done prior to the transient initiation.

Signal filter responses for a fast and normal ramp rate are shown in Figure 29-1 and Figure 29-2, respectively. The figures show the core power, the lagged power, and the flux rate trip signal versus time for a linear ramp increase and decrease in power. The fast ramp rate simulated in Figure 29-1 is 1%/msec and the normal ramp rate in Figure 29-2 is 10%/minute.

For the fast ramp rate, each point represents a sampling rate of once every 25 milliseconds. The fast ramp rate illustrates the signal response during a prompt excursion. The excore power will indicate no higher than 200 percent power when the actual power is above 200 percent power. For the fast ramp rate figure, the flux rate signal is nearly equal to the delta power observed from $t=0$ because the lagged power signal does not change in this short time frame relative to the 30 second lag time. The flux rate signal remains high throughout the transient even though the power is going down. The flux rate values for 20 second gain and lag constants is indistinguishable from the values with 30 second time constants. The label of normal ramp rate corresponds to a 10%/minute ramp rate, which is a relatively fast maneuvering rate. Figure 29-2 shows an asymptotic 5 percent rate signal, which agrees with the ramp rate (10%/60 seconds) times the gain constant (30). The flux rate signal with the gain and lag set to 20 reaches its maximum value of 3.3 (10%/60 seconds times 20) more quickly than the gain and lag set to 30.

Figure 29-3 and Figure 29-4 show the core power and the flux rate trip signal for each excore detector versus time for the BOC HFP and EOC HZP transient simulations, respectively. As shown in Figure 29-3 for the BOC HFP ejected rod transient, only one of the four flux rate signals exceeded the trip limit and the reactor did not trip. The highest detector response is the detector location closest to the ejected rod. In Figure 29-4 for the EOC HZP ejected rod transient, each point represents a sampling rate of once every 25 ms and three detectors indicated a trip signal twice leading to a trip signal being activated.

Figure 29-1—Flux Rate Signal Fast Ramp Rate

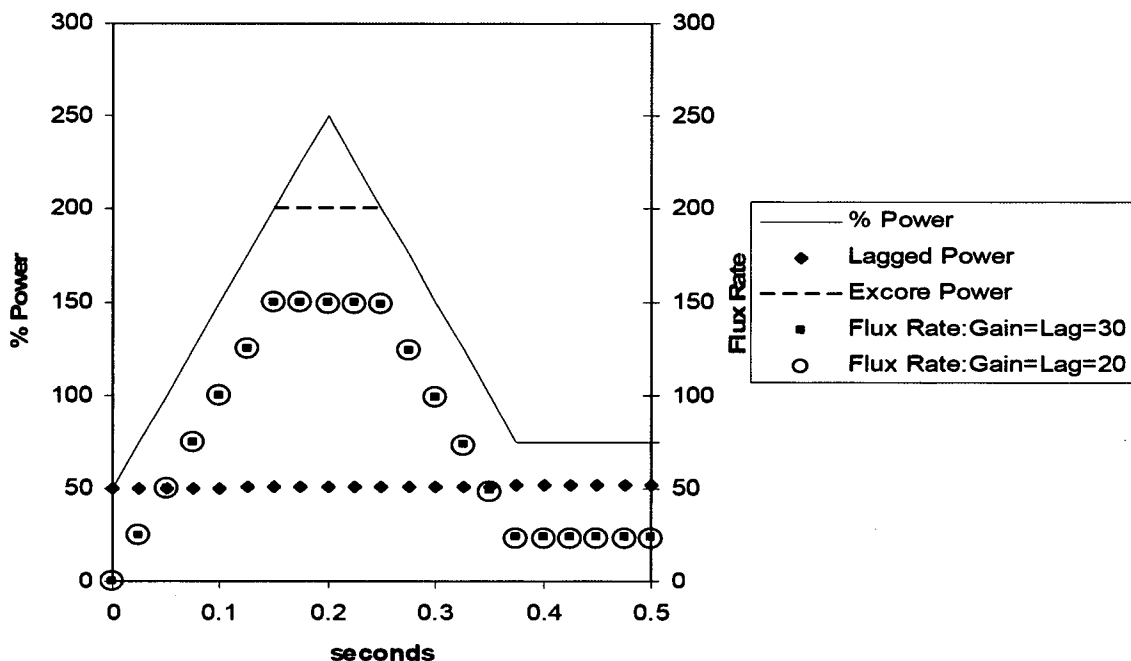


Figure 29-2—Flux Rate Signal – Normal Ramp Rate

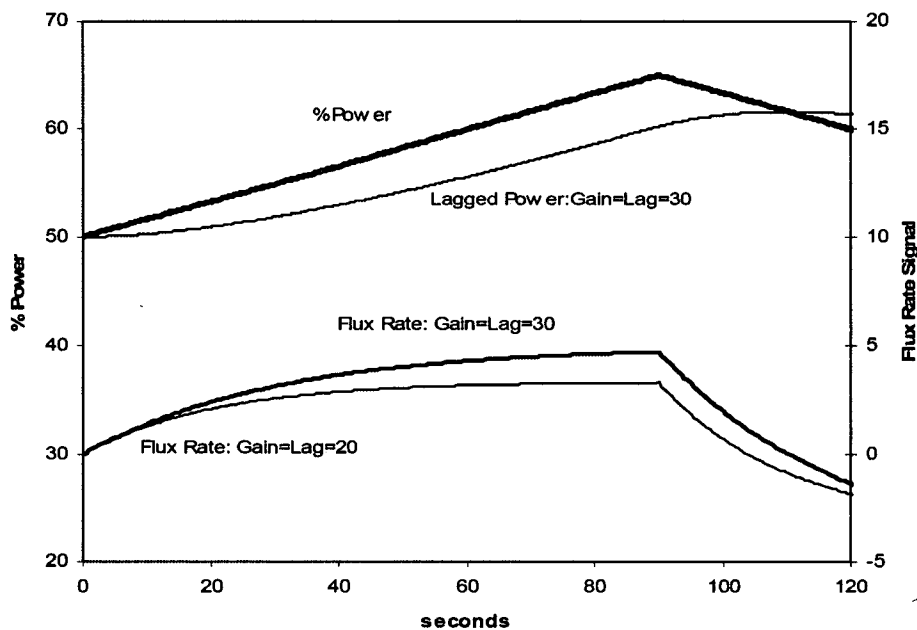


Figure 29-3—BOC HFP – Flux Rate Signals

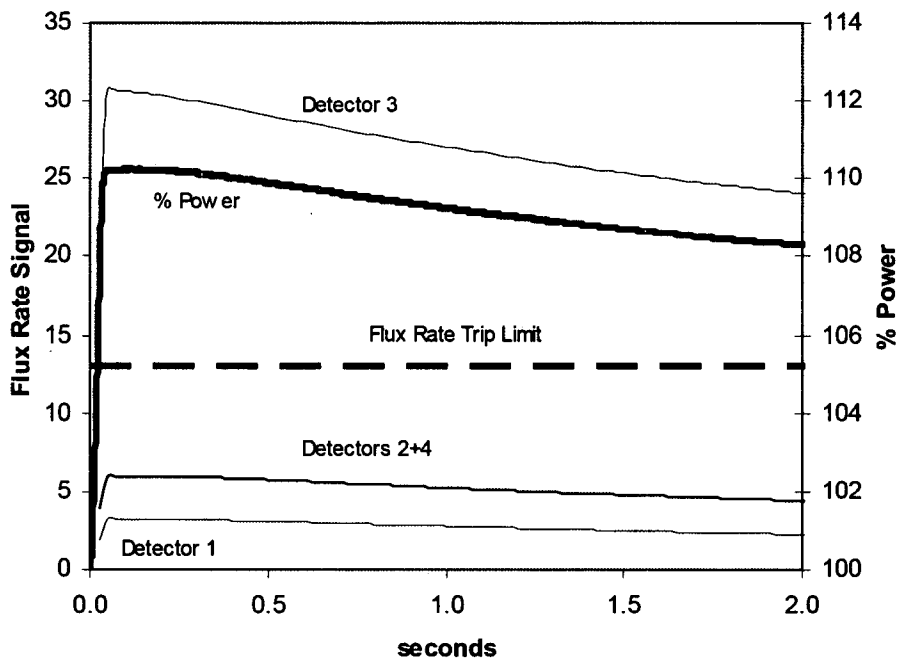
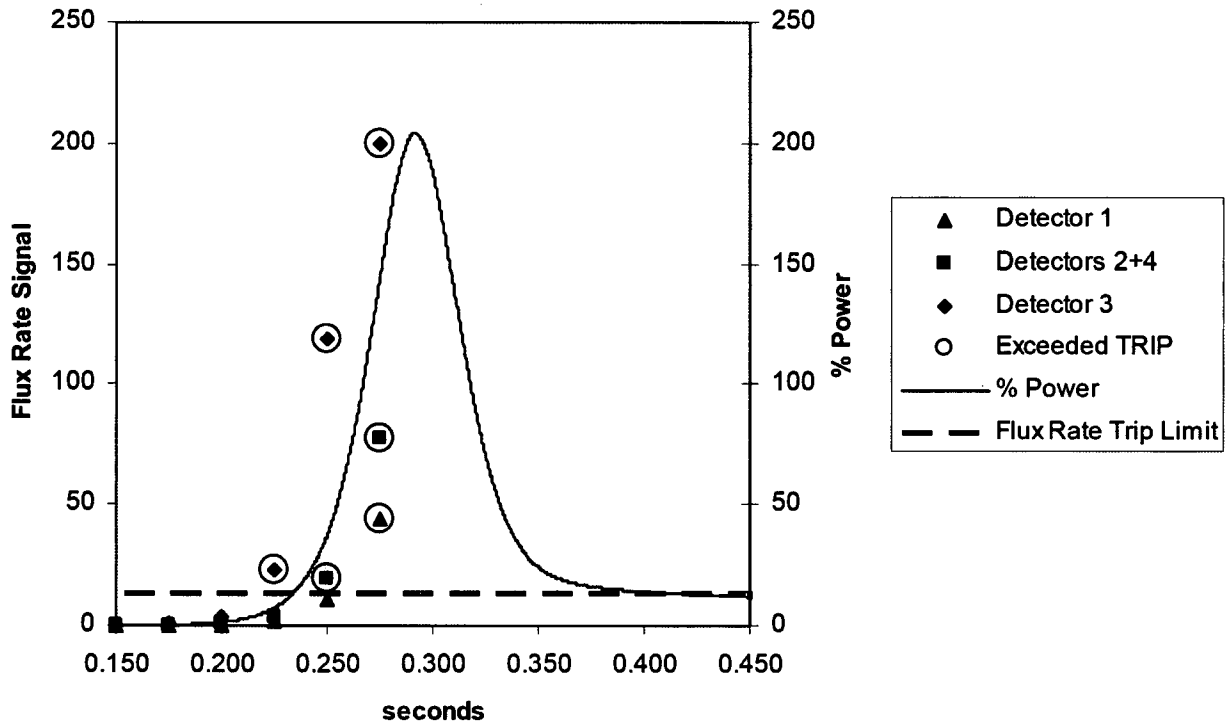


Figure 29-4—EOC HZP – Flux Rate Signals



RAI-30. Section 7.2.4 – Please explain why the assembly pin power radial power distribution in LYNXT is conservative for the assumed power distribution within the fuel assembly of interest.

Response to RAI-30:

The radial power distribution for the sample problem fuel rods is based on the distribution used in other MDNBR analyses for the U.S. EPR (e.g., U.S. EPR FSAR Tier 2, Chapter 15 events).

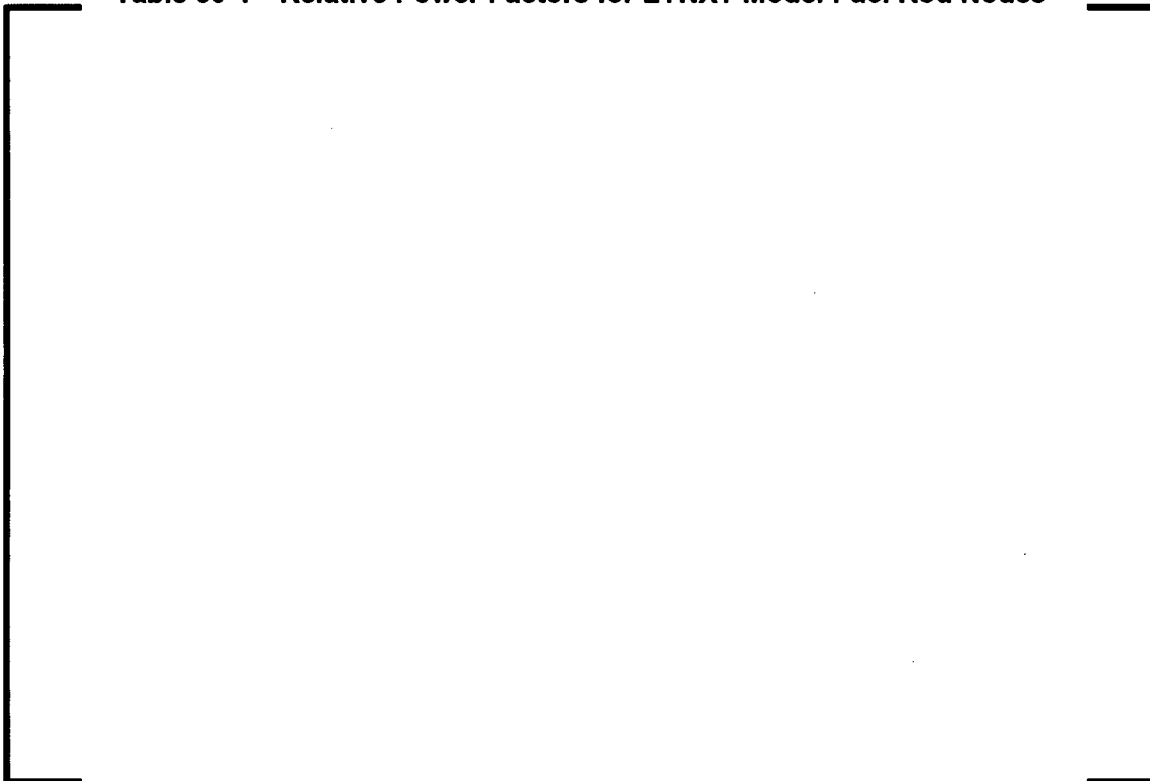
[

] The power

distribution selected for DNBR analysis was based on investigations of the fuel assembly lattice fuel rod power distribution from several cycles and burnups. The power distribution used for the U.S. EPR analysis is presented in Table 30-1. As described in TR Section 7.2.4, [

] The equation to provide the proper core normalized $F_{\Delta H}$ for the last [] nodes is provided in TR Section 7.2.4.

Table 30-1—Relative Power Factors for LYNXT Model Fuel Rod Nodes



RAI-31. Please provide an explanation for the discontinuities of the LYNXT results relative to the COPERNIC temperature transients in Figures 6-23 and 6-27.

Response to RAI-31:

The discontinuities of the LNYXT results in TR Figures 6-23 and 6-27 are related to the interpolation for the value of the gap conductance from the table values input as part of the CG/TDP option. The model assumptions for LYNXT and COPERNIC are described in the response to RAI-24. For LYNXT, the gap conductance (HGAP) input is a [] The format of the HGAP property set is described in the response to RAI-16. The fuel average temperature and HGAP values from LYNXT and COPERNIC are shown in Figure 31-1. The fuel temperatures are the same as the values shown in TR Figure 6-24. During the transient, the average [] temperature is maintained between [], which are [] index into the HGAP table. The fuel average temperature transitions from [] during the [] seconds of the simulation. Also indicated in Figure 31-1 are the time points of the []

[] The fuel temperatures transition through [] These are the times at

which the temperature cusping inflections occur in Figure 31-1 and in TR Figures 6-23 and 6-27. The slope of the HGAP changes at these points; therefore, the response in LYNXT will be affected.

During the transient, the LYNXT fuel surface temperatures in TR Figure 6-23 are at most [] °F lower and at the [] second end of transient, the LYNXT value is approximately [] °F higher than the COPERNIC value. Because the HGAP value is [] in the LYNXT results than in the COPERNIC results, during the initial phases of the transient, the heat flux from the fuel rod will be [], the fuel surface will tend to be [], and the cladding maximum temperature will tend to be []. This is shown in TR Figure 6-27.

While developing the response to RAI-31, a typographical error was found in the input for LYNXT gap conductance for the BOL cases. The input typo resulted in the HGAP for [] being set to an incorrect low value. The LYNXT calculations were re-run and the correct results once again compared to the COPERNIC results. The change in the results of the LYNXT transient occur only after [] seconds and results in changes less than [] percent (i.e., [] °F) in fuel and clad temperatures and changes less than [] percent ([]) for the temperature ratios for the HFP BOL case in TR Table 6-3. The maximum ratio of the cladding maximum temperature changed from []. The minimum ratio for the fuel surface temperature changed from [] and for the average fuel temperature changed from []. The rest of the ratios in the table remained the same. A revised TR Table 6-3, TR Figure 6-23, and TR Figure 6-27 are provided in the attachment to this RAI response. The above error was also documented in the AREVA corrective action program.

Figure 31-1—LYNXT and COPERNIC Fuel Average Temperature and Gap Conductance for Comparison Model REA from HFP/BOC



RAI-32. *Please explain why the BOC HZP was not analyzed in LYNXT in Sections 8.1 and 8.3*

Response to RAI-32:

The BOC HZP power case was not analyzed for MDNBR response in LYNXT because the power response at HZP BOC changes less than 6 percent power from 0 to 5 seconds, as shown in TR Figure 8-1. In TR Figure 8-2, the power response at BOC for 25 percent power increases more than 25 percent power in less than 0.2 seconds and clearly bounds the changes seen at HZP BOC. Because the ejected rod reactivity worth is less than the effective delayed neutron fraction β_{eff} , the power rise is caused by the prompt jump in reactivity and is not a prompt critical excursion. The prompt jump is a fractional change of the initial power so that a higher initial power results in a higher change in power. Therefore, the BOC HZP case was not analyzed with LYNXT because it was bounded by the conditions at 25 percent power. To indicate that the BOC HZP case was not analyzed beyond the neutronic calculation, the number of fuel rods failed in TR Table 8-4 at 0 percent power should be labelled with a dash rather than a value of 0 indicating that the results are bounded by the results at 25 percent power. A marked up revision to TR Table 8-4 is provided in the attachment to this RAI.

ANP-10286 Markups

Table 6-3 LYNXT and COPERNIC Transient Temperature Ratio Comparisons

Comparison parameter	Fuel temperature				Cladding maximum temperature
	Surface	Average	Centerline	Maximum	
HZP EOL					
Average					
Std. dev.					
Maximum					
Minimum					
Sample size					
HFP EOL					
Average					
Std. dev.					
Maximum					
Minimum					
Sample size					
HZP BOL					
Average					
Std. dev.					
Maximum					
Minimum					
Sample size					
HFP BOL					
Average					
Std. dev.					
Maximum					
Minimum					
Sample size					

Notes:

1. The data is based on (COPERNIC result) / (LYNXT CG/TDP result).
2. "Std. dev." is the standard deviation of the data about the average. Sample size is the number of transient time steps.

Figure 6-23 HFP/BOL Transient Fuel Surface Temperature



Figure 6-24 HFP/BOL Transient Fuel Average Temperature



Figure 6-27 HFP/BOL Transient Cladding Maximum Temperature



burnup for a 2.0 and 5.0 w/o U-235 pellet is estimated to be 50 and 70 GWD/MTU, respectively. The MDNBR performance is shown in Figure 7-9 for these cases. [

] This is due to higher gap conductance values and higher pellet rim power peaking. Calculations are performed with 5.0 w/o U-235 fuel at 2.5 and 50 GWD/MTU burnup levels for the BOC cases and 20 and 70 GWD/MTU burnup levels for the EOC cases in order to bound the potential burnup thermal property states of the fuel rods.

Fuel loaded with gadolinia has a lower thermal conductivity than pure UO_2 . The higher the gadolinia content, the lower the thermal conductivity of the fuel pellet. This increases the fuel temperatures of the gadolinia fuel if operated at the same LHGR as a UO_2 fuel rod. However the gadolinia rods typically have low maximum powers because of lower fuel uranium enrichments and parasitic neutron absorption by the residual gadolinium isotopes. To determine if the analysis can be performed using only UO_2 properties, a sensitivity study was run on the BOC HFP power excursion with gadolinia loadings of 4 w/o and 8 w/o gadolinia. The gadolinia rods were run with the same power history as the pure UO_2 rod and with the maximum power level anticipated for a gadolinia loaded rod. [

] Figure 7-10 shows the peak fuel temperatures for 0, 4, and 8 w/o gadolinia loadings. Note that the fuel temperatures with gadolinia are higher when operating at the same linear heat rate as UO_2 , ~~and~~ When the transient temperatures for gadolinia fuel are adjusted by the power reduction factor, are the maximum temperature during the transient is bounded by the UO_2 maximum temperatures. For the thermally limiting transient for HFP at BOC, the temperatures never exceed the lowest fuel melt limit for a rim burnup, even when the peak power is not decreased by the maximum expected value for a gadolinia rod. Because the UO_2 rod bounds the temperatures, the LYNXT calculations use the

[

]

Table 8-4 Ejected Rod Analysis Results for BOC

Parameter	Criterion	0	25	35	60	100
Maximum Ejected Rod Worth, pcm	-	433	362	346	286	64
β_{eff}	-	0.0055	0.0055	0.0055	0.0055	0.0055
MTC, pcm/°F	-	2.16	1.32	1.35	0.34	0.01
DTC, pcm/°F	-	-1.22	-1.14	-1.11	-1.05	-0.96
Initial F_Q	-	NA ^a	3.01	2.88	2.63	2.36
Maximum Transient F_Q	-	9.46	5.75	5.23	5.06	2.70
Initial $F_{\Delta H}$	-	NA ^a	2.15	2.09	1.94	1.70
Maximum Transient $F_{\Delta H}$	-	5.21	3.75	3.58	3.01	2.11
Maximum Neutron Power, FOP	-	0.32	0.55	0.69	0.98	1.10
Maximum cal/g	≤ 150	-	70.4	50.4	63.9	109.4
Maximum $\Delta\text{cal/g}$, prompt	≤ 110	-	10.0	10.9	11.8	7.2
Maximum Fuel Temperature, °F	[]	-	2655	1901	2529	4014
Maximum Cladding Temperature, °F	[]	-	1098	727	951	1461
MDNBR/SAFDL Ratio For Failure	≤ 1.0	-	0.71	1.86	0.96	0.33
Time of Trip (initiation of safety bank insertion), seconds	-	No Trip	No Trip ^b	0.850	0.825	No Trip
Equivalent nominal rods failed, %	≤ 30	0	1.8	0	0	7.2

Notes:

^a Not applicable since initial stored energy above the coolant temperature is zero.

^b Trip is disabled to bound consequences of powers lower than 25%.



UNITED STATES
NUCLEAR REGULATORY COMMISSION
WASHINGTON, D.C. 20555-0001

February 27, 2009

Mr. Ronnie L. Gardner
AREVA NP Inc.
3315 Old Forest Road
P.O. Box 10935
Lynchburg, VA 24506-0935

SUBJECT: THIRD REQUEST FOR ADDITIONAL INFORMATION REGARDING
ANP-10286P, "U.S. EVOLUTIONARY POWER REACTOR ROD EJECTION
ACCIDENT METHODOLOGY TOPICAL REPORT"

Dear Mr. Gardner:

By letter dated November 20, 2007, which can be accessed through the U.S. Nuclear Regulatory Commission's (NRC Agencywide Document Access and Management System ADAMS) Accession No. ML073310620, AREVA NP submitted for U.S. Nuclear Regulatory Commission (NRC) staff review Topical Report ANP-10286, "Rod Ejection Accident Methodology" (ML073310629). The first set of request for additional information (RAI) was issued by the NRC on May 16, 2008 (ML081360008), and the AREVA NP responses were received on July 15, 2008 (ML081970402). The second set of request for additional information (RAI) was issued by the NRC on July 29, 2008 (ML081850297), and the AREVA NP responses were received on October 14, 2008 (ML082880502).

The NRC staff's review has determined that some areas of this report require additional information in order to complete the review. The specific information requested is contained in the enclosure to this letter. The draft RAI was discussed with your staff in meetings on February 18, 2009. AREVA NP has agreed to provide a response to the first two questions within 30 days and a response to the third question within 90 days of the receipt of this letter.

If you have any questions regarding this matter, I may be reached at 301-415-3361.

Sincerely,

A handwritten signature in black ink, appearing to read "Getachew Tesfaye".

Getachew Tesfaye, Sr. Project Manager
EPR Projects Branch
Division of New Reactor Licensing
Office of New Reactors

Docket No. 52-020
Enclosure:
Request for Additional Information

cc: DC AREVA – EPR Mailing List

DC AREVA - EPR Mailing List

(Revised 01/05/2009)

cc:

Mr. Glenn H. Archinoff
AECL Technologies
481 North Frederick Avenue
Suite 405
Gaithersburg, MD 20877

Mr. Gary Wright, Director
Division of Nuclear Facility Safety
Illinois Emergency Management Agency
1035 Outer Park Drive
Springfield, IL 62704

Ms. Michele Boyd
Legislative Director
Energy Program
Public Citizens Critical Mass Energy
and Environmental Program
215 Pennsylvania Avenue, SE
Washington, DC 20003

Dr. Charles L. King
Licensing Manager, IRIS Project
Westinghouse Electric Company
Science and Technology Department
20 International Drive
Windsor, CT 06095

Ms. Sherry McFaden
Framatome NP, Inc.
3315 Old Forest Road, OF-16
Lynchburg, VA 24501

Mr. Steve Seitz
AREVA
100 Dean Road
East Lyme, CT 06333

Mr. Tom Sliva
Vice President
New Plants Project Management
AREVA, NP, Inc. 3315
Old Forest Road
P.O. Box 10935
Lynchburg, VA 24506-0935

Mr. Robert E. Sweeney
IBEX ESI
4641 Montgomery Avenue
Suite 350
Bethesda, MD 20814

DC AREVA - EPR Mailing List

Email

alex.miller@hse.gsi.gov.uk (Alex Miller)
APH@NEI.org (Adrian Heymer)
awc@nei.org (Anne W. Cottingham)
bob.brown@ge.com (Robert E. Brown)
BrinkmCB@westinghouse.com (Charles Brinkman)
carey.fleming@constellation.com (Carey Fleming)
CFessler@ameren.com (Chris Fessler)
chris.maslak@ge.com (Chris Maslak)
cwaltman@roe.com (C. Waltman)
david.hinds@ge.com (David Hinds)
david.lewis@pillsburylaw.com (David Lewis)
dlochbaum@UCSUSA.org (David Lochbaum)
erg-xl@cox.net (Eddie R. Grant)
gcesare@enercon.com (Guy Cesare)
greshaja@westinghouse.com (James Gresham)
james.beard@gene.ge.com (James Beard)
james.p.mcquighan@constellation.com (Jim McQuighan)
jason.parker@pillsburylaw.com (Jason Parker)
jgutierrez@morganlewis.com (Jay M. Gutierrez)
jim.riccio@wdc.greenpeace.org (James Riccio)
JJD1@nrc.gov (John Donohue)
JINesrsta@cpsenergy.com (James J. Nesrsta)
John.O'Neill@pillsburylaw.com (John O'Neill)
Joseph_Hegner@dom.com (Joseph Hegner)
junichi_uchiyama@mnes-us.com (Junichi Uchiyama)
KSutton@morganlewis.com (Kathryn M. Sutton)
kwaugh@impact-net.org (Kenneth O. Waugh)
lchandler@morganlewis.com (Lawrence J. Chandler)
Marc.Brooks@dhs.gov (Marc Brooks)
maria.webb@pillsburylaw.com (Maria Webb)
mark.beaumont@wsms.com (Mark Beaumont)
matias.travieso-diaz@pillsburylaw.com (Matias Travieso-Diaz)
mbowling@numarkassoc.com (Marty Bowling)
media@nei.org (Scott Peterson)
mike_moran@fpl.com (Mike Moran)
MSF@nei.org (Marvin Fertel)
mwetterhahn@winston.com (M. Wetterhahn)
nirsnet@nirs.org (Michael Mariotte)
patriciaL.campbell@ge.com (Patricia L. Campbell)
paul.gaukler@pillsburylaw.com (Paul Gaukler)
Paul@beyondnuclear.org (Paul Gunter)
pshastings@duke-energy.com (Peter Hastings)
RJB@NEI.org (Russell Bell)
RKTemple@cpsenergy.com (R.K. Temple)

DC AREVA - EPR Mailing List

roberta.swain@ge.com (Roberta Swain)
Ronda.pederson@areva.com (Ronda Pederson)
rrsgarro@pplweb.com (Rocco Sgarro)
russell.wells@areva.com (Russell Wells)
sabinski@suddenlink.net (Steve A. Bennett)
sandra.sloan@areva.com (Sandra Sloan)
sfrantz@morganlewis.com (Stephen P. Frantz)
steven.hucik@ge.com (Steven Hucik)
tkkibler@scana.com (Tria Kibler)
tlharpster@pplweb.com (Terry Harpster)
tom.miller@hq.doe.gov (Tom Miller)
trsmith@winston.com (Tyson Smith)
Vanessa.quinn@dhs.gov (Vanessa Quinn)
VictorB@bv.com (Bill Victor)
vijukrp@westinghouse.com (Ronald P. Vijuk)
Wanda.K.Marshall@dom.com (Wanda K. Marshall)
wayne.marquino@ge.com (Wayne Marquino)
whorin@winston.com (W. Horin)

THIRD REQUEST FOR ADDITIONAL INFORMATION (RAI)

ANP-10286P, "U. S. EPR ROD EJECTION ACCIDENT

METHODOLOGY TOPICAL REPORT"

DOCKET NO. 52-020

RAI-33. [Intentionally deleted.]

RAI-34. Figure 8-41 provides the transient post-to-pre-ejection power ratio versus static post-to-pre-ejection power ratio plot, and the rod failure census.

- a. Why is the static ratio always larger than the transient ratio?
- b. Does this imply a built-in conservatism? If yes, what is the implied conservatism?
- c. Provide a qualitative discussion of the uncertainty in the methodology used to determine the number of failed rods for transients terminated by 5 seconds.

RAI-35. Provide a discussion of the uncertainty in the analysis regarding the number of rods failed in the quasi-static analysis using S-RELAP and LYNXT for transients lasting longer than approximately 5 seconds.

RAI-36. In order to assess the NEMO-K/LYNX-T Computational Engine reactivity insertion accident analyses, we request that AREVA perform comparison analyses of reactor excursion tests performed during the mid-1960s at the National Reactor Testing Station. These data were taken during the E-Core campaign as part of the Special Power Reactor Test III (SPERT) program. This comparison analysis will assist the verification of compliance of the rod ejection analysis with the Standard Review Plan (SRP), Section 15.4.8.

ENCLOSURE



March 26, 2009
NRC:09:021

Document Control Desk
U.S. Nuclear Regulatory Commission
Washington, D.C. 20555-0001

Response to a Third Request for Additional Information Regarding ANP-10286P, "U.S. EPR Rod Ejection Accident Methodology Topical Report"

Ref. 1: Letter, Ronnie L. Gardner (AREVA NP Inc.) to Document Control Desk (NRC), "Request for Review and Approval of ANP-10286P, 'U.S. EPR Rod Ejection Accident Methodology Topical Report'," NRC:07:065, November 20, 2007.

Ref. 2: Letter, Getachew Tesfaye (NRC) to Ronnie L. Gardner (AREVA NP Inc.), "Third Request for Additional Information Regarding ANP-10286P, 'U.S. EPR Rod Ejection Accident Methodology Topical Report'," February 27, 2009.

AREVA NP Inc. (AREVA NP) requested the NRC's review and approval of topical report ANP-10286P, "U.S. EPR Rod Ejection Accident Methodology Topical Report" in Reference 1. The NRC provided a third Request for Additional Information (RAI) regarding this topical report in Reference 2. The response to the RAI is enclosed with this letter, ANP-10286Q3P, "Response to a Request for Additional Information – ANP-10286P, 'U.S. EPR Rod Ejection Accident Methodology Topical Report'."

AREVA NP considers some of the material contained in the attachments to this letter to be proprietary. As required by 10 CFR 2.390(b), an affidavit is enclosed to support the withholding of the information from public disclosure. Proprietary and non-proprietary versions of the response are attached.

If you have any questions related to this submittal, please contact Ms. Sandra M. Sloan, Regulatory Affairs Manager for New Plants. She may be reached by telephone at 434-832-2369 or by e-mail at sandra.sloan@areva.com.

Sincerely,

A handwritten signature in cursive script that reads "Ronnie L. Gardner".

Ronnie L. Gardner, Manager
Corporate Regulatory Affairs
AREVA NP Inc.

Enclosure

cc: G. Tesfaye
Docket No. 52-020

AREVA NP INC.

An AREVA and Siemens company

3315 Old Forest Road, P.O. Box 10935, Lynchburg, VA 24506-0935
Tel.: 434 832 3000 - Fax: 434 832 3840 - www.areva.com

requested qualifies under 10 CFR 2.390(a)(4) "Trade secrets and commercial or financial information."

6. The following criteria are customarily applied by AREVA NP to determine whether information should be classified as proprietary:

- (a) The information reveals details of AREVA NP's research and development plans and programs or their results.
- (b) Use of the information by a competitor would permit the competitor to significantly reduce its expenditures, in time or resources, to design, produce, or market a similar product or service.
- (c) The information includes test data or analytical techniques concerning a process, methodology, or component, the application of which results in a competitive advantage for AREVA NP.
- (d) The information reveals certain distinguishing aspects of a process, methodology, or component, the exclusive use of which provides a competitive advantage for AREVA NP in product optimization or marketability.
- (e) The information is vital to a competitive advantage held by AREVA NP, would be helpful to competitors to AREVA NP, and would likely cause substantial harm to the competitive position of AREVA NP.

The information in the Document is considered proprietary for the reasons set forth in paragraphs 6(b) and 6(c) above.

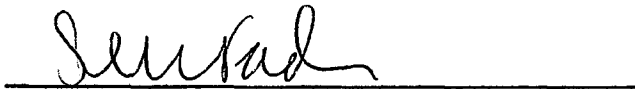
7. In accordance with AREVA NP's policies governing the protection and control of information, proprietary information contained in this Document have been made available, on a limited basis, to others outside AREVA NP only as required and under suitable agreement providing for nondisclosure and limited use of the information.

8. AREVA NP policy requires that proprietary information be kept in a secured file or area and distributed on a need-to-know basis.

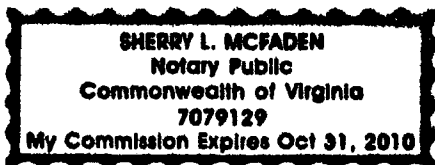
9. The foregoing statements are true and correct to the best of my knowledge, information, and belief.

A handwritten signature in black ink, appearing to be 'A. P. N.', written over a horizontal line.

SUBSCRIBED before me this 25th
day of March 2009.

A handwritten signature in black ink, appearing to be 'Sherry L. McFaden', written over a horizontal line.

Sherry L. McFaden
NOTARY PUBLIC, COMMONWEALTH OF VIRGINIA
MY COMMISSION EXPIRES: 10/31/10
Reg. # 7079129



**Response to a Request for Additional Information – ANP-10286P
“U.S. EPR Rod Ejection Accident Methodology Topical Report”**

RAI-33. [Intentionally deleted.]

RAI-34:

Figure 8-41 provides the transient post-to-pre-ejection power ratio versus static post-to-pre-ejection power ratio plot, and the rod failure census.

- a. *Why is the static ratio always larger than the transient ratio?*
- b. *Does this imply a built-in conservatism [and if yes, what is it]?*
- c. *Provide a qualitative discussion of the methodology used to determine the number of failed rods for transients terminated by 5 seconds.*

Response to RAI-34:

- a. The reactivity feedback (Doppler and moderator) is frozen at the pre-ejection conditions, while the transient calculation includes thermal reactivity feedback at all conditions including the time period during the ejection of the control rod. Therefore, the static value of the power ratio is always larger than the transient value. The power ratios are addressed in the Response to RAI-28, Reference 34-1.
- b. The use of the static ratios does not add additional conservatism relative to the use of the transient ratios. There is additional conservatism included due to the determination of the relationship of static ratio to transient ratio. This is described in the Response to RAI-34c.
- c. [] fuel rods (chosen from those represented in the Rod Ejection Topical Report, Figure 8-41) are chosen to have their transient power histories individually analyzed by LYNXT for each condition (e.g., beginning-of-cycle (BOC), hot full power (HFP)). The highest corresponding transient ratio data point (corresponding to a particular fuel assembly) for a given static ratio data point is chosen to be conservative. The power histories are augmented by applicable uncertainty components as described in the Rod Ejection Topical Report, Table 7-2 throughout the entire transient as analyzed by LYNXT.

For example, for the BOC HFP case, the total two dimensional uncertainty plus an additional design allowance results in a total multiplier of [] on the peak fuel rod power, which is included throughout the entire transient. Each of the [] transient power histories is analyzed using LYNXT to determine a corresponding multiplier on the fuel rod power which causes the fuel rod to reach the departure from nucleate boiling ratio (DNBR) design limit. The multipliers are then applied to the corresponding static pre-ejection and post-ejection peaking factors (F_{AH} and F_Q) in order to generate a set of failure criteria to be applied to all fuel rods in the static census analysis. This process and example peaking factors are also provided in the Response to RAI-28, Reference 34-1. The LYNXT analysis calculated power multipliers resulted in 0.3 percent of fuel rods failed for the BOC HFP case. If the uncertainties and allowances were removed to simulate best estimate values, no failures would be calculated for this example.

The primary conservatisms in the control rod ejection methodology, which result in a conservative number of failed fuel rods are:

- 1) The power response versus time for the reference has the following conservatisms:
 - a) The deterministic choice of the highest ejected control rod worth or peaking versus a statistical evaluation of the range of potential ejected control rod worths.

- b) The 15% uncertainty applied to the ejected control rod worth (Rod Ejection Topical Report, Table 7-3).
 - c) The uncertainties applied to Doppler and moderator temperature reactivity coefficients (DTC and MTC) and delayed neutron fraction beta effective (β -eff).
 - d) The reference cycle has additional biases on ejected rod worth, DTC, MTC, and β -eff that will be less limiting for the actual cycles.
- 2) The peaking factor uncertainties defined in the Rod Ejection Topical Report, Table 7-2.
- 3) The choice of the assemblies with the highest values of []
for the DNBR evaluation.

Reference:

34-1, ANP-10286Q2P, Response to Second Request for Additional Information - ANP-10286P
"U.S. EPR Rod Ejection Accident Methodology Topical Report."

RAI-35:

Provide a discussion of the analysis regarding the number of rods failed in the quasi-static analysis using S-RELAP and LYNXT for transients lasting longer than approximately 5 seconds.

Response to RAI-35:

The analysis for the number of rods failed in the steady state analysis is analogous to the transient analysis except that [] fuel rods reduce to a single fuel rod because all rod powers include the full Doppler and moderator feedback effects. The fuel rod with the peak steady state power (F_{dh}) and corresponding normalized axial shape is analyzed using LYNXT for the DNBR performance. The fuel rod power is augmented by applicable uncertainty components as described in Table 7-2.

For example, for the BOC HFP case, the total two dimensional uncertainty plus an additional design allowance results in a total multiplier of [] which is multiplied times the peak pin power. The power distribution (radial and axial) for the fuel assembly is analyzed with LYNXT in a static solution mode to determine a corresponding multiplier on the fuel rod power, which causes the fuel rod to reach the DNBR design limit. The thermal hydraulic boundary conditions for system pressure, core inlet temperature, and inlet mass flux are from the S-RELAP calculation at the time of interest during the transient (this is described in the Response to RAI-26 in Reference 35-1). The multiplier is then applied to the steady state post-ejection peaking factors ($F_{\Delta H}$ and F_Q) in order to generate failure criteria to be applied to fuel rods in the steady state census analysis. The LYNXT analysis calculated multiplier resulted in 7.2 percent of fuel rods failed. If the uncertainties and allowances were removed to simulate best estimate values, less than 0.6 percent of fuel rods would be calculated to fail for this example.

The primary conservatisms in the control rod ejection methodology which result in a conservative number of failed fuel rods for transients lasting longer than approximately five seconds are the same as the first two described in the Response to RAI-34.

Reference:

35-1, ANP-10286Q2P, Response to Second Request for Additional Information - ANP-10286P
"U.S. EPR Rod Ejection Accident Methodology Topical Report."



June 15, 2009
NRC:09:067

Document Control Desk
U.S. Nuclear Regulatory Commission
Washington, D.C. 20555-0001

Response to a Request for Additional Information Regarding ANP-10286P, "U.S. EPR Rod Ejection Accident Methodology Topical Report"

- Ref. 1: Letter, Ronnie L. Gardner (AREVA NP Inc.) to Document Control Desk (NRC), "Request for Review and Approval of ANP-10286P, 'U.S. EPR Rod Ejection Accident Methodology Topical Report'," NRC:07:065, November 20, 2007.
- Ref. 2: Letter, Getachew Tesfaye (NRC) to Ronnie L. Gardner (AREVA NP Inc.), "Third Request for Additional Information Regarding ANP-10286P, 'U.S. EPR Rod Ejection Accident Methodology Topical Report'," February 27, 2009.
- Ref. 3: Letter, Ronnie L. Gardner (AREVA NP Inc.) to Document Control Desk (NRC), "Response to a Third Request for Additional Information Regarding ANP-10286P, 'U.S. EPR Rod Ejection Accident Methodology Topical Report'," NRC:09:021, March 24, 2009.

AREVA NP Inc. (AREVA NP) requested the NRC's review and approval of topical report ANP-10286P, "U.S. EPR Rod Ejection Accident Methodology Topical Report" in Reference 1. The NRC provided a third Request for Additional Information (RAI) regarding this topical report in Reference 2. The responses to all but one of the questions in this RAI were provided in Reference 3. The response to the final question, RAI-36, is enclosed with this letter, ANP-10286Q4P, "Response to a Request for Additional Information – ANP-10286P, 'U.S. EPR Rod Ejection Accident Methodology Topical Report'."

If you have any questions related to this submittal, please contact Ms. Sandra M. Sloan, Regulatory Affairs Manager for New Plants. She may be reached by telephone at 434-832-2369 or by e-mail at sandra.sloan@areva.com.

Sincerely,


For

Ronnie L. Gardner, Manager
Corporate Regulatory Affairs
AREVA NP Inc.

Enclosures

cc: G. Tesfaye
Docket No. 52-020

AREVA NP INC.

An AREVA and Siemens company

**Response to a Request for Additional Information – ANP-10286P
“U.S. EPR Rod Ejection Accident Methodology Topical Report”**

RAI-36. *In order to assess the NEMO-K/LYNX-T Computational Engine reactivity insertion accident analyses, we request that AREVA perform comparison analyses of reactor excursion tests performed during the mid-1960s at the National Reactor Testing Station. These data were taken during the E-Core campaign as part of the Special Power Reactor Test III (SPERT) program. This comparison analysis will assist the verification of compliance of the rod ejection analysis with the Standard Review Plan (SRP), Section 15.4.8.*

Response to RAI-36:

Two of the SPERT III-E facility (Reference 1) rod ejection experiments were selected for evaluation against the test results provided in Reference 2. Test 60 was selected for a hot zero power (HZP) condition and Test 86 for a hot full power (HFP) condition. These are simulated with NEMO-K using cross-sections and delayed neutron precursor data provided by the NRC. The cross-sections are converted to NEMO-K cross-section tables. The SPERT III-E experiments do not require the use of LYNXT to simulate the experiment. The majority of the remaining information is obtained from References 1 and 2, or as noted in the text. Assumptions are made where the information is not readily available. Several model assumptions are required to perform these benchmarks due to the difficulty of finding applicable reference information for modeling. A number of the key modeling assumptions are listed below.

- The cross-sections and neutron precursor data provided by the NRC are used as provided.
- The regulating control rod fuel follower is not modeled in the lower reflector region.
- The axial reflectors are modeled with a standard PWR model since it represents a similar metal to water ratio for the SPERT III-E core.
- The regulating control rod position is adjusted until the NEMO-K initial K-effective is 1.0 prior to the ejection of the transient control rod. The initial transient control rod is positioned so that it yields the measured ejected control rod worth or is within the uncertainty quoted for the test.
- The control rod ejection begins to move at zero seconds. Note that the ascension to full power and the start of the ejection for test 86 is not described in enough detail to determine whether the core is in thermal equilibrium with the power or whether significant xenon is produced. Zero xenon is assumed.
- The direct energy deposition into the coolant is based on a PWR value of 2.7 percent of the total energy produced.
- The power density in the fuel rod model for each assembly is scaled by the number of fuel rods in the assembly to obtain an accurate nodal average fuel temperature.
- The number of fuel rods per assembly and flow areas for the 5x5 fuel assembly are used for all assemblies for the hydraulic calculations. This assumption should cause an overprediction of the Moderator Temperature Coefficient (MTC) feedback in the 4x4 assemblies.
- The gap conductance for HZP and HFP are assumed constant and are 1.3042 and 2.0000 W/cm²K, respectively (as provided by the NRC).

The base neutronic model is validated with two static comparisons. First, the hot zero power (HZP) static control rod worths at 500°F versus the initial position are calculated and compared

in Figure 36-1 to the measured test results from Reference 2. Second, the calculated moderator temperature coefficient (MTC) is $-3.8\phi/^{\circ}\text{F}$ and the measured MTC is listed as $-4.0\phi/^{\circ}\text{F}$. The agreement with the measured results is good (within 5%) and indicates that the assumptions made are reasonable.

Test 60 - HZP

Test 60 is an ejected control rod test initiated from a core power of 50 watts at 500 °F. In Test 60 the initial transient control rod position is set to yield a worth of 1.23\$ when ejected (which is equal to the measured worth).

The mean generation time, which is controlled by the thermal neutron velocity in a 3-D kinetics code, is not directly measurable. However, if the ejected control rod worth and the beta-effective are known, then the mean generation time can be estimated from the measured reactor period. The thermal neutron velocity is adjusted to yield a reactor period of 9.6 milliseconds which is approximately equivalent to the measured reactor period of 9.7 milliseconds for Test 60. The value used for the thermal neutron velocity is within 3 percent of the values used for the U.S. EPR NEMO-K model at BOC and EOC.

The Test 60 power versus time results, as measured and calculated, are shown in Figure 36-2. The calculated peak power is 439 MW and the measured is reported as 410 ± 41 MW. The calculated integrated power at the peak is 8.6 MW-sec and the measured is reported as 8.5 ± 1.1 MW-sec. Both of these calculated values are within the measurement uncertainty of the test.

Test 86 - HFP

Test 86 is a prompt critical ejected control rod test initiated from a core power of 19 MW with a measured ejected rod worth of 1.17 ± 0.05 \$. Test 86 is simulated with an ejected control rod worth of 1.22\$. This value is equal to the measured worth at the high end of its uncertainty (4.3 percent higher than the reported measured value). Reference 2 states that the ejected control rod worth can not be measured directly at power and its uncertainty is higher because the feedback is immediate and a stable reactor period was not established. The difference in control rod position between a 1.17\$ and a 1.22\$ ejected control rod worth is less than one-quarter inch, which highlights the sensitivity of this small core to the initial control rod position. Also, a PWR typically has to eject a full length control rod which is at least 10 feet in length to become prompt critical whereas the SPERT III-E core becomes prompt critical with less than 8.5 inches of control rod movement. This sensitivity indicates that the experimental uncertainty for control rod worth is larger than 4.3 percent, the difference between the reported worth and the worth used in the NEMO-K calculations.

The same thermal neutron velocity derived for Test 60 is used for modelling Test 86.

The Test 86 power versus time results, measured and calculated, are shown in Figure 36-3. The calculated peak power response is in agreement with the measured response yielding a calculated peak power of 604 MW compared to a measured value of 610 ± 60 MW. The calculated time integrated power at the peak is 13.7 MW-sec and the measured is reported as 17 ± 2 MW-sec.

The calculated result for the integrated power for this test is outside of the quoted measured uncertainty. As stated in the Table VII of Reference 2, the definition of this result is the time integrated power above the initial power. The possible causes of the difference between the measured and calculated integrated power for Test 86 could be a higher uncertainty in the

measured results attributed to the “at power” conditions or a lack of refinement in the model to represent the small SPERT III-E core configuration which is not typical of a PWR. Neither of these conditions affects the ability of NEMO-K to calculate at-power ejected rod transients in PWRs as evidenced by the benchmarks included in NEMO-K topical report BAW-10221PA (Reference 3).

Conclusion

NEMO-K has been benchmarked against the SPERT III-E tests reported above and against a set of international standard problems reported in the NEMO-K topical report BAW-10221PA (Reference 3). These results demonstrate the adequacy of NEMO-K to simulate a control rod ejection transient.

References for RAI 36:

1. J. Dugone, “SPERT III Reactor Facility, E-Core Revision,” IDO-17036, U.S. Atomic Energy Commission, November 1965.
2. “Reactivity Accident Test Results and Analyses for the SPERT III E-Core—A Small, Oxide-Fueled, Pressurized Water Reactor,” IDO-17281, U.S. Atomic Energy Commission, March 1969.
3. BAW-10221PA, “NEMO-K a Kinetics Solution in NEMO,” September 1998.

Figure 36-1—SPERT III-E Test 60 Ejected Control Rod Worths

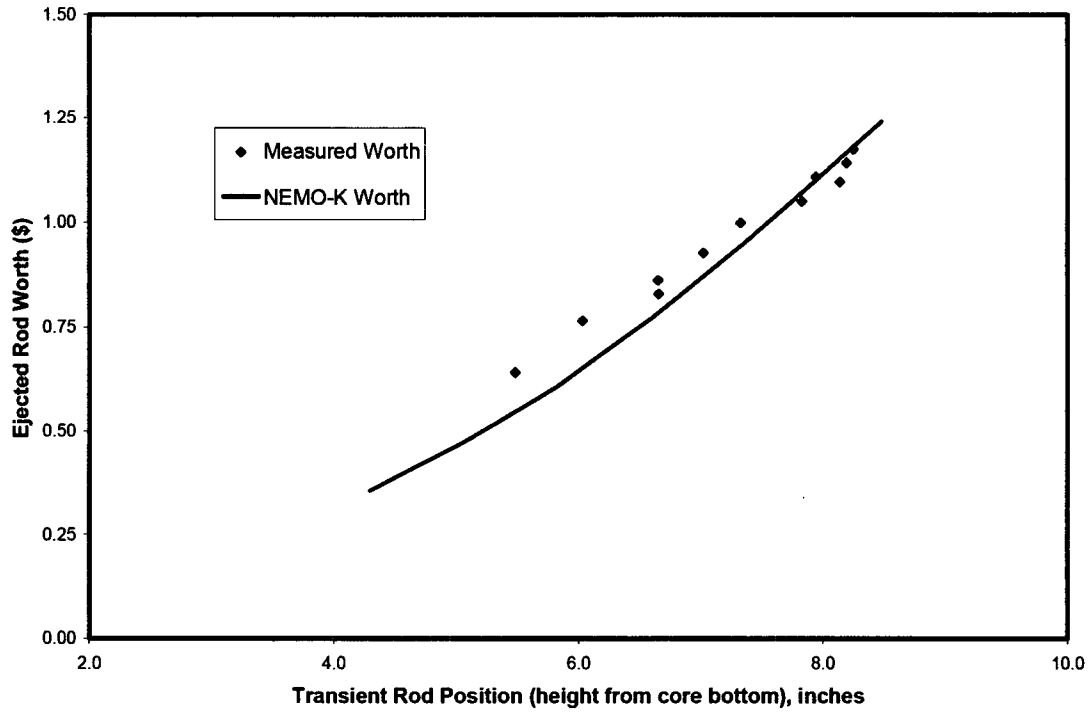


Figure 36-2—SPERT III-E Test 60 Power Response

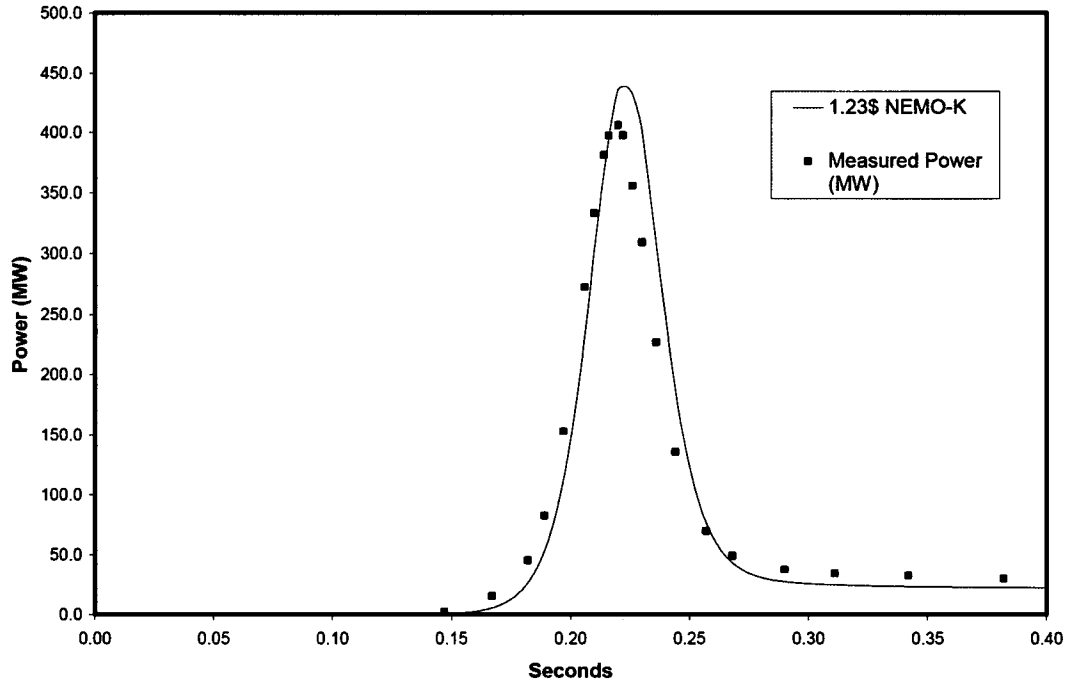
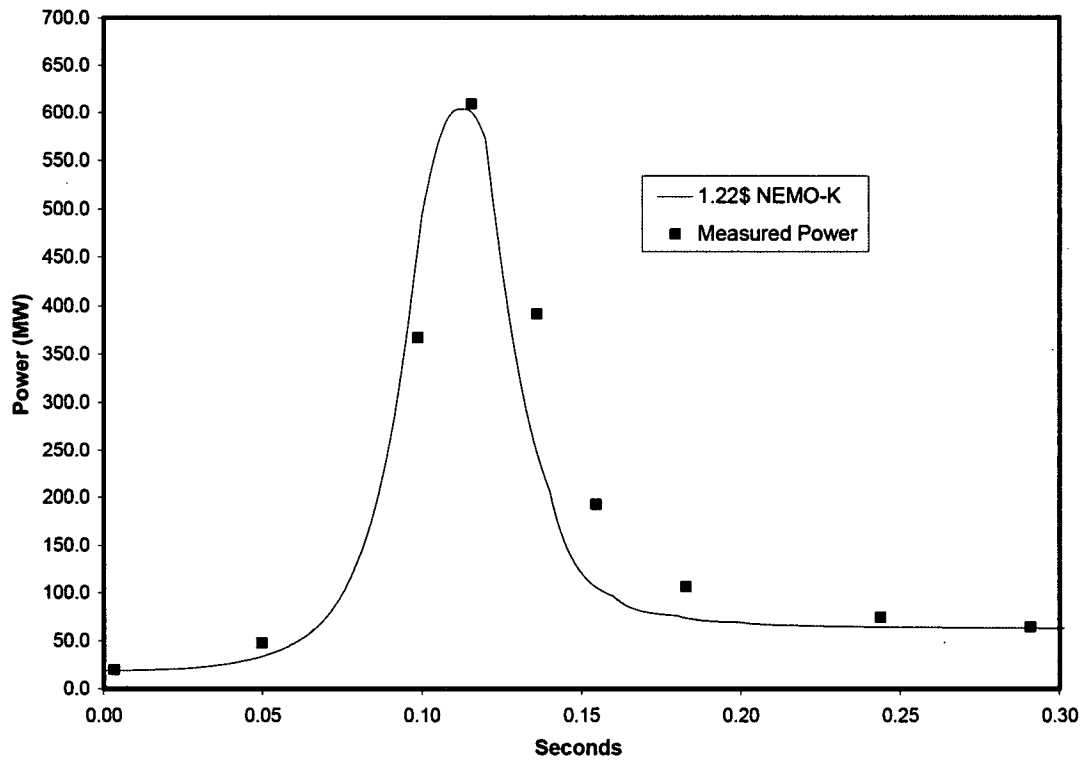


Figure 36-3—SPERT III-E Test 86 Power Response





ANP-10286NP
Revision 0

U.S. EPR Rod Ejection Accident Methodology Topical Report

November 2007

AREVA NP Inc.

Nature of Changes

Item	Section(s) or Page(s)	Description and Justification
Original Issue	NA	NA

Contents

	<u>Page</u>
1.0 INTRODUCTION.....	1-1
2.0 REA REGULATORY REQUIREMENTS.....	2-1
2.1 Cladding Failure.....	2-1
2.1.1 PCMI Criteria for M5™ Cladding.....	2-1
2.1.2 Cladding Failure Due to Total Energy Deposition	2-2
2.1.3 DNBR.....	2-2
2.2 Coolability	2-2
2.3 Radiological Consequences	2-3
2.4 Licensing Criteria for the U.S. EPR.....	2-4
3.0 COMPUTER CODE REQUIREMENTS.....	3-1
4.0 MODEL BOUNDARY CONDITIONS AND UNCERTAINTIES REQUIREMENTS.....	4-1
4.1 Plant Transient Analysis	4-1
4.1.1 Maximum Ejected Rod Worth.....	4-2
4.1.2 Rate of Reactivity Insertion	4-2
4.1.3 Moderator Feedback	4-3
4.1.4 Fuel Temperature Feedback.....	4-3
4.1.5 Delayed Neutron Fraction	4-3
4.1.6 Reactor Trip Reactivity.....	4-3
4.1.7 Fuel Cycle Design	4-4
4.1.8 Heat Resistances and Transient Cladding to Coolant Heat Transfer	4-4
4.1.9 Heat Capacities.....	4-4
4.1.10 Fractional Heat Deposited in Coolant.....	4-6
4.1.11 Pellet Radial Power Profile.....	4-6
4.1.12 Rod Peaking Factors.....	4-6
4.1.13 Neutron Velocities	4-7
4.1.14 System T-H Conditions	4-7
4.2 Fuel Rod Transient Model for Fuel and Cladding Temperatures and DNBR	4-7
4.2.1 Pellet and Cladding Dimensions	4-8
4.2.2 Burnup Distribution.....	4-8

4.2.3	Cladding Oxidation	4-8
4.2.4	Power Distribution	4-8
4.2.5	Initial Coolant Conditions	4-8
4.2.6	Transient Power Specification	4-9
4.2.7	Heat Resistances in Fuel, Gap, and Cladding	4-9
4.2.8	Transient Cladding-to-Coolant Heat Transfer Coefficient	4-9
4.2.9	Heat Capacities of Fuel and Cladding	4-9
4.2.10	Coolant Conditions	4-10
4.2.11	System T-H Conditions	4-10
4.3	Time Dependent Analysis	4-10
4.4	Failure Analysis	4-10
5.0	U.S. EPR REA METHODOLOGY	5-1
6.0	COMPUTER CODES	6-1
6.1	COPERNIC	6-1
6.2	Plant Transient Model	6-1
6.2.1	Trip Function	6-2
6.2.2	Adiabatic cal/g Edit	6-5
6.2.3	Adjustment Factors	6-5
6.2.4	Pellet Weighted Temperature for DTC	6-6
6.2.5	NEMO-K Summary	6-7
6.3	Transient Fuel Rod Model	6-8
6.3.1	General Overview of Existing LYNXT Fuel Rod Models	6-8
6.3.2	Enhancements to the Fuel Rod Models	6-9
6.3.3	LYNXT Benchmark Review	6-11
6.3.4	LYNXT Conclusions	6-14
6.4	System T-H Model	6-16
7.0	APPLICATION OF BOUNDARY CONDITIONS AND UNCERTAINTIES	7-1
7.1	NEMO-K Boundary Conditions and Uncertainties	7-1
7.1.1	Ejected Rod Worth	7-1
7.1.2	MTC	7-2
7.1.3	DTC	7-2
7.1.4	β_{eff}	7-2
7.1.5	Fuel Cycle Design	7-2

7.1.6	Transient Power and Rod Power Peaking	7-4
7.1.7	Sensitivity Calculations for Plant Transient Calculations	7-4
7.2	LYNXT Boundary Conditions and Uncertainties	7-5
7.2.1	Pellet and Cladding Dimensions (Geometry)	7-5
7.2.2	Cladding Oxidation	7-6
7.2.3	Coolant Conditions	7-7
7.2.4	Transient Power	7-7
7.2.5	Heat Resistances in Fuel, Gap and Cladding	7-8
7.2.6	Coolant Heat Transfer Coefficient and Transient Coolant Conditions	7-10
7.3	Failure Boundary Conditions	7-10
8.0	U.S. EPR SAMPLE PROBLEM RESULTS	8-1
8.1	NEMO-K Results	8-1
8.2	S-RELAP5 Evaluation	8-1
8.3	LYNXT Results	8-2
8.4	Rod Census	8-4
8.5	Summary Results	8-5
9.0	CONCLUSIONS AND CYCLE SPECIFIC CHECKS	9-1
10.0	REFERENCES	10-1

List of Tables

Table 2-1 REA Limits for U.S. EPR.....	2-5
Table 4-1 PIRT Plant Transient Analysis.....	4-12
Table 4-2 PIRT Fuel Rod Transient Analysis for Fuel and Cladding Temperatures..	4-12
Table 6-1 NEACRP Kinetic Results.....	6-17
Table 6-2 Cylindrical and Planar Geometry Collocation Points for LYNXT	6-18
Table 6-3 LYNXT and COPERNIC Transient Temperature Ratio Comparisons	6-19
Table 6-4 LYNXT Fuel Rod Model Options	6-20
Table 7-1 Design and REA Analysis Conditions	7-12
Table 7-2 Peaking Uncertainties	7-13
Table 7-3 Plant Transient Sensitivity Study Summary.....	7-14
Table 8-1 Trip Signal Parameters in Analysis	8-6
Table 8-2 Static Power Search.....	8-7
Table 8-3 Estimated Rod Failures	8-7
Table 8-4 Ejected Rod Analysis Results for BOC	8-8
Table 8-5 Ejected Rod Analysis Results for EOC	8-9
Table 9-1 Ejected Rod Analysis Checklist.....	9-2
Table 9-2 Cycle 1 Ejected Rod Parameters	9-3

List of Figures

Figure 6-1 Scram Position Versus Drop Time	6-21
Figure 6-2 Core Power Fraction – Case B2	6-22
Figure 6-3 Power Distribution at Initial Conditions – Case A1	6-23
Figure 6-4 Power Distribution at Maximum Core Power – Case A1	6-24
Figure 6-5 Power Distribution at 5 Seconds – Case A1	6-24
Figure 6-6 Comparison of Radial Power at Max Power – C1	6-25
Figure 6-7 Comparison of Radial Power at Max Power – C2	6-25
Figure 6-8 HZP/EOL Transient Fuel Surface Temperature	6-26
Figure 6-9 HZP/EOL Transient Fuel Average Temperature	6-26
Figure 6-10 HZP/EOL Transient Fuel Centerline Temperature	6-27
Figure 6-11 HZP/EOL Transient Fuel Maximum Temperature	6-27
Figure 6-12 HZP/EOL Transient Cladding Maximum Temperature	6-28
Figure 6-13 HFP/EOL Transient Fuel Surface Temperature	6-29
Figure 6-14 HFP/EOL Transient Fuel Average Temperature	6-29
Figure 6-15 HFP/EOL Transient Fuel Centerline Temperature	6-30
Figure 6-16 HFP/EOL Transient Fuel Maximum Temperature	6-30
Figure 6-17 HFP/EOL Transient Cladding Maximum Temperature	6-31
Figure 6-18 HZP/BOL Transient Fuel Surface Temperature	6-32
Figure 6-19 HZP/BOL Transient Fuel Average Temperature	6-32
Figure 6-20 HZP/BOL Transient Fuel Centerline Temperature	6-33
Figure 6-21 HZP/BOL Transient Fuel Maximum Temperature	6-33
Figure 6-22 HZP/BOL Transient Cladding Maximum Temperature	6-34
Figure 6-23 HFP/BOL Transient Fuel Surface Temperature	6-35
Figure 6-24 HFP/BOL Transient Fuel Average Temperature	6-35
Figure 6-25 HFP/BOL Transient Fuel Centerline Temperature	6-36
Figure 6-26 HFP/BOL Transient Fuel Maximum Temperature	6-36

Figure 6-27 HFP/BOL Transient Cladding Maximum Temperature.....	6-37
Figure 7-1 Average Coolant Temperature with Power	7-16
Figure 7-2 Rod Position Technical Specification Limits/Analysis	7-17
Figure 7-3 BOC 25%, FOP Comparison between Equilibrium Cycle and []	7-18
Figure 7-4 BOC HFP, FOP Comparison between Equilibrium Cycle and []	7-18
Figure 7-5 EOC HZP Equilibrium Cycle and [] Comparison	7-19
Figure 7-6 EOC HFP Equilibrium Cycle and [] Comparison	7-19
Figure 7-7 EOC HZP Equilibrium Cycle and []	7-20
Figure 7-8 17-Channel LYNXT Model Diagram.....	7-21
Figure 7-9 MDNBR Uranium Enrichment Response for EOC HZP	7-22
Figure 7-10 UO ₂ and Gadolinia Fuel Temperatures for BOC HFP	7-23
Figure 8-1 BOC 0% Power Transient.....	8-10
Figure 8-2 BOC 25% Power Transient.....	8-11
Figure 8-3 BOC 35% Power Transient.....	8-12
Figure 8-4 BOC 60% Power Transient.....	8-13
Figure 8-5 BOC 100% Power Transient.....	8-14
Figure 8-6 EOC 0% Power Transient.....	8-15
Figure 8-7 EOC 25% Power Transient.....	8-16
Figure 8-8 EOC 35% Power Transient.....	8-17
Figure 8-9 EOC 60% Power Transient.....	8-18
Figure 8-10 EOC 100% Power Transient.....	8-19
Figure 8-11 BOC 100% Power Transient for N05 Ejected	8-20
Figure 8-11 BOC 100% Power Transient for N05 Ejected	8-20
Figure 8-12 S-RELAP5 Results for BOC 25%.....	8-21
Figure 8-13 S-RELAP5 Results for HFP	8-21
Figure 8-14 MDNBR for BOC 25%.....	8-22
Figure 8-15 Fuel and Cladding Temperatures for	8-23
Figure 8-16 Peak Enthalpy Rise for BOC 25%.....	8-24

Figure 8-17 MDNBR for BOC 35%.....	8-25
Figure 8-18 Fuel and Cladding Temperatures for BOC 35%.....	8-26
Figure 8-19 Peak Enthalpy Rise for BOC 35%.....	8-27
Figure 8-20 MDNBR Excursion for BOC 60%	8-28
Figure 8-21 Fuel and Cladding Temperatures for BOC 60%.....	8-29
Figure 8-22 Peak Enthalpy Rise Excursion for BOC 60%	8-30
Figure 8-23 MDNBR for BOC HFP	8-31
Figure 8-24 Fuel and Cladding Temperatures for BOC HFP.....	8-32
Figure 8-25 Peak Enthalpy Rise for BOC HFP.....	8-33
Figure 8-26 MDNBR for EOC HZP	8-34
Figure 8-27 Fuel and Cladding Temperatures for EOC HZP.....	8-35
Figure 8-28 Peak Enthalpy Rise for EOC HZP.....	8-36
Figure 8-29 MDNBR for EOC 25%.....	8-37
Figure 8-30 Fuel and Cladding Temperatures for EOC 25%.....	8-38
Figure 8-31 Peak Enthalpy Rise for EOC 25%.....	8-39
Figure 8-32 MDNBR for EOC 35%.....	8-40
Figure 8-33 Fuel and Cladding Temperatures for EOC 35%.....	8-41
Figure 8-34 Peak Enthalpy Rise for EOC 35%.....	8-42
Figure 8-35 MDNBR for EOC 60%.....	8-43
Figure 8-36 Fuel and Cladding Temperatures for EOC 60%.....	8-44
Figure 8-37 Peak Enthalpy Rise for EOC 60%.....	8-45
Figure 8-38 MDNBR for EOC HFP	8-46
Figure 8-39 Fuel and Cladding Temperatures for EOC HFP.....	8-47
Figure 8-40 Peak Enthalpy Rise for EOC HFP.....	8-48
Figure 8-41 Static Ejected Rod Peak Correlated to Transient Peak.....	8-49

Nomenclature

Acronym	Definition
β_{eff}	Beta effective (effective total delayed neutron fraction)
BOC	Beginning Of Cycle
BOL	Beginning Of Life (of a fuel rod)
cal/g	Calories per gram
CG/CP	Constant Gap/Constant Properties
CG/TDP	Constant Gap/Temperature Dependent Properties
CHF	Critical Heat Flux
DNBR	Departure From Nucleate Boiling Ratio
DTC	Doppler Temperature Coefficient
EOC	End Of Cycle
EOL	End Of Life (of a fuel rod)
FGR	Fission Gas Release
FGRF	Fission Gas Release Failures
FOP	Fraction Of Power
$F_{\Delta H}$	Peak rod power (in the core)
F_Q	Peak local power (in the core)
Gd ₂ O ₃	Gadolinium Oxide
GWD/MTU	GigaWatt Days per Metric Ton Uranium
HCF	Hot Channel Factor
HFP	Hot Full Power
HZP	Hot Zero Power
IR	Importance Ratios
KN	Knowledge Ratios
LOCA	Loss-Of-Coolant Accident
MDNBR	Minimum Departure from Nucleate Boiling Ratio
MTC	Moderator Temperature Coefficient
NEACRP	Nuclear Energy Agency Committee on Reactor Physics
pcm/°F	PerCent Milli-rho per degree Fahrenheit
PCMI	Pellet Cladding Mechanical Interaction
PIRT	Phenomena Importance Ranking Tables
REA	Rod Ejection Accident
RIA	Reactivity Initiated Accident

Acronym	Definition
SA	Safety Analysis
SAFDL	Specified Acceptable Fuel Design Limit
SRSS	Square Root Sum of the Squares
TFGR	Transient Fission Gas Release
T-H	Thermal Hydraulics
TS	Technical Specifications
μm	Micrometers
UO ₂	Uranium Dioxide
VG/TDP	Variable Gap/Temperature Dependent Properties
w/o	Weight percent
3-D	Three Dimensional

1.0 INTRODUCTION

The methodology to analyze the rod ejection accident (REA) for the U.S. EPR is presented. The methodology includes the use of a nodal 3-D kinetics solution with both thermal-hydraulic (T-H) and fuel temperature feedback and a separate peak rod thermal evaluation with an open channel T-H and fuel thermal model. These models provide more precise localized neutronic and thermal conditions than previous methods to show compliance with the interim Reactivity Initiated Accident (RIA) criteria in the SRP Section 4.2 (Reference 1). The boundary conditions and uncertainty values are defined for the REA methodology. The overall REA sample problem results for the U.S. EPR are well within the limiting criteria for this REA methodology, with maximum $\Delta\text{cal/g}$ less than 14 and failures less than 8 percent of the rods in the core. This report presents the REA regulatory requirements, followed by the code and model requirements, U.S. EPR methodology, computer codes, application of boundary conditions and uncertainties, sample problem results, and conclusions.

2.0 REA REGULATORY REQUIREMENTS

The first step of the methodology is to use the appropriate regulatory requirements to define the specific criteria that the REA analysis will meet. This methodology addresses the requirements in Reference 1 for cladding failure, core coolability, and radiological consequences. The requirements for radiological assessment and the maximum pressure are not addressed by this methodology.

2.1 Cladding Failure

Reference 1 contains several criteria to determine whether the cladding is assumed failed. The failure criteria to be assumed for the U.S. EPR are provided for pellet cladding mechanical interaction (PCMI), total energy deposition, and departure from nucleate boiling ratio (DNBR). Each rod is examined to determine whether it has exceeded any of these criteria and is considered failed if it does.

2.1.1 PCMI Criteria for M5™ Cladding

The prompt PCMI cladding failure criteria for M5™ Cladding is based on Figure B-1 from Reference 1. The maximum corrosion expected for U.S. EPR fuel cladding with M5™ at end of life is less than 35 μm . This oxide thickness is based on a conservative COPENIC (Reference 2) analysis for a limiting rod using a bounding rod power history at burnups in excess of 62 GWD/MTU. The corresponding oxide to wall thickness ratio is 0.061, which leads to a conservative PCMI failure limit of 110 cal/g.

The maximum prompt energy deposition in the RIA simulations is shown to be less than 110 cal/g for all burnups. Hence, no cladding failures occur based on the PCMI criteria for all initial power levels from hot zero power (HZP) to hot full power (HFP).

In order to calculate the fuel enthalpy rise to assess PCMI failures, the prompt fuel enthalpy rise is defined as the radial average fuel enthalpy increase from the initial conditions to the time corresponding to one pulse width after the peak of the prompt pulse.

2.1.2 Cladding Failure Due to Total Energy Deposition

The maximum total enthalpies are shown as less than 150 cal/g, which precludes failures in fuel rods below and above system pressure. This is demonstrated for powers from HZP to HFP.

2.1.3 DNBR

For powers greater than 5 percent rated thermal power, fuel cladding failure is assumed if the cladding surface heat flux exceeds the thermal design limits for MDNBR.

2.2 Coolability

The coolability requirements from Reference 1 are as follows:

1. Peak radial average fuel enthalpy must remain below 230 cal/g.
2. Peak fuel temperature must remain below incipient fuel melting conditions.
3. Mechanical energy generated as a result of (1) non-molten fuel-to-coolant interaction and (2) fuel rod burst must be addressed with respect to reactor pressure boundary, reactor internals, and fuel assembly structural integrity.
4. No loss of coolable geometry due to (1) fuel pellet and cladding fragmentation and dispersal and (2) fuel rod ballooning.

From conditions set forth in Sections 2.1.1 and 2.1.2, energetic ejection of fuel into the coolant is prevented by preserving the cladding integrity during high energy deposition pulses by staying below the cladding and fuel cal/g limits and below the fuel melt temperature.

Coolability for fuel rods undergoing DNB (DNBR failures) is established by limiting rod heatup during post critical heat flux (CHF). If the rod does not heatup enough to rupture, there are no coolability issues. Rupture and significant ballooning are unlikely if the maximum cladding temperature is below [], and there is no significant exothermic oxidation of the cladding. Therefore, coolability is maintained by precluding

PCMI failures, maximum total enthalpies above 150 cal/g, fuel melt, and maximum cladding temperatures greater than [].

2.3 Radiological Consequences

The radiological consequence evaluation associated with the postulated REA is based on the guidance in SRP Section 15.0.3 and RG 1.183, Appendix H. Consideration is also given to the fission-product gap inventory for RIA, and the interim acceptance criteria and guidance provided in Reference 3. One of the objectives of the evaluation is to determine the maximum cladding failure for an REA without exceeding 90 percent of the dose acceptance criterion at any receptor. The acceptable fuel cladding percent failure (DNBR) that meets this objective is approximately 30 percent of the rods in the core dictated by the dose at the exclusion area boundary (EAB).

The radiological consequences could be more severe for failed pins that experience high local energy depositions during an REA causing transient fission gas release. The formula in Section D of Reference 1 is used to increase the fission product gap activity for those rods that fail and is shown below.

$$TFGR = (0.2286 \times \Delta H) - 7.1419$$

where:

TFGR = Transient Fission Gas Release, percent (must be ≥ 0)

ΔH = Increase in prompt fuel enthalpy, Δ cal/g

The gap activity of the axial node rod segments experiencing delta prompt fuel enthalpies greater than 31.2 cal/g ($\Delta H = 31.2$ when $TFGR = 0$) will increase by the above equation. The radiological consequences will incorporate two relative source terms for rods that fail due to DNBR during the REA event. The radiological consequences can be simplified to a function of the equivalent number of rods failed and can be represented by the following equation.

$$EQP = F + FGRF \leq A$$

where:

- EQP = The equivalent number of rods failed
- F = Total number of rods failed due to DNBR or fuel melt
- FGRF = Equivalent number of additional rods failed due to Transient Fission Gas Released from high $\Delta\text{cal/g}$
- A = The maximum allowed number of rods that could fail due to only DNBR failures and stay within the dose limits.

TFGR will be calculated for every rod that failed using the relationship with delta cal/g and converted to FGRF. The total effective number of rods failed will be reported when failed rods are counted for radiological consequences. The radiological assessment remains valid when the equivalent number of pins failed due to REA yields less than 30 percent of the core due to DNBR failures.

2.4 Licensing Criteria for the U.S. EPR

The conditions in Table 2-1 define the limits to be met for the U.S. EPR.

Table 2-1 REA Limits for U.S. EPR

Criterion Description	Limit
Maximum enthalpy of the fuel	≤ 150 cal/g
Maximum energy deposition during prompt power pulse for core powers <5%	≤ 110 cal/g
Fuel Melt	0%
Maximum Cladding Temperature	[]
After power pulse, number of equivalent rods failed due to DNBR or fuel melt	$\leq 30\%$ *

Notes:

* For sample problem.

3.0 COMPUTER CODE REQUIREMENTS

The use of a nodal 3-D kinetics solution with both T-H and fuel temperature feedback and a peak rod thermal evaluation model with an open channel T-H and fuel thermal model are required. The requirement for the computational codes is that they are qualified and approved by the U.S. NRC for time-dependent solutions.

In general, the 3-D neutronic solution will calculate the core power and the local power distribution response to an ejected rod. This information will then be used by an open channel T-H and fuel thermal code to calculate the fuel enthalpy, the temperature distributions, and the DNBR for the peak rod in the core. If the peak rod fails due to DNBR, the open channel T-H and fuel thermal code is also used to establish the power conditions at which a rod will not fail. The boundary conditions and uncertainties used in the codes for the REA simulation are addressed in Section 4.0.

4.0 MODEL BOUNDARY CONDITIONS AND UNCERTAINTIES REQUIREMENTS

This section addresses the boundary conditions and uncertainties considered for the REA. The analysis can be divided into two parts, the plant transient analysis and the fuel rod transient analysis as defined in the Phenomenon Identification and Ranking Tables (PIRT) in Reference 4. A list of the phenomena, their importance ratio and knowledge ratio is presented in Table 4-1 for the plant transient analysis.

A similar list is presented in Table 4-2 for fuel and cladding temperatures. Many of the items included in Table 3-3 in Reference 4 are not included in Table 4-2 because they are captured by a cal/g limit or have little relevance to a DNBR limit. The items that are categorized relative to "PCMI loading to cladding" effects are captured by the cal/g failure limit. The gap size, gas pressure, gas composition, gas distribution, fuel-cladding gap friction coefficient and rod volume are essentially captured in the context of gap conductance. The hydrogen concentration, hydrogen distribution, and spallation effects on the cladding are captured in the cal/g failure limit. Fast fluence, porosity, rim size, bubble size, and bubble distribution are captured by the fuel pellet conductivity and/or the cal/g limit. Therefore, these items are not included in Table 4-2.

Reference 4 states that the phenomena with importance ratios above 75 are important and those with knowledge ratios above 75 are well known. It also warns that parameters near the threshold should not necessarily be ignored. Additional parameters address impacts on DNBR since the scope of Reference 6 was primarily concerned with PCMI type failures and not DNBR. Each of the parameters are addressed with respect to the requirements for modeling relative to the need to bound, apply uncertainty, or to demonstrate a negligible consequence.

4.1 Plant Transient Analysis

The plant transient analysis is dominated during the first 5-10 seconds (less than the loop time) by the core kinetics, nodal fuel temperatures and nodal T-H conditions. Inlet

temperature, core pressure, and flow are relatively constant during an REA so that the 3-D core kinetics can be used with, or independently of, a system T-H code. The results and dependencies of a 3-D kinetics solution are identical to a point kinetics solution for uniform changes to a core. The difference in the two solutions is the local weighting of the changes that occur, which become very important during an REA. Therefore, many of the dependencies of the parameters from the point kinetics models remain applicable to 3-D kinetics. Since a static reactivity calculation provides a 3-D weighting of the core effects, standard static methods to calculate reactivity coefficients, delayed neutron fractions, and rod worths can be used to evaluate the initial conditions for the sensitivities. This section is a review of the parameters listed in Table 4-1 relative to 3-D kinetics and other effects that could impact the results.

4.1.1 *Maximum Ejected Rod Worth*

The maximum ejected rod worth is a limiting parameter and is the driver for the event. It is integral to the neutronic nodal simulator solution through the input of the initial insertion of the rod bank(s) and the control rod cross sections. The worth is not a direct input and is calculated using standard static methods with moderator temperature and fuel temperature held constant. The worth depends on fuel cycle design, cycle lifetime, and initial xenon conditions. The initial conditions are required to be a reasonable representation of the limiting conditions allowed by Technical Specifications that maximize the worth. In addition, an uncertainty is applied that is equal or greater than the approved uncertainty value. Additional conservatisms can be applied to bound future fuel cycle designs.

4.1.2 *Rate of Reactivity Insertion*

Rate of reactivity insertion is not rated as an important parameter for prompt critical rod ejections. A sensitivity study is performed to confirm the impact for the range of conditions analyzed.

4.1.3 Moderator Feedback

Moderator feedback (i.e., Moderator Temperature Coefficient, (MTC)) is not rated as an important parameter relative to the power pulse. However, the MTC does affect the power after the pulse, which can affect DNBR. The MTC is not a direct input to the neutronics computer code and is required to be adjusted to represent an uncertainty.

4.1.4 Fuel Temperature Feedback

The fuel temperature feedback (i.e., Doppler Temperature Coefficient, (DTC)) terminates a prompt critical power excursion and is an important parameter. The DTC is calculated using standard static methods with moderator temperature held constant. The DTC is dependent upon core design and cycle lifetime. The magnitude of DTC is conservatively reduced by the uncertainty.

4.1.5 Delayed Neutron Fraction

For a given reactivity insertion, the sensitivity of total delayed neutron fraction (β_{eff}) is addressed from a point kinetics viewpoint. The β_{eff} determines the rate of neutron flux change from an initial static condition. The higher the reactivity relative to β_{eff} , the faster the flux increases. For reactivity insertions less than β_{eff} , a higher reactivity will increase the prompt jump and decrease the subsequent doubling time. When the reactivity insertion exceeds β_{eff} , the core becomes critical on prompt neutrons and the doubling time can decrease by more than an order of magnitude. For step reactivity insertions as with an REA, a low β_{eff} results in higher core powers. Therefore, the β_{eff} is lowered by the uncertainty for the cases where fast increases are limiting.

4.1.6 Reactor Trip Reactivity

For prompt critical excursions, the power excursion is terminated by DTC and the core returns to a much lower power level. Also, the excore flux or flux rate trip is reached shortly after the rod is ejected. After the DTC terminates the pulse, the core power flattens with time until the rods are inserted from the reactor trip. The reactor trip reactivity reduces the core power to shutdown conditions. The trip reactivity sensitivity

is most important for the “at power” cases where a trip limits the amount of time the core is at elevated powers and can limit the core damage due to potential DNBR failures. The timing of the trip is also important relative to the excore response of the detectors to the asymmetric flux caused by the ejected rod. As with the ejected rod worth, the trip reactivity is not an input quantity to the 3-D kinetics calculations. It can be adjusted by changing the amount of banks inserted prior to the accident, the control rod cross sections, and the trip time parameters. The sensitivity of the trip reactivity to the “at power” events is used to determine the level of conservatism required.

4.1.7 Fuel Cycle Design

Most of the fuel cycle design dependencies are captured by examining the beginning of cycle (BOC) and end of cycle (EOC) behavior on ejected rod worth, β_{eff} , DTC, MTC, and peaking. The fuel cycle design can also influence the proximity of the high burnup rods to the ejected rod location. When burnup dependent limits are used, a lower ejected rod worth in a high burnup assembly could be more limiting than a higher worth rod. More than the maximum ejected rod location is evaluated for burnup dependent limits if they are used. These fuel cycle design elements are addressed in Section 7.1.5.

4.1.8 Heat Resistances and Transient Cladding to Coolant Heat Transfer

The heat resistances and transient cladding to coolant heat transfer are not viewed as sensitive parameters to the ejected rod event and sensitivity calculations are used to confirm their use. The heat resistances comprise the thermal conductivity of the fuel and cladding, and the gap conductance. Nominal gap conductance values can vary by more than a factor of ten for an open gap between the fuel pellet and cladding versus a closed gap.

4.1.9 Heat Capacities

The heat capacity is rated as an important parameter in Reference 4. The heat capacity determines how much the fuel temperature increases as the energy is deposited into the fuel; therefore, the energy deposited is proportional to the heat capacity. For prompt

critical power excursions, the point kinetics equations can be approximated by the following analytical equation representing the energy deposition:

$$ED = \frac{2(\rho - \beta) \cdot C_p}{DTC}$$

where:

ED = Energy Deposition

ρ = Step Reactivity Change

β = Beta Effective

C_p = Heat Capacity of the Fuel

DTC = Doppler Temperature Coefficient

This equation shows the dependence of the energy deposition on heat capacity. If the temperature is the parameter of interest, then the delta temperature reached from an energy deposition with no heat loss can be represented as follows:

$$\Delta T = ED / C_p$$

where:

ΔT = Temperature rise

Substituting the first equation yields:

$$\Delta T = \frac{2 \cdot (\rho - \beta)}{DTC}$$

The temperature increase from the power excursion with a step change in reactivity is not a function of heat capacity of the fuel. For slow transients near static conditions, the

fuel temperature is dominated by the heat resistance of the rods. Therefore, for fuel temperature predictions, heat capacity is not an important parameter.

Reference 5 is considered a standard for defining heat capacity for UO_2 . The variation of the UO_2 heat capacity is only a function of temperature. Using the heat capacity consistently in the different codes will yield consistent results. No error estimate or special treatment is used for the UO_2 heat capacity.

4.1.10 Fractional Heat Deposited in Coolant

The fraction of heat deposited in the coolant can affect the relative amount of direct heating of the water and the fuel. The different prompt temperatures of the water and the fuel can result in different feedback between the MTC and DTC during a power pulse. The direct heating of the coolant could have an impact on the results since MTC can vary from small positive to large negative values from BOC to EOC conditions, respectively. This parameter is assumed constant throughout the transient because it has few or no dependencies upon other core parameters. A sensitivity evaluation is used to determine its importance.

4.1.11 Pellet Radial Power Profile

The pellet radial power profile could affect the rate of energy transferred from the fuel pellet to the coolant or it could affect the weighting of the pellet temperature distribution on the DTC. This parameter has very weak dependencies upon other core parameters. A sensitivity evaluation is used to determine its importance.

4.1.12 Rod Peaking Factors

The rod peaking factors are important relative to the weighting of the local powers to the overall core reactivity as well as the local energy deposition during the power pulse. As with the ejected rod worth, the rod peaking is not an input quantity to the 3-D kinetics calculations. If the peaking factors increased, the local fuel temperatures would increase so that the Doppler response would lower the core power. Therefore, the peaking factors that are used in the kinetics calculation are best estimate and the

peaking factors for the fuel rod thermal model are conservatively increased by the expected uncertainties.

4.1.13 Neutron Velocities

Since the dominant fission reactions occur with thermal neutrons, the thermal neutron velocities determine the rate at which the neutrons multiply. The mean generation time in point kinetics is calculated based on the neutron velocities. The impact of neutron velocities on the REA energy deposition is negligible because the energy deposition in the first equation in Section 4.1.9 is not a function of mean generation time. However, the pulse width is roughly inversely proportional to the thermal neutron velocity and narrow pulse widths could become more important when evaluating potential coolability concerns when PCMI failures occur. Since this methodology shows that energy deposition is below the cal/g for PCMI failure criteria for M5™, any reasonable value for thermal neutron velocity is acceptable.

4.1.14 System T-H Conditions

The kinetics solution can be affected by changes in inlet temperature, pressure, and flow. The longer the transient is modeled (greater than 5 seconds) the more the system T-H conditions can influence the neutronic kinetic solution. It is expected that prompt critical excursions will not be affected by the system T-H conditions since the maximum power deposition and maximum fuel temperatures are reached in less than a second. Non-prompt excursions may require modeling for more than a few seconds. Sensitivity studies are performed to assess these impacts.

4.2 Fuel Rod Transient Model for Fuel and Cladding Temperatures and DNBR

The fuel and cladding temperatures are dominated by the initial temperatures and the energy deposition versus time. Similar to the previous section, inlet temperature, core pressure, and flow are relatively constant and the fuel rod transient model can be used independently of a system T-H code. The discussion in this section is a review of the parameters listed in Table 4-2 relative to the fuel rod transient model for fuel and

cladding temperatures. Additional parameters address impacts on DNBR since the scope of Reference 4 was primarily concerned with PCMI type failures and not DNBR.

4.2.1 Pellet and Cladding Dimensions

Pellet and cladding dimensions are considered important and well known. Nominal dimensions are appropriate and application of the uncertainty for manufacturing allowances is acceptable. Approximations of the full core geometry model surrounding the limiting rod can affect the results. These approximations are shown to be appropriate for the REA analysis.

4.2.2 Burnup Distribution

The local rod radial burnup distribution is rated as a relatively low importance parameter and a homogenized pellet is acceptable.

4.2.3 Cladding Oxidation

The cladding oxidation is rated as a relatively low importance parameter and can be modeled on a best estimate basis or ignored.

4.2.4 Power Distribution

The power distribution is assumed to be the radial pellet power distribution and is weighted as an important parameter. The radial pellet power profile is a strong function of pellet burnup and uranium enrichment. A typical or bounding fuel performance power history from an approved fuel performance code can provide this information and is acceptable for the REA. Sensitivity calculations are used to define the impact of this parameter.

4.2.5 Initial Coolant Conditions

Initial coolant conditions for inlet temperature, flow and pressure are defined by the initial power level and operational mode. These parameters are already defined conservatively for other safety analyses. Existing methods are applicable.

4.2.6 *Transient Power Specification*

The transient core power and peaking factors are defined by the results generated from the plant transient analysis, which also includes the initial power distributions. The uncertainties applied to the REA power distributions are consistent with the current uncertainties applied for $F_{\Delta H}$ and F_Q for other accidents. Initial distributions are representative of the worst conditions allowed by Technical Specifications. The uncertainties of the power peaking factors are addressed.

4.2.7 *Heat Resistances in Fuel, Gap, and Cladding*

A typical or bounding fuel performance power history from an approved fuel performance code can provide the heat resistances in fuel, gap, and cladding, and is acceptable for the REA. Sensitivity studies are used to define the bounding conditions. Decreased thermal conductivity can increase the maximum fuel temperature but reduce the heat flux (DNBR). Therefore, two calculations modeling the limiting direction of the resistances are needed. One is used for maximum fuel temperature prediction and the other to predict MDNBR.

4.2.8 *Transient Cladding-to-Coolant Heat Transfer Coefficient*

The importance of the cladding to coolant heat transfer coefficient for prompt critical power excursions is rated of little importance. Since DNBR is a fuel failure criterion, transient cladding-to-coolant heat transfer becomes an important parameter. Transient heat transfer and critical heat flux (CHF) are not as well understood as static CHF. In general, the application of the static heat transfer, CHF, and failure when exceeding MDNBR is considered conservative for rapidly changing conditions. Therefore, the use of existing approved T-H codes, CHF correlations, and MDNBR cladding failure criterion is considered acceptable.

4.2.9 *Heat Capacities of Fuel and Cladding*

The heat capacity of UO_2 is primarily dependent upon temperature. Therefore, the local rod model requirement for heat capacity is the same as that used in the plant transient

model. Section 4.1.9 addresses the heat capacity as a non-critical parameter for REA when predicting temperatures and no uncertainty is needed.

4.2.10 Coolant Conditions

The transient water temperatures, local flows, and pressure are important to estimate fuel and cladding temperatures and DNBR of the fuel rods. An approved T-H computer code with time dependent capability is used with the approved uncertainties defined for licensing.

4.2.11 System T-H Conditions

The inlet temperature, core flow, and system pressure can affect the fuel rod transient analysis. The longer the transient is modeled (greater than 5 seconds) the more the system T-H conditions can impact the transient fuel rod model. Prompt critical excursions will not be impacted by the system T-H conditions because the maximum power deposition and maximum fuel temperatures are reached in less than a second. Non-prompt excursions may require modeling for more than a few seconds and the impact of plant conditions on the overall results is evaluated.

4.3 Time Dependent Analysis

The sensitivity of the time dependent calculations to time step meshing is addressed.

4.4 Failure Analysis

There are many ways to count the number of rod failures. The failure criteria defined for this methodology in Section 2.1.3 must be used. Rod by rod explicit analysis is acceptable. Rod by rod explicit analysis models the power versus time of every rod and counts each rod that has a DNBR less than the design limit as failed. Also, setting a conservative value for $F_{\Delta H}$ and F_Q and counting any rod above either value as a rod failed is acceptable. Exceeding a 95/95 tolerance/confidence limit on DNBR is conservative as a failure criterion. If the number of rods is statistically counted, only 5 percent or less of the rods having powers equal to the criteria would be failed. This is far less than the 100 percent as defined. Therefore, no additional DNBR propagation

needs to be assumed since the maximum fuel enthalpy is less than 150 cal/g and the maximum cladding temperature is less than [].

Table 4-1 PIRT Plant Transient Analysis

Subcategory	Phenomenon	IR*	KR**
Calculation of power history during pulse (includes pulse width)	Ejected control rod worth	100	100
	Rate of reactivity insertion	61	88
	Moderator feedback	38	93
	Fuel temperature feedback	100	96
	Delayed-neutron fraction	95	96
	Reactor trip reactivity	0	96
	Fuel cycle design	92	100
Calculation of rod fuel enthalpy increase during pulse (includes cladding temperature)	Heat resistances in high burnup fuel, gap, and cladding (including oxide layer)	58	67
	Transient cladding-to-coolant heat transfer coefficient	56	64
	Heat capacities of fuel and cladding	94	90
	Fractional energy deposition in pellet	4	93
	Pellet radial power distribution	63	88
	Rod-peaking factors	97	100

Notes:

* Importance Ratio IR>75 Important

**Knowledge Ratio KR<75 Not completely understood

Table 4-2 PIRT Fuel Rod Transient Analysis for Fuel and Cladding Temperatures

Subcategory	Phenomenon	IR*	KR**
Initial conditions	Pellet and cladding dimensions	91	96
	Burnup distribution	55	89
	Cladding oxidation	46	73
	Power distribution	100	89
	Coolant conditions	93	96
	Transient power specification	100	94
Fuel and cladding temperature changes	Heat resistances in fuel, gap, and cladding	75	77
	Transient cladding-to-coolant heat transfer coefficient (oxidized cladding)	50	58
	Heat capacities of fuel and cladding	88	93
	Coolant conditions	85	88

Notes:

* Importance Ratio IR>75 Important

**Knowledge Ratio KR<75 Not completely understood

5.0 U.S. EPR REA METHODOLOGY

The major difference in this methodology compared to past methods is that it replaces the point kinetics model with a 3-D kinetics model. A bounding sample problem analysis is presented in the following sections to define the overall process, computer codes, boundary conditions, uncertainties, and results for the REA event for the U.S. EPR. This methodology also provides the static conditions that a future cycle must meet for this analysis to remain valid. A cycle specific analysis can be repeated for those cycle parameters that do not meet the REA design parameters or a complete re-analysis can be performed to meet more challenging fuel designs. The following sections describe the U.S. EPR REA methodology and describe how the requirements are met.

6.0 COMPUTER CODES

The computer codes used to demonstrate the applicability of this methodology are COPERNIC², NEMO-K⁶, LYNXT⁷, and S-RELAP5⁸. Other approved computer codes which perform the same types of calculations are also acceptable.

6.1 COPERNIC

COPERNIC is used to define the fuel and cladding thermal properties for both NEMO-K and LYNXT. These properties include the fuel and cladding thermal conductivity which includes oxide formation, the heat capacity for the fuel pellet and cladding, the radial power distribution in the fuel pellet, and the gap conductance. Fuel burnup affects the fuel conductivity, the pellet radial power profile, the gap conductance, and cladding oxide. The gap conductance is a complex function of the gap and surface temperatures, gap size (i.e., creep and thermal expansion), contact pressure, and fission gas content. To capture these effects in the downstream codes using a constant fuel geometry model, the gap conductance is interpolated from a table of gap conductances [

] Repeating these calculations of gap conductance values at various burnup levels, a complete table is developed that captures the complex effects of burnup on the gap as well as the transient effects due to thermal expansion.

6.2 Plant Transient Model

The approved NEMO-K code is used as the plant transient model. It is a 3-D neutronic kinetics solution with time dependent fuel and coolant models. Benchmarks presented in Reference 6 include three HZP and three HFP ejected rod code benchmarks and confirm that NEMO-K is applicable for calculating core power and peaking response during an ejected rod event. This section provides an overview of the features added to NEMO-K and its applicability to the U.S. EPR.

6.2.1 Trip Function

The U.S. EPR uses an excore power rate lagged trip signal to sense severe RIAs and subsequently shutdown the core. This trip function requires three different models: excore detector signals, a rate lagged processed signal, and a control rod drop model. The excore detectors are located near the minor axis of each quadrant, which causes the excore signal response to differ from the core average value when an asymmetric rod is ejected. These signals are processed with a rate lagged function to compare to the trip values. Once the criteria for trip are reached (2/4 logic when trip signal is exceeded), a time delay is employed before the control rods are moved. The rod position with time in NEMO-K is defined by the safety analysis control rod drop position versus time from an input table. The physical models for the excore signals, the flux lagged signal, and the dropping of the control rods are discussed in the following subsections.

6.2.1.1 Excore Detector Model

Reactor plant protection systems typically sense and respond to the plant excore power detector signals. These signals measure the fast flux exiting the reactor core and are an indication of the actual incore reactor conditions. The incore assembly powers are multiplied by weighting factors to translate the incore conditions to the excore signals. These weighting factors are typically generated using detailed transport calculations. As demonstrated in Reference 6, a simple weighting of the peripheral location closest to the excore detector provides good simulated results compared to the actual results in an operating reactor when a control rod is dropped.

The excore detector model in NEMO supports a top and bottom detector at four radial locations. Detector response is computed by:

$$E_n^{T/B} = C_n^{T/B} \cdot F(T_n^{T/B}) \cdot \left[\sum_{j=1}^J W_j \cdot \sum_{k=1}^K D_k^{T/B} \cdot P_{jk} \right] \cdot P_{th}$$

where:

- $E_n^{T/B}$ = top or bottom excore response in terms of percent power for radial detector n
- $C_n^{T/B}$ = top or bottom excore response calibration factor for radial detector n
- $F(T_n^{T/B})$ = top or bottom excore response correction function for coolant temperature compensation for radial detector n
- W_j = weighting factor for the assembly j contribution to the excore detector response
- $D_k^{T/B}$ = weighting factor for the axial level k contribution to the top or the bottom detector response
- P_{jk} = normalized power density for assembly j at axial level k
- P_{th} = percent thermal power

The calibration factor represents the actual calibration performed at the plant when the excore detectors are periodically normalized to the measured thermal power. The calibration factor is either input or calculated by NEMO-K, if requested. For the requested calibration, the detectors are calibrated to core power using a static case that is run before the transient. The temperature correction factors, the radial and the axial weighting factors are input by the user.

6.2.1.2 Rate Lagged Processed Signal

NEMO-K simulates the instrumentation and processing that determines a reactor scram based on excore flux signals. The model combines the top and bottom signals previously described to treat four distinct radial detectors. The user specifies the magnitude of the signal to cause a detector to trip and the number of detectors required to trigger a reactor scram. A maximum (i.e., saturation) signal can be specified, along with a low signal that will reset the state of the detector. The relationship between the rate lagged signal ($F(t)$) that is used for the trip function and the unfiltered excore detector signal ($I(t)$) is defined by the following first order filter equations:

$$F(t) = \tau_d \frac{dP(t)}{dt}$$

$$\frac{dP(t)}{dt} = \frac{1}{\tau} (I(t) - P(t))$$

where:

τ_d = the derivative lead time constant

$P(t)$ = the lagged excore signal (power)

τ = the lagged signal time constant

These equations are approximated with a finite difference formulation based on the dt as the sampling rate. When the trip criteria are reached, the time to start the rod movement is set based on an input delay time between the trip measured and the start of physical movement.

6.2.1.3 Control Rod Drop

Rod movement during a scram is characterized by several distinct conditions:

- An initial acceleration period.
- Free fall above the dashpot.
- Deceleration due to the dashpot.
- Free fall within the dashpot.
- Stop at the bottom position.

The NEMO-K implementation models the movement for each rod or bank regardless of its initial position before scram. This leads to two different starting conditions:

- Rods that begin above dashpot.

- Rods that begin at the top of or within the dashpot.

When rod movement begins from a trip actuation, NEMO-K drops the rods or banks from their current height to the fully inserted position. The position versus time of a rod or bank depends upon the initial position prior to the trip. [

] This control rod drop model allows the rods to fall from any initial position in a manner consistent with the safety analysis assumptions without user intervention.

6.2.2 *Adiabatic cal/g Edit*

An edit is provided that calculates the change in pellet enthalpy during a transient. The method integrates the change in rod segment power produced (relative to the beginning of the transient) over each timestep. The total energy deposited is the change in enthalpy. This method conservatively estimates the cal/g as defined for RIA because it neglects the energy lost from the fuel rod by heat transfer to the coolant. This definition provides a useful means of identifying the relative impact of different conditions in two or more NEMO-K transients.

6.2.3 *Adjustment Factors*

In NEMO, there are four types of adjustment factors that can be used to account for uncertainty and conservative allowances. These adjustment factors are multipliers on the following parameters:

- Fuel conductivity
- Gap conductance
- Cross section changes due to fuel temperature variation (Doppler adjustment)
- Cross section changes due to control rod insertion (rod worth adjustment)

For the first three parameters the multipliers are applied to every node location. The control rod multiplier can be applied by bank or assembly location. These multipliers are factors that can be applied to examine sensitivities or to formulate a limiting case with uncertainties and/or conservative allowances.

6.2.4 Pellet Weighted Temperature for DTC

The cross sections are generated for NEMO-K using a flat pellet temperature profile. The pellet temperature distribution can vary significantly with time during an REA. For a pellet with a temperature distribution, a simple approach is to use volume averaging to obtain the effective temperature for the cross sections. Another common method uses a weighting of the centerline and surface temperatures as shown below:

$$T_{\text{eff}} = T_{\text{S}} \cdot \text{wt}_{\text{SC}} + T_{\text{CL}} \cdot (1 - \text{wt}_{\text{SC}})$$

where:

T_{eff} = the effective flat temperature

T_{S} = the fuel surface temperature

T_{CL} = the fuel centerline temperature

wt_{SC} = the weighting factor for the surface/centerline formula

For example, Reference 9 uses this formulation with a weighting factor of 0.7. The disadvantages of this formulation are that it uses only two temperatures of the pellet and that it is based on the typical radius squared variation of the fuel pellet temperature at static conditions. An improved weighting method is employed in NEMO-K [

]

6.2.5 NEMO-K Summary

Some of the results from Reference 6 that are pertinent to the REA are summarized to illustrate the accuracy of NEMO-K to a fine mesh reference solution. Table 6-1 shows the current NEMO-K results for each of the six rod ejection benchmark cases. These results are comparable to Table 4-5 in Reference 6. The six cases include a HZP (x1) and a HFP (x2) rod ejection with three different core geometries (where x is A, B, or C). As stated in Reference 6, the agreement between NEMO-K and the reference solution is excellent. The only item that stands out in the table is case B2, where the time of the peak is predicted to be 0.10 seconds rather than 0.12 seconds as the reference solution. Although this is a large percentage difference, the absolute difference is small considering the relatively flat peak core power in this transient as shown in Figure 6-2.

Additionally, Figure 6-3 through Figure 6-5 show the power distribution comparisons for case A1 at initial, peak core power, and 5 seconds during the transient, respectively. These figures correspond to figures 4-17, 4-18, and 4-19 in Reference 6. As shown in the figures, NEMO-K agrees with the reference PANTHER solutions.

Figure 6-6 and Figure 6-7 show power distribution results that have not been previously published with NEMO-K for cases C1 and C2, respectively. These figures show the assembly planar power at a fixed height along the major axis at maximum transient core

power. This dimensional slice includes the ejected rod location at B08. The power density values are normalized to the maximum value in this slice. The figures show excellent agreement between NEMO-K and the reference solution. The results demonstrate that NEMO-K accurately models REA time dependent phenomena and is applicable for the methodology presented.

6.3 Transient Fuel Rod Model

The fuel rod model in LYNXT⁷, an approved code, is used as the transient fuel rod model. Changes to the core thermal-hydraulic code LYNXT are implemented in the fuel rod modeling for the REA analysis. This section contains a brief overview of the approved fuel rod model as well as the changes in the fuel rod model made for the REA and other static and transient fuel rod modeling applications.

6.3.1 General Overview of Existing LYNXT Fuel Rod Models

The approved fuel rod model in LYNXT is based on a two-dimensional conduction equation with a radial and optional axial dependence. The solution is based on the orthogonal collocation method where the solution locations within the fuel and cladding are determined based on the collocation order. Two fuel rod models exist in LYNXT as approved by the U.S. NRC:

- **Constant Gap/Constant Properties (CG/CP)** – This is the same model in COBRA-IV-I¹⁰, which served as the basis for LYNXT. The fuel-to-cladding gap dimension remains invariant throughout the modeled event as do all the thermal properties, with the exception of the fuel thermal conductivity which can optionally be modeled using a third order temperature dependence.
- **Variable Gap/Temperature Dependent Properties (VG/TDP)** – This fuel rod model is based on the thermal and mechanical properties of the TAFY¹¹, TACO¹², and TACO2¹³ fuel performance codes. The VG/TDP fuel rod model allows the fuel and cladding dimensions to change during the event due to temperature and pressure difference effects (i.e., pressure difference between

coolant and internal fuel rod pressure), based on the TAFY, TACO, and TACO2 models. The VG/TDP fuel rod model uses the same gap conductance model from TAFY, TACO, and TACO2 with the gas inventory at the start of the event being invariant throughout the event. The LYNXT VG/TDP model allows the radial power profile data from the three fuel performance codes to be used as an optional input, which is held invariant during the modeled event.

6.3.2 Enhancements to the Fuel Rod Models

The enhancements to the approved LYNXT fuel rod models increase the number of solution locations in the fuel pellet and increase the modeling flexibility of the fuel rod model (including the cladding). Increasing the number of solution locations in the fuel allows the fuel rod model to more accurately represent various radial power profiles across the fuel pellet, including those with the peak radial power in the outer portions of the fuel pellet. Expanding the modeling capability allows various fuel performance codes, such as (but not limited to) TACO3¹⁴ or COPERNIC², to be used as the basis of a LYNXT time dependent analysis. The enhancements use the same fuel and cladding energy equations and solution process as the CG/CP and VG/TDP models (defined in Equations 2-6 through 2-13 for the energy equations and Equations 2-117 through 2-125 for the solution process in Reference 7), but use input property values for the pellet, gap, and cladding instead of the code specific values relative to TAFY, TACO, and TACO2.

The maximum number of solution locations in the cylindrical fuel is increased from 6th order collocation in Reference 7 to 20th order collocation. The additional solution locations are available for the enhanced fuel rod model and the approved CG/CP and VG/TDP fuel rod models. Table 6-2 contains the collocation locations, both the cylindrical and planar data up to 6th order collocation are from Figure 2-5 of Reference 7, as well as the additional 8th, 10th, 12th, 16th, and 20th order radial locations in the fuel pellet. The planar data is unchanged from COBRA-IV-I¹⁰.

The enhancements to the fuel rod model to expand the modeling capability allow the various temperature dependent properties and radial power profile characteristics used in the fuel/cladding energy equation calculations to be based on a number of potential fuel performance codes. The enhancements provide a fuel rod model that is based on the following parameters being invariant during the modeled event:

- Fuel Dimensions - Thermal and lateral pressure changes to the geometry are not modeled. Gap conductance is allowed to change in a transient [

]

- Cladding, gap, and fuel properties dependent on parameters other than temperature, such as pressure difference across the cladding.
- Gas inventory during the event - This is consistent with the VG/TDP model.
- Radial power profile - This is consistent with the VG/TDP model.

The new fuel rod model is called the Constant Gap/Temperature Dependent Property (CG/TDP) model because the fuel-to-cladding gap dimension is invariant and various thermal properties may be temperature dependent.

The CG/TDP model allows the input of the following temperature dependent properties, in tabular form:

- Thermal conductivity for the fuel and/or cladding
- Specific heat for the fuel and/or cladding
- Gap conductance
- Fuel enthalpy

[

] The CG/TDP model also allows the application of a radial power profile across the fuel pellet.

6.3.3 LYNXT Benchmark Review

The LYNXT thermal equations have not changed; only the user inputs to those equations have changed. Therefore, the validation of the code equations remains valid. This subsection reviews the past qualification of the code and provides some example cases with the new input options to illustrate the new coupling of inputs.

6.3.3.1 Past Qualification

The benchmarks for the CG/CP and VG/TDP fuel rod models included:

- Analytical solution of the fuel and cladding with the gap conductance assumed as negligible.
- Power ramp comparisons to TACO (Reference 12).
- Non-crossflow transient fuel temperature and DNBR code, RADAR¹⁵, using the four pump coastdown and the four pump locked rotor transients.
- Sensitivity studies using the hot full power ejected rod (HPPER) event.

The Reference 7 CG/CP and VG/TDP benchmark cases indicated the following in terms of the maximum difference:

- Agreement between the CG/CP LYNXT fuel rod model and the analytical solution was within 0.5 percent on the fuel centerline temperature.
- Agreement between the VG/TDP LYNXT fuel rod model (initialized to 102 percent rated power with TACO) and TACO over a power ramp range from 60 to 135 percent rated power was within 2 percent on centerline temperature and 4 percent on fuel surface temperature for BOL conditions.

- Agreement between the VG/TDP LYNXT fuel rod model and the RADAR fuel rod model for the transients was within 3 percent on the fuel centerline temperature, within 4.5 percent on the radial average temperature, and 2.5 percent on the transient minimum DNBR (MDNBR). These comparisons are based on BOL conditions.

The fuel rod model benchmark cases for LYNXT, based on Reference 7, confirm that the VG/TDP LYNXT fuel rod model is capable of predicting consistent results with fuel performance codes (limited to TAFY, TACO, and TACO2). The CG/CP and VG/TDP fuel rod models are capable of predicting the fuel temperatures, cladding temperatures and DNBR from other transient fuel performance and DNBR codes such as RADAR over a wide range of static and transient events typically encountered in plant operations.

These benchmarks are repeated with the new LYNXT version which produced equivalent results (within roundoff). In addition, several cases were repeated with the higher collocation orders and with the CG/TDP fuel option which produced equivalent results. Therefore, the conclusions made for LYNXT in Reference 7 remain valid for the CG/TDP fuel option.

6.3.3.2 LYNXT-to-COPERNIC Example Cases

The CG/TDP LYNXT fuel rod model is compared to COPERNIC (Reference 2) using a representative rod ejection transient starting at HZP and HFP conditions. Even though COPERNIC is not approved for fast transients like REA, this comparison highlights any significant differences between LYNXT and a more precise treatment of the fuel rod thermal parameters. These calculations were repeated for both BOL and EOL burnup-based fuel rod conditions. The CG/TDP LYNXT inputs for these rod ejection cases are thermal properties (including gap conductance) and radial/axial power profiles based on static COPERNIC calculations. In addition to any temperature dependence, the COPERNIC-based LYNXT inputs consider the burnup effects, the uranium enrichment, the porosity of the fuel, and the oxide thickness on the cladding. The same transient

boundary conditions for power, $F_{\Delta H}$, axial shape, and cladding outer wall temperature versus time are used in both the COPERNIC and LYNXT transient analyses.

The following four example cases are performed for LYNXT and COPERNIC:

- HZP/EOL – Based on EOL burnup conditions (60 GWD/MTU) for HZP transient boundary conditions.
- HFP/EOL – Based on EOL burnup conditions for HFP transient boundary conditions.
- HZP/BOL – Based on BOL burnup conditions (2.5 GWD/MTU) for HZP transient boundary conditions.
- HFP/BOL – Based on BOL burnup conditions for the HFP transient boundary conditions.

The transient comparisons of the fuel surface, fuel radial average, fuel centerline, fuel maximum, and the cladding maximum temperatures for the four different cases are presented in Figure 6-8 through Figure 6-27 as illustrated in the following table.

Condition	Fuel temperature				Cladding maximum temperature
	Surface	Average	Centerline	Maximum	
HZP/EOL	Figure 6-8	Figure 6-9	Figure 6-10	Figure 6-11	Figure 6-12
HFP/EOL	Figure 6-13	Figure 6-14	Figure 6-15	Figure 6-16	Figure 6-17
HZP/BOL	Figure 6-18	Figure 6-19	Figure 6-20	Figure 6-21	Figure 6-22
HFP/BOL	Figure 6-23	Figure 6-24	Figure 6-25	Figure 6-26	Figure 6-27

Table 6-3 contains a numerical summary for the LYNXT and COPERNIC comparisons for each of the four transient cases when transient time steps are the same in both codes.

With the exception of the HZP/EOL fuel surface temperatures in the 0.15 to 0.20 second time frame, the maximum difference between the transient COPERNIC and LYNXT

CG/TDP fuel temperatures is less than [] percent. During this 0.05 second interval for HZP/EOL, which represents the time of the neutron power spike due to the rod ejection, the differences between the COPERNIC and the CG/TDP LYNXT fuel surface temperatures are [

]. This difference in the gap conductance is for a short duration and has little impact on the maximum fuel temperature comparisons, which are within [] percent. The maximum difference in the maximum cladding temperatures between COPERNIC and LYNXT is within [] percent, with LYNXT predicting higher temperatures than COPERNIC. Since this LYNXT model tends to yield higher peak cladding temperatures and accurately predicts peak fuel temperatures, this model with the gap conductance fitting tables is acceptable to predict fuel melt and minimum DNBR conditions for REA.

6.3.4 LYNXT Conclusions

Three different fuel rod models are available in LYNXT (i.e., CG/CP, VG/TDP, and CG/TDP). These models are summarized in Table 6-4. The enhancements used to form the CG/TDP model provide LYNXT the ability to use thermal properties and other conditions from any fuel performance code, such as (but not limited to) TACO3 (Reference 14) or COPERNIC (Reference 2). The CG/TDP fuel rod model allows LYNXT to mimic the behavior of various fuel performance codes without the need to implement each of the various fuel performance code models and properties within LYNXT. The CG/TDP model allows the specification of the following, based on input:

- Temperature dependent thermal properties for the fuel and cladding
- Gap conductance based on the []

- Radial power profile across the fuel pellet

The limitations of the CG/TDP LYNXT fuel rod model are as follows:

- Cladding, gap, and fuel dimensions are invariant throughout the event.
- Cladding, gap, and fuel properties are only temperature dependent.
- Cladding, gap, and fuel properties apply throughout the event.
- Radial power profile is invariant throughout the event.
- Gas inventory during the event is invariant.

The last two limitations are also limitations of the VG/TDP fuel rod model.

Three different types of cases to verify that the CG/TDP fuel rod model is accurately predicting the results of various fuel performance codes are as follows:

- Analytical benchmark (same as in Reference 7).
- Original fuel performance code benchmarks using a variable gap conductance fuel rod model (same as in Reference 7).
- Example cases with COPERNIC.

The code comparisons indicate that the CG/TDP fuel rod model predicts the known solution (analytical or from a fuel performance code) to within [] percent, based on the input gap conductance table accurately predicting the fuel performance code gap conductance behavior. As the burnup increases and the power excursion gets larger it becomes [

]. For these higher burnups and large power excursions, the difference between the CG/TDP LYNXT local fuel temperature predictions and COPERNIC is [], with LYNXT

producing higher temperatures. Even with these differences for short durations, the maximum difference in the maximum fuel temperature is less than [] percent. Therefore, this model with the gap conductance fitting tables is acceptable to predict fuel melt and minimum DNBR conditions for REA analyses.

6.4 System T-H Model

The plant transient model uses a constant pressure, inlet temperature, and flow model. A system T-H model is needed to model the trip functions, primary and secondary systems to address those conditions that may change pressure, inlet temperature and/or flow during an REA. S-RELAP5 (Reference 8) is used for non-LOCA safety analyses and is also used to estimate changing plant conditions during an REA. Its applicability to the U.S. EPR for the maximum pressure boundary consequences of REA is addressed in Reference 16. The only significant change to this model for REA simulations would be to turn off the point kinetics model and substitute the power versus time obtained from NEMO-K.

Table 6-1 NEACRP Kinetic Results

	NEMO-K	Ref	Diff	% Diff
A1				
Maximum Core Power Fraction	1.223	1.179	0.044	3.7
Core Power Fraction @ 5 sec	0.200	0.196	0.004	2.0
Time of Maximum Power	0.550	0.560	-0.010	-1.8
Fuel Temperature at Max Power	294.7	294.5	0.200	0.1
Fuel Temperature @ 5 sec	325.1	324.3	0.800	0.2
A2				
Maximum Core Power Fraction	1.082	1.080	0.002	0.2
Core Power Fraction @ 5 sec	1.036	1.035	0.001	0.1
Time of Maximum Power	0.1	0.1	0.000	0.0
Fuel Temperature at Max Power	544.6	546.5	-1.900	-0.3
Fuel Temperature @ 5 sec	553.0	554.6	-1.600	-0.3
B1				
Maximum Core Power Fraction	2.431	2.441	-0.010	-0.4
Core Power Fraction @ 5 sec	0.324	0.320	0.004	1.3
Time of Maximum Power	0.520	0.517	0.003	0.6
Fuel Temperature at Max Power	301.4	301.4	0.000	0.0
Fuel Temperature @ 5 sec	350.3	349.9	0.400	0.1
B2				
Maximum Core Power Fraction	1.062	1.063	-0.001	-0.1
Core Power Fraction @ 5 sec	1.038	1.038	0.000	0.0
Time of Maximum Power	0.10	0.12	-0.020	-16.7
Fuel Temperature at Max Power	542.1	544.1	-2.000	-0.4
Fuel Temperature @ 5 sec	550.0	552.0	-2.000	-0.4
C1				
Maximum Core Power Fraction	4.735	4.773	-0.038	-0.8
Core Power Fraction @ 5 sec	0.148	0.146	0.002	1.4
Time of Maximum Power	0.268	0.268	0.000	0.0
Fuel Temperature at Max Power	298.2	297.9	0.300	0.1
Fuel Temperature @ 5 sec	316.1	315.9	0.200	0.1
C2				
Maximum Core Power Fraction	1.074	1.071	0.003	0.3
Core Power Fraction @ 5 sec	1.031	1.030	0.001	0.1
Time of Maximum Power	0.1	0.1	0.000	0.0
Fuel Temperature at Max Power	544.5	546.4	-1.900	-0.3
Fuel Temperature @ 5 sec	551.8	553.5	-1.700	-0.3

Table 6-2 Cylindrical and Planar Geometry Collocation Points for LYNXT

Cylindrical geometry				
<u>N = 2</u>	<u>N = 3</u>	<u>N = 4</u>	<u>N = 5</u>	<u>N = 6</u>
0.393765	0.297637	0.238965	0.199524	0.171220
0.803087	0.639896	0.526159	0.444987	0.384810
	0.887502	0.763931	0.661797	0.580504
		0.927491	0.833945	0.747443
			0.949455	0.877060
				0.962780
 Planar Geometry				
	<u>N = 2</u>		<u>N = 3</u>	
	0.285232		0.209299	
	0.765055		0.591700	
			0.871740	

Notes:

1. All collocation points are normalized, based on fuel pellet/plate outer surface.
2. The point, based on a normalized location, of 1.0 is a collocation point for all orders. This represents the fuel surface.
3. N denotes the collocation order.

Table 6-3 LYNXT and COPERNIC Transient Temperature Ratio Comparisons

Comparison parameter	Fuel temperature				Cladding maximum temperature
	Surface	Average	Centerline	Maximum	
HZP EOL					
Average					
Std. dev.					
Maximum					
Minimum					
Sample size					
HFP EOL					
Average					
Std. dev.					
Maximum					
Minimum					
Sample size					
HZP BOL					
Average					
Std. dev.					
Maximum					
Minimum					
Sample size					
HFP BOL					
Average					
Std. dev.					
Maximum					
Minimum					
Sample size					

Notes:

1. The data is based on (COPERNIC result) / (LYNXT CG/TDP result).
2. "Std. dev." is the standard deviation of the data about the average. Sample size is the number of transient time steps.

Table 6-4 LYNXT Fuel Rod Model Options

Fuel/cladding parameter	CG/CP	VG/TDP	CG/TDP
Collocation orders	See Note 1	See Note 1	All values in Table 6-2
Fuel thermal conductivity	Constant or user-supplied third order polynomial	TAFY, TACO, TACO2 property	User-supplied function of fuel temperature
Fuel specific heat		Temperature-dependent function	
Cladding thermal conductivity		TAFY, TACO, TACO2 property	User-supplied function of cladding temperature
Cladding specific heat		Temperature-dependent function	
Fuel-to-cladding gap dimension		Variable	Constant
Gap conductance		TAFY, TACO, TACO2 model	User-supplied function of []
Radial power profile	Uniform	User-supplied as a function of fuel pellet radial location	User-supplied as a function of fuel pellet radial location
Fuel enthalpy	Not available	Not available	User-supplied function of fuel temperature

Notes:

1. The collocation orders in Reference 7 are 2, 3, 4, 5, and 6 (cylindrical). The potential collocation orders were expanded to include all the locations in Table 6-2.
2. In the CG/TDP fuel rod model the input of each of the user-supplied functions is optional and if used is supplied in tabular form.

Figure 6-1 Scram Position Versus Drop Time

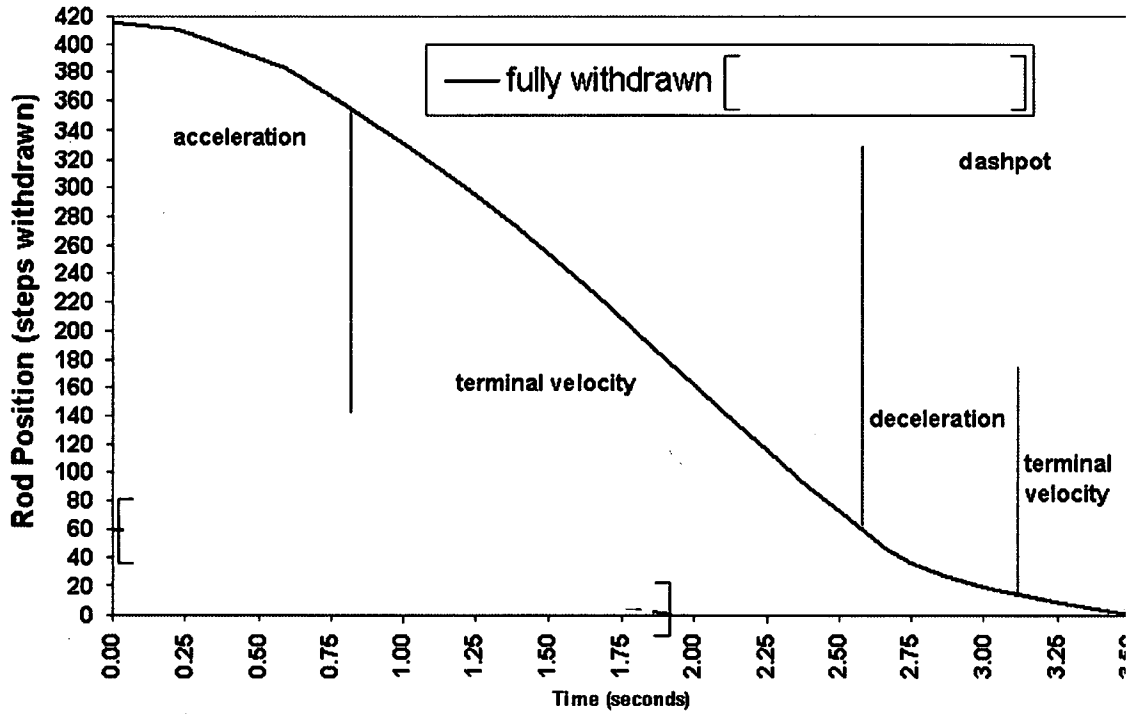


Figure 6-2 Core Power Fraction – Case B2

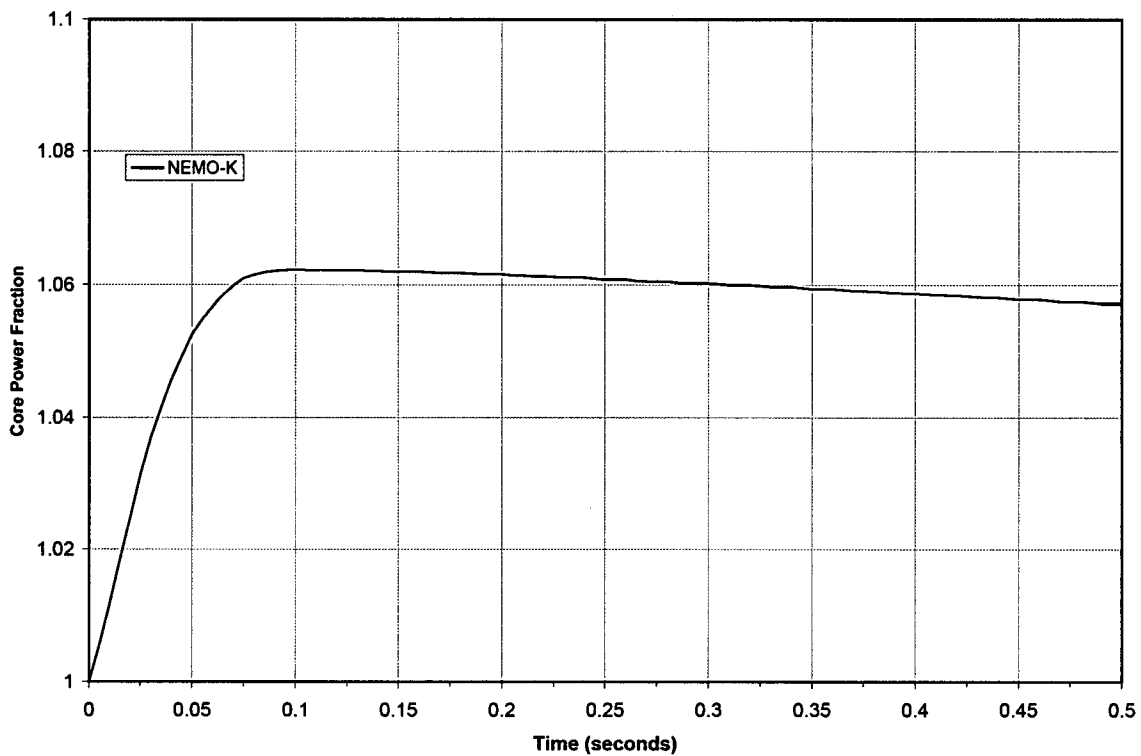


Figure 6-3 Power Distribution at Initial Conditions – Case A1

1/8th Core Assembly Power Map at Plane 6

PANTHER

				0.293	0.354		
			0.752	0.533	0.497	0.285	
		0.545	0.757	0.393	0.380	0.206	
	0.964	0.867	1.000	0.745	0.301	0.294	0.226
0.533	0.793	0.575	0.945	0.951	0.527	0.214	0.285

NEMO-K

Nodal Layer Peak	2.372			0.284	0.353		
			0.752	0.532	0.496	0.284	
		0.530	0.757	0.382	0.380	0.200	
	0.965	0.868	1.000	0.745	0.292	0.293	0.225
0.518	0.794	0.559	0.945	0.950	0.527	0.207	0.284

DIFFERENCE (N-P)

STD	0.006			-0.009	-0.001		
			0.000	-0.001	-0.001	-0.001	
		-0.015	0.000	-0.011	0.000	-0.006	
	0.001	0.001	0.000	0.000	-0.009	-0.001	-0.001
-0.015	0.001	-0.016	0.000	-0.001	0.000	-0.007	-0.001

Figure 6-4 Power Distribution at Maximum Core Power – Case A1

1/8th Core Assembly Power Map at Plane 6

PANTHER							
				0.128	0.150		
			0.362	0.242	0.214	0.120	
		0.316	0.390	0.188	0.169	0.088	
	0.790	0.562	0.540	0.371	0.140	0.126	0.093
1.000	0.778	0.390	0.513	0.474	0.248	0.093	0.117
NEMO-K							
				0.124	0.149		
			0.362	0.242	0.213	0.119	
		0.307	0.391	0.183	0.169	0.085	
	0.790	0.562	0.540	0.371	0.136	0.126	0.093
1.000	0.778	0.379	0.513	0.474	0.248	0.090	0.117
DIFFERENCE (N-P)							
	STD	0.003		-0.004	-0.001		
			0.000	0.000	-0.001	-0.001	
		-0.009	0.001	-0.005	0.000	-0.003	
	0.000	0.000	0.000	0.000	-0.004	0.000	0.000
0.000	0.000	-0.011	0.000	0.000	0.000	-0.003	0.000

Figure 6-5 Power Distribution at 5 Seconds – Case A1

1/8th Core Assembly Power Map at Plane 6

PANTHER							
				0.143	0.168		
			0.392	0.266	0.239	0.135	
		0.333	0.417	0.205	0.188	0.099	
	0.802	0.581	0.569	0.397	0.153	0.142	0.106
1.000	0.785	0.403	0.540	0.505	0.269	0.104	0.134
NEMO-K							
				0.139	0.169		
			0.392	0.266	0.239	0.135	
		0.323	0.417	0.199	0.188	0.096	
	0.802	0.582	0.570	0.397	0.149	0.142	0.106
1.000	0.785	0.392	0.541	0.505	0.270	0.101	0.134
DIFFERENCE (N-P)							
	STD	0.003		-0.004	0.001		
			0.000	0.000	0.000	0.000	
		-0.010	0.000	-0.006	0.000	-0.003	
	0.000	0.001	0.001	0.000	-0.004	0.000	0.000
0.000	0.000	-0.011	0.001	0.000	0.001	-0.003	0.000

Figure 6-6 Comparison of Radial Power at Max Power – C1

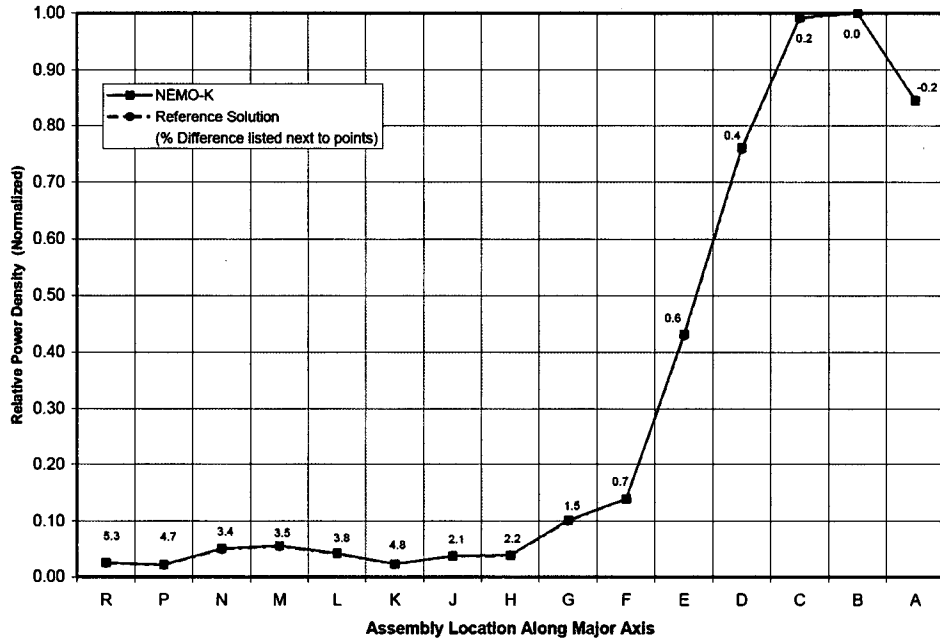


Figure 6-7 Comparison of Radial Power at Max Power – C2

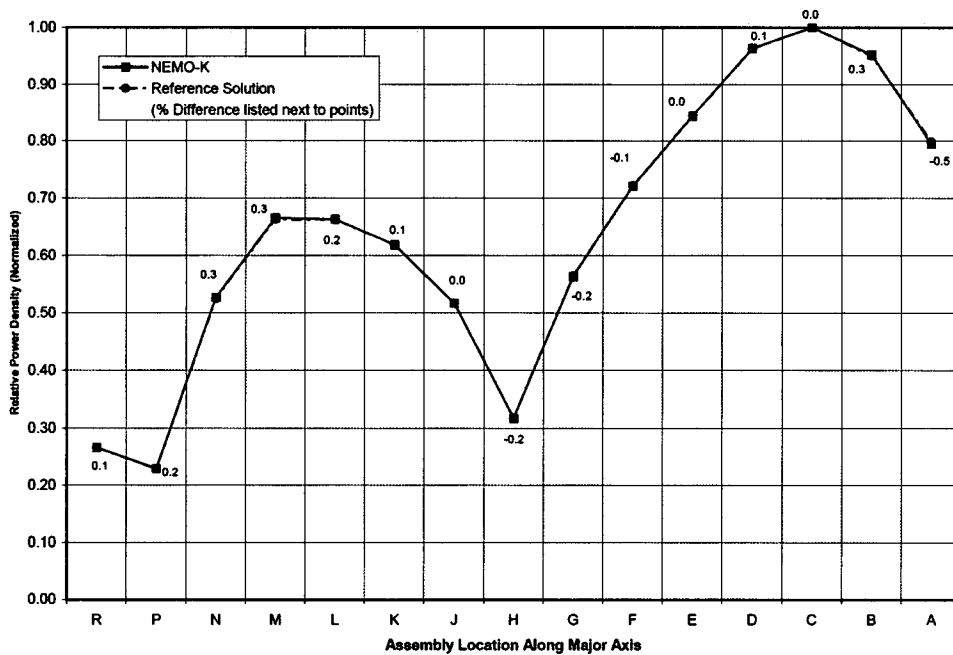


Figure 6-8 HZP/EOL Transient Fuel Surface Temperature



Figure 6-9 HZP/EOL Transient Fuel Average Temperature



Figure 6-10 HZP/EOL Transient Fuel Centerline Temperature



Figure 6-11 HZP/EOL Transient Fuel Maximum Temperature



Figure 6-12 HZP/EOL Transient Cladding Maximum Temperature



Figure 6-13 HFP/EOL Transient Fuel Surface Temperature



Figure 6-14 HFP/EOL Transient Fuel Average Temperature



Figure 6-15 HFP/EOL Transient Fuel Centerline Temperature

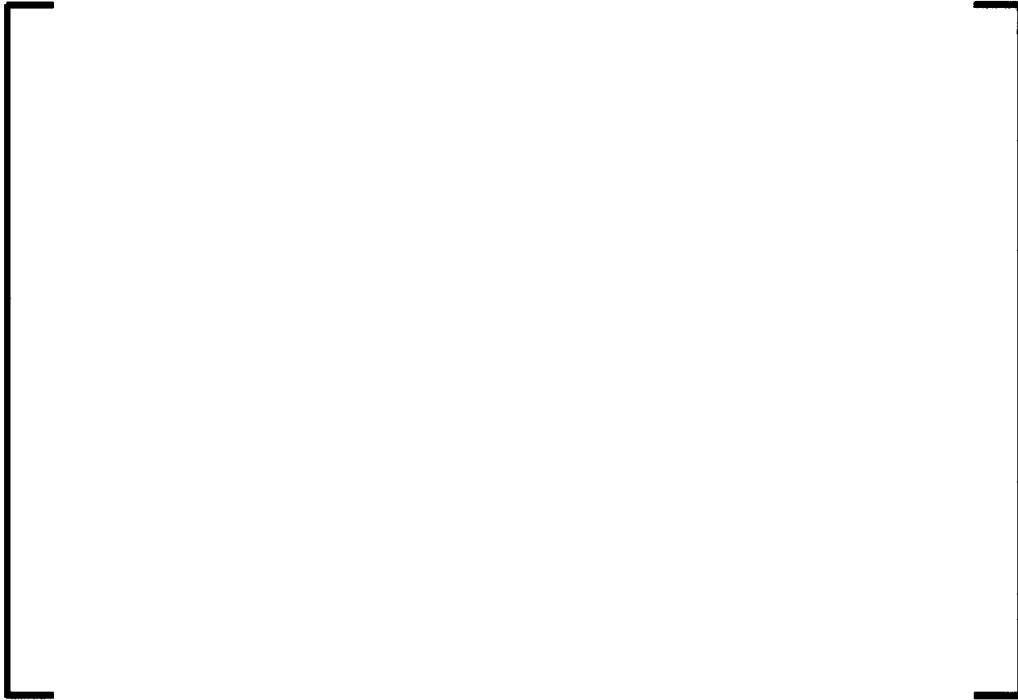


Figure 6-16 HFP/EOL Transient Fuel Maximum Temperature



Figure 6-17 HFP/EOL Transient Cladding Maximum Temperature



Figure 6-18 HZP/BOL Transient Fuel Surface Temperature



Figure 6-19 HZP/BOL Transient Fuel Average Temperature

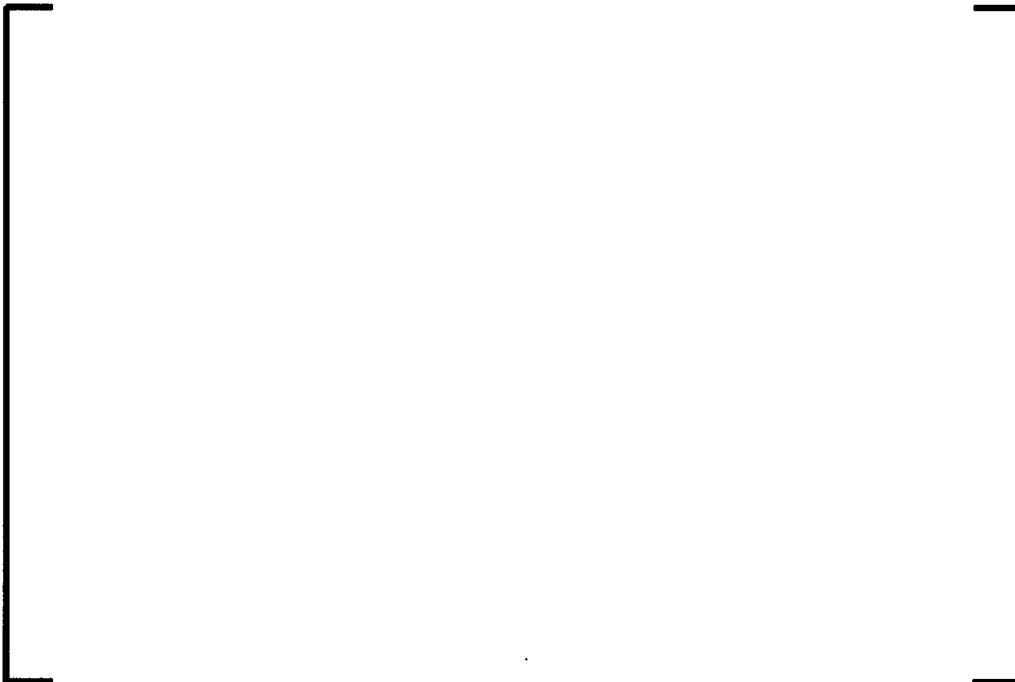


Figure 6-20 HZP/BOL Transient Fuel Centerline Temperature



Figure 6-21 HZP/BOL Transient Fuel Maximum Temperature



Figure 6-22 HZP/BOL Transient Cladding Maximum Temperature



Figure 6-23 HFP/BOL Transient Fuel Surface Temperature



Figure 6-24 HFP/BOL Transient Fuel Average Temperature

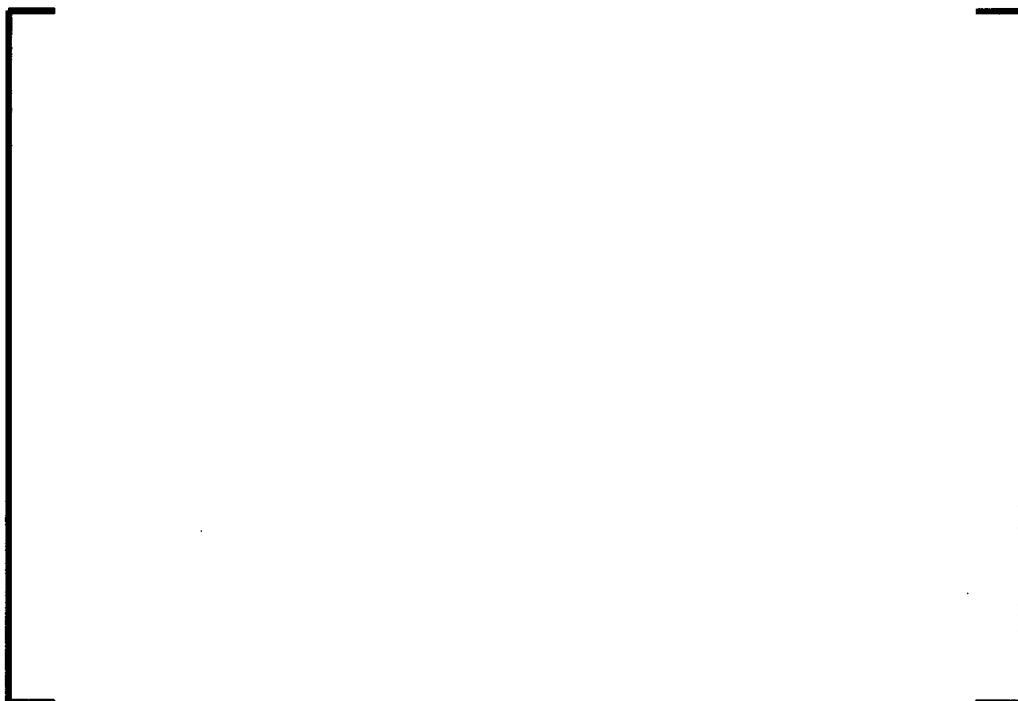


Figure 6-25 HFP/BOL Transient Fuel Centerline Temperature



Figure 6-26 HFP/BOL Transient Fuel Maximum Temperature



Figure 6-27 HFP/BOL Transient Cladding Maximum Temperature



7.0 APPLICATION OF BOUNDARY CONDITIONS AND UNCERTAINTIES

This section discusses the REA analysis boundary conditions and uncertainties for the plant transient model, the fuel rod model, and the failure analysis. The minimum requirement is to analyze/bound the limits of operation from BOC to EOC and from HZP to HFP. The U.S. EPR average temperature versus power level is shown in Figure 7-1. Since DNBR is one of the main failure criteria and it can be sensitive to the coolant temperature, the core powers of 0, 25, 35, 60, and 100 percent (i.e., at the transition temperatures) are analyzed to demonstrate where the limiting conditions occur relative to initial power level.

7.1 NEMO-K Boundary Conditions and Uncertainties

The treatment of the NEMO-K boundary conditions and uncertainties is addressed in this section. The parameters which have conservatisms and/or uncertainties and sensitivity results are presented to illustrate the conservatisms in the calculations. The application of conservatisms and uncertainties of the ejected rod worth, MTC, DTC, β_{eff} , fuel cycle design, and rod power peaking is addressed in the following sections.

7.1.1 Ejected Rod Worth

The uncertainty for the ejected rod worth is 15 percent for NEMO-K. This uncertainty is consistent with the currently employed methods that use NEMO¹⁷. The initial rod position prior to rod ejection and the change in fuel assembly cross sections due to the presence of control rods can be conservatively changed to bound the cycle-to-cycle variation of the observed ejected control rod worths and the uncertainty of 15%. The rod position insertion limit for the U.S. EPR is shown in Figure 7-2 and is compared to the assumed position in the REA analysis. The maximum calculated ejected rod worths for BOC and EOC at HFP and HZP are shown in Table 7-1 for the proposed cycles 1, 2, 3, and equilibrium cycle with PRISM and the bounding analysis values in NEMO-K for the REA example analysis.

7.1.2 MTC

A 2 pcm/°F uncertainty is used. The MTC uncertainty of 2 pcm/°F has been used as the acceptance criterion for current licensed cores. Both PRISM and NEMO comparisons to measurement results support a value lower than 2 pcm/°F.

7.1.3 DTC

A DTC uncertainty of 10 percent is used.

7.1.4 β_{eff}

A β_{eff} uncertainty of 5 percent is used. [

] and

therefore a 5 percent β_{eff} uncertainty is a reasonable upper bound.

7.1.5 Fuel Cycle Design

Eighteen month core designs for cycle 1, cycle 2, cycle 3 and an equilibrium cycle are used to define the bounding initial conditions. The base REA analysis model uses the equilibrium cycle. The proximity of the fuel to the ejected rod location will affect the local cal/g. Since there are no burnup dependencies of the limits (see Section 2.1.1) and the MDNBR is evaluated for the full range of burnups (see Section 7.2.5), only the maximum ejected rod worth is investigated to determine the maximum power response of the peak assembly. Table 7-1 lists the nominal range of the key parameter values and the REA analysis values at BOC and EOC for both HZP and HFP for the available core designs.

A point kinetics model has very few inputs and the applicability to core designs has been demonstrated by using conservative reactivity core coefficients. To demonstrate that 3-D kinetics can be used similarly, sensitivity studies are performed with the [] and compared to the equilibrium core design. []

]

Figure 7-3 through Figure 7-6 show the power versus time for both cores at BOC 25 percent power, BOC HFP, EOC HZP, and EOC HFP conditions, respectively. Very similar power excursions for the initial pulse are shown for these cases. Figure 7-5 shows that the []].

Figure 7-7 shows the EOC HZP core power []. The equilibrium cycle is now more limiting than []

] The results show that the selected base case is bounding and representative of the REA conditions for the U.S. EPR.

In Figure 7-3 and Figure 7-4, the ejected rod location at BOC is in assembly J03 for [] and in assembly N05 for the equilibrium cycle. A different location of the ejected rod does not significantly change the results and indicates a low sensitivity to ejected rod location. Therefore, future cycle results can be compared to the equilibrium cycle results to verify the applicability of this analysis for the U.S. EPR.

7.1.6 Transient Power and Rod Power Peaking

The example uncertainties and peaking allowances that are used for the REA analyses are shown in Table 7-2. These values are consistent with values employed for other chapter 15 events. The $F_{\Delta H}$ and F_Q uncertainty components are statistically combined (square root sum of the squares) and determined to be [] percent on $F_{\Delta H}$ and [] percent on F_Q . An overall allowance of [] percent is also applied to the calculated local $F_{\Delta H}$ and F_Q values. This allowance is defined as the maximum expected difference between measured to predicted values of $F_{\Delta H}$ and F_Q . These uncertainties will only be applied to the fuel rod model.

7.1.7 Sensitivity Calculations for Plant Transient Calculations

Table 7-3 provides a list of parameters, the range of transients sampled, and the estimated range of sensitivity in terms of estimated power differences. The difference in core power, core power times peaking factor ($F_{\Delta H}$ and F_Q), and/or maximum adiabatic cal/g (see section 6.2.2) are compared at the time of peak power and after the pulse has flattened out. The largest of the range of results are tabulated. The first sensitivity case is the base model with the uncertainties removed on ejected rod worth, β_{eff} , DTC, and MTC. The results can be significantly different for a prompt critical rod ejection calculation versus a non prompt critical rod ejection. The prompt critical excursion at EOC HZP has approximately [] percent conservatism or a delta of [] cal/g over the first second. The BOC HZP ejected rod worth is not prompt critical and is not as limiting as a higher initial power. Therefore, the BOC 25 percent power transient is used to replace the sensitivities of the analysis for BOC HZP. The BOC 25 percent power case has between [] percent conservatism. The HFP cases have the least conservatism [] depending on the time of the comparison. The minimum conservatism at peak power is [] percent. The smaller value corresponds to the near static condition at greater than 5 seconds. The trend of decreasing conservatism as power increases is expected. The uncertainties are applied to

maximize the resultant power change for a given reactivity insertion and the full power cases have the smallest change for the ejected rod worth.

For the remaining studies it is shown that [

] These conclusions are applicable to the results presented in this report. If in future analyses, the cal/g of the analysis exceeds the cal/g presented herein, the HZP sensitivity cases would need to be repeated for those conditions.

7.2 LYNXT Boundary Conditions and Uncertainties

The treatment for the LYNXT boundary conditions and uncertainties demonstrates which parameters need to be modeled and what conservatisms and uncertainties are applied. The application of boundary conditions and uncertainties for the pellet and cladding dimensions (geometry), cladding oxidation, coolant conditions, transient power, heat resistances, transient coolant heat transfer coefficient, and transient coolant conditions is addressed in the following sections.

7.2.1 Pellet and Cladding Dimensions (Geometry)

The LYNXT geometry model used for the rod ejection accident analysis is based upon a base 17-channel model used for the majority of the thermal-hydraulic and MDNBR evaluations. The model is developed to be consistent with the methods and geometries described in References 7 and 16. The fuel assembly is a 17x17 array of lattice locations with 265 fuel rods and 24 guide tubes. The U.S. EPR fuel assembly has 165.4 inches of active fuel height and a fuel rod in the center location. The LYNXT core model uses a 1/8th symmetric model with [

] Figure 7-8 shows the baseline geometry for the radial layout of LYNXT model, which is constant for each axial node.

The geometry model for the temperature and enthalpy calculations within the fuel rod is based on the nominal cold dimensions for all cases. Engineering hot channel factors on the local heat flux and enthalpy rise are used to account for the off nominal dimensions and other manufacturing tolerances not covered by the power factors applied to NEMO-K peak rod powers.

The fuel rod selected to be modeled is the U.S. EPR reference fuel rod described in Reference 16. Axially, the overall cladding length for the coolant heat transfer model is extended beyond the active fuel length to 179.1 inches to account for the lower and upper gas plenums.

7.2.2 Cladding Oxidation

The thermal conductivity of a zirconia corrosion layer on the cladding is lower than the M5™ cladding. The LYNXT code does not currently allow two regions of cladding properties to be used, but the decrease in the effective cladding thermal conductivity can be modeled with the CG/TDP property sets. To determine the impact of the maximum anticipated oxide layer thickness on DNBR and temperatures, a sensitivity study was performed using a cladding conductivity reduced to 60 percent of the nominal temperature dependent values. The study was run on the BOC HFP and EOC HZP rod ejection cases. The results showed that the peak cladding temperatures increased by less than [] and the peak fuel temperatures increased by less than []. The timing of the DNBR response was minimally impacted and results indicated higher DNBR values. For the evaluation of the spectrum of rod ejections, the cladding

conductivity properties with no oxide thickness are used in order to provide lower predictions of the MNDBR.

7.2.3 Coolant Conditions

The coolant boundary conditions used in the LYNXT models are the system pressure, inlet coolant temperature, and inlet mass flux. For the system pressure, the pressurizer pressure is used instead of the core exit pressure. This is conservative because the pressurizer pressure is typically 40 psi lower than the core exit pressure. The minimum thermal design volumetric flow rate, which is 4 percent below the nominal, is reduced by 5.5 percent for the core bypass to obtain the inlet mass flux boundary condition for the core. An additional local reduction in the inlet mass flux is applied to the bundle of interest. This provides a low value estimate of the inlet mass flux. The inlet temperature and mass flux are determined by a heat balance performed in conjunction with the coolant average temperature as a function of power level. The average coolant temperature as a function of the core power is given in Figure 7-1. In the LYNXT calculations no further temperature or pressure errors are applied to the determined values. For transients less than 5-10 seconds, these thermal boundary conditions are held constant. For longer duration transients, time varying inputs may be used. Boundary conditions generated with S-RELAP5 are evaluated to estimate the thermal performance for the 25 percent power case at BOC and the HFP cases for both BOC and EOC.

7.2.4 Transient Power

Each fuel rod node is assigned time dependent normalized axial power shapes and radial peaking factors. The fraction of core power is also assigned a time dependent array of values. These are used to approximate the relative global and local heating rates as determined by the NEMO-K neutronics calculations within the number of time-step limitations of the LYNXT code. For DNBR performance, one assembly of the core is considered as the "assembly of interest." A detailed channel analysis is performed for the peak rod from this assembly. The transient axial shape factors are taken to be that of the fuel assembly of interest and are used for the entire core.

The rod powers for the 17 fuel rod nodes in the assembly of interest are conservatively assumed for this analysis to have [

]

No sensitivities are performed because this is a conservative model.

7.2.5 Heat Resistances in Fuel, Gap and Cladding

A representative approach is used to treat the heat resistances of the fuel and gap. The effect of the cladding resistance is addressed in section 7.2.2. A single uranium enrichment at the extreme burnups is evaluated. Sensitivity studies are run for burnup, uranium enrichment, and gadolinia content to illustrate the analysis conditions.

The EOC HZP power excursion is run with 2.0 and 5.0 w/o U-235 at two different burnup conditions to determine the uranium enrichment and burnup dependence. The two different burnup conditions are maximum gap (near BOL) and end of life. [

] The practical maximum burnup for a 2.0 and 5.0 w/o U-235 pellet is estimated to be 50 and 70 GWD/MTU, respectively. The MDNBR performance is shown in Figure 7-9 for these cases. [

]

This is due to higher gap conductance values and higher pellet rim power peaking. Calculations are performed with 5.0 w/o U-235 fuel at 2.5 and 50 GWD/MTU burnup levels for the BOC cases and 20 and 70 GWD/MTU burnup levels for the EOC cases in order to bound the potential burnup thermal property states of the fuel rods.

Fuel loaded with gadolinia has a lower thermal conductivity than pure UO_2 . The higher the gadolinia content, the lower the thermal conductivity of the fuel pellet. This increases the fuel temperatures of the gadolinia fuel if operated at the same LHGR as a UO_2 fuel rod. However the gadolinia rods typically have low maximum powers because of lower fuel uranium enrichments and parasitic neutron absorption by the residual gadolinium isotopes. To determine if the analysis can be performed using only UO_2 properties, a sensitivity study was run on the BOC HFP power excursion with gadolinia loadings of 4 w/o and 8 w/o gadolinia. The gadolinia rods were run with the same power history as the pure UO_2 rod and with the maximum power level anticipated for a gadolinia loaded rod. [

] Figure 7-10 shows the peak fuel temperatures for 0, 4, and 8 w/o gadolinia loadings. Note that the fuel temperatures with gadolinia are higher when operating at the same linear heat rate as UO_2 . When the transient temperatures for gadolinia fuel are adjusted by the power reduction factor, the maximum temperature during the transient is bounded by the UO_2 maximum temperature. For the thermally limiting transient for HFP at BOC, the temperatures never exceed the lowest fuel melt limit for a rim burnup, even when the peak power is not decreased by the maximum expected value for a gadolinia rod. Because the UO_2 rod bounds the temperatures, the LYNXT calculations use the [

]

7.2.6 Coolant Heat Transfer Coefficient and Transient Coolant Conditions

Minimum flow is used and if the local DNBR is less than a LYNXT code input safety design limit, the heat transfer correlation conservatively switches from Dittus-Boelter to include consideration of the inception of film boiling and post-CHF conditions. The DNBR safety design limit used for this sample problem is [] (Reference 21).

For the short duration scenarios (i.e., 0-5 seconds), the coolant boundary conditions are assumed constant and only the power distribution history is modeled. For the events that do not have an excore neutron flux rate trip (usually occurs within the first 2 seconds), coolant boundary conditions from S-RELAP5 calculations using the NEMO-K core power history instead of the point kinetics were used to further degrade the LYNXT transient boundary conditions for the calculation of the thermal performance of the fuel rods.

7.3 Failure Boundary Conditions

For a core that has a peak rod exceeding the DNBR criterion or has melted the fuel, a fuel census will be performed. The minimum DNBR Safety Design Limit criterion is [] from Reference 21.

The UO₂ melting temperature is a function of burnup. The best estimate melt temperature is adjusted downward by a [

] The limiting centerline fuel melt (CFM) temperature is represented by the following equations from Reference 2 (Equation 12-3, pg 12-7):

$$[\quad \quad \quad]$$

where:

T_{LC} = reduced melt temperature, C

T_{LF} = reduced melt temperature, F

Bu = pellet burnup, GWD/tU

For very fast transients, when the maximum pellet temperature may be close to the rim, the melting temperature limit must also account for local burnup levels being higher than the pellet average. During pellet irradiation, the radial pellet power distribution shifts from [] the pellet average power on the rim. So at the point of maximum pellet average burnup, the ratio of the rim burnup to the average burnup will be no higher than []. This factor is used conservatively to lower the fuel melt limit for these regions. Using 70 GWD/MTU as the maximum average pellet burnup, the maximum rim burnup is no larger than [].

]. The peak fuel temperature can not exceed this temperature.

The magnitude of assembly power distribution change due to the ejected rod varies relative to its proximity to the ejected rod location. Several different power shapes versus time are run in LYNXT with different changes in the peaking. The $F_{\Delta H}$ of the assembly is either scaled up or down until the rod DNBR reaches [] or higher. Peaking conditions between the rods analyzed are linearly interpolated for the failure value. Rods with powers higher than this value in terms of $F_{\Delta H}$ and F_Q are considered failed.

Table 7-1 Design and REA Analysis Conditions

Parameter		Unc ¹	BOC, HZP	BOC, HFP	EOC, HZP	EOC, HFP
Ejected Rod Worth (pcm)	PRISM ²	+15%	180 to 242	17 to 22	264 to 402	22 to 25
	REA Analysis	-	433	64	634	97
MTC (pcm/°F)	PRISM ²	+2	-5.57 to -2.36	-11.89 to -7.68	-26.94 to -22.29	-38.81 to -31.73
	REA Analysis	-	2.16	0.01	-19.40	-28.47
DTC (pcm/°F)	PRISM ²	-10%	-1.59 to -1.53	-1.40 to -1.34	-1.82 to -1.81	-1.63 to -1.61
	REA Analysis	-	-1.22	-0.96	-1.52	-1.28
Beta Effective (10 ⁻⁵)	PRISM ²	-5%	640 to 740	640 to 740	510 to 530	510 to 530
	REA Analysis	-	550	550	470	470

Notes:

1. Unc = Uncertainty to be applied to nominal conditions.
2. PRISM conditions are without uncertainties, rod position at rod insertion limits, and nominal Xenon.

Table 7-2 Peaking Uncertainties

3-D Uncertainty	%
Measurement	[]
HCF	[]
Rod Bow	[]
Assembly Bow	[]
Core Power	[]
Total SRSS	[]
2-D Uncertainty	%
Measurement	[]
Assembly Bow	[]
Core Power	[]
Total SRSS	[]

Table 7-3 Plant Transient Sensitivity Study Summary

Parameter	Δ Case Conditions	Range of Evaluation	% difference (Δ /base-1) *100% ^a	Comments
Ejected rod worth, DTC, β_{eff} , and MTC	-15% ejected rod worth 10% increase in Doppler magnitude 5% increase in β_{eff} -2 pcm/ ^o F MTC	BOC 25 BOC HFP EOC HZP EOC HFP		
Rate of Reactivity Insertion	0.1 to 0.2 sec for full length ejection	BOC 25 BOC HFP EOC HZP EOC HFP		
Reactor Trip Reactivity	9% increase in trip worth Base analysis is 9% less than nominal	BOC 60 EOC HZP		
Power Peaking	13%	Not tested in plant model		
Heat Resistances and Transient cladding to Coolant Heat Transfer				
Fuel conductivity,	-20% change in Fuel conductivity	EOC HZP		
Gap Conductance	Gap conductance increased by 100%	BOC 25 BOC HFP EOC HZP EOC HFP		
Coolant Heat Transfer	-4% flow assumed by fuel rod model	BOC 25 EOC HZP EOC HFP		

Parameter	Δ Case Conditions	Range of Evaluation	% difference (Δ /base-1) *100% ^a	Comments
Others				
Fractional Heat Deposited in Fuel	0.974 to 0.966	BOC 25 BOC HFP EOC HZP EOC HFP		
Pellet Radial Power Profile	5 w/o fuel to 2 w/o fuel	BOC 25 BOC HFP EOC HZP EOC HFP		
Neutron Velocities	+10%	BOC HFP EOC HZP EOC HFP		
Time step	Flux Δt 2x Fuel Δt =4x Moderator Δt =4x	BOC 25 BOC HFP EOC HZP EOC HFP		
Number of Fuel Rod Nodes	15 to 20 fuel nodes 3 to 5 cladding nodes	BOC HFP EOC HZP EOC HFP		
Effective Temperature	Weighting by the pellet average temperature	BOC 25 BOC HFP EOC HZP EOC HFP		

Notes:

^a Negative values indicate that the base case yields more conservative results.

Figure 7-1 Average Coolant Temperature with Power

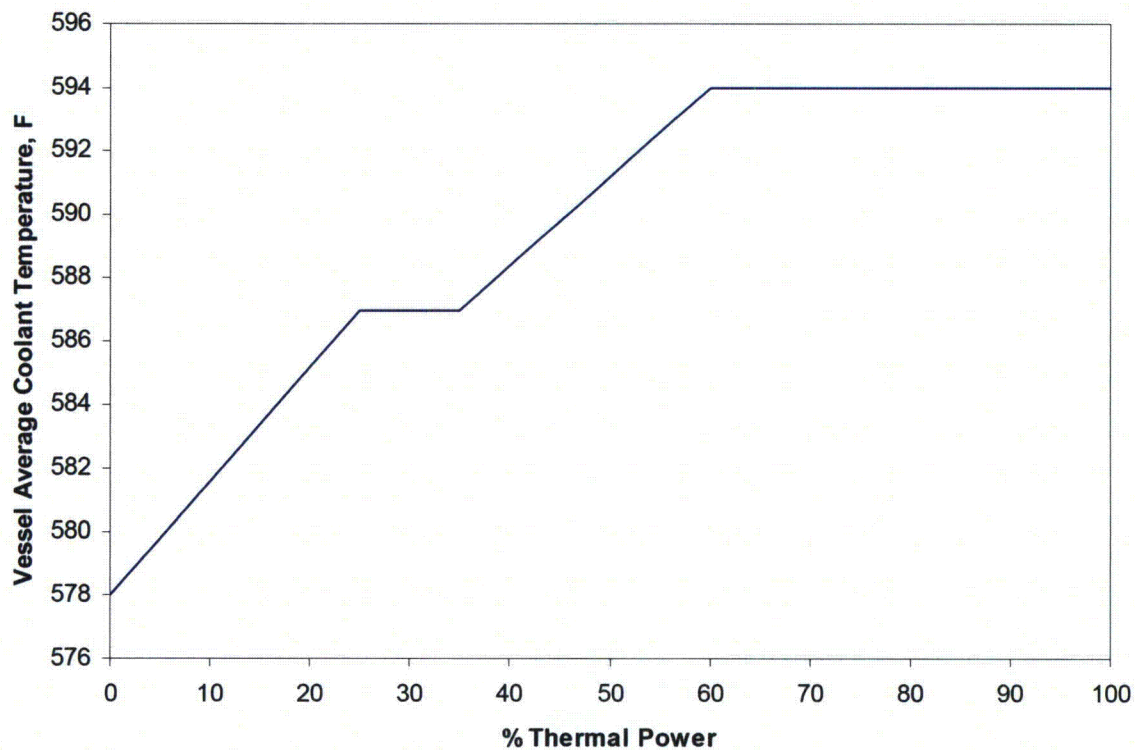
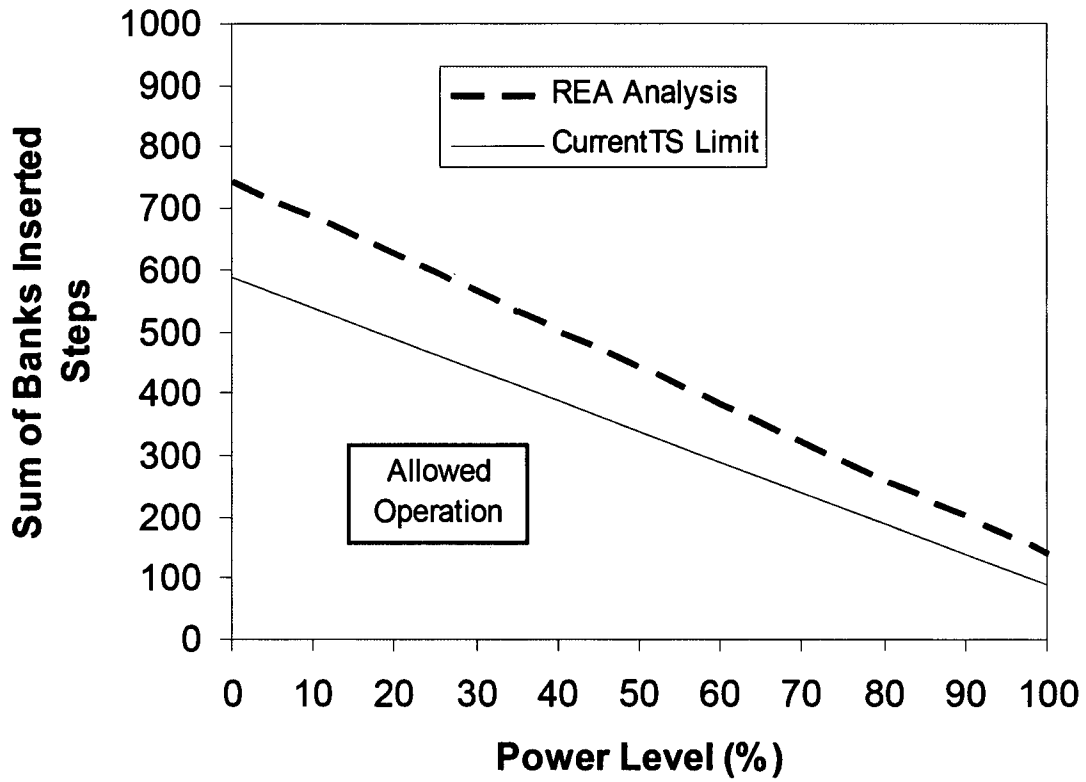


Figure 7-2 Rod Position Technical Specification Limits/Analysis



**Figure 7-3 BOC 25%, FOP Comparison between Equilibrium Cycle
and []**



**Figure 7-4 BOC HFP, FOP Comparison between Equilibrium Cycle
and []**



Figure 7-5 EOC HZP Equilibrium Cycle and [] Comparison



Figure 7-6 EOC HFP Equilibrium Cycle and [] Comparison



Figure 7-7 EOC HZP Equilibrium Cycle and []



Figure 7-8 17-Channel LYNXT Model Diagram



NOTE: channel numbers are shown in normal font and rod numbers are shown in bold

Figure 7-9 MDNBR Uranium Enrichment Response for EOC HZP

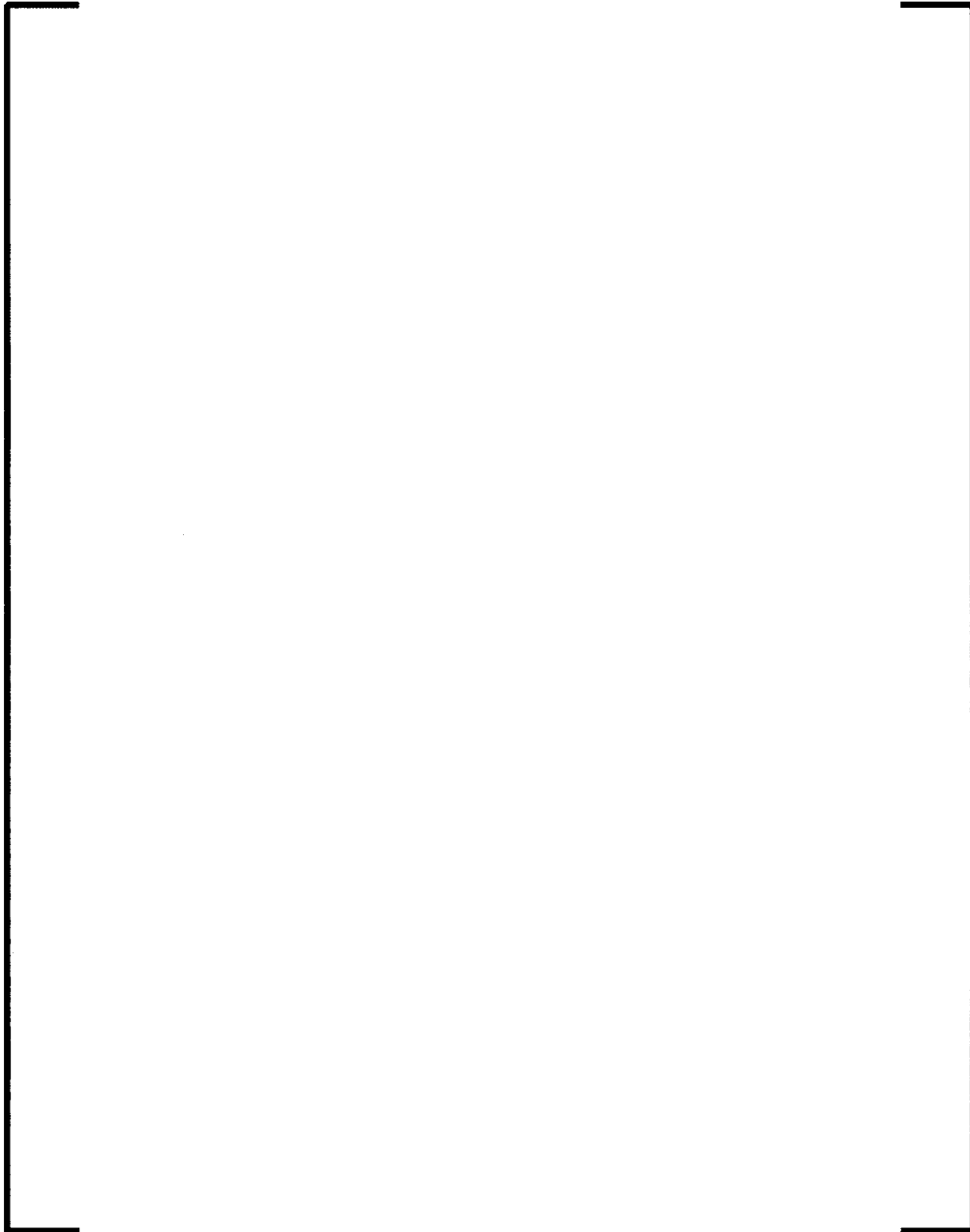
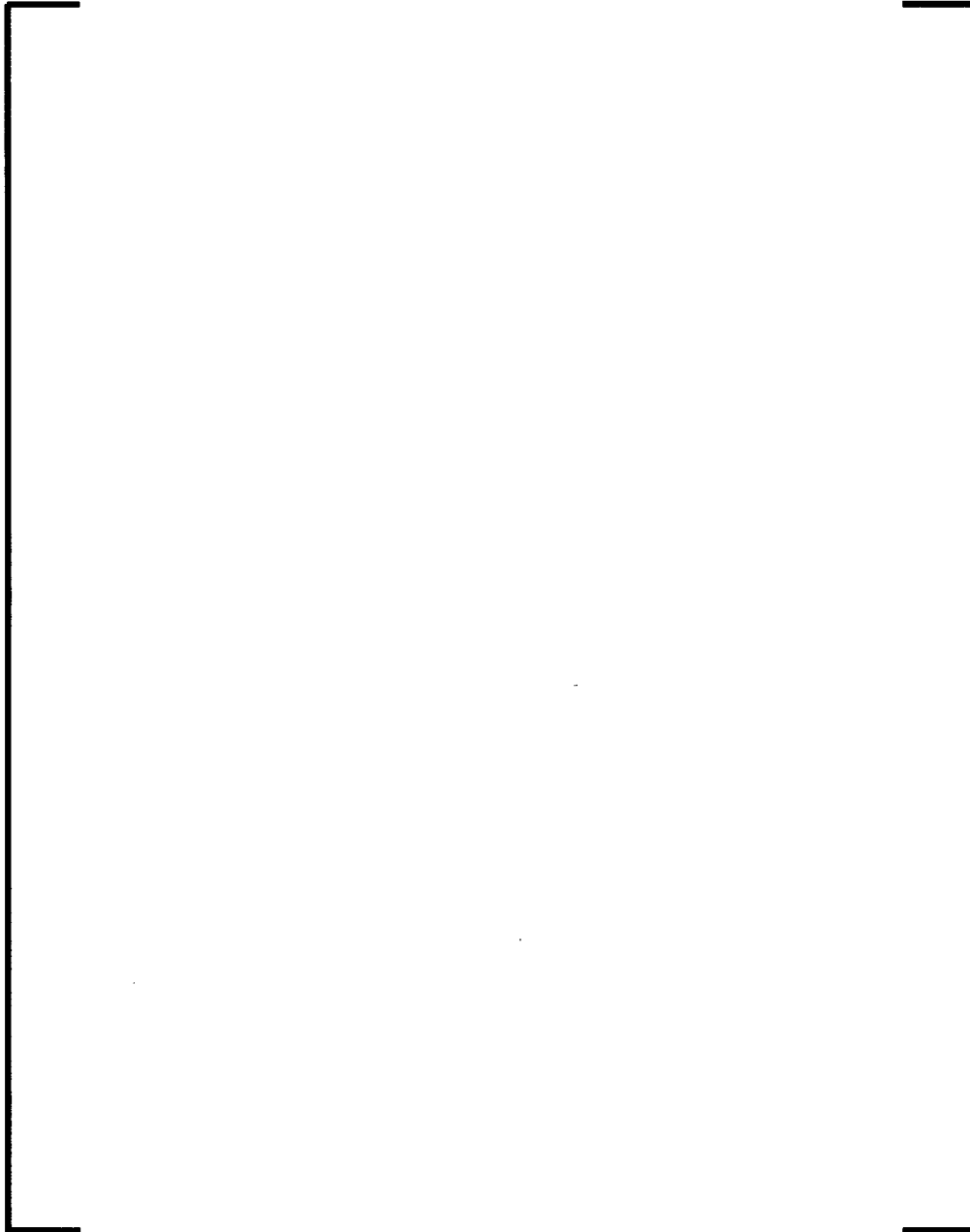


Figure 7-10 UO₂ and Gadolinia Fuel Temperatures for BOC HFP



8.0 U.S. EPR SAMPLE PROBLEM RESULTS

The U.S. EPR sample problem results section contains the detailed results of this REA methodology. The trip functions that are used by this sample problem are shown in Table 8-1.

8.1 NEMO-K Results

The transient simulations for 0, 25, 35, 60, and 100 percent full power are performed at BOC and EOC. The results for core power, $F_{\Delta H}$ and F_Q are shown in Figure 8-1 through Figure 8-10. Because the ejected rod starts out at a lower power than the surrounding assemblies a separate analysis can be performed for the ejected rod location. As an example, Figure 8-11 shows the nominal peaking from NEMO-K for the ejected rod and peak locations for the BOC HFP condition. The HZP BOC ejected rod worth is not prompt critical and does not trip on the high flux rate trip. To bound the results below 25 percent power at BOC where the reactor may not trip on the flux rate trip, the transient model is run with and without the trip function. Core pressure, flow, and inlet temperature are held constant during these simulations. BOC and EOC HFP transients do not reach a trip signal. Those conditions without trip require a S-RELAP5 analysis, which is described in the following section.

8.2 S-RELAP5 Evaluation

The S-RELAP5 evaluation section reviews the consequences of using a constant pressure, inlet temperature and flow in the NEMO-K and estimates its impact on the fuel rod model. For the plant model in NEMO-K, two conditions are reviewed:

- an increase in pressure due to the power insertion.
- operation without trip.

A calculation is performed to determine how an increase in pressure affects the core reactivity. The power pulse after the ejection could cause an increase in the pressure if

there is no hole in the primary system from the ejected rod. A pressure increase of 40 psia is estimated for the EOC HFP REA. A power search is performed at EOC HFP at +40 psia. The temperature increase occurred after the peak power and would only affect the static power thereafter. The power difference is [].

For the condition of no trip with a leak in the primary, two S-RELAP5 calculations, a full power and 25 percent power transient, are performed to estimate the range of thermal conditions that could be reached. The break area is calculated using the 75 mm (0.246 ft) inside diameter of the control rod flange as the break diameter and applied to the top of the upper head volume. The simulations continue until a trip in the S-RELAP5 model is reached. This simulation did not include any actions for the non-safety control systems that would tend to improve the situation. The S-RELAP5 results for 25 percent power and HFP are shown in Figure 8-12 and Figure 8-13, respectively. The REA simulations for the 25 percent and HFP initial conditions without a high flux rate trip eventually tripped on high secondary steam pressure and low primary pressure, respectively. For these cases, the duration is slow enough that the core is in near equilibrium with the thermal conditions. Rather than running this specific transient in NEMO-K, several static power searches are performed with the rod ejected at various thermal conditions from S-RELAP5 to determine the limiting power that may be reached after the initial ejection. These results are shown in Table 8-2. The maximum power and the time dependent range of thermal conditions from these cases are evaluated using the fuel rod model with LYNXT.

8.3 LYNXT Results

The transient simulations are performed for 0, 25, 35, 60, and 100 percent full power at BOC and EOC. The BOC HZP ejected rod worth is not simulated in LYNXT because the results are bounded by the 25 percent power response and are not presented. The results for the MDNBR, peak fuel temperature, peak cladding temperature, and peak radially averaged enthalpy rise are shown in Figure 8-14 through Figure 8-40.

The BOC 25 percent power, BOC HFP, and the EOC HFP transient simulations did not trip. The LYNXT models the S-RELAP5 thermal boundary conditions with time. The NEMO-K power results for the first 5 to 8 seconds are followed by a linear progression to the highest power predicted by the static NEMO-K cases. For the 25% power BOC case with no trip, the minimum DNBR for the peak power assembly does not exceed the design limit until after 16 seconds into the transient. After this point the post-CHF heat transfer mode is simulated causing the rapid rise in the peak cladding temperature.

For the BOC and EOC 100 percent power cases, the power level stabilizes at a power level to balance the reactivity. A conservative estimate of 108 percent for BOC and 104 percent for EOC with no void reactivity feedback in NEMO-K is used. The minimum DNBR for the peak power assembly rapidly drops below the DNBR design limit and continues to degrade as the plant heats up and system pressure drops. The thermal boundary conditions continue to degrade and increase the peak fuel and cladding temperatures. The rate of increase reduces as the system approaches thermal equilibrium. The S-RELAP5 simulation did not include the low DNBR reactor trip function, which would terminate the transient before the plant system trip on low pressure. There is a design requirement for the low DNBR reactor trip function to trip at any static power, temperature, and pressure combination of conditions that would compromise the minimum DNBR design criteria for a non skewed design peak type condition. This requirement provides added protection in the event that the core achieves different powers, temperatures, and pressures than analyzed by the S-RELAP5 by enabling the same relative DNBR protection. Based on this requirement applied to the S-RELAP5 core conditions, a trip is estimated to occur before 30 seconds for the HFP REA transients.

Even though the DNBR design limit is exceeded for five of the evaluated cases, in no case did the peak fuel temperatures exceed the fuel melt limit for the expected higher burnup fuel [

]. The maximum temperatures calculated were 4014°F for the fuel and 1461°F for the cladding with the limiting temperature case of BOC HFP at 30 seconds into the

transient (time of estimated RCSL trip). The maximum prompt radially averaged fuel enthalpy rise determined for the entire spectrum of cases was less than 20 cal/g (EOC HZP) and a maximum integrated total enthalpy was less than 110 cal/g (BOC HFP).

8.4 Rod Census

The number of rods failed was estimated for BOC 25 percent, BOC 60 percent, BOC HFP, EOC 60 percent and EOC HFP. For each transient, the rods may need to be counted for two different thermal conditions, the prompt response (i.e., 0-5 seconds) and the delayed response (i.e., greater than 5 seconds) when trip does not occur from the power pulse. The latter case reduces to a static case where the neutron power is in equilibrium with the thermal output of the core. None of the assemblies experienced an enthalpy rise of more than 20 cal/g so that the fuel failure analysis does not need to consider the elevated dose requirements outlined in Section 2.3.

LYNXT cases are run for each condition to determine the power at which the limiting fuel rod has a MDNBR of []. The $F_{\Delta H}$ and F_Q for this condition are used as the failure criteria. Any rod with an $F_{\Delta H}$ or F_Q exceeding this value is assumed failed. For the prompt response at power, each location has a different amount of thermal margin to the limit based on its initial power. This dependence is captured [] in LYNXT to determine when a rod may fail.

A correlation is then made between the []
[]. In Figure 8-41 []

The failed rod counting can be based on the static peaking rather than detailed time dependent evaluations. For each transient condition the limiting transient $F_{\Delta H}$ and F_Q values are correlated to []. All rods

exceeding the static $F_{\Delta H}$ or F_Q for these cases are counted as failed for the prompt response.

The cases with no trip (delayed response) can be treated simply as a static case and therefore, only one assembly of interest distribution is needed to define the limiting $F_{\Delta H}$ and F_Q prior to reaching the MDNBR. Table 8-3 contains the estimated rod failures for each of the transients.

8.5 Summary Results

The overall REA results for the plant transient analysis and fuel rod model are shown in Table 8-4 and Table 8-5 for BOC and EOC, respectively. The maximum prompt $\Delta\text{cal/g}$ is calculated at one pulse width after the peak. For those cases that have no discernable pulse, the value at 1.0 second is used. For all the transients modeled, the maximum $\Delta\text{cal/g}$ is less than the threshold value (31.2 $\Delta\text{cal/g}$) to consider increased fission gas release and there is no fuel melt. Therefore, no equivalent pin failure adjustments are needed to the DNBR failures calculated. The results are within the criteria listed in Table 2-1. Also, the limiting conditions for all the criteria are at either HZP or HFP.

Table 8-1 Trip Signal Parameters in Analysis

Parameter	Value
Type of Trip Signal	Flux Rate
Trip Signal, %	13 ⁽¹⁾
Sampling Rate, seconds	0.025
Scram Lag, seconds	≤ 0.7 ⁽²⁾
Number of Detectors Required to Trip	3 ⁽³⁾
Lag Rate Constant, seconds	30
Gain Constant, seconds	30
High Steam Generator Pressure (Setpoint/Analysis), psia	1384.7/1414.7
Low Saturation Margin (Setpoint/Analysis), BTU/lbm	430/0
Low Pressurizer Pressure (Setpoint/Analysis), psia	2005/1980
High Pressurizer Level (Setpoint/Analysis), % range	75.0/80.5
High Pressurizer Pressure (Setpoint/Analysis), psia	2414.9/2439.9

Notes:

- (1) 11% plus 2% uncertainty.
- (2) Conservatively used 0.725 in analysis.
- (3) Need 3 to account for 2 out of 4 logic with 1 detector assumed failed.

Table 8-2 Static Power Search

Core Condition	ΔPressure (psi)	ΔTinlet (°F)	Flow, (%)	Resultant FOP
BOC HFP	0 to -250	0 to +10	0 to -2.5%	1.0034 to 1.0817
EOC HFP	0 to -250	0 to +10	0 to -2.5%	0.8405 to 1.0399
BOC 25%	0 to -100	0 to +10	0 to -2.0%	0.5246 to 0.5507

Table 8-3 Estimated Rod Failures

Core Condition	% Failed Rods in Census	
	Prompt	Static
BOC 25% (no trip)	-	1.8
BOC 60%	none*	-
BOC HFP	0.3	7.2
EOC 60%	none*	-
EOC HFP	none*	1.9

Note:

- * Although MDNBR [] for the conservative peak analysis to bound future cycles, the actual distribution did not result in any failures.

Table 8-4 Ejected Rod Analysis Results for BOC

Parameter	Criterion	0	25	35	60	100
Maximum Ejected Rod Worth, pcm	-	433	362	346	286	64
β_{eff}	-	0.0055	0.0055	0.0055	0.0055	0.0055
MTC, pcm/°F	-	2.16	1.32	1.35	0.34	0.01
DTC, pcm/°F	-	-1.22	-1.14	-1.11	-1.05	-0.96
Initial F_Q	-	NA ^a	3.01	2.88	2.63	2.36
Maximum Transient F_Q	-	9.46	5.75	5.23	5.06	2.70
Initial $F_{\Delta H}$	-	NA ^a	2.15	2.09	1.94	1.70
Maximum Transient $F_{\Delta H}$	-	5.21	3.75	3.58	3.01	2.11
Maximum Neutron Power, FOP	-	0.32	0.55	0.69	0.98	1.10
Maximum cal/g	≤ 150	-	70.4	50.4	63.9	109.4
Maximum $\Delta\text{cal/g}$, prompt	≤ 110	-	10.0	10.9	11.8	7.2
Maximum Fuel Temperature, °F	[]	-	2655	1901	2529	4014
Maximum Cladding Temperature, °F	[]	-	1098	727	951	1461
MDNBR/SAFDL Ratio For Failure	≤ 1.0	-	0.71	1.86	0.96	0.33
Time of Trip (initiation of safety bank insertion), seconds	-	No Trip	No Trip ^b	0.850	0.825	No Trip
Equivalent nominal rods failed, %	≤ 30	-	1.8	0	0	7.2

Notes:

^a Not applicable since initial stored energy above the coolant temperature is zero.

^b Trip is disabled to bound consequences of powers lower than 25%.

Table 8-5 Ejected Rod Analysis Results for EOC

Parameter	Criterion	0	25	35	60	100
Maximum Ejected Rod Worth, pcm	-	634	516	484	389	97
β_{eff}	-	0.0047	0.0047	0.0047	0.0047	0.0047
MTC, pcm/°F	-	-19.40	-23.44	-23.31	-26.68	-28.47
DTC, pcm/°F	-	-1.52	-1.41	-1.40	-1.35	-1.28
Initial F_Q	-	NA ^a	5.28	4.24	3.28	2.10
Maximum Transient F_Q	-	20.10	13.32	10.91	7.38	3.30
Initial $F_{\Delta H}$	-	NA ^a	2.15	2.09	1.94	1.70
Maximum Transient $F_{\Delta H}$	-	6.51	4.87	4.53	3.61	2.22
Maximum Neutron Power, FOP	-	2.04	1.75	1.75	1.58	1.17
Maximum cal/g	≤ 150	33.9	62.2	64.6	73.1	103.4
Maximum $\Delta\text{cal/g}$, prompt	≤ 110	13.8	10.2	9.0	6.0	7.9
Maximum Fuel Temperature, °F	[]	1140	2402	2534	2987	3856
Maximum Cladding Temperature, °F	[]	741	777	774	1062	1337
MDNBR/SAFDL Ratio For Failure	≤ 1.0	1.82	1.36	1.33	0.97	0.46
Time of Trip (initiation of safety bank insertion)	-	1.000	0.850	0.850	0.825	No Trip
Equivalent nominal rods failed, %	≤ 30	0	0	0	0	1.9

Notes:

^a Not applicable since initial stored energy above the coolant temperature is zero.

Figure 8-1 BOC 0% Power Transient

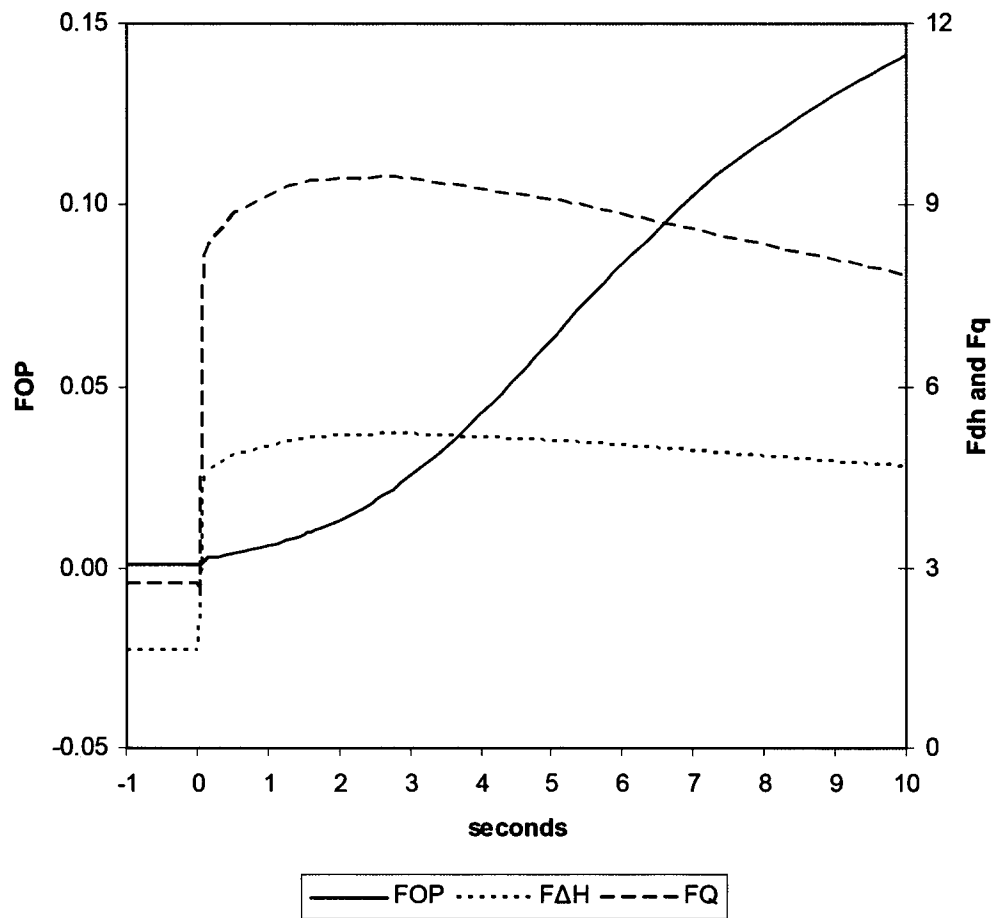


Figure 8-2 BOC 25% Power Transient

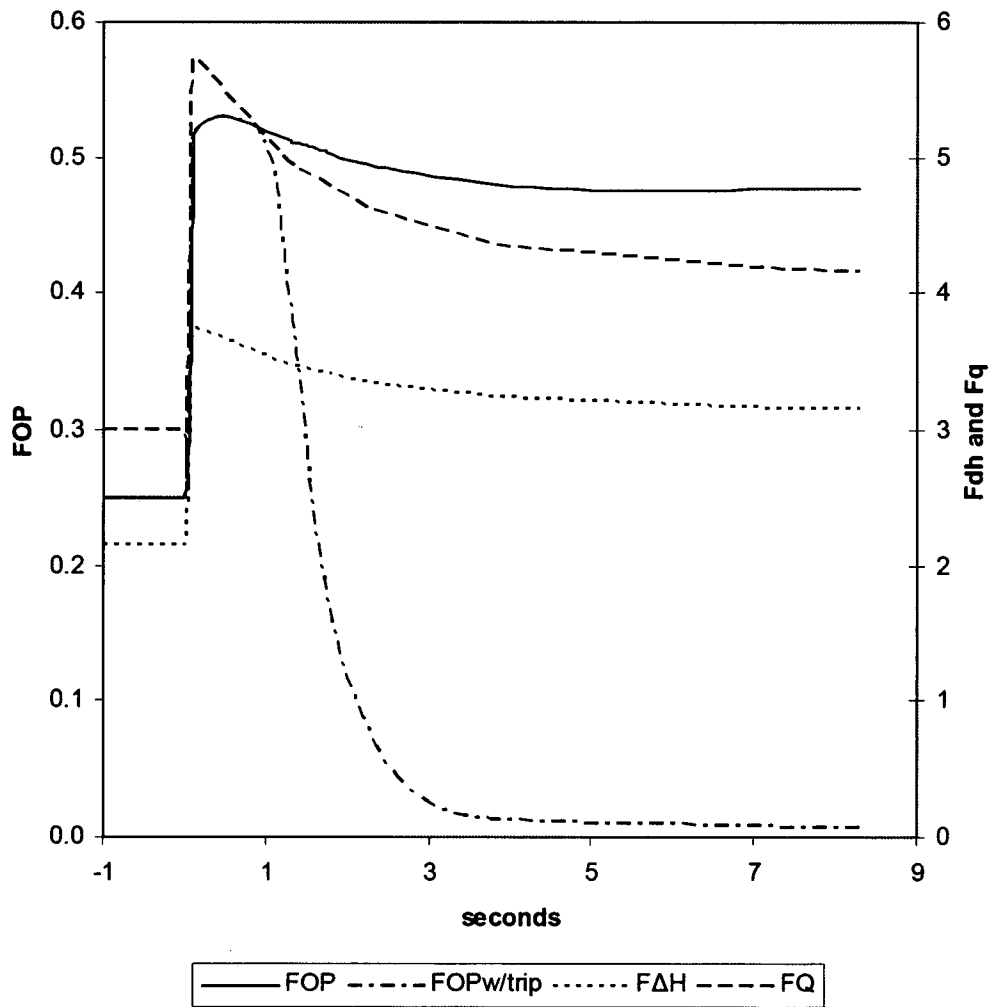


Figure 8-3 BOC 35% Power Transient

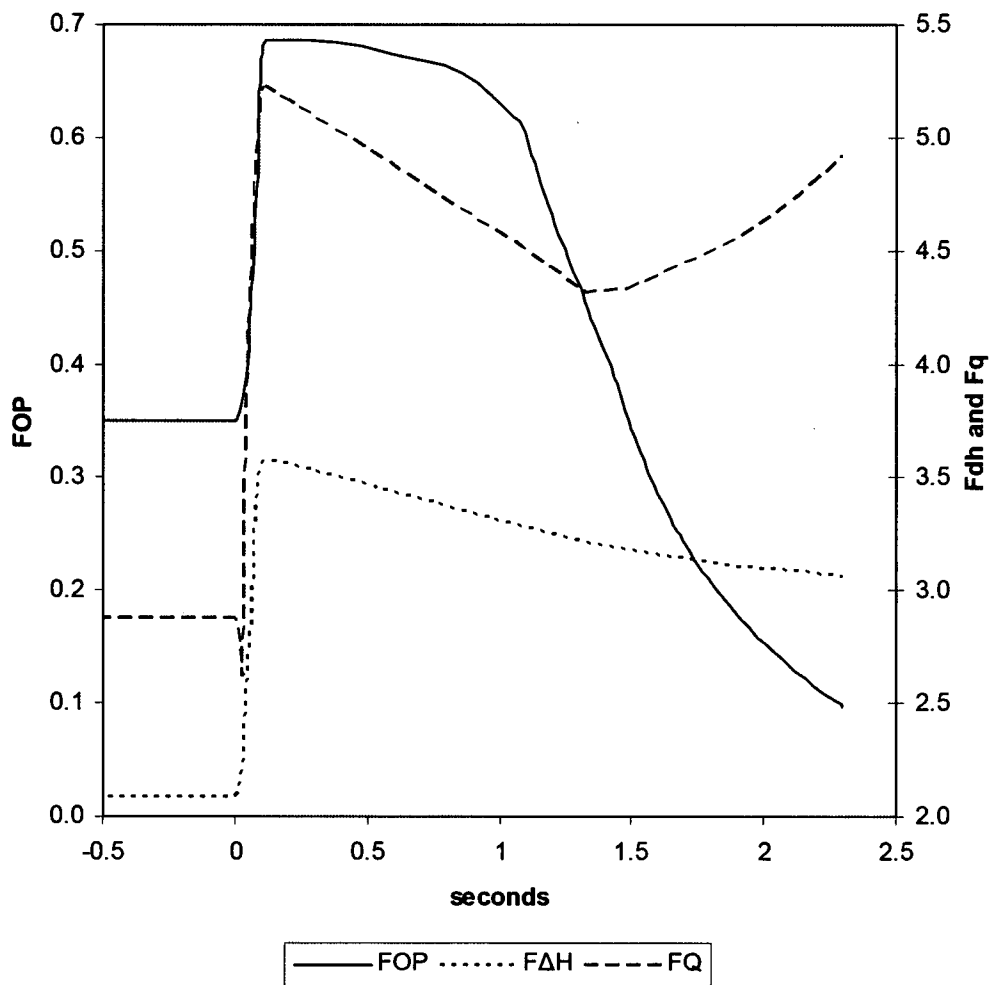


Figure 8-4 BOC 60% Power Transient

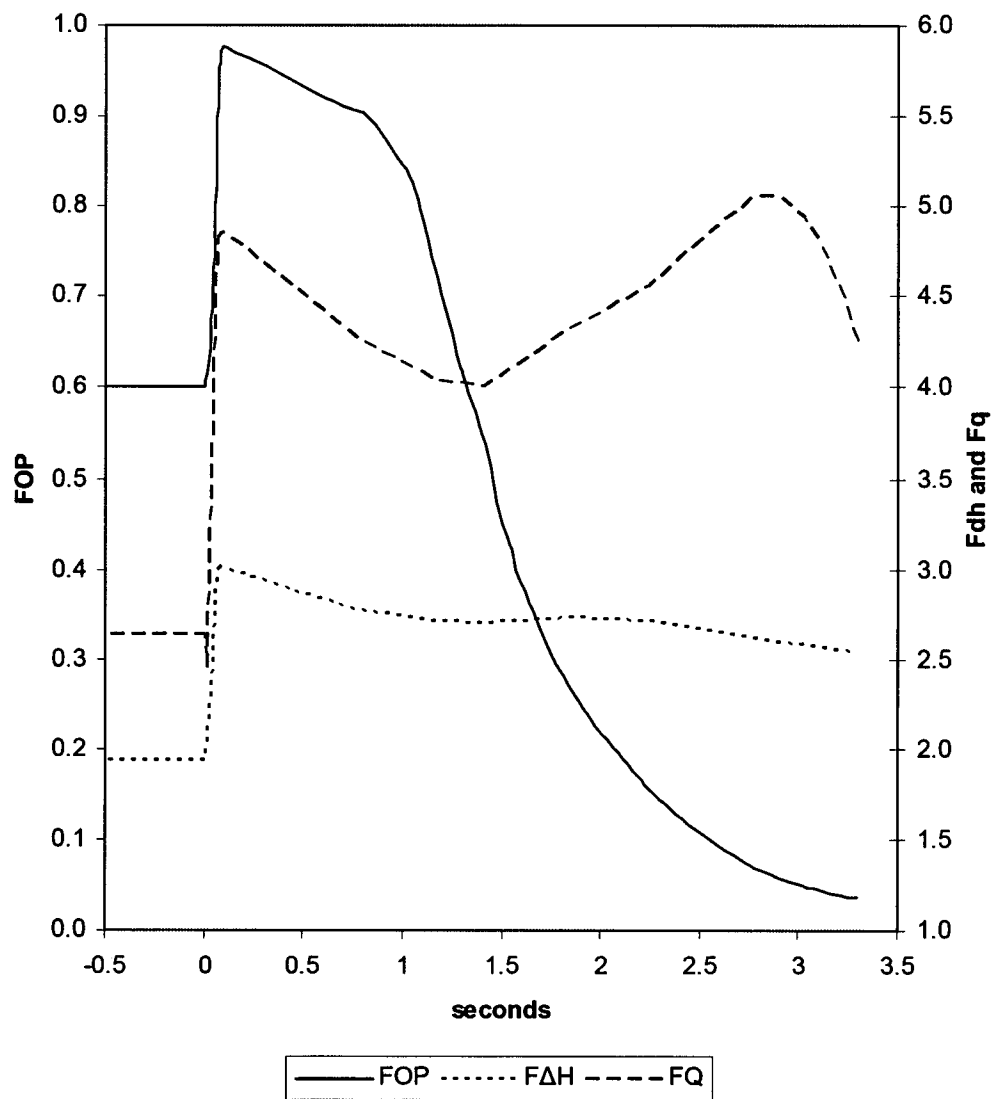


Figure 8-5 BOC 100% Power Transient

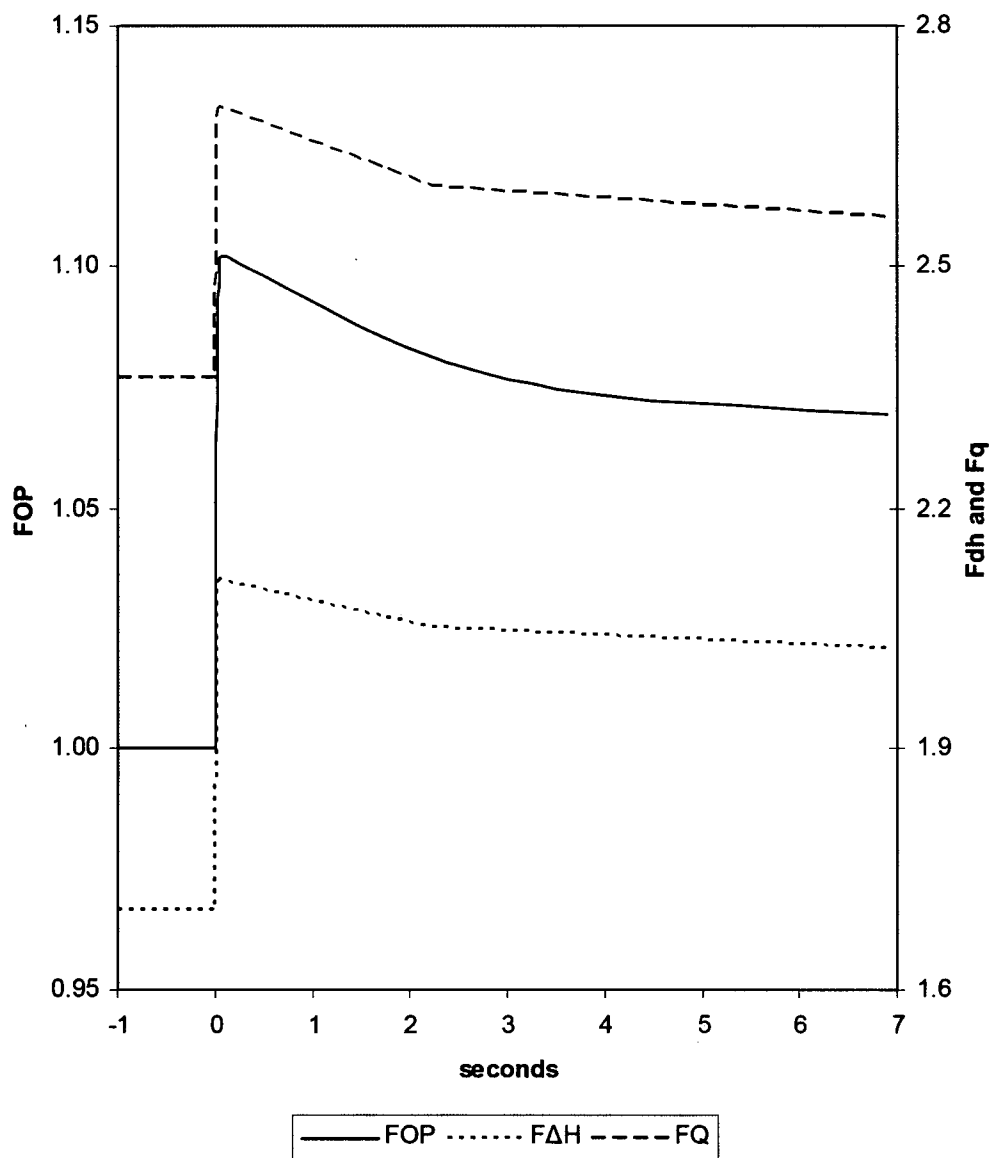


Figure 8-6 EOC 0% Power Transient

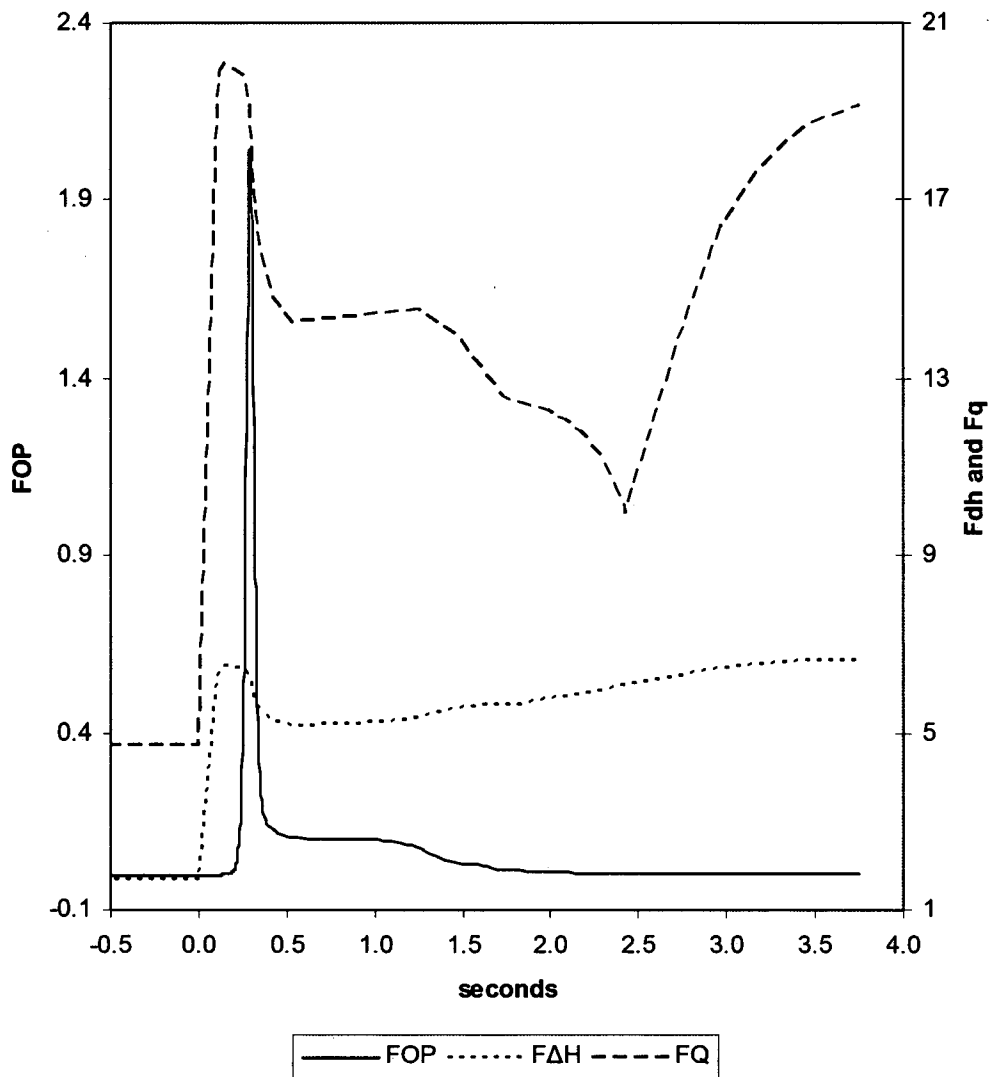


Figure 8-7 EOC 25% Power Transient

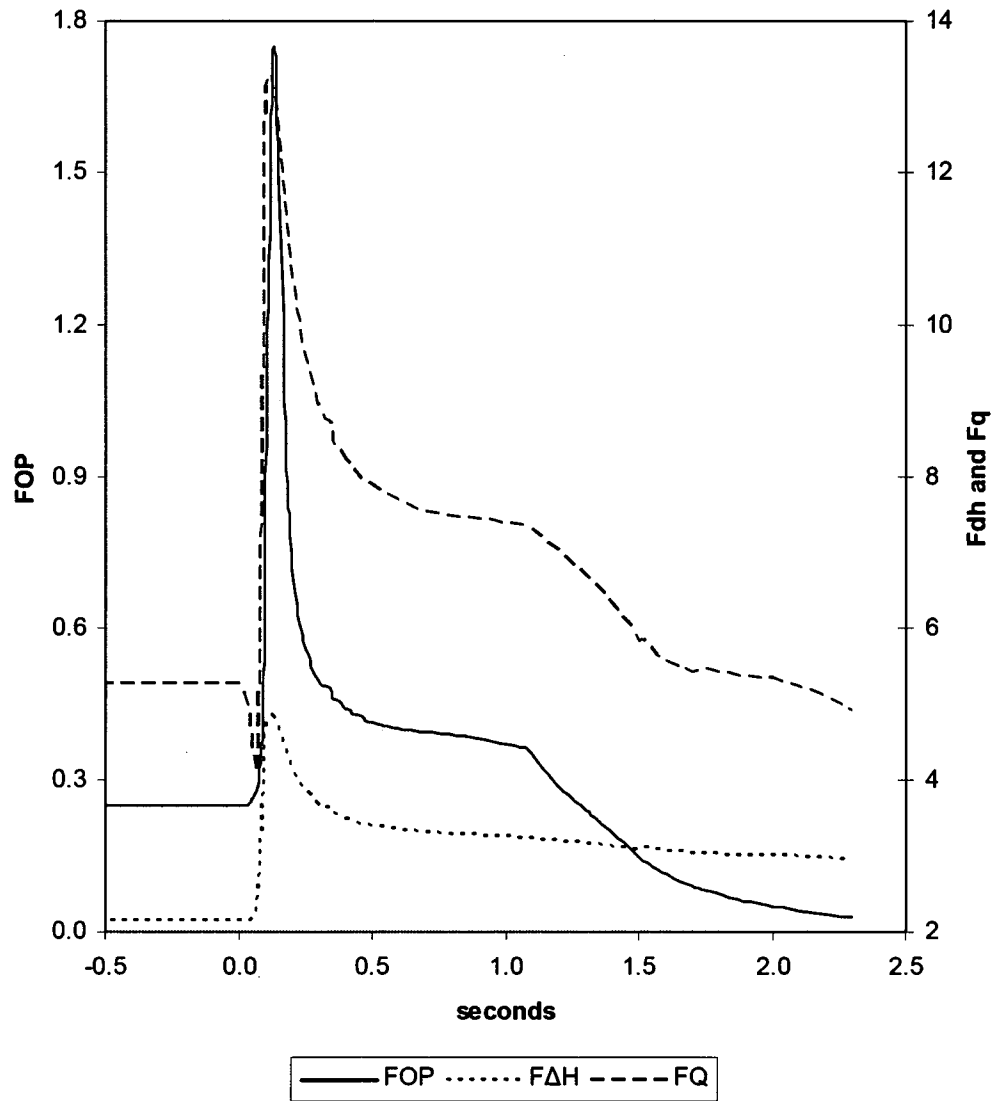


Figure 8-8 EOC 35% Power Transient

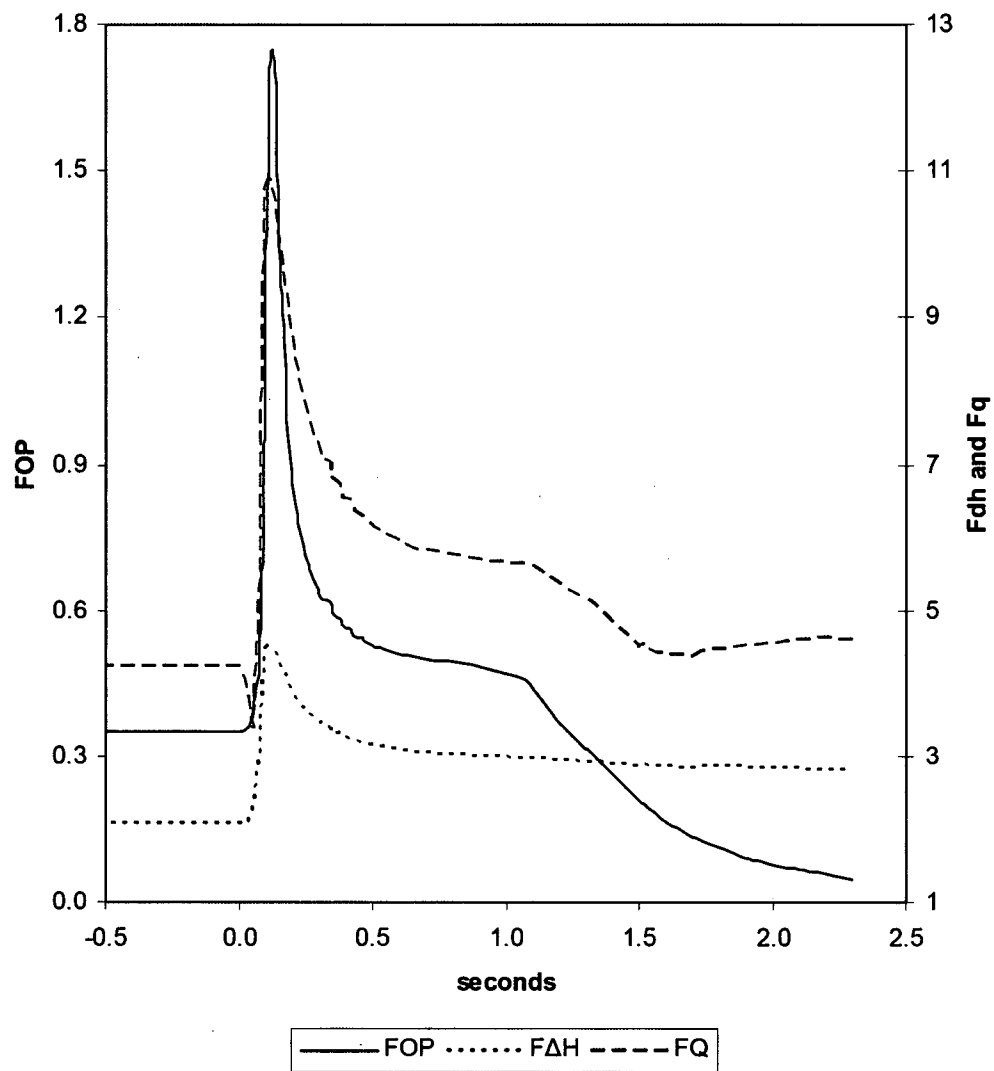


Figure 8-9 EOC 60% Power Transient

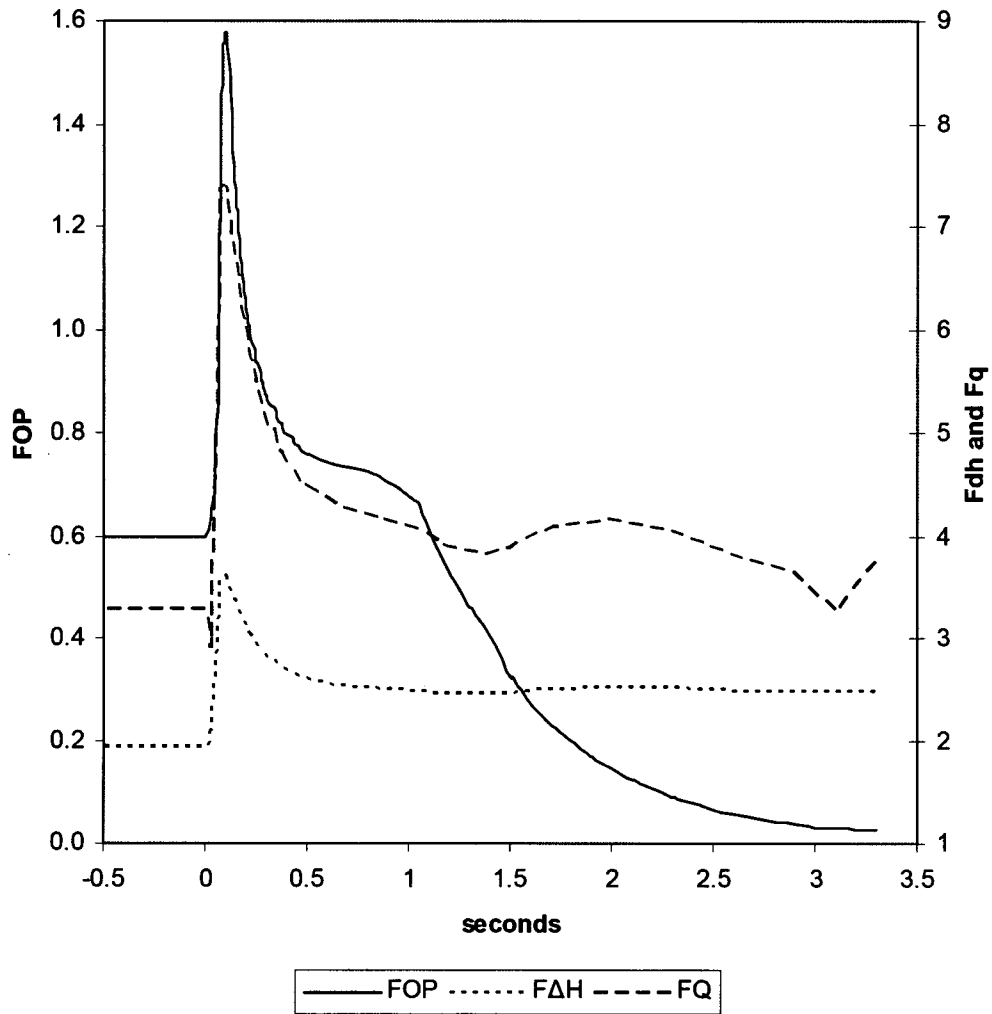


Figure 8-10 EOC 100% Power Transient

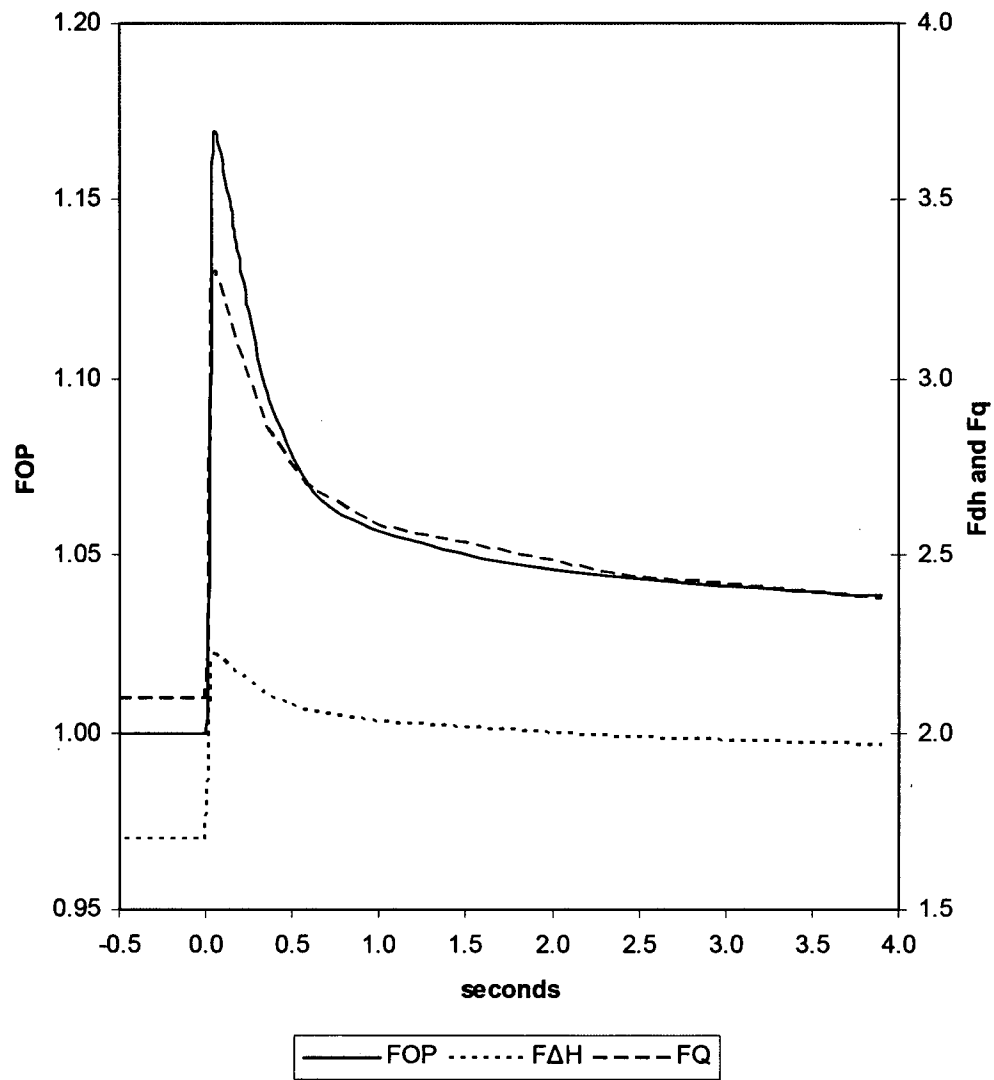


Figure 8-11 BOC 100% Power Transient for N05 Ejected

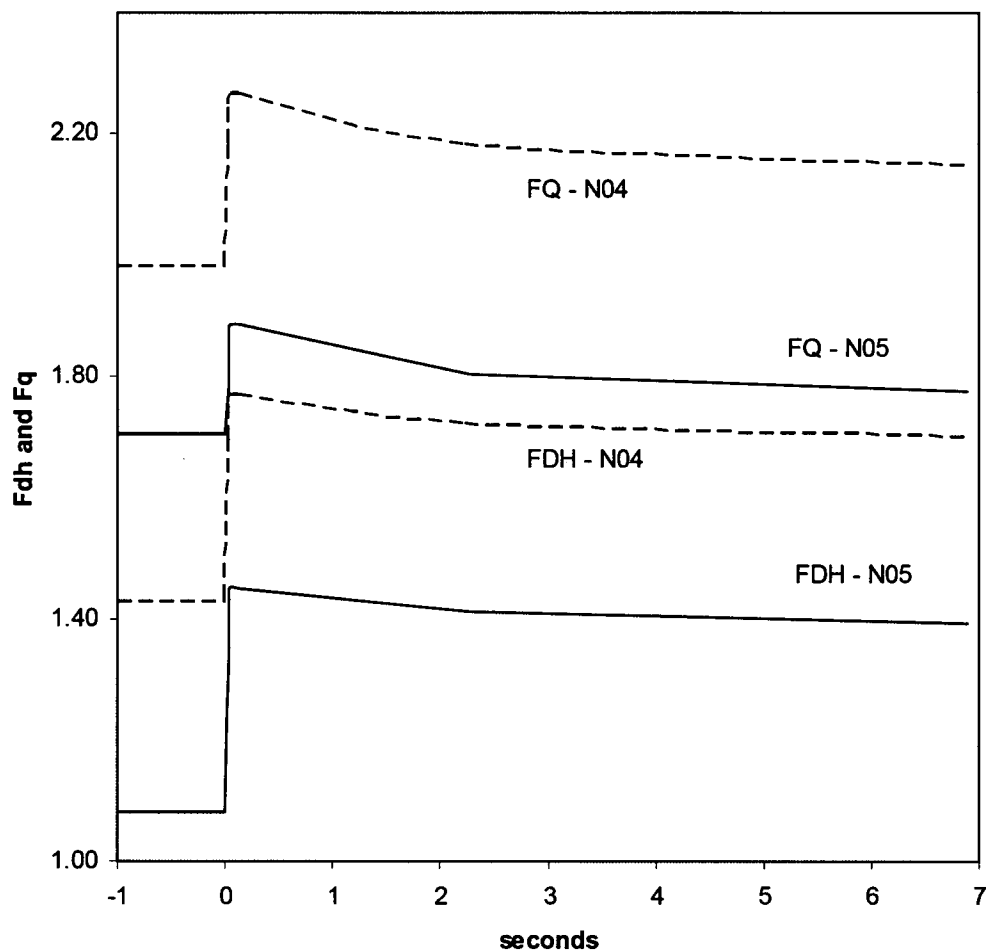


Figure 8-12 S-RELAP5 Results for BOC 25%

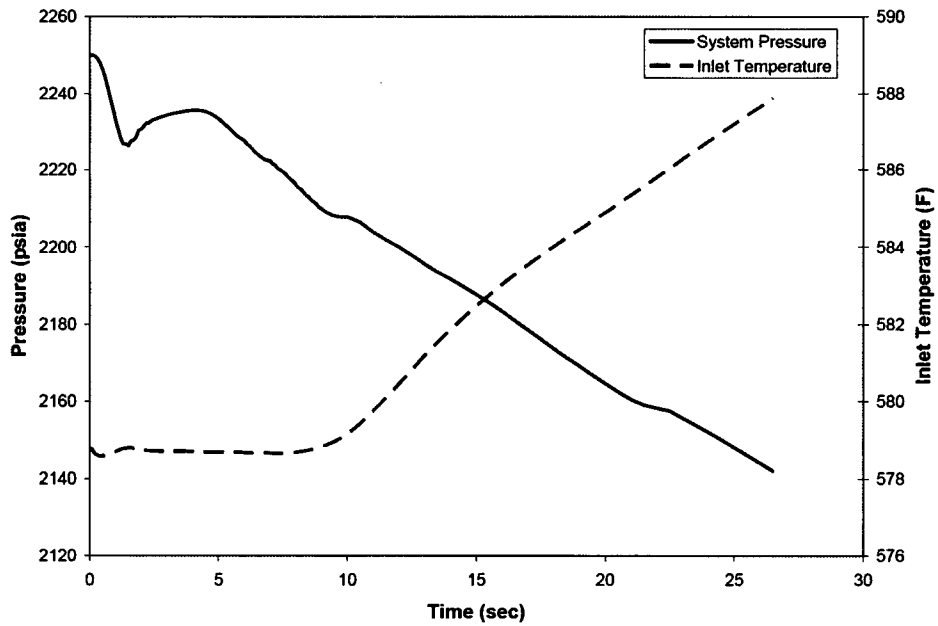


Figure 8-13 S-RELAP5 Results for HFP

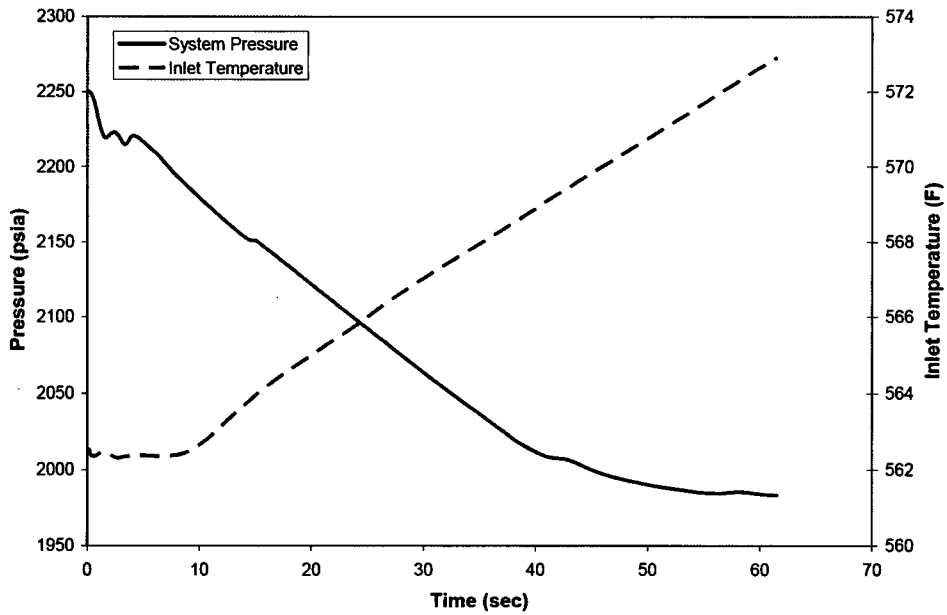


Figure 8-14 MDNBR for BOC 25%

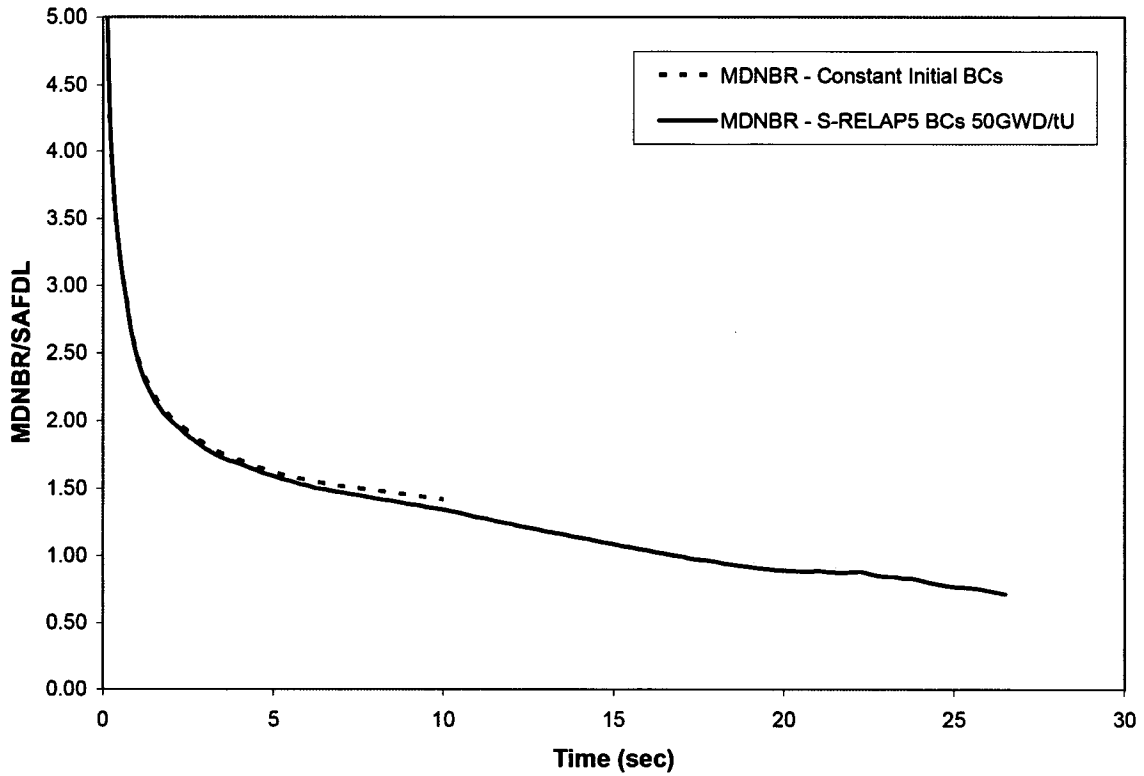


Figure 8-15 Fuel and Cladding Temperatures for BOC 25%

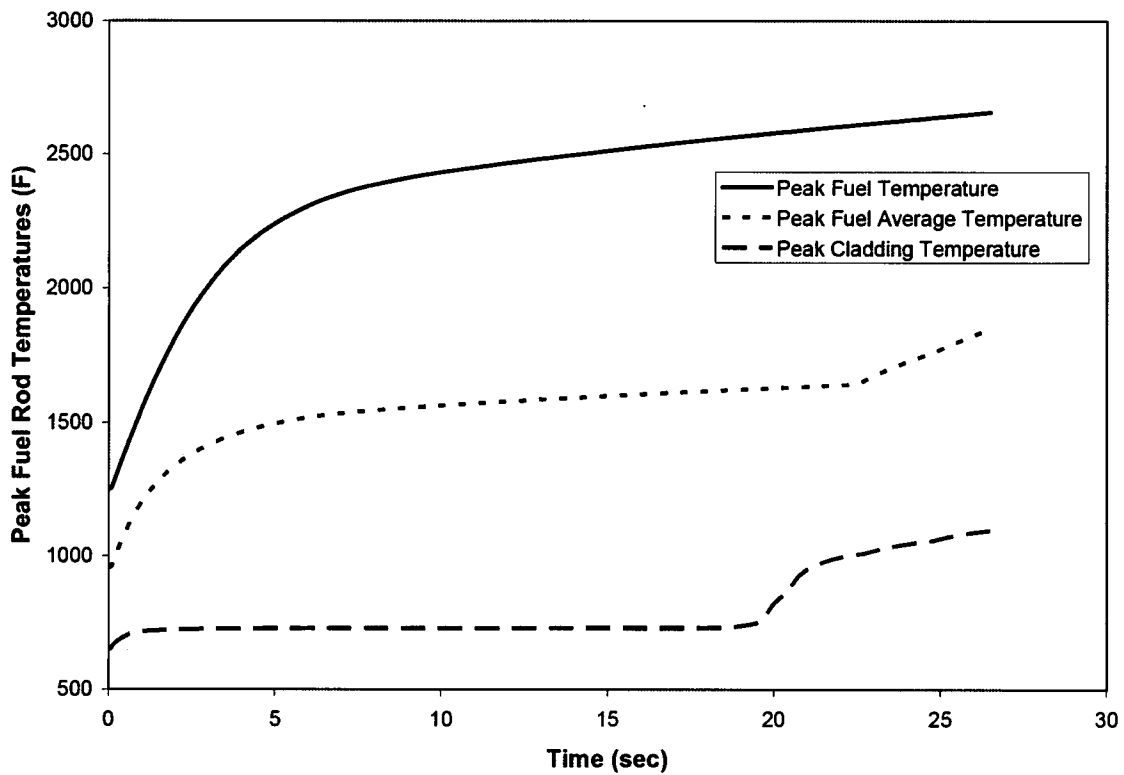


Figure 8-16 Peak Enthalpy Rise for BOC 25%

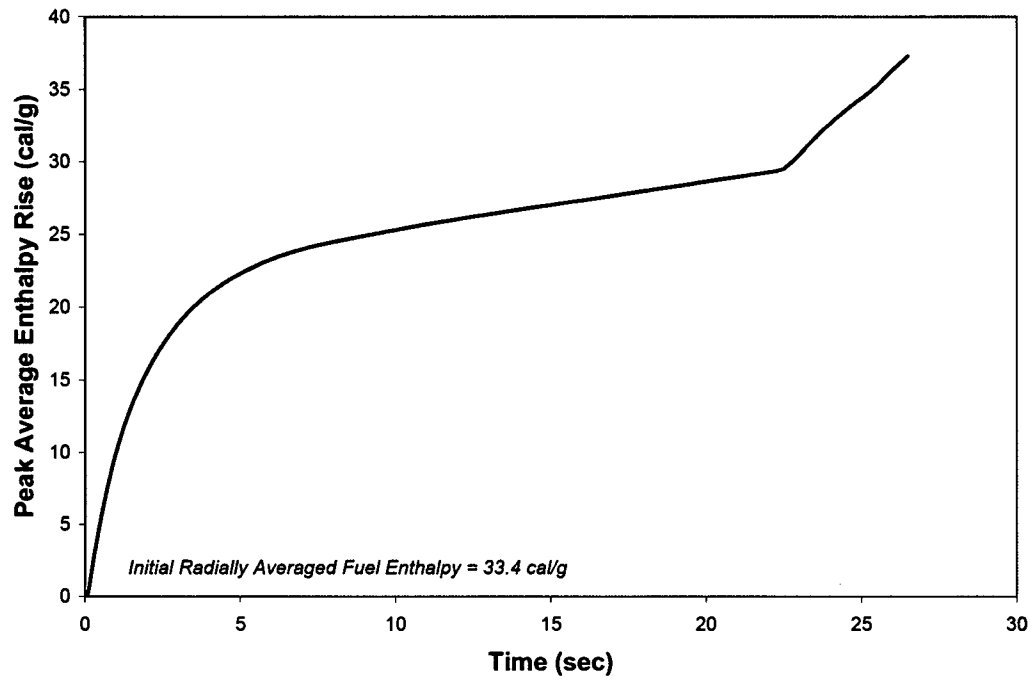


Figure 8-17 MDNBR for BOC 35%

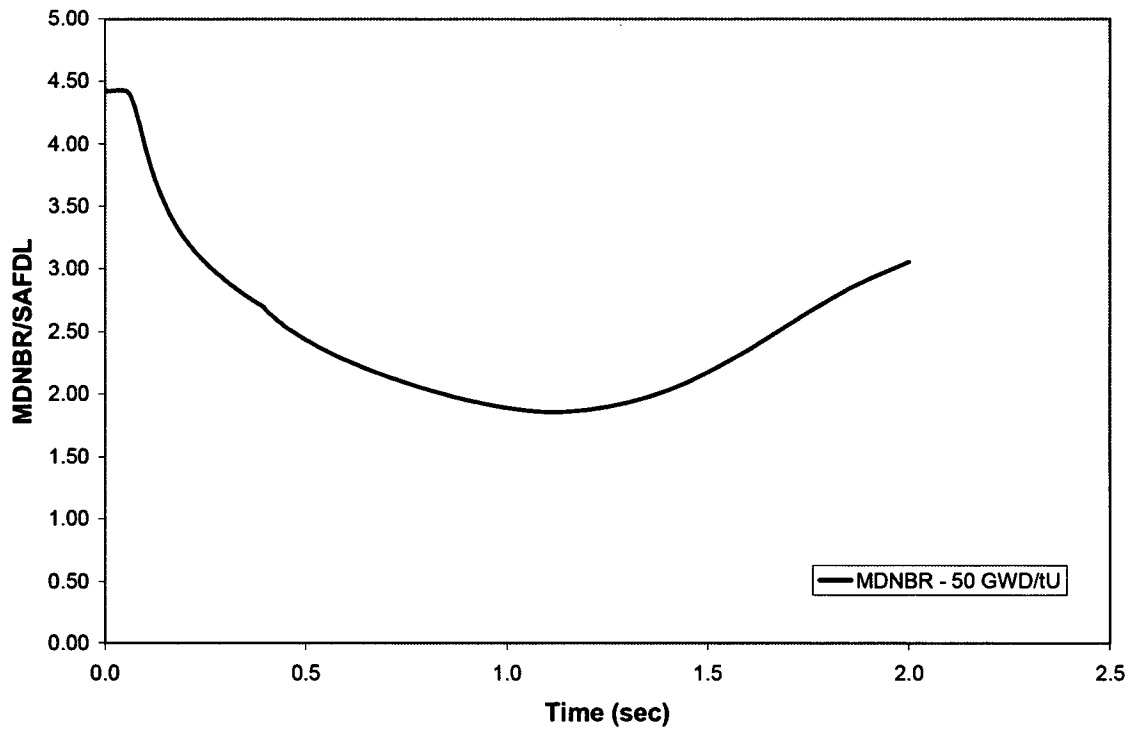


Figure 8-18 Fuel and Cladding Temperatures for BOC 35%

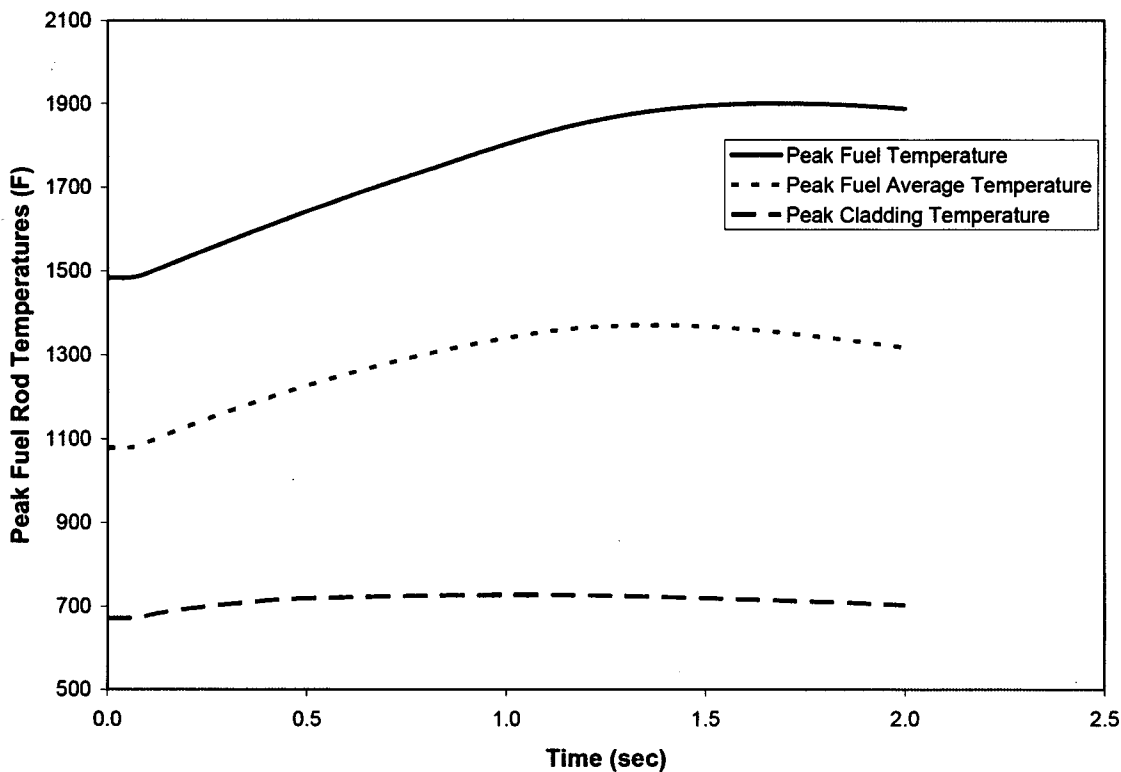


Figure 8-19 Peak Enthalpy Rise for BOC 35%

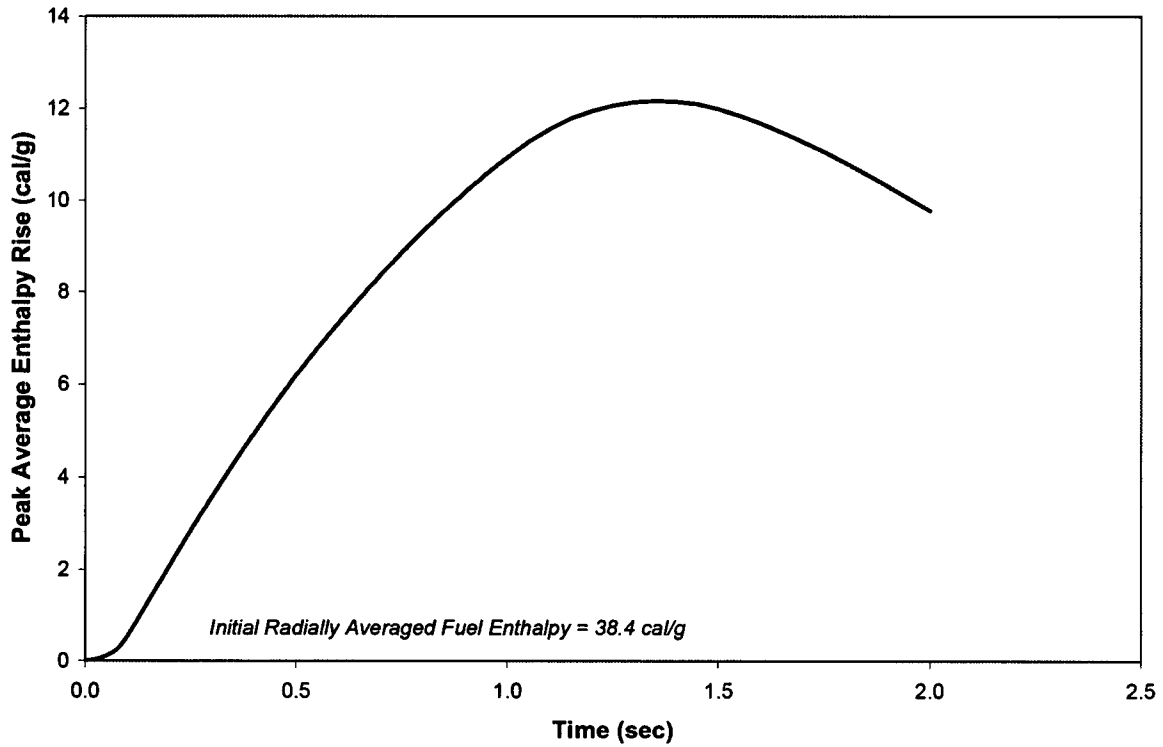


Figure 8-20 MDNBR Excursion for BOC 60%

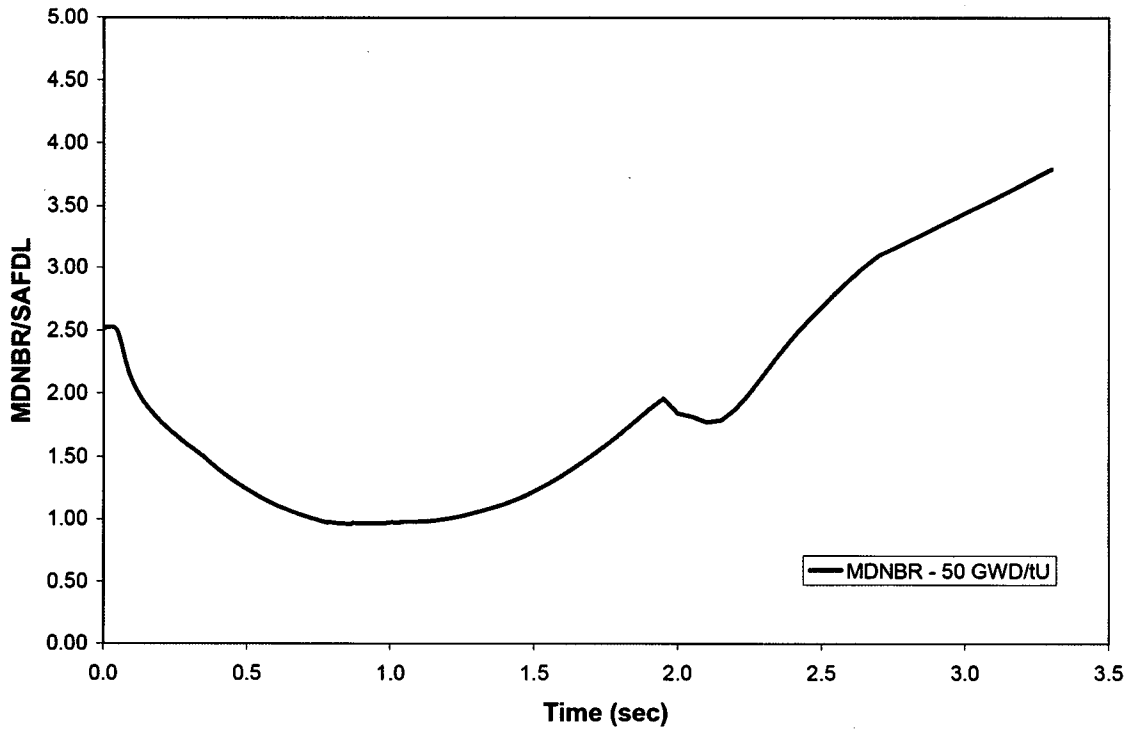


Figure 8-21 Fuel and Cladding Temperatures for BOC 60%

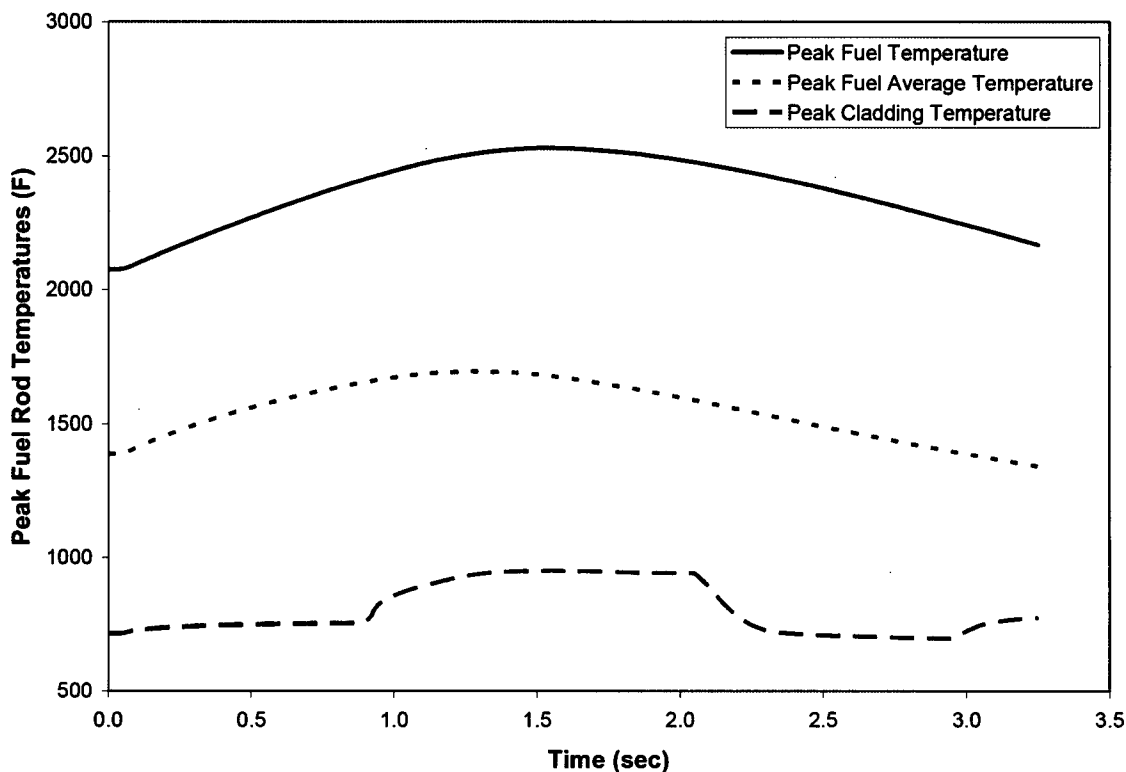


Figure 8-22 Peak Enthalpy Rise Excursion for BOC 60%

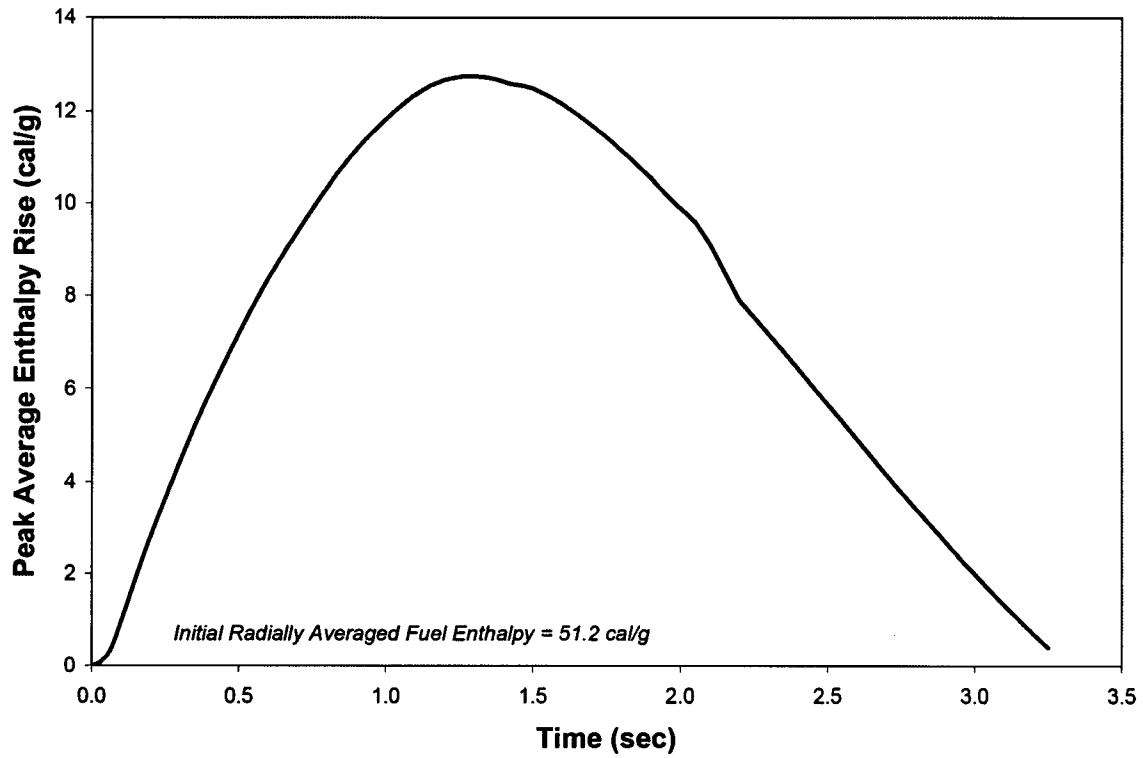


Figure 8-23 MDNBR for BOC HFP

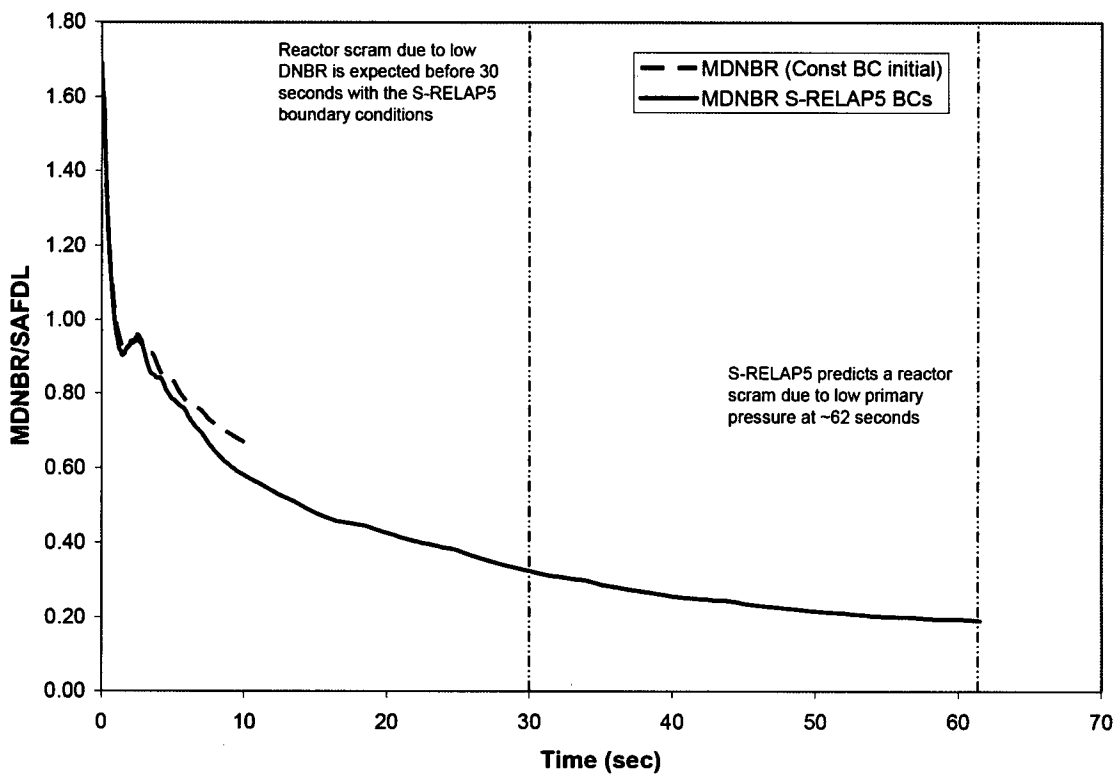


Figure 8-24 Fuel and Cladding Temperatures for BOC HFP

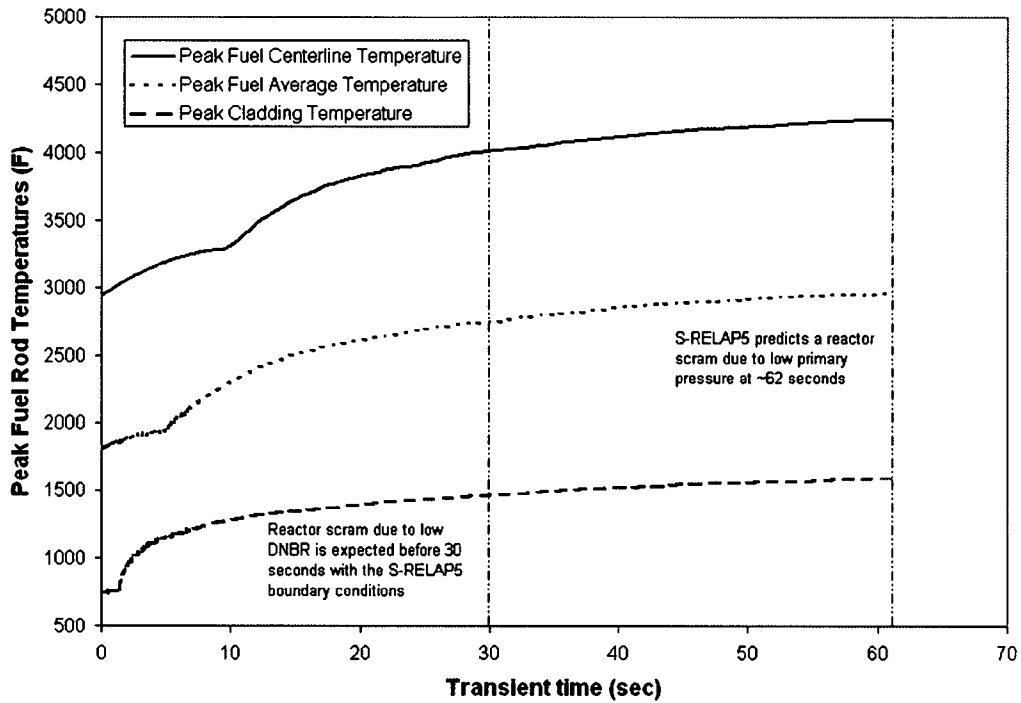


Figure 8-25 Peak Enthalpy Rise for BOC HFP

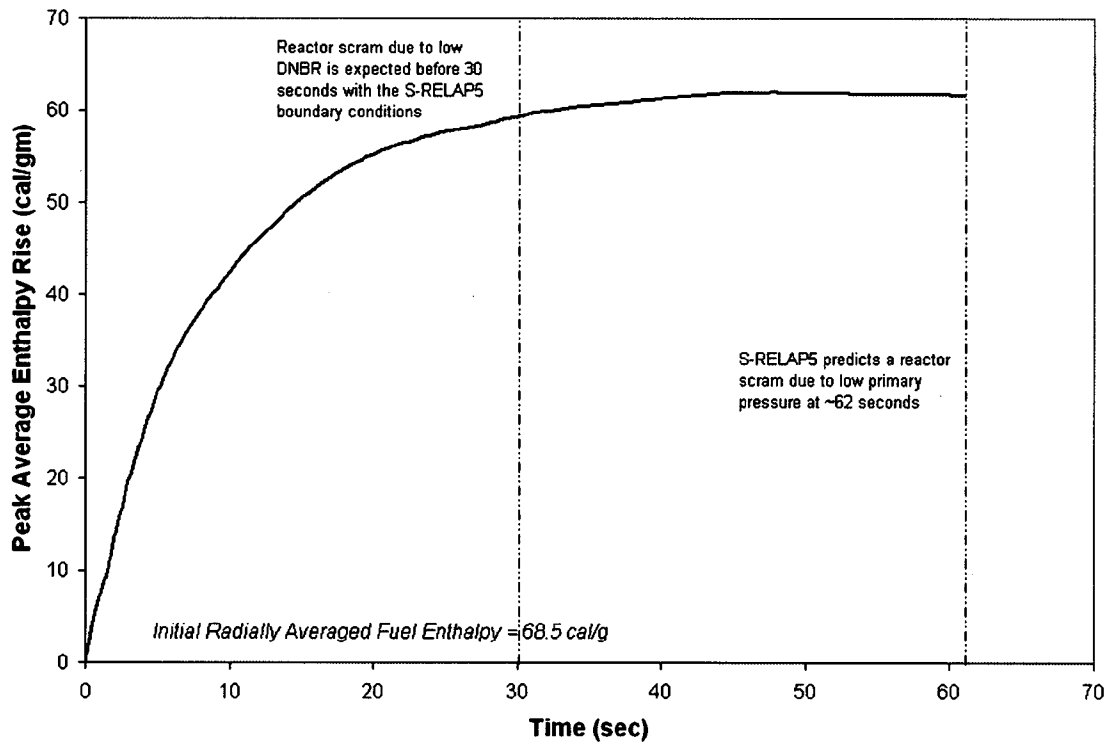


Figure 8-26 MDNBR for EOC HZP

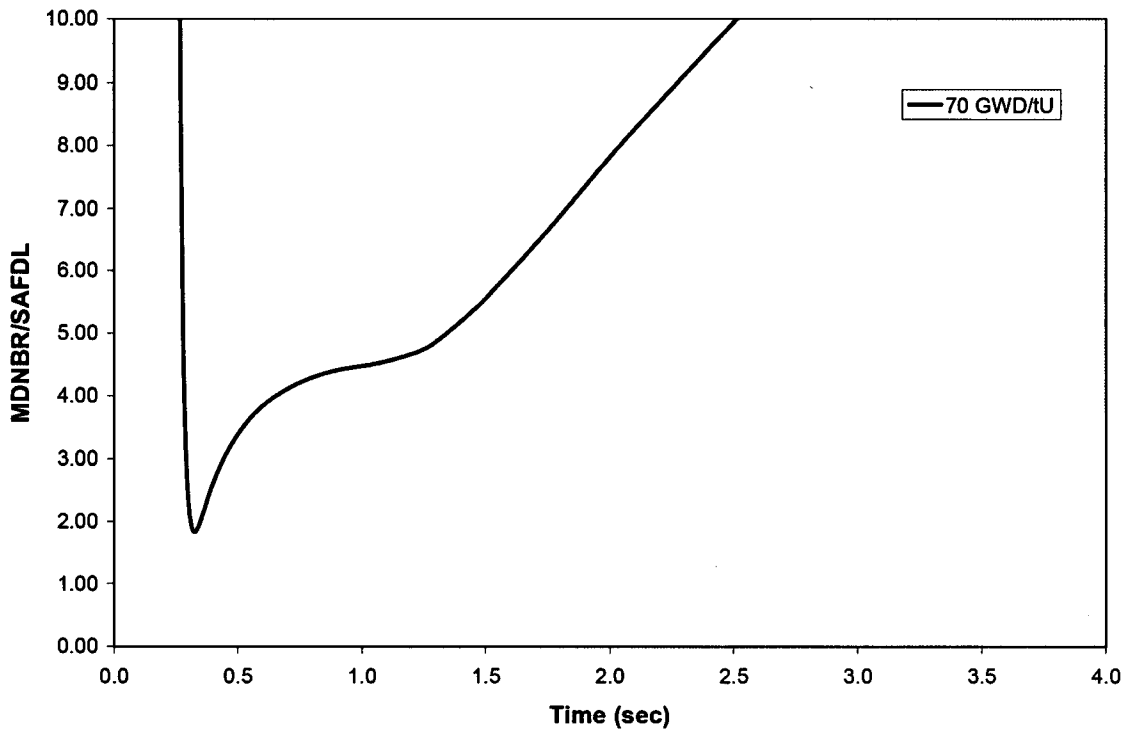


Figure 8-27 Fuel and Cladding Temperatures for EOC HZP

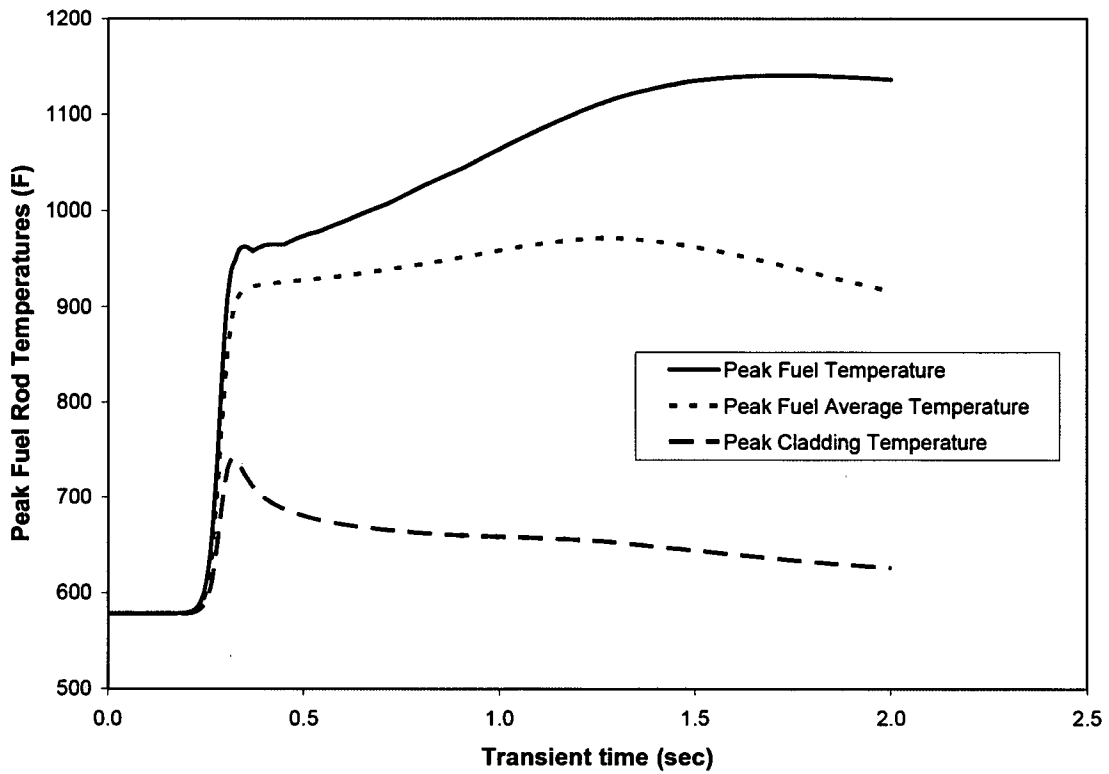


Figure 8-28 Peak Enthalpy Rise for EOC HZP

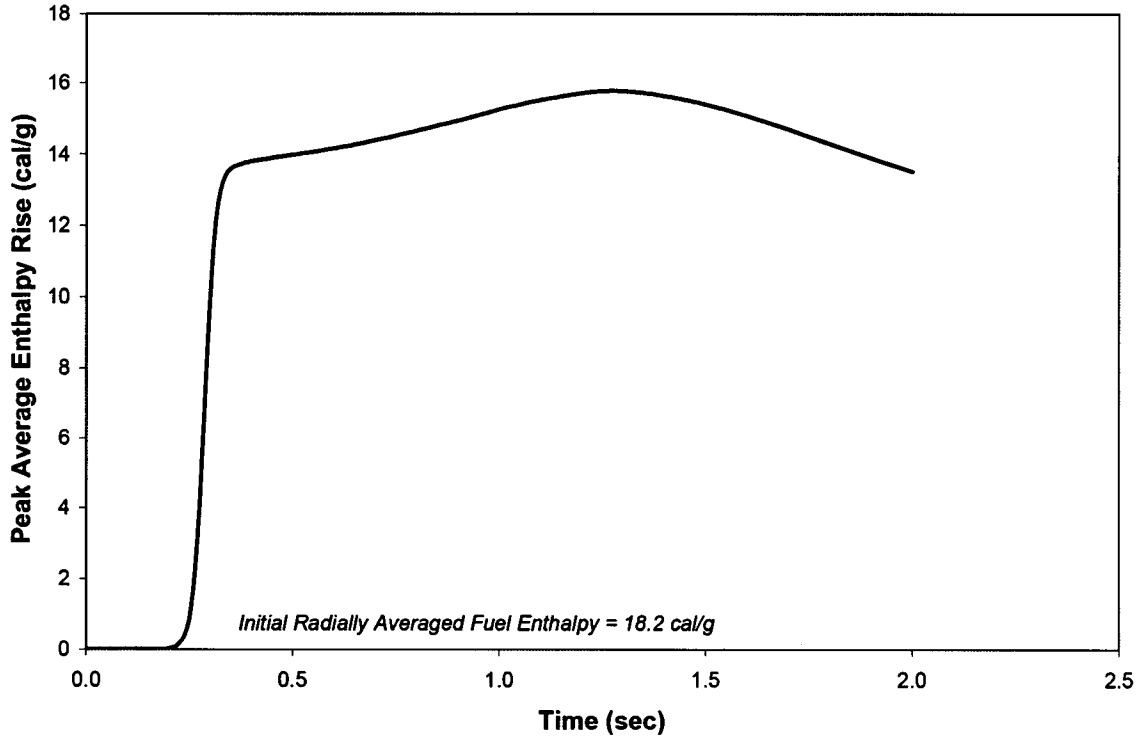


Figure 8-29 MDNBR for EOC 25%

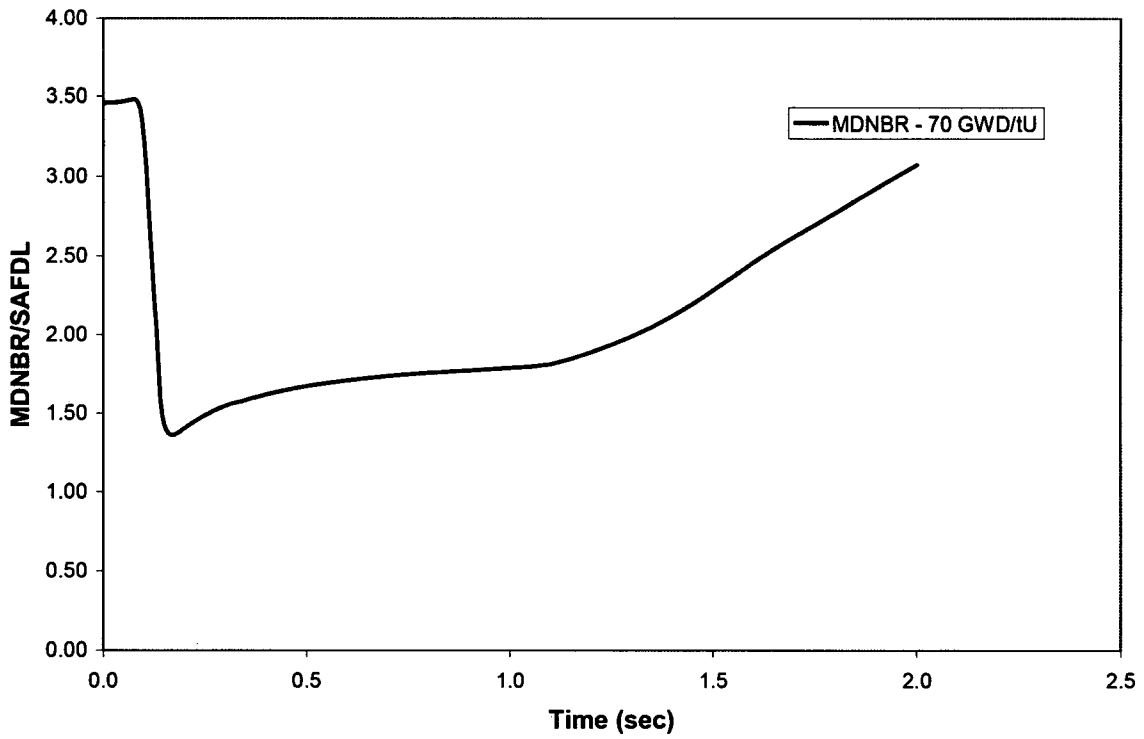


Figure 8-30 Fuel and Cladding Temperatures for EOC 25%

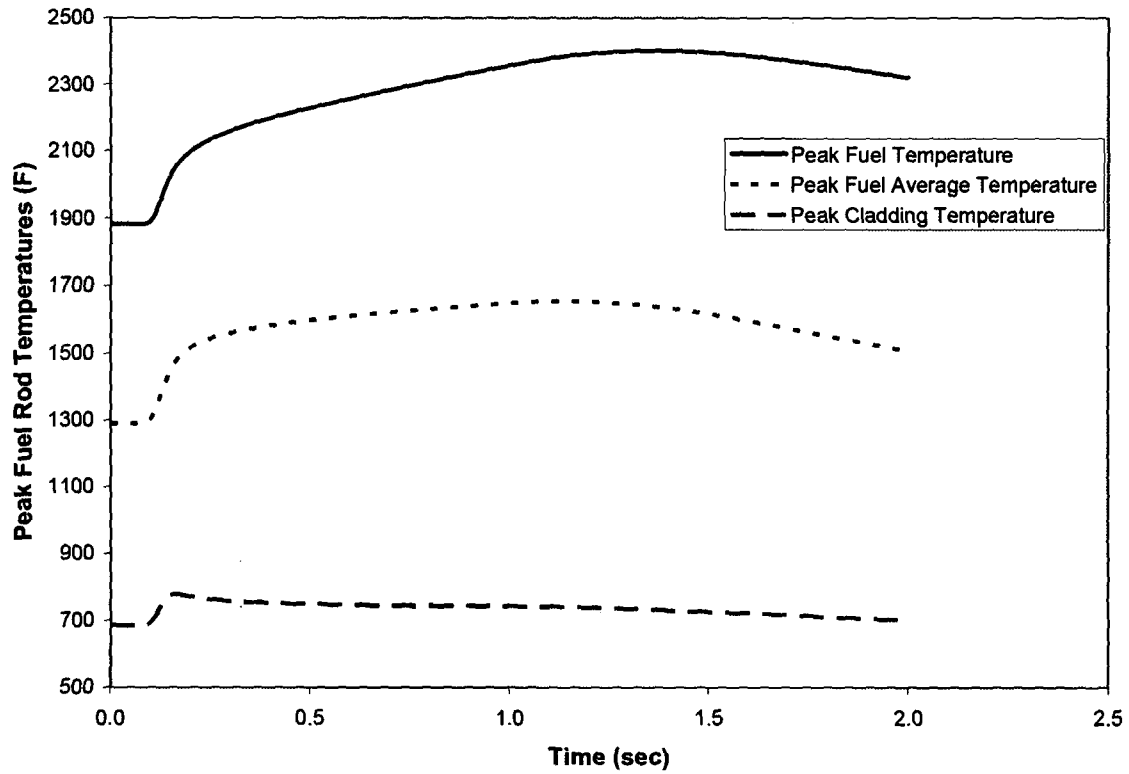


Figure 8-31 Peak Enthalpy Rise for EOC 25%

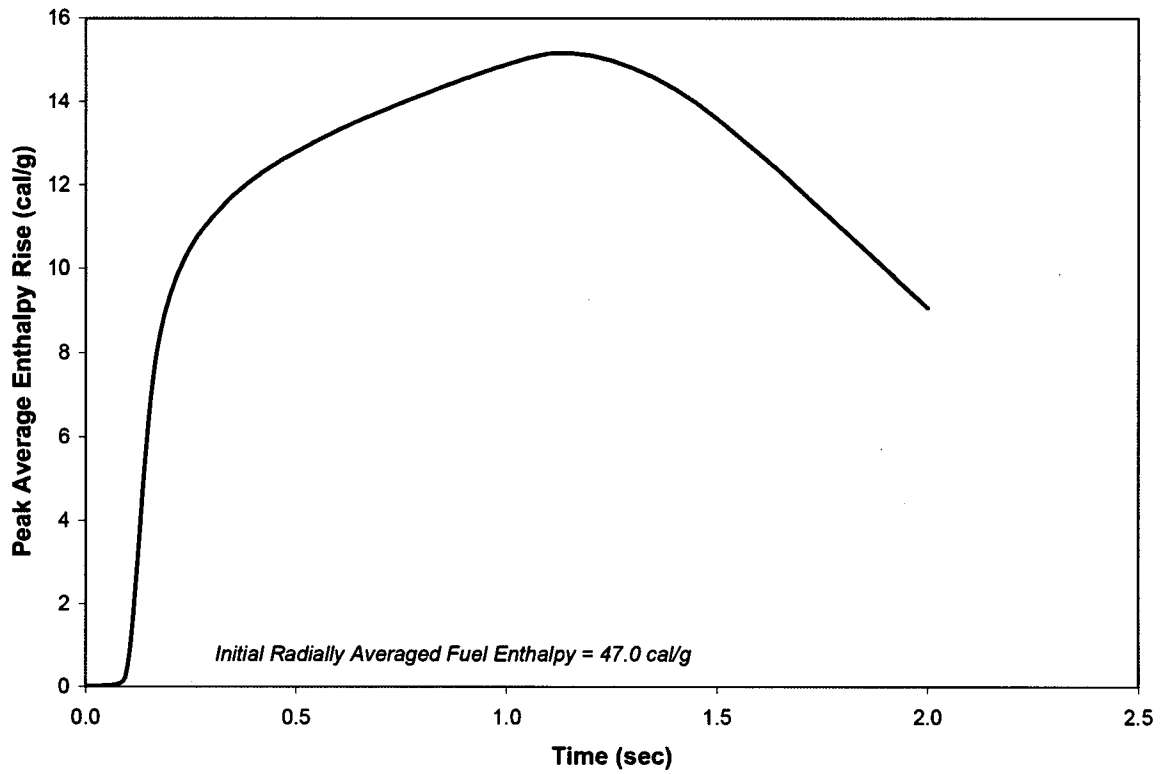


Figure 8-32 MDNBR for EOC 35%

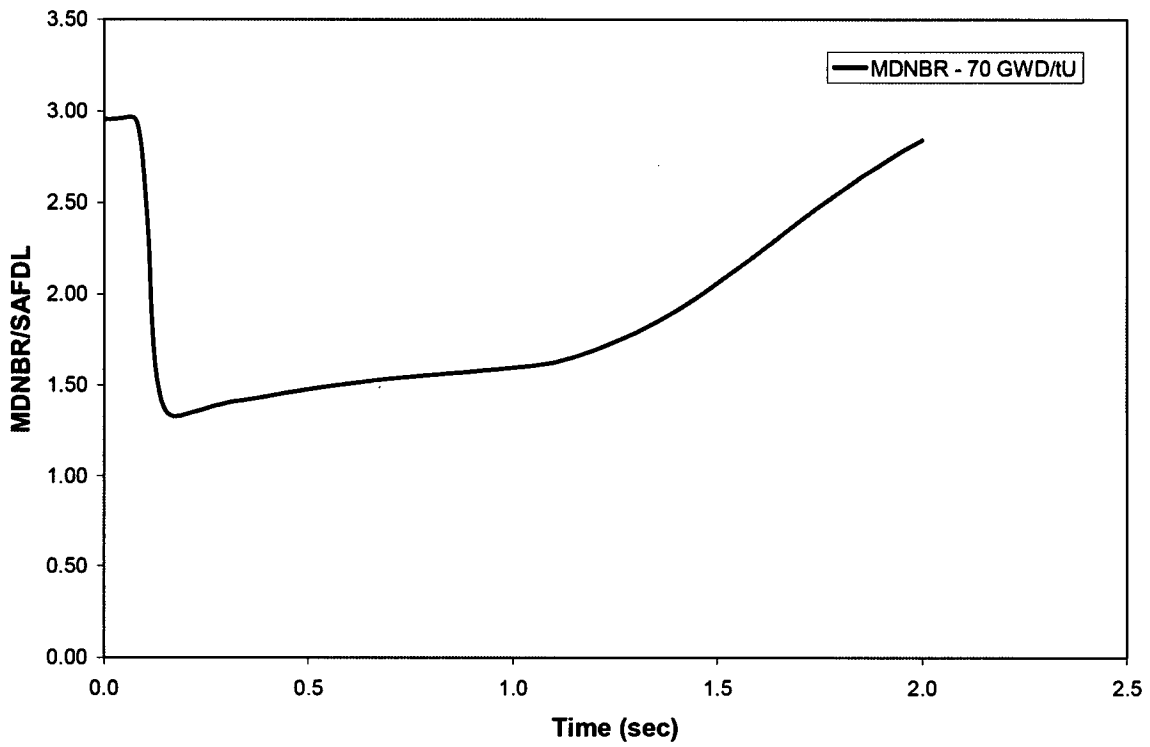


Figure 8-33 Fuel and Cladding Temperatures for EOC 35%

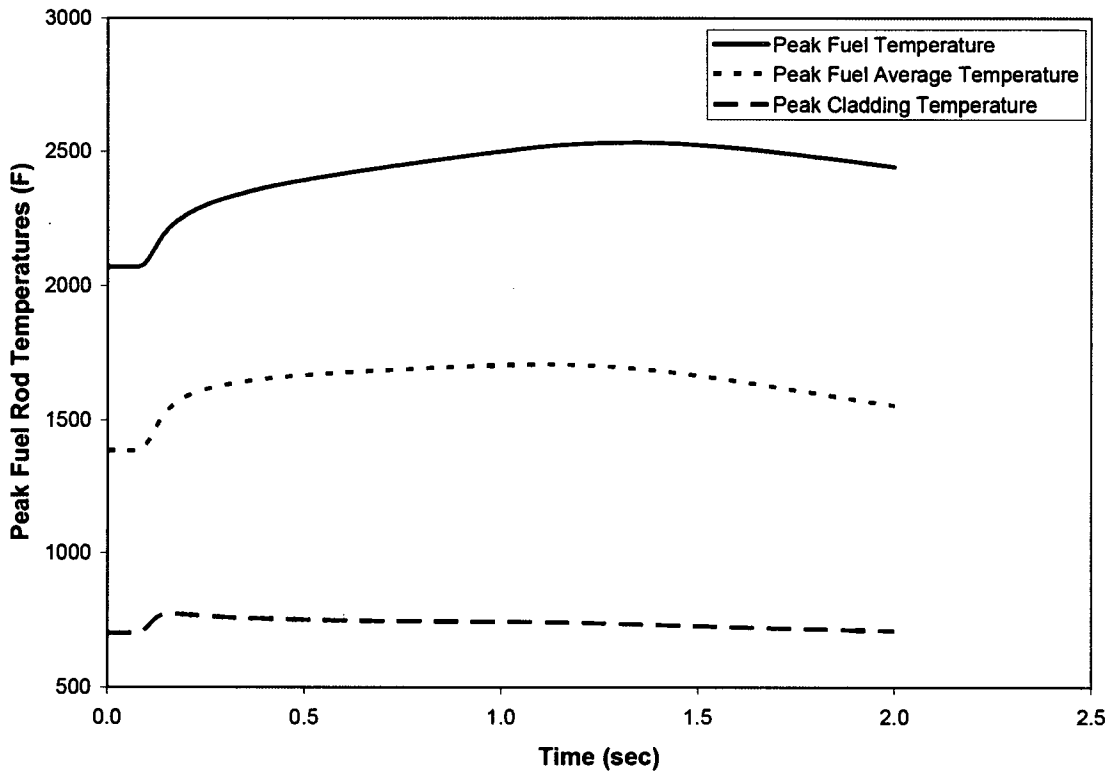


Figure 8-34 Peak Enthalpy Rise for EOC 35%

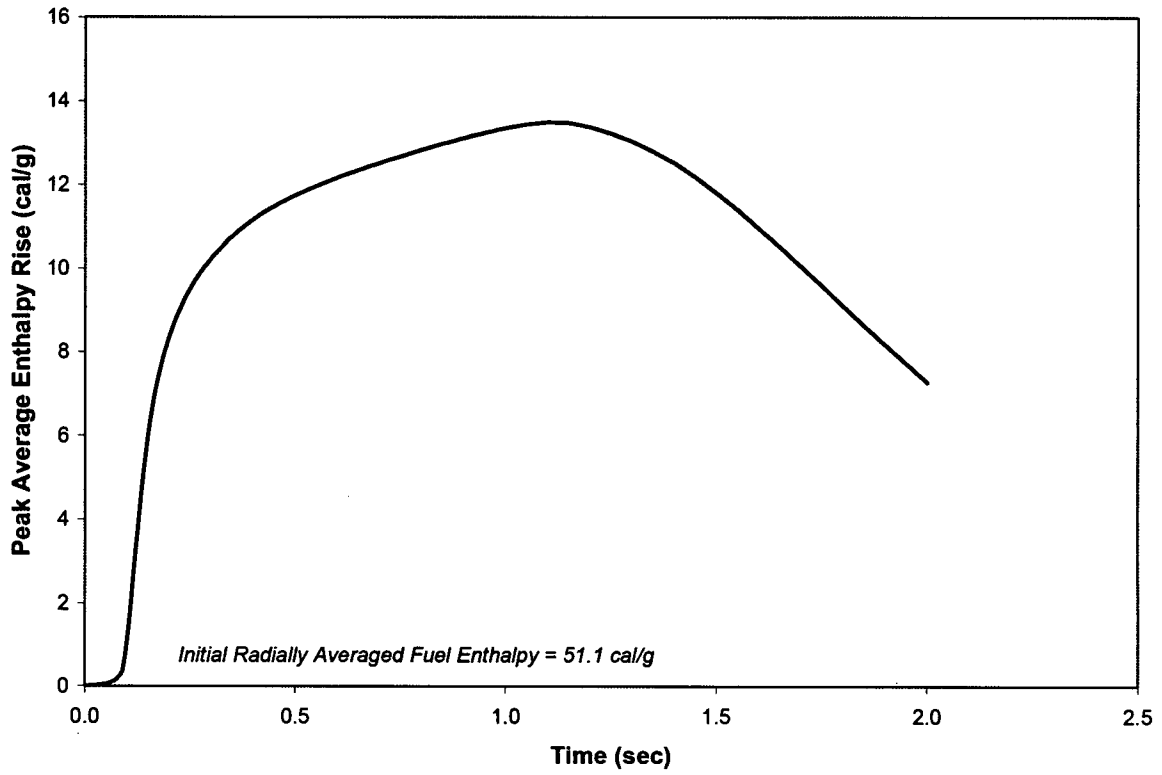


Figure 8-35 MDNBR for EOC 60%

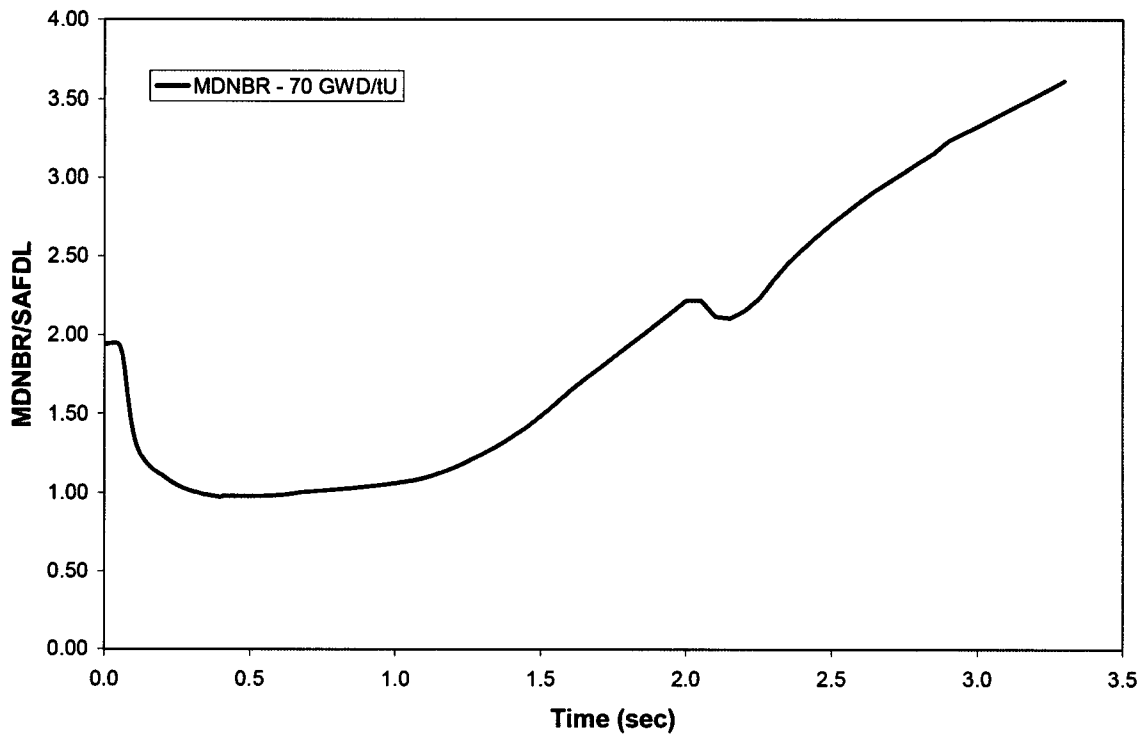


Figure 8-36 Fuel and Cladding Temperatures for EOC 60%

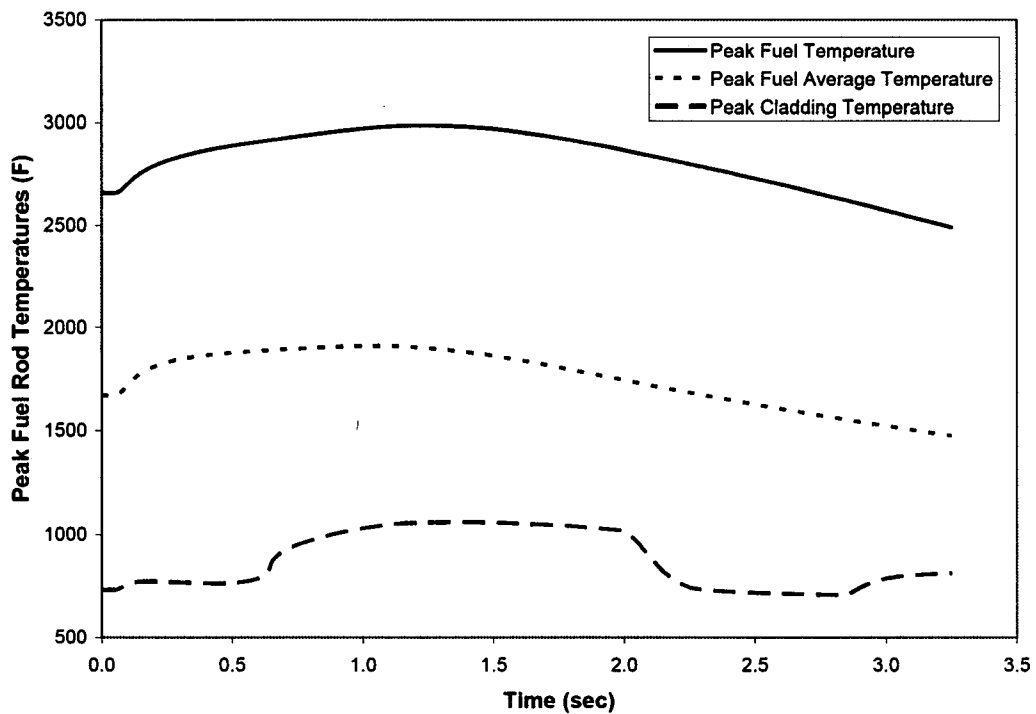


Figure 8-37 Peak Enthalpy Rise for EOC 60%

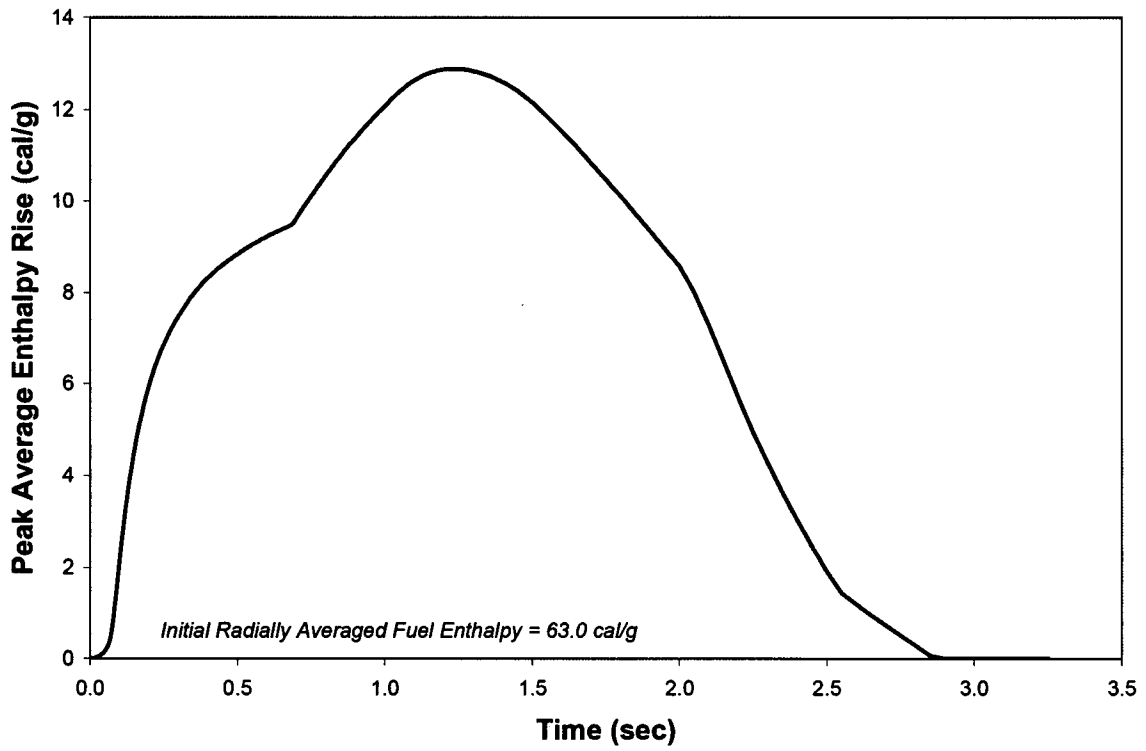


Figure 8-38 MDNBR for EOC HFP

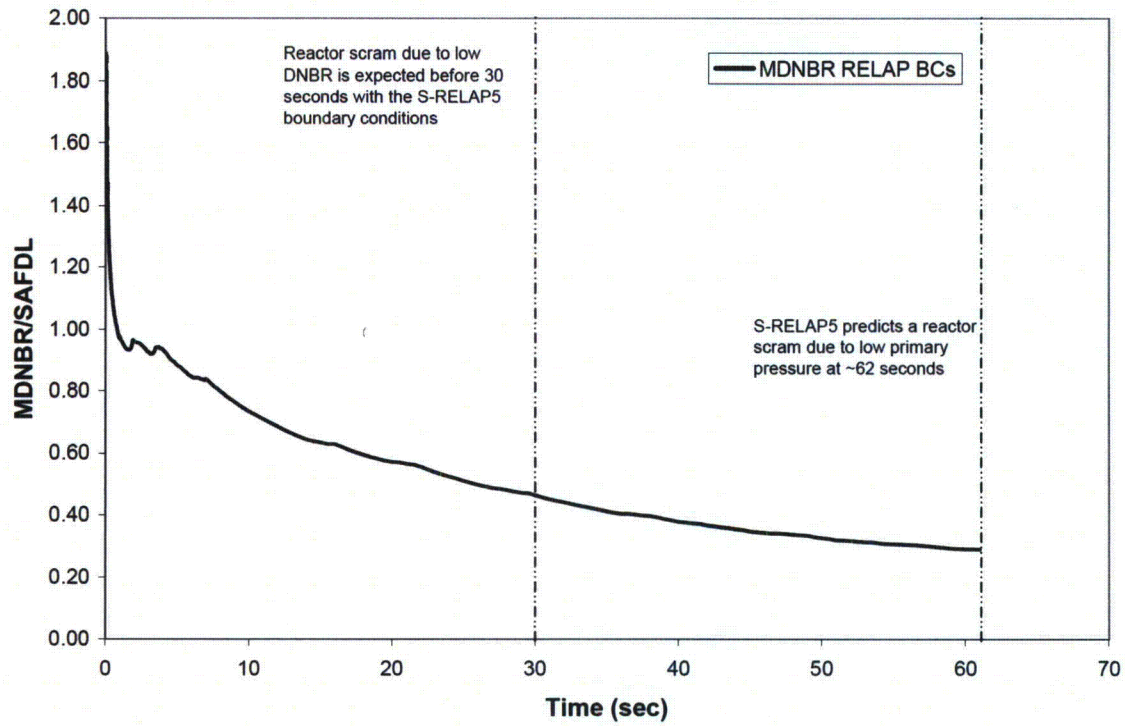


Figure 8-39 Fuel and Cladding Temperatures for EOC HFP

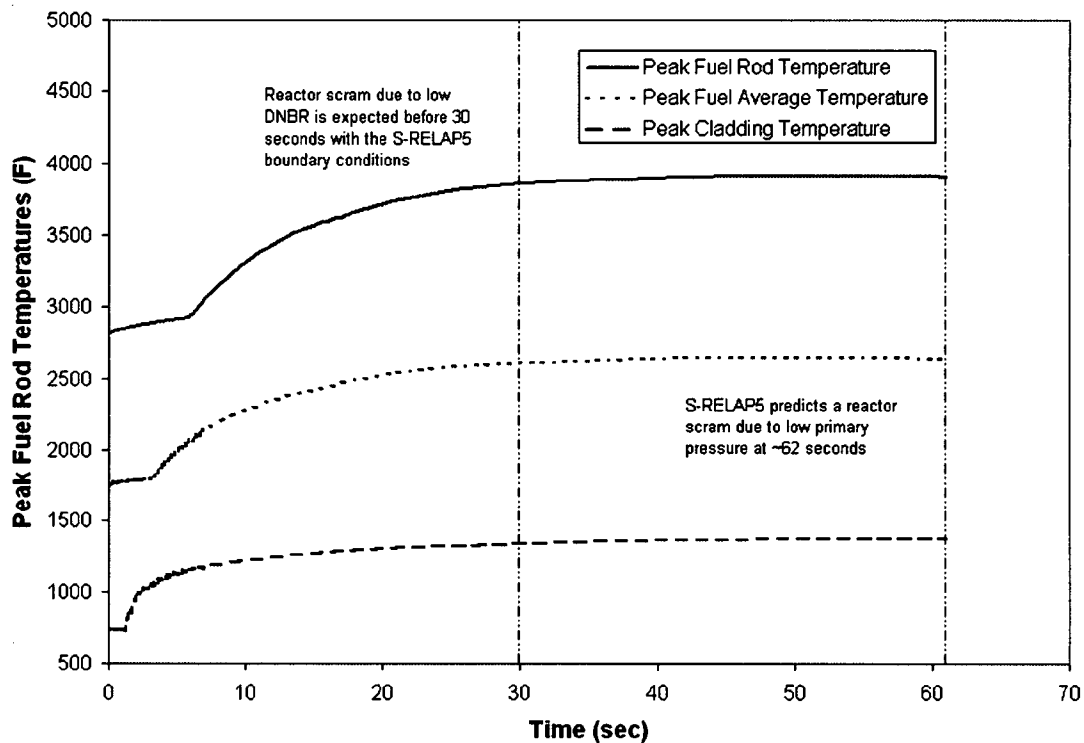


Figure 8-40 Peak Enthalpy Rise for EOC HFP

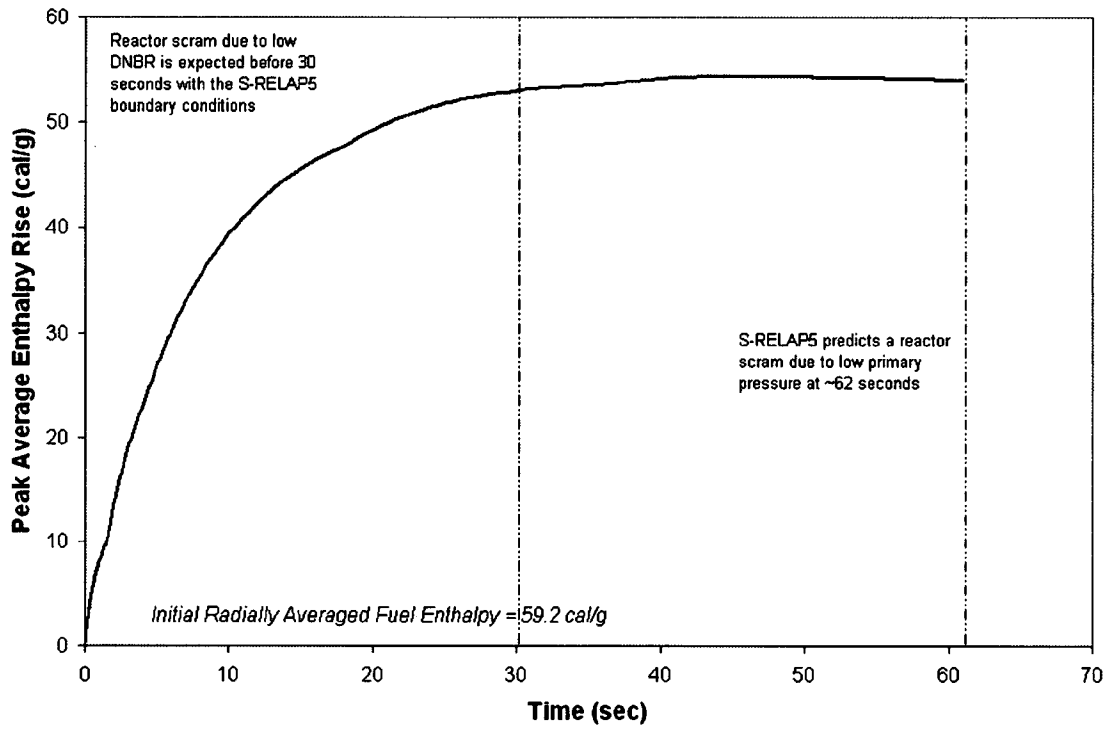


Figure 8-41 Static Ejected Rod Peak Correlated to Transient Peak



9.0 CONCLUSIONS AND CYCLE SPECIFIC CHECKS

This topical report provides a method and sample analysis to demonstrate acceptable results relative to the interim RIA criteria for the U.S. EPR. One of three options can be performed in order to meet any changes in cycle design requirements:

1. Portions of the example analysis can be repeated for each cycle.
2. The current record of analysis can be shown to be applicable to another core design.
3. A complete reanalysis.

Based on the analysis results of Section 8.0, a table to check for each new fuel cycle design can be composed of the limiting values. As concluded in Section 8.0, the limiting conditions occurred at either HZP or HFP. Therefore, only the HZP and HFP parameters need to be verified each cycle. Table 9-1 presents the checklist to validate the cycle specific verification of this sample problem. Table 9-2 presents the cycle 1 limiting values to compare to this sample problem.

Table 9-1 Ejected Rod Analysis Checklist

Parameter	Acceptable values	Cycle Specific Criteria			
		BOC		EOC	
		HZP	HFP	HZP	HFP
Maximum ejected rod worth, pcm	\leq	433	64	634	97
β_{eff}	\geq	0.0055	0.0055	0.0047	0.0047
MTC, pcm/°F	\leq	2.16	0.01	-19.4	-28.47
DTC, pcm/°F	\leq	-1.22	-0.96	-1.52	-1.28
Initial F_Q	\leq	NA ^a	2.36	NA ^a	2.10
Static F_Q after ejection	\leq	9.89	3.39	20.33	4.78
Maximum design $F_{\Delta H}$	\leq	NA ^a	1.70	NA ^a	1.70
Static $F_{\Delta H}$ after ejection	\leq	5.34	2.37	6.51	2.63
Equivalent nominal rods failed, %	\leq	0	30	0	30
Trip setpoints	Not Affected ^b				

Notes:

^a Not applicable since initial stored energy above the coolant temperature is zero.

^b Any changes to the trips listed in Table 8-1 would have to be reviewed relative to their impact on this accident analysis.

Table 9-2 Cycle 1 Ejected Rod Parameters

Parameter	Acceptable values	Cycle 1 values			
		BOC ^b		EOC	
		HZP	HFP	HZP	HFP
Maximum ejected rod worth, pcm ^a	Yes	335	47	539	59
β_{eff}	Yes	0.0061	0.0061	0.0048	0.0048
MTC, pcm/°F	Yes	1.62	-3.38	-20.29	-29.73
DTC, pcm/°F	Yes	-1.35	-1.17	-1.63	-1.45
Initial F_Q	Yes	-	2.20	-	1.69
Static F_Q after ejection	Yes	6.66	2.68	17.76	3.33
Maximum design $F_{\Delta H}$	Yes	-	1.59	-	1.41
Static $F_{\Delta H}$ after ejection	Yes	3.08	1.68	5.01	1.86
Equivalent nominal rods failed, %	Yes	0	0.8	0	0.4
Trip setpoints	NV ^c				

Notes:

^a Ejected rod worths are calculated with the offset skewed to LCO limits and the rods inserted to the Technical Specification Limit for the inserted banks.

^b Composite of BOC and burnup at which the most positive MTC occurs if not BOC

^c Not verified – plant information not available

10.0 REFERENCES

1. NUREG 800, Revision 3, "Standard Review Plan for the Review of Safety Analysis Reports for Nuclear Power Plants," March 2007, ML070740002.
2. BAW-10231PA, Revision 1, "COPERNIC Fuel Rod Design Computer Code," Framatome ANP, January 2004.
3. Letter, Ralph Landry, Acting Chief, Nuclear Performance and Code Review Branch, Division of Safety Systems, NRR, to Thomas Martin, Director, Division of Safety Systems, NRR, "Technical and Regulatory Basis for the Reactivity Initiated Accident Interim Acceptance Criteria and Guidance," January 2007, ML070220400.
4. NUREG/CR-6742 LA-UR-99-6810, "Phenomenon Identification and Ranking Tables (PIRTs) for Rod Ejection Accidents in Pressurized Water Reactors Containing High Burnup Fuel," Los Alamos National Laboratory, September 2001.
5. NUREG/CR-0497, TREE-1280, Revision 2, D. L. Hagman, G. A. Reymann, and R.E. Mason, MATPRO Version 11 (Revision 2), "A Handbook of Material Properties for Use in the Analysis of Light Water Reactor Fuel Rod Behavior," August 1981.
6. BAW-10221PA, "NEMO-K a Kinetics Solution in NEMO," September 1998.
7. BAW-10156A, Revision 1, "LYNXT Core Transient Thermal-Hydraulic Program," B&W Fuel Company, August 1993.
8. EMF-2310PA Revision 1, "SRP Chapter 15 Non-LOCA Methodology for Pressurized Water Reactors," May 2004.
9. NEACRP-L-335 (Revision 1), H. Finnemann and A. G. Galati, "NEACRP 3-D LWR Core Transient Benchmark," Final Specifications, October 1991 (January 1992).
10. BNWL-1962, UC-32, "COBRA-IV-I: An Interim Version of COBRA for Thermal-Hydraulic Analysis of Rod Bundle Nuclear Fuel Elements and Cores," Battelle Pacific Northwest Laboratories, March 1976.
11. BAW-10044, "TAFY – Fuel Pin Pressure and Gas Pressure Analysis," Babcock & Wilcox, April 1972.
12. BAW-10087P, "TACO – Fuel Pin Performance Analysis," Babcock & Wilcox, December 1975.

13. BAW-10141PA, "TACO2 – Fuel Pin Performance Analysis," Babcock & Wilcox, June 1983.
14. BAW-10162PA, "TACO3 – Fuel Pin thermal Analysis Computer Code," BW Fuel Company, October 1989.
15. BAW-10069A, Revision 1, "RADAR – Reactor Thermal and Hydraulic Analysis During Reactor Flow Coastdown," Babcock & Wilcox, October 1974.
16. ANP-10263PA, Revision 0, "Codes and Methods Applicability Report for the U.S. EPR," August 2007.
17. Letter J. H. Taylor to U.S. Nuclear Regulatory Commission, "Revised Measurement Uncertainty for Control Rod Worth Calculations," JHT/96-01, January 3, 1996.
18. Letter J. H. Taylor to U.S. Nuclear Regulatory Commission, "Revised Measurement Uncertainty for Control Rod Worth Calculations," JHT/95-124, December 20, 1995.
19. Letter J. H. Taylor to U.S. Nuclear Regulatory Commission, "Revised Measurement Uncertainty for Westinghouse 193 Plant Control Rod Worth Calculations," JHT/97-20, April 11, 1997.
20. BAW-10150A, "Control Rod Assembly Ejection," pp. 2-26, June 1986.
21. ANP-10269P, Revision 0, Supplement, "The ACH-2 CHF Correlation for the U.S. EPR, Topical Supplement," August 2007.

The original versions of pages 6-19, 6-35, 6-37, 7-9 and 8-8 follow

Table 6-3 LYNXT and COPERNIC Transient Temperature Ratio Comparisons

Comparison parameter	Fuel temperature				Cladding maximum temperature
	Surface	Average	Centerline	Maximum	
HZP EOL					
Average					
Std. dev.					
Maximum					
Minimum					
Sample size					
HFP EOL					
Average					
Std. dev.					
Maximum					
Minimum					
Sample size					
HZP BOL					
Average					
Std. dev.					
Maximum					
Minimum					
Sample size					
HFP BOL					
Average					
Std. dev.					
Maximum					
Minimum					
Sample size					

Notes:

1. The data is based on (COPERNIC result) / (LYNXT CG/TDP result).
2. "Std. dev." is the standard deviation of the data about the average. Sample size is the number of transient time steps.

Figure 6-23 HFP/BOL Transient Fuel Surface Temperature



Figure 6-24 HFP/BOL Transient Fuel Average Temperature



Figure 6-27 HFP/BOL Transient Cladding Maximum Temperature



] This is due to higher gap conductance values and higher pellet rim power peaking. Calculations are performed with 5.0 w/o U_{235} fuel at 2.5 and 50 GWD/MTU burnup levels for the BOC cases and 20 and 70 GWD/MTU burnup levels for the EOC cases in order to bound the potential burnup thermal property states of the fuel rods.

Fuel loaded with gadolinia has a lower thermal conductivity than pure UO_2 . The higher the gadolinia content, the lower the thermal conductivity of the fuel pellet. This increases the fuel temperatures of the gadolinia fuel if operated at the same LHGR as a UO_2 fuel rod. However the gadolinia rods typically have low maximum powers because of lower fuel uranium enrichments and parasitic neutron absorption by the residual gadolinium isotopes. To determine if the analysis can be performed using only UO_2 properties, a sensitivity study was run on the BOC HFP power excursion with gadolinia loadings of 4 w/o and 8 w/o gadolinia. The gadolinia rods were run with the same power history as the pure UO_2 rod and with the maximum power level anticipated for a gadolinia loaded rod. [

] Figure 7-10 shows the peak fuel temperatures for 0, 4, and 8 w/o gadolinia loadings. Note that the fuel temperatures with gadolinia are higher when operating at the same linear heat rate as UO_2 and the transient temperatures for gadolinia fuel adjusted by the power reduction factor are bounded by the UO_2 temperatures. For the thermally limiting transient for HFP at BOC, the temperatures never exceed the lowest fuel melt limit for a rim burnup, even when the peak power is not decreased by the maximum expected value for a gadolinia rod. Because the UO_2 rod bounds the temperatures, the LYNXT calculations use the [

]

Table 8-4 Ejected Rod Analysis Results for BOC

Parameter	Criterion	0	25	35	60	100
Maximum Ejected Rod Worth, pcm	-	433	362	346	286	64
β_{eff}	-	0.0055	0.0055	0.0055	0.0055	0.0055
MTC, pcm/°F	-	2.16	1.32	1.35	0.34	0.01
DTC, pcm/°F	-	-1.22	-1.14	-1.11	-1.05	-0.96
Initial F_Q	-	NA ^a	3.01	2.88	2.63	2.36
Maximum Transient F_Q	-	9.46	5.75	5.23	5.06	2.70
Initial $F_{\Delta H}$	-	NA ^a	2.15	2.09	1.94	1.70
Maximum Transient $F_{\Delta H}$	-	5.21	3.75	3.58	3.01	2.11
Maximum Neutron Power, FOP	-	0.32	0.55	0.69	0.98	1.10
Maximum cal/g	≤ 150	-	70.4	50.4	63.9	109.4
Maximum $\Delta\text{cal/g}$, prompt	≤ 110	-	10.0	10.9	11.8	7.2
Maximum Fuel Temperature, °F	[]	-	2655	1901	2529	4014
Maximum Cladding Temperature, °F	[]	-	1098	727	951	1461
MDNBR/SAFDL Ratio For Failure	≤ 1.0	-	0.71	1.86	0.96	0.33
Time of Trip (initiation of safety bank insertion), seconds	-	No Trip	No Trip ^b	0.850	0.825	No Trip
Equivalent nominal rods failed, %	≤ 30	0	1.8	0	0	7.2

Notes:

^a Not applicable since initial stored energy above the coolant temperature is zero.

^b Trip is disabled to bound consequences of powers lower than 25%.